THE UNIVERSITY OF HULL

DEVELOPING GPS RIVER FLOW TRACERS (GRiFTers) TO INVESTIGATE LARGE SCALE RIVER FLOW PHENOMENA

being a Thesis submitted for the Degree of PhD
in the University of Hull

by

Richard-James Stockdale BSc

September 2009

Contents

Figures

Tables

Abstract

Existing flow measurement methods in natural gravel rivers are largely based on a series of point measurements detached from the dynamic nature of river flow. Traditional measurement methods are limited in many environments and locations due to an inability to access directly the channel; this situation is further complicated at high discharges where entry into the channel becomes impossible. The inadequacy of currently utilised flow measurement methods is highlighted in the study of riffle-pool sequences where limited data has produced gaps in the understanding of these fundamentally important bedform structures. Within the study of riffle-pool sequences the most prominent debates concern the precise means of sequence development and maintenance, the existence / operation of the velocity reversal hypothesis and the spatial compositions and periodicity of these quasi-regular bedform features.

The expanding usage of remote sensor monitoring techniques, the incorporation of GPS receivers into drifters to provide improved positioning, and the adaptation of drifters for use in the surf zone and in estuaries and lakes have combined to highlight the potential of producing a GPS river flow tracer (GRiFTer). The development of a GRiFTer suitable for deployment in a natural gravel bed river system is described whilst the logistics of performing a field based GRiFTer investigation, data acquisition and analysis methods and the achievable accuracy of the approach are also considered.

The development of a GPS River Flow Tracer provides an innovative approach to the acquisition of surface velocity measurements through the development of a series of GRiFTer based analysis tools and techniques. The suite of tools developed to date includes; the ability to measure a single primary flowline through a reach, a means of independently measuring the effective width of channel flow, the identification of low velocity zones (and the direction of flow within these areas), three different methods for the measurement of surface flow velocity (primary flowline, cross-sectional averaged and reach scale) and a means of defining riffles and pools from the relationship between depth and surface flow velocities.

The study ultimately concludes with a conceptual model for the development and maintenance of riffle-pool sequences based on an adaptation of the flow convergence routing hypothesis.

Acknowledgements

I would firstly like to thank the Department of Geography, University of Hull, and EPSRC for giving me the opportunity, support and ability to complete my PhD research.

The thesis you are about to read represents four years of work, effort and sacrifices by many people, several of which I would like to take the opportunity to thank now.

My supervisor committee have been amazing and provided the perfect balance for every aspect of my research. Many thanks go to Tom Coulthard for having so much passion for my work and for constantly providing new ideas and enthusiasm. Incredible gratitude goes to Dick Middleton for teaching me so much, guiding virtually all technical aspects of my work and being directly responsible for the invention, development and operation of the GRiFTer concept. Sincerest thanks go to Stuart McLelland; your knowledge, guidance and insistence on accuracy and brevity have made the research process both possible and extremely valuable. You have played the single biggest role in my education through both degree and PhD and all my achievement are at least in part down to you. Thank you.

Special thanks go to my best friend Matt Dowson for waking up stupidly early and spending many hours stood / laid in freezing cold water in the middle of nowhere, you're the best friend anyone could have and this is yet another thing I am very glad I didn't have to do without you.

To Helen, you're the best discovery I made during my PhD; you're the best person I know, have helped me so much and your love and support makes me want to be better everyday. Special thanks to Lynn and Colin for their support, for feeding me and essentially letting me move in for weeks on end.

Thanks also go to my family (Mum, Dad, Aaron, Aidan & Biscuit) for their continued support and for providing me with the place I always did my best writing and work.

Thanks also go to; David Keir, David Boyd, James Tait, Josh Comitale, Mark Golding and Brendan Murphy for help with field work and thanks to anyone else who helped in the research process.

1.0 Introduction

1.1 Thesis Overview

1.1.1 Review of Existing Velocity Measurement Methods

A variety of methods are currently utilised to measure flow velocities in fluid environments. These can be broadly categorised as invasive and non-invasive approaches. Invasive approaches can be further categorised as mechanical methods, which include propeller meters (Wolman, 1958; Ferguson et al., 1989; Carling, 1991; Thompson et al., 1999) and electromagnetic current meters (ECMs) (Lane et al., 1998; Markham et al., 1992; Fulford, 2001; Lamarre et al., 2005; Wang et al., 2007; MacVicar et al., 2007) and acoustic approaches that include acoustic Doppler current profilers (ADCP) (Richardson et al., 1996; Lane et al., 1999, Yorke and Obeng, 2002; Nystrom et al., 2002; Kostaschuk et al., 2004; Muste and Spasojevic, 2004; Shields and Rigby, 2005; MacVicar et al., 2007) and acoustic Doppler velocimetry (ADV) (Voulgaris and Trowbridge, 1997; Rodriguez et al., 1999; Lohrmann et al., 1994; Hosseini et al., 2006; MacVicar et al., 2007) . Non-invasive approaches include image based techniques (PIV, PTV, and LS-PIV) (Tait et al., 1996; Ettema et al., 1997; Costa et al., 2000; Holland et al., 2001; Weibrecht et al., 2002; Creutin et al., 2003; Muste et al., 2005; Jodeau et al., 2008; Fox et al., (2008) and surface drifter buoys (Grudlingh, 1998; Bushnell, 1998; Bogard et al., 1999; Manda et al., 2000; Grodsky et al., 2002; Jakobsen et al., 2002; Tseng et al., 2002; Johnson et al., 2003; Ohlmann et a., 2005).

In order to perform velocity measurements both mechanical and acoustic devices require operators to wade into the channel or use boats, scaffolding and / or cabling to facilitate measurements (Wolman, 1958; Carling et al., 1991; Lane et al., 1998; Thompson et al., 1999; Yorke and Obeng, 2002; Kostachuk et al., 2004; Lamarre et al., 2005). Regardless of the measurement technique, traditional methods are generally time consuming and labour intensive which result in the high cost of river monitoring. Traditional measurement methods become increasingly difficult to utilise during periods of high flow where greater depths and velocities make entry into the channel dangerous (Carling, 1991; Creutin et al., 2003). Most traditional velocity measurements are also Eulerian in nature, presenting point velocity values both spatially and temporally detached from the dynamic nature of river flow. All velocity results are also arbitrary since the path of measurement is predetermined prior to investigation providing results that are further detached from the dynamic nature of river flows (Stockdale et al., 2007).

Alternative velocity measurement methods are therefore required when natural flow conditions do not permit the use of conventional techniques (Jodeau et al., 2008). A potential solution lies in the use of large-scale particle image velocimetry (LSPIV); an image-based technique that provides surface velocities by measuring the displacement of floating fluid-markers between successive digital images (Fox et al., 2008). LSPIV is a non-invasive method and therefore does not require entry into the channel (Creutin et al., 2003). This increases the speed of potential repeat measurements and allows for measurements up to and beyond bankfull flow conditions (Creutin et al., 2003; Muste et al., 2005). LSPIV can also make flow measurements in heavily sediment laden and vegetated flows (Muste et al., 2005). Uniquely, LSPIV also provides the potential for the measurement of surface flow velocities, particularly in shallow water environments (Weibrecht et al., 2002; Jodeau et al., 2008).

LSPIV is not without limitation; difficulties arise in ensuring sufficient natural light is available to allow the recording of clear images particularly in adverse weather conditions (Ettema et al., 1997, Cruetin et al., 2003). The potential exists to utilise artificial lighting but this introduces additional complexity, time and costs and is not always possible in all environments (Cruetin et al., 2003). Additional problems arise in providing sufficient coverage and uniformity of particle seeding throughout the channel (Ettema et al., 1997; Weibrecht et al., 2002).

In recent years there has been an increase in the use of drifter buoys for the acquisition of data from remote and often inhospitable environments (Clearwater, 2007). It has also been highlighted that drifter buoys can be customised to meet the specific requirements of varied environments and investigations (Grudlingh, 1998; Bogard et al., 1999; Grodsky et al., 2002; Jakobsen et al., 2002). Structurally; the size, shape and material of the surface housing and subsurface drogue can be changed dependent upon the environment within which the drifter is to be deployed (Clearwater, 2007). Additionally, the type of positioning, data recording and transmission equipment must be selected specifically dependent upon the intended deployment environment and resultant structural constraints (Bushnell, 1998; Tseng et al., 2002). Similarly, the designated sampling strategy determines both the acquisition of data and the power requirement of the integrated equipment (Bograd et al., 1999; Jakobsen et al., 2002 and Barth, 2003). Through the combination of each of these elements it is possible to construct a drifter suitable for deployment in a wide variety of fluid environments. This fact is highlighted by the increasing use of drifter buoys in lakes, estuaries and surf-zone areas (Manda et al., 2000; Johnson et al., 2003; Ohlmann et al., 2005). Deployment in such environments has required both structural and technical alterations to currently available drifter designs (Manda et al., 2000; Johnson et al., 2003; Ohlmann et al., 2005). Drifters buoys are non-invasive and have the advantage that they can be used in high velocity and high sediment flows where traditional measurement methods would be compromised. The use of drifter buoys also removes the potential of user error in the performance of measurements since there is no user intervention prior to the processing and interpretation of collected measurements.

1.1.2 Large-Scale Surface Flow Dynamics

Riffle-pool sequences are fundamentally important to understanding flow and flow processes in natural gravel-bed river systems (Yang, 1971). A riffle-pool sequence is a periodic stream morphology consisting of longitudinal bedform undulations with larger alluvial bars, spanning the channel, and intervening deeper pools (Leopold and Wolman, 1957; Richards, 1976a; Wilkinson et al., 2004). Riffles are thought to occur periodically, having an average wavelength of several channel widths (Leopold and Wolman, 1957; Keller and Melhorn, 1978), although there may be significant variability about the mean (Keller and Melhorn, 1978; Carling and Orr, 2000; Wilkinson et al., 2004).

Existing literature has highlighted several key areas of debate regarding riffle-pool sequences; development and maintenance (Yang, 1971; Keller, 1971; Carling 1991; Clifford and Richards, 1992; Clifford, 1993a; Lofthouse and Robert, 2007) structure and periodicity (Melton, 1962; Leopold et al., 1964; Church, 1972; Keller, 1971; Richards, 1976b; Keller and Melhorn, 1978; Clifford and Richards, 1992; Clifford, 1993b; Sear, 1996; Thompson, 2001) and hydraulic parameters of which the velocity-reversal hypothesis remains the most prominent (Lisle, 1979; O'Connor et al., 1986; Clifford and Richards, 1992; Keller and Florsheim, 1993; Carling and Wood, 1994; Sear, 1996; Thompson et al., 1998, 1999; Booker et al., 2001; Milan et al., 2001; Cao et al., 2003 and MacWilliams et al., 2006).

The difficulties highlighted with the use of traditional measurement methods are particularly prominent in the study of riffle-pool sequences and are at least partly responsible for existing literature failing to address many fundamental questions (Wilkinson et al., 2004; MacWilliams et al., 2006). Quantative measures for defining riffles and pools are lacking largely because most attempts to develop criteria rely on mean or point flow measurements which are inadequate to describe the complex flow processes (Richards, 1976a; Clifford and Richards, 1992). The pre-determined and often random collection of data (often dictated by access / safety issues) further limits current understandings by spatially and temporally restricting available measurements (Carling, 1991). Measurements are particularly lacking at high flow conditions where entry into the channel is not possible meaning traditional mechanical measurements cannot be made (Carling, 1991; Clifford and Richards, 1992). In addition to limitations in measurement methods, inconsistent definitions (regarding elements of flow phenomenon and channel structure), sampling strategies and methodologies have complicated experimental findings and therefore the understanding of riffle-pool sequences (Cherkauer, 1973, Milan et al., 2001). Expanded and improved flow data is therefore required from natural formed riffle-pool sequences. Specifically there is a need for a data that; (i) extends through multiple, consecutive riffle-pool sequences (ii) includes both straight and curved reaches comprising higher intensity hydraulic measurements (iii) covers a wider range of discharge conditions (Milan et al., 2001).

Despite the existing literature providing a widely agreed upon criteria and explanation for the classification and operation of riffle-pool sequences, there are areas of continued debate, methodological criticism and fundamentally important questions remaining to be addressed.

1. There is significant debate regarding the periodicity of ripple-pool sequences. The majority of research agrees that riffles form with a periodicity to the inter-riffle spacing of 5 to 7 channel widths (Melton, 1962; Leopold et al., 1964; Church, 1972; Keller, 1971; Keller and Melhorn, 1978; Richards, 1976b; Clifford and Richards, 1992; Sear, 1996; Thompson, 2001). Additional research is however required to determine the appropriate definition and measurement of channel width and to establish whether there is a relationship between discharge and inter-riffle spacing.

2. In response to the debate concerning the provision of consistent definitions and methodologies, Cherkauer (1973) introduced 'effective width' which corresponds to only the active zone of flow (Clifford and Richards, 1992). Although the concept of effective width has been utilised in other investigations (Thompson, 2004; Harrison and Keller, 2007) there remains no means of independently measuring effective width.

3. The majority of riffle-pool sequences investigations have focused on the velocity-reversal hypothesis (Lane and Borland, 1954; Keller, 1971; Lisle, 1979; Andrews, 1982; Carling, 1991; Keller and Florsheim, 1993; Carling and Wood, 1994; Thompson et al., 1996; Booker et al., 2001; Milan et al., 2001). Despite the prominence of this phenomenon and volume of research attached to it, there has been no universal agreement upon the occurrence or operation of a reversal. Many investigations are criticised for being based upon limited spatial and temporal field evidence (Thompson, 2001; MacWilliams et al., 2006). Furthermore, however with currently utilised measurement methods it may not be feasible to provide the data necessary to clarify the debate regarding the velocity-reversal hypothesis (Cao et al., 2003) particular due to the lack of measurement at very high discharges.

4. Whilst the majority of velocity based research has focused on identifying the relative differences between riffles and pools, (Lane and Borland, 1954; Keller, 1971; Lisle, 1979; Andrews, 1982; Carling, 1991; Keller and Florsheim, 1993; Carling and Wood, 1994; Thompson et al., 1996; Booker et al., 2001; Milan et al., 2001) little attention has been placed upon the velocity structures observed in individual riffles and pools. For example, the point of maximum velocity throughout a reach, theoretically located at the riffle midpoint is thought to migrate with changes in discharge (Wilkinson et al., 2004). The unique velocity structure of individual riffles and pool must therefore be considered with respect to changes in discharge to provide a more complete understanding of large-scale surface flow phenomena.

1.1.3 The Potential of Utilising a GPS Based Flow Measurement Method (GRiFTers)

Using existing velocity measurement methods, the data required to address the issues and inadequacies associated with flow phenomena in riffle-pool sequences is difficult, if at all possible to acquire. Therefore an alternative approach to velocity measurement is required. The growth in the use of drifter buoys in a variety of flow environments, including lakes, estuaries and surf-zone areas (Manda et al., 2000; Johnson et al., 2003; Ohlmann et al., 2005) and the incorporation of GPS receivers providing improved positioning and velocity measurements, raises the potential of engineering a GPS river flow tracer (Stockdale et al., 2007).

The use of a GPS receiver provides the potential to measure accurate positions and velocities anywhere on the earth's surface (Hofmann-Wellenhof et al., 2001; DePriest, 2003). The removal of selective availability and the introduction of WAAS-enabled GPS receivers theoretically offer dramatically improved positioning within the same cheap, lightweight GPS receivers (Adrados et al., 2002; El-Rabbany, 2002; Witte et al., 2005). In addition to positioning, GPS receivers can provide accurate velocity measurements utilising instantaneous Doppler measurements or calculations made from deviations in positioning over known time periods (Witte et al., 2004; Witte et al., 2005; Stockdale et al., 2007).

There are several potential difficulties associated with utilising GPS receivers in natural river environments. Steep slopes and channel banks dramatically increase the angle of the satellite mask, therefore limiting the number of visible satellites and the quality of over-head satellite geometry relative to the GPS receiver. Additionally, signal blockage and multipathing would be a likely result of dense bank vegetation or channel crossing bridges which would again be detrimental to the quality of GPS measurements (Pace *et al.,* 1995; Garmin, 2000; El-Rabbany, 2002; Leick, 2004; Witte et al., 2005).

The engineering of a drifter buoy suitable for use in a natural gravel-bed river would require several fundamental changes to be made to the drifters utilised in other fluid environments. The exterior body or casing would need to be made smaller to allow passage through the channel; the internal components would therefore also need to be reduced in size. Additionally, the potential of utilising a GPS in natural, shallow water environments must be determined since no other method would provide sufficiently accurate position and velocity measurements. The appropriate approach to data recording and or transmission must be determined, as must the ability to recover and redeploy individual drifters. GPS river flow tracer measurements would also be unique in providing genuine Lagrangian surface velocity measurements, with the measurement path being independently determined by the natural path of flow.

Extensive field testing must be conducted to determine the operational limitations of GPS receivers specifically in natural river environments. Similarly the design, construction, internal configuration and usage of a GPS river flow tracer must be examined to determine whether it is possible to acquire higher resolution spatial and temporal flow data, and if so what is the best approach to this. In addition to the development of a GPS river flow tracer, unique data presentation and analysis methods would also be required to utilise the collected information and apply the data to address the limitations and questions that remain in the understanding of riffle-pool sequences.

1.2 Research Objectives

1. **Review currently utilised flow measurement methods and critique their respective advantages and limitations with particular reference to measurements in riffle-pool sequences.**

Initially a review of currently utilised velocity measurement methods will be conducted to highlight the limitations and inadequacies of making velocity measurement, particularly in natural gravel-bed river environments. The associated limitations of field-based data collection in these environments will then be linked to the fragmented understanding of the large-scale flow processes operating within riffle-pool sequences.

2. **Determine the precision and accuracy with which GPS can measure velocity and positioning.**

The expanding usage of GPS within drifter buoys for remote sensed positioning and velocity measurement has highlighted the potential of developing a GPS River Flow Tracer. In order to determine the feasibility of such an approach a series of experiments will be conducted to ascertain the precision and accuracy with which both positioning and velocity measurement can be made.

3. **Engineer a GPS River Flow Tracer to facilitate the measurement of surface flow patterns in natural gravel-bed river systems.**

The process of engineering a GPS River Flow Tracer requires the completion of a series of individual objectives.

Initially the appropriate structural composition of the flow tracer must be determined in order to maximise the water following capability and the provide the maximum range of flow conditions to which the technique can be applied.

A suitable means of data capture will also be developed - the potential exists to utilise data transmission directly from the GPS Flow Tracer or to capture data within an internal memory in each GPS Flow Tracer.

The logistics of GPS Flow Tracer deployment and recovery must be established to minimise equipment redundancy and maximise the repeatability to flow measurements. Furthermore, the potential of utilising multiple GPS Flow Tracers (a flotilla) will be investigated to maximise achievable data coverage of a single flow event.

Following the successful capture of data, a method of disseminating information from extremely large datasets will be developed based upon a cellular grid approach similar to that utilised in two-dimensional flow modelling (in order to provide flexibility to environment variables such as the size of reach under investigation). This approach will allow for the development of unique analysis tools based on the averaged behaviour of flow across cells such as attempts to determine the effective width of channel flow and an independent main line of channel flow.

1.3 Thesis Outline

Chapter 1: Introduction.

Current chapter.

Chapter 2: Literature review.

The second chapter will comprise a three part literature review. The first section will focus on currently utilised flow measurement methods and provide a description, example usage, achievable accuracies and the advantages and disadvantages of each approach. The final part of the first section will focus on the subject of drifter buoy and consider their development and expanding usage.

The second section will review the published literature referencing riffle-pool sequences in gravel bed river systems. This section will provide a definition and description criteria then reference each of the fundamental research areas; development and maintenance, structure and periodicity and the velocity-reversal hypothesis. This section will conclude with an analysis of the limitations of current understandings and outstanding research questions which have remained as the result of technological limitations and / or inadequate field data.

The third literature review section considers the operation and suitability of GPS receivers to be utilised in natural river environments. This section will include subsections providing a definition, description and operation of the global positioning system, an explanation of the available velocity measurement methods, indicators of the quality of GPS measurements, potential sources of error and extension to the global positioning system (DGPS and WAAS).

Chapter 3: Method.

Chapter three provides a unique method chapter, comprising seven linear sections spanning the initial concept and development of the GRiFTer through to validating its performance against a comparable velocity measurement method.

Chapter 4: Results - Flow Phenomena in Riffles and Pools.

Chapter 4 details the development of a series of GPS River Flow Tracer (GRiFTer) based tools and techniques for the measurement and description of surface flow phenomena in natural gravel bed river systems.

Chapter 5: Conclusions and Future Work.

Chapter 5 provides a summary of the main findings regarding large-scale flow phenomena in riffle pools sequences; including the primary flowline, effective channel width, low velocity zones, surface flow velocities and flow depth and structures of individual riffles and pools, and the operation of the flow convergence routing hypothesis. Following these summaries, an adapted conceptual model of the develop and maintenance of riffle-pool sequences, primarily based on the flow convergence routing hypothesis will be presented. This chapter will also include an outline of potential future work to explore with the GRiFTer technique.

2.0 Literature Review

2.1 Flow Measurement Methods

A variety of methods are currently utilised to measure flow velocities in fluid environments. These can be broadly categorised into invasive and non-invasive approaches. Invasive approaches can be further classified as mechanical methods which include propeller meters and electromagnetic current meters (ECMs) and acoustic approaches which include acoustic Doppler current profilers (ADCP) and acoustic Doppler velocimetry (ADV). Non-invasive approaches include image based techniques (PIV, PTV, and LS-PIV) and surface drifter buoys. In order to understand the difficulties associated with the measurement of surface flow dynamics in natural river environments and the need for an alternative approach to velocity measurements, a review of existing flow measurement methods is presented (Table 2.0).

		DESCRIPTION	EXAMPLE USAGE	ACCURACY	ADVANTAGES	DISADVANTAGES
INVASIVE APPROACHES	**PROPELLER METERS**	Mechanical device comprising rotating impeller blade attached to an electronic unit which converts propeller rotations into point velocity values.	Carling et al., (1991) utilised customised installation of six OTT current meters on a single wading rod. Thompson et al., (1999) performed velocity and discharge measurement across multiple riffle-pool sequences.	0.02 ms^{-1} +/- 2% for Marsh-McBirney Propeller Meter (Thompson et al., 1999).	o Robust. o Simple. o Adaptable. o Portable. o Cheap.	o Cannot make surface flow measurements. o Time consuming. o Requires entry into the channel. o Limited in deep / high flow conditions. o Equipment malfunctions in high sediment flows. o Eulerian and predetermined. o Only 1-Dimensional Measurement.
	ECMs	A streamline epoxy modelled sensor head features two electrodes. Movement of water past the sensor head causes electric potential which is processed to provide a digitized velocity.	Clifford (1993b) made high-frequency velocity measurements using an array of electromagnetic current meters in the study of differential bed sedimentology and the maintenance of riffle-pool sequences.	Valeport Model 808: velocities ranging between 0 - 5 ms^{-1} with an accuracy of 1% +/- 0.005 ms^{-1} Marsh-McBirney Flowmate; range of 0 - 6 ms^{-1} at an accuracy of +/- 2% + 0.015 ms^{-1}	o Measures flow direction. o Does not suffer inertia effects. o Robust. o Simplified user interface (doesn't require accurate flow orientation).	o Instrument noise / electromagnetic interference. o Poor in aerated flows. o Requires entry into the channel. o Limited in deep / high flow conditions. o Eulerian and predetermined. o Only 2-Dimensional Measurement.
NON INVASIVE	**ADCP**	ADCPs measure the Doppler shift of emitted acoustic signals reflected by suspended matter (sediment, biological matter, bubbles) in the water.	Kostaschuk et al., (2004) performed ADCP measurements in the Fraser River estuary and Lilloet Lake.	According to Lane et al., (1999) ADCP are usually set up for accuracy better than +/- 1.0 cms^{-1} in currents around 1 ms^{-1}.	o Simultaneous flow and sediment measurements. o Increased time-effectiveness. o ADCPs make three-dimensional velocity measurements.	o Cannot measure top 0.25 m of flow. o Poor at making measurement in channels with large channel floor roughness. o Cannot provide point velocity values. o Eulerian and predetermined.

APPROACHES	**ADV**	ADV differs from ADCP by providing high frequency three-dimension point velocity values from very small volumes of flow away from the sensor head.	Maa and Kwon (2007) highlighted how ADVs have been used to measure both the current velocity and the suspended sediment concentration in natural river environments.	Hosseini et al., (2006) quoted accuracies of +/- 2.5 mm/s +/- 1%.	o Instantaneous three dimensional point velocities. o Small volume of flow. o Detached from sensing element. o High frequency measurements.	o Indirect method since measure particles not flow. o Changes in density of fluid effect velocity measurements. o Increasing sediment concentrations effect velocity measurements.
	PIV / PTV	PIV is a velocity calculation technique that measures movement of areas of flow over known time periods utilising time lapse photography (Ettema et al., 1997). PTV differs from PIV by measuring the movement of individual particles as opposed to areas of flow.			o Make rapid repeated measurement. o Non-invasive. o Measurements at full range of flow conditions. o Can measure heavily sedimented flows. o Provides flow direction. o Surface flow velocities. o Lagrangian. o Natural selected flow path.	o Amount and uniformity of particle seeding. o Insufficient natural / available light (precludes using PIV / PTV in the majority of natural environments). o Poor in bad weather conditions.
	LSPIV	LSPIV is an image based technique that measures the displacement of floating fluid particles between successive digital images.	Costa et al., (2000) LSPIV for surface velocity measurement at the River Skagit, Washington. Fox et al., (2008) investigated the use of LSPIV to make measurements of macro scale turbulence features using the resultant surface velocity fields.	LSPIV measurement of surface flow velocities were underestimated by 0.7 ms^{-1} on average Jodeau et al., (2008) Velocities measured below 0.2ms^{-1} were removed from collected results Fox et al., 2008.		
	SURFACE	The term drifter buoy	Shipping and weather	Ohlmann et al., (2005)	o Autonomous.	o May not be suitable for

	DRIFTERS	refers to any (often custom designed) floating platform upon which a series of environmental sensors can be mounted to collect and either store and / or transmit data.	forecasts and international climate investigations such as the Surface Velocity Programme (SVP) and the World Ocean Circulation Experiment (WOCE) (Data Buoy Cooperation Panel. 2005). Johnson et al., (2003) utilised customised surface drifters for the measurement of flow irregularities in the near-shore zone.	Intermittent GPS Positioning = 4.06m SD Johnson et al., (2003) Continuous GPS Positioning = 1.3m E and 1.6m N Water following capability: 0.32 cms^{-1} at low velocities and 1.72 cm^{-1} higher velocities Ohlmann et al., (2005)	o Flexible / Adaptable. o Lagrangian. o Robust. o Cost efficient. o Free from user error. o Non-invasive. o Easily deployable. o Deployable in the full range of flow conditions.	application to natural river environments. o Size. o Positioning (GPS performance). o Buoyancy. o Only measures surface flow velocities.

Table 2.0 Summary table reviewing both invasive (propeller meters and ECMs) and non-invasive (ADCPs, ADVs, PIV / PTV, LSPIV and surface drifters) flow measurement methods.

2.1.1 Invasive Approaches

2.1.1.2 Propeller Meters

One of the most important tools for the measurement of velocity in natural river environments is the propeller meter. A propeller meter is a mechanical device which comprises a precisely calibrated rotating impeller blade attached to an electronic unit which converts the number of propeller rotations over specified time periods into point velocity values (Figure 2.1).

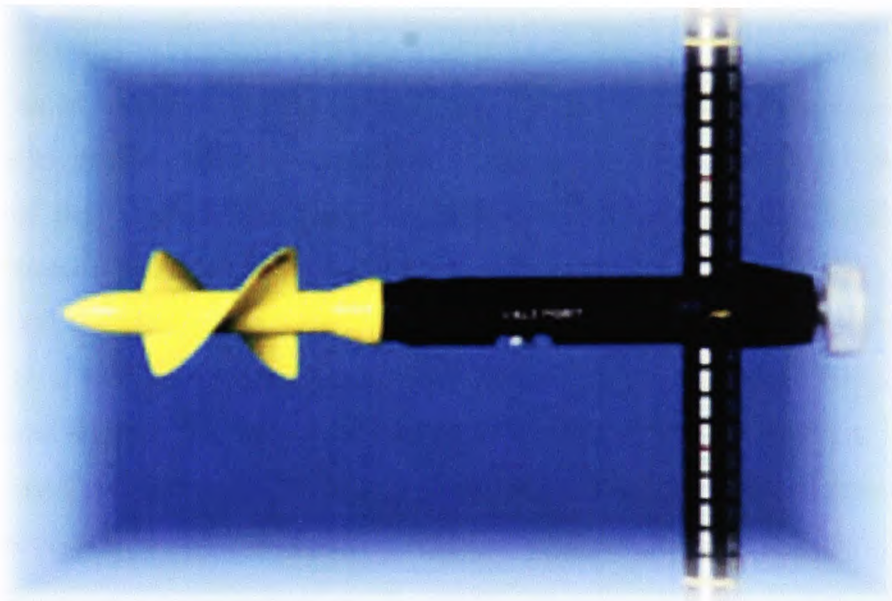

Figure 2.1 Valeport 001 "Braystoke" Propeller Flow Meter (Valeport, 2009)

The majority of commercially available propeller meters are designed for flow measurement in combination with hand-held wading rods, cabling or scaffolding installations from a bridge or from a boat (OTT 2006). Examples of the simplest propeller meter deployments were presented by Wolman (1958). Wolman (1958) used propeller meters for the investigation of Brandywine Creek, Pennsylvania by conducting measurements by wading into the channel or in higher discharge conditions from channel spanning bridges. Thompson et al., (1999) conducted similar flow measurements using a single propeller meter from a small inflatable raft.

Carling (1991) opted for a customised installation featuring an array of six OTT current meters equally spaced over the lower 0.5m of a 1m wading rod which was lowered into the channel from a boat. Raising and lowering the installation provided a complete profile through the entire water column, Ferguson et al., (1989) utilised similar installations to Carling (1991) performing flow measurements using arrays of three or four mechanical current meters with 5 cm impellers on a single wading rod. Particularly prominent to this work are the investigations of the velocity reversal hypothesis conducted by Carling (1991) and Thompson et al., (1999) who both performed velocity and discharge measurements across multiple riffle-pool sequences at a variety of flow conditions using propeller meters.

A description of measurement procedures and achievable accuracies in the use of propeller meters for flow measurements is provided by Thompson et al., (1999). Thompson et al., (1999) used a single Marsh-McBirney propeller meter to measure 30s averaged velocities in North Saint Vrain Creek, Rocky Mountain National Park, for the investigation of sediment sorting patterns and the velocity reversal hypothesis. Five point velocity profiles were constructed from measurements at 20%, 40%, 60%, 80% and 95% of flow depths. Measured velocities were then used to produce five cross-sections spaced at 3m intervals across a pool-riffle sequence. According to Thompson et al., (1999) the sampling error for the Marsh-McBirney propeller meter is approximately 0.02 ms^{-1} +/- 2% of the measurement reading. The accuracy of specific propeller meters will however depend on the manufacturer, unit calibration, environment, sampling procedure used and user error, the Marsh-McBirney (2008) figures are representative of the magnitude of achievable accuracy.

Propeller meters provide a robust, reliable and relatively cheap option for the measurement of velocities and discharges in natural gravel-bed river systems. Propeller meters also benefit from being portable, flexible in application and relatively accurate.

Propeller meters cannot however be used to measure surface velocities or velocities near the channel bed or banks (depth is limited by the dimensions of the impellor blades, approximately 5cm). Similarly, propeller meters do not allow for the measurement of flow direction, simply providing a detached value with only a magnitude. Propeller meter measurements are also time-consuming both in terms of set-up time, if complex installations are to be used or movement is required between consecutive measurements in different areas of the channel and in allowing sufficient time for the averaging of individual velocity measurements. The use of propeller meters is also limited in high discharge conditions where entry into the channel is restricted due to flow speed / depth requiring alternative applications such as from a boat or bridge. The need for an alternative deployment strategy can then be further limiting in terms of time and cost. These limitations restrict the range of flow conditions that can be investigated leaving significant gaps in the understanding of flow patterns. Carling (1991) also found that at the highest discharges equipment frequently malfunctioned limiting the collection of velocity results. Ferguson et al., (1989) found that in flows with large amounts of sediment, impellor blades or bearings became clogged and rotations restricted thereby falsifying results. Similar difficulties would arise if propeller meters were to be utilised in highly vegetated channels. All propeller meter measurements are also limited by the fact that they are Eulerian in nature, presenting point velocity values both spatially and temporally detached from the dynamic nature of river flow. Furthermore, the majority of velocity measurements are arbitrary since the path of data acquisition is predetermined prior to investigation returning results that are further detached from the dynamic nature of river flows.

2.1.1.3 Electromagnetic Current Meters (ECMs)

Electromagnetic current meters (ECMs) have allowed major progress to be made in the understanding of flow dynamics in a variety of fluvial environments (Lane et al., 1998, Wang et al., 2007). They have the advantage of measuring in more than one orthogonal direction and therefore do not need accurate orientation. ECMs also lack the inertial limitations of comparable mechanical current meters and therefore have been increasingly utilised to measure flow velocities in rapidly fluctuating, turbulent gravel-bed rivers (Lane et al., 1998). MacVicar et al., (2007) further detailed that no evidence had been found of ECM failure with increasing velocities and turbulence, demonstrating their suitability for flow measurement in upland river environments.

The basic construction of an ECM (Sensa) was described by Robert (1997). The meter uses an electromagnetic sensor housed in a streamlined epoxy moulding. Movement of water past the sensor head causes an electric potential in the water which is detected by two electrodes; this is then transmitted to the display unit where the signal is processed to provide a digitized velocity (Figure 2.2).

The operation of ECMs is based on Faraday's 1831 law of electromagnetic induction. Faraday stated that when an electrical conducting fluid moves through a magnetic field, the induced voltage is proportional to the velocity of the fluid (Lane et al., 1998, MacVicar et al., 2007, Wang et al., 2007).

Figure 2.2 Valeport 801 Electromagnetic Open Channel Flow Meter (Valeport, 2009)

Lamarre et al., (2005) collected 65 velocity profiles using ECMs mounted on a vertical wading rod to characterize turbulent flow characteristics. According to Lamarre et al, (2005) ECMs were utilised since they are designed to measure simultaneously the stream wise and vertical velocity components. Markham et al., (1992) similarly collected both long stream and cross-channel velocity data using two-component ECMs. Measurements were made exclusively from channel spanning bridges to ensure that data could be collected irrespective of discharge and channel flow conditions.

Lane et al., (1999) identified two commercial manufacturers of ECMs (Colnbrook / Valeport and Marsh McBirney) in widespread use for studies of turbulence and sediment transport in shallow river environments. According to Valeport (2009) the Model 808 ECM can measure velocities ranging between 0 - 5 ms^{-1} with an accuracy of 1% +/- 0.005 ms^{-1} whereas the Marsh-McBirney Flowmate has a range of 0 - 6 ms^{-1} at an accuracy of +/- 2% + 0.015 ms^{-1} (Marsh-McBirney, 2008). Fulford (2001) performed an independent validation of the accuracy and consistency of water-current measurement techniques and found that a Marsh-McBirney ECM (2000-model) returned measurements mostly within the manufacturers accuracy specifications but performed less well at and below velocities of 0.15 ms^{-1}.

The use of ECM has allowed for considerable progress in the study of natural fluid dynamics and the local short-term relationships between flow and sediment transport (Lane et al., 1998). ECMs measure in more than one orthogonal direction, allowing flow directions to be calculated. Furthermore, unlike instruments with moving parts (e.g. propeller meters) ECM do not suffer form inertial effects which produces inaccuracies in the measurement of rapidly fluctuating velocities characteristic of turbulent flow conditions (Kanwisher and Lawson in Lane et al., 1998). This further highlights that the relative robustness of the ECM makes it particularly suited to monitoring velocities in turbulence flows with sediment transport. Lane et al., (1998) also concluded that ECM velocities are likely to be more reliable than propeller meter measurements due to simplified user interface (reduced need for correct sensor head alignment).

The use of ECM for flow measurement in open channels is however not without limitation. According to Lane et al., (1998) instrument noise / electromagnetic interferences occur in the measurement of flow velocities. Particularly problematic is instrument noise that is reproduced at frequencies comparable to fluctuation in the flow being measured. Although these errors can be removed through low pass filtering it becomes necessary to sample at twice the output filter frequency. Lane et al., (1998) warns that if the sampling frequency is less than twice the output frequency then aliasing will occur within the record and that sampling at twice the output filter frequency, extreme caution must be exhibited in the interpretation of the time series records themselves.

According to Hemp (2001) the need for accurate calibration of ECMs adds considerably to instrument costs. MacVicar et al., (2007) considered that although voltage measurements need to be calibrated to water velocity, these are sometimes prone to zero drift. Most modern ECM utilise dc (direct current) excitation which allows the flow meter to read signal noise between pulses and therefore continuously establishes zero and eliminate zero drift.

Sensor head shape and electrode spacing are also important to the performance of ECMs for flow velocity measurements. According to Lane et al., (1993) a discoidal sensor head shape is preferable to cylindrical models since its shape is more hydrodynamically efficient, limiting the development of micro scale turbulence around the instrument itself. The difference in sensor head shape will, in most cases, determine the positioning and spacing of the electrodes. This is important since any flow fluctuation that is of a smaller wavelength than the electrode spacing will be undetectable. Therefore, just as there is a temporal control on the ECM sensitivity due to the effects of the electronic design, there is also a spatial control through sensor head shape and the electrode separation effect (Lane et al., 1998).

Additional problems can arise with the use of ECM in highly aerated flows since electrodes cannot distinguish air bubbles within fluid flows and therefore return artificially elevated velocity measurements. The electrodes themselves are also prone to coating from fine sediment, and metallic deposits within the channel which disrupts electromagnetic conduction.

Furthermore, ECMs suffer from difficulties similar to those observed with the use of other invasive measurement methods. ECMs require user entry into the channel or sensor deployment from channel-spanning bridges. This results in many locations and flow conditions remaining immeasurable. Finally, ECM cannot measure genuine surface flow conditions due to the design and dimensions of the instrument and instrument components.

2.1.1.4 Summary of Invasive Measurement Methods

The term invasive flow measurement method refers to any instrument / approach that requires direct or indirect entry into the channel, of either the operator or the equipment itself. Two types of equipment are outlined here; a mechanical propeller meter and an electromagnetic current meter; both types of apparatus are commercially available and present unique groups of advantages and disadvantages. As previously described, propeller meters either require the operator to wade into the channel or for the apparatus to be lowered into the flow from scaffolding installation or from bridges or boats. Similarly, ECMs are principally utilised on wading rods or scaffolding rigs again through the operator entering the channel or from banks and bridges. Invasive approaches have the advantages that they are generally robust, reliable and relatively cheap with the added advantages of being portable, flexible in application and relative accurate.

The use of invasive methods is however limited in high flow conditions where entry into the channel is restricted due to flow speed / depth requiring alternative applications such as from a boat or bridge. The need for an alternative deployment strategy can then be further limiting in terms of time and cost. These limitations restrict the range of flow conditions that can be investigated leaving significant gaps in available data and therefore the current understandings of flow patterns. Additionally, invasive methods are also time-consuming both in terms of set-up and equipment arrangement (if complex installations are to be used or movement is required between consecutive measurements in different areas of the channel and in allowing sufficient time for the averaging of individual velocity measurements.)

Neither propeller meters nor ECM can be utilised to measure surface velocities or velocities near the channel bed or banks. Propeller meters are further limited by the inability to record flow direction therefore providing a detached value with only a magnitude. Additional problems were outlined in the use of propeller meters at higher discharge (Carling, 1991) and in sediment laden flows (Ferguson et al., 1989). The use of ECMs removes several of these limitations. ECMs can also measure in more than one orthogonal direction, allowing flow direction to be calculated. Similarly, as previously described the accuracy of ECMs does not deteriorate in high velocity, turbulent (except for highly aerated flows) and highly sedimented flows. ECMs also benefit from having a more simplified user interface which according to Lane et al., (1998) is likely to produce more accurate velocity measurements.

Ultimately however, all invasive methods are limited by the fact that they are Eulerian in nature, presenting point velocity values both spatially and temporally detached from the dynamic nature of river flow. Furthermore, the majority of velocity measurements are arbitrary since the path of data acquisition is predetermined prior to investigation returning results that are further detached from the dynamic nature of river flows.

2.1.2 Non-Invasive Approaches

2.1.2.1 Acoustic Measurement Techniques

Kostaschuk et al., (2004) and MacVicar et al., (2007) highlighted that the increased demand for the measurement of flow velocities is critical for understanding the dynamics of flow in rivers where mean and turbulent quantities play important roles. As a result, acoustic non-intrusive instruments using the Doppler Effect have become increasingly popular for velocity measurements in both laboratory and field conditions (Kostaschuk et al., 2004).

There are two prominent forms of Acoustic Doppler measurement techniques; acoustic Doppler current profilers provide mean velocity measurements at specified spatial and temporal positions through virtually the entire water column and acoustic Doppler velocimetry which provides instantaneous three-dimensional point velocity measurements.

2.1.2.2 Acoustic Doppler Current Profilers (ADCPs)

An ADCP system requires the combination of an acoustic Doppler profiler, a laptop computer, and a platform / vessel for mounting the instrumentation. The type of acoustic Doppler current profiler and deployment strategy depends on the characteristics of the river being measured. For deployment in a small river, the ADCP can be mounted in the bottom of a small raft or on a pulley system whilst deployment in a large river would require the ADCP to be suspended in the water column from a larger floating vessel or boat (Yorke and Obeng, 2002). Examples of these two types of deployment are shown in Figure 2.3.

ADCPs measure the Doppler shift of acoustic signals emitted from the transducer face and then reflected by suspended matter (sediment, biological matter, bubbles) in the water. The Doppler principle states that if a source of sound is moving relative to the receiver, the frequency of the sound at the receiver is shifted from the transmitting frequency. Therefore assuming that the echo-producing targets have the same velocity as the water, the instrument computes a weighted mean velocity from the distribution of reflected pulses (Shields and Rigby, 2005).

The receiver echoes are range-gated to produce successive segments along the axis of the acoustic beam, called depth cells or bins, which are processed independently returning individual temporally and spatially, averaged mean velocities. These calculations are performed by grouping together echoes from given depths based on the speed of sound in water (Muste and Spasojevic, 2004).

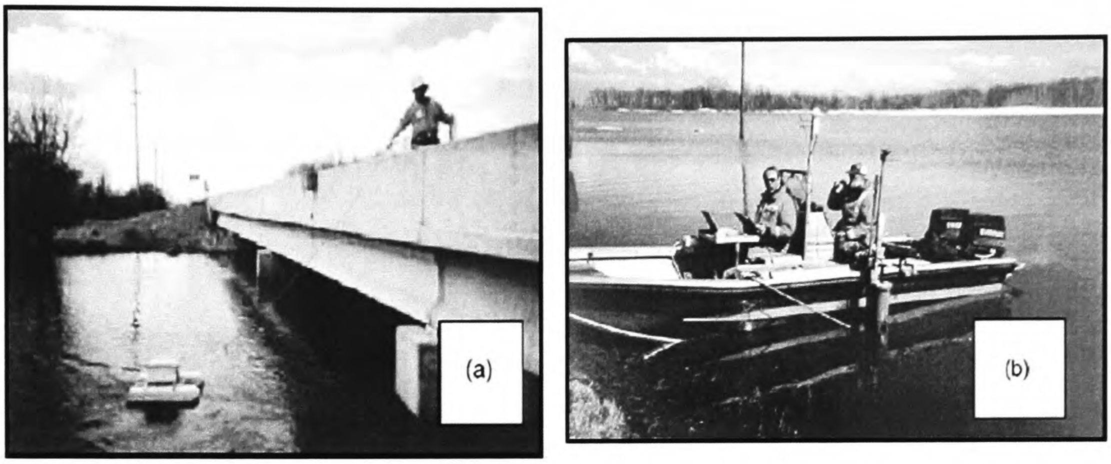

Figure 2.3 Photographs showing acoustic Doppler profilers deployed on a small catamaran (a) and a power boat (b). Yorke and Obeng, 2002.

ADCPs measure velocities in the water column relative to the vessel to which they are attached. Therefore, if the vessel moves, its velocity relative to the channel bed needs to be measured to calculate the actual water velocity. The most popular procedure for measuring boat translation velocity is bottom-tracking, which determines the relative velocity between vessel and river bed using long acoustic pulses (Muste and Spasojevic, 2004). This is achieved through the measurement of an ensemble of water pings and bottom-tracking pings interleaved during transmission (Yorke and Obeng, 2002).

According to Kostaschuk et al., (2004) acoustic Doppler current profilers are now widely used for measuring fluid velocity in geophysical flows (e.g. Admiraal and Demissie, 1996; Wewtzer et al., 1999; Best et al., 2002). Kostaschuk et al., (2004) performed ADCP measurements in the Fraser River estuary and Lilloet Lake.

ADCPs have been increasingly used for measurements in shallower waters, such as rivers. Muste and Spasojevic (2004) described how multiple velocity measurements can be obtained in rivers as shallow as 1 m from moving vessels improving the speed of measurements and allowing measurements where conventional methods are expensive or impractical. According to Lane et al., (1999) ADCP is usually set up for accuracy better than +/- 1.0 cms^{-1} in currents around 1 ms^{-1}.

According to Muste and Spasojevic (2004) acoustic instruments using Doppler Effects have become increasingly popular for velocity measurements in both laboratory and field conditions. ADCPs offer many advantages over traditional point current meters; firstly, an ADCP is a single instrument that can be used for simultaneous flow and sediment measurements. Secondly, ADCPs have increased time-effectiveness allowing flow measurements at sites where the use of conventional meters is expensive or impractical. Thirdly, ADCPs make three-dimensional velocity measurements through virtually the whole depth of the water column (Kostaschuk et al., 2004).

Acoustic Doppler profilers do however have some limitations for measuring flow velocities; they cannot be used to make measurements near the water surface, the bed or river banks (Yorke and Obeng, 2002). Shields and Rigby, (2005) also concedes these limitations when stating that the ADCP used in this study cannot measure velocity in the top 0.25 m of flow. This occurs because there is a vertical distance from the transducer face in which no velocity measurements are made since insufficient time is allowed for vibrations in the profiler transducer to be damped out immediately following pulse transmission (referred to as the blanking distance) (Yorke and Obeng, 2002). Describing the same limitation, Muste et al., 2005 explains this process as ringing errors affecting velocity measurement near the free surface whilst considering that the blanking distance varies with ADCP design and frequency.

The river and channel characteristics also affect the performance of ADCPs. A river with a deep centre and shallower sides may pose problems for measuring with a single system because the optimal frequency and configuration of the internal parameters of the profilers will be different for the deep and shallow parts of the channel (Yorke and Oberg, 2002).

The uncertainty of measurements is also affected by the degree of turbulent fluctuations present in the particular river reach being measured. Rivers with a large part of the sediment load transported as bed load, or having high sediment concentrations near the bed pose other problems since these will falsify the measurement of particle velocities and therefore the measured water velocities.

Nystrom et al., (2002) additionally notes that ADCPs cannot resolve velocity fields into instantaneous point values since velocities produced by ADCPs are temporal and spatial averages over finite domains. Considering increased ADCP usage and the persistent technical limitations, Muste et al., (2004) discussed the need for further analysis of the ADCP measurements conducted from moving and stationary vessels to assess the relationship between the flow and ADCP operational parameters, in order to accurately capture mean and turbulent characteristics in river environments. (Muste et al., 2004).

2.1.2.3 Acoustic Doppler Velocimetry (ADV)

The principal of acoustic Doppler velocimetry (ADV) has been used for some time to monitor three-dimensional velocities in laboratory flumes and more recently in natural river systems (e.g. Richardson et al., 1996). The acoustic Doppler velocimeter (ADV) offers accuracy of laboratory devices even under field conditions providing unobstructed three-dimensional flow measurements at high sampling rates and with a small sample volume (Lohrmann et al., 1994).

A typical ADV system incorporates a probe head mounted on a long stem attached by a flexible cable to the signal conditioning module. This module contains analogue electronics, which detect and amplify acoustic signals and is connected to a digital signal processor (which controls the ADV system) by a shield cable (McLelland and Nicholas, 2000).

ADVs utilise the Doppler frequency shift of emitted acoustic signals after reflection by small sound scattering particles in the flow. The frequency of the shift is proportional to the particle velocity (Voulgaris and Trowbridge, 1997; Lane et al., 1999). Assuming that the particles are small enough to be neutrally buoyant, there movement can be assumed to be equal to the speed of the flow. ADVs use a technique known as pulse-to-pulse coherent Doppler sonar for measuring the velocity vector. The phase shift between successive backscattered signals sampled at each receiver is converted to a measurement of velocity along each beam (Hosseini et al., 2006). Instruments are calibrated to sample as quickly as possible to increase the precision of the estimate since the larger the number of samples used to determine the mean velocity the more precise the estimate will be (Lane et al., 1999).

Maa and Kwon (2007) highlighted how ADVs have been used to measure both the velocity and the suspended sediment concentration in natural river environments. According to Hosseini et al., (2006) following mythological comparisons, ADVs have replaced traditional methods such as ECMs, propeller meters, hot film and hot wire for the measurement of instanteous velocities. Analysing the use of ADV sensors to measure mean velocity within natural river channels, Volugaris and Trowbridge (1997) found that mean velocity can be estimated to within 1% of the true velocities value whilst Hosseini et al., (2006) quoted accuracies of +/- 2.5 mm/s +/- 1%. MacVicar et al., (2007) considering the simulated flow series performed by Garcia et al., (2005) developed curves for ADV performance under a range of flow conditions, finding that ADV will generally underestimate signal variance when turbulence is high during sampling procedures.

ADVs are vital for flow measurement in turbulence studies providing a robust and portable instrument that has great potential for small-scale, intensive investigations of the interaction between river channel form and flow processes (Lane et al., 1998). According to Hosseini et al., (2006) an important advantage of the ADV is its ability to measure the flow in a small sampling volume (approximately 0.25 cm^3) that is located 5-10 cm away from the sensing element. Lane et al., (1998) further highlighted that ADVs can measure instantaneous three-dimensional point velocity measurements. Voulgaris and Trowbridge (1997) add that although the probe must be inserted within the flow, the fact that the sensing volume is several centimetres away from all physical parts of the probe mean that the presence of the device does not disturb the flow that is being measured.

Hosseini et al. (2006) described three limitations when utilising ADVs for velocity measurement. The first is that ADVs measure the velocity of acoustic targets but not the fluid velocities themselves and are therefore indirect measurements. In flows with highly varied sediment composition this may result in flow velocities being subjected to additional uncertainties. Secondly, the spatial changes in the density of fluid throughout the channel will change the speed of sound through the respective area of flow. Thirdly, when sediment concentrations increase, emitted acoustic waves are absorbed by sediment laden flows and attenuated.

MacVicar et al., (2007) highlights additional difficulties, specifically that raw ADV signals are often contaminated by electronic errors and Doppler noise / interference. Furthermore, acoustic reflections can become contaminated by air bubbles in highly turbulent fluids (Rodriguez et al., 1999) and aliasing of the return signal above the Nyquist frequency (Goring and Nikora, 2002).

2.1.2.4 Particle Imaging Techniques

Particle imaging techniques are a member of a broader class of velocity measurement methods that determine the motion of marked regions of a fluid. By observing the location of areas flow (and flow markers) at two or more times, velocities can then be established from known time-steps between recorded images (Adrian, 1991). One group of particle-imaging techniques is classified as pulsed-light velocimetry (PLV) of which particle-tracking velocity (PTV) and particle-image velocimetry (PIV) are two prominent types.

PIV is a velocity calculation method that measures the movement of specified areas of flow (interrogation areas) over known time periods (Ettema et al., 1997). Establishing interrogation areas involves the seeding of an illuminated flow region with visible particles (either artificially or naturally present within the channel) to facilitate the recording of a sequence of images of particle motion (Creutin et al., 2003). These particles must scatter light effectively, be small but visible and be approximately neutrally buoyant so that they can accurately follow flow (Tait et al., 1996). An image analysis algorithm is then used to determine the displacement of the surface tracers between successive frames with velocities computed by dividing these displacements with the time interval between frames. An entire vector field is obtained by repeating the PIV analysis over a grid encompassing the flow field image (Creutin et al., 2003).

PTV (particle-tracking velocity) differs from PIV since velocity calculations are made based on the displacement of individual particles as opposed to areas of flow. As a result, the flow must be seeded with a small enough number of particles so that individual particles or particle streaks can be determined as a function of time (Holland et al., 2001).

A typical commercially available PLV package comprises a PC, PIV and control software, programmable timing-unit (PTU), camera / recording device, particles, particle-dispenser and source of illumination. The PTU is provided by a customised PC that specifies a precise time management for triggering pulses of light for illumination and the recording of flow images (Figure 2.4). To control the capture process and the analysis of images, customised software packages are provided by manufactures and often include algorithms for both PIV and PTV measurements.

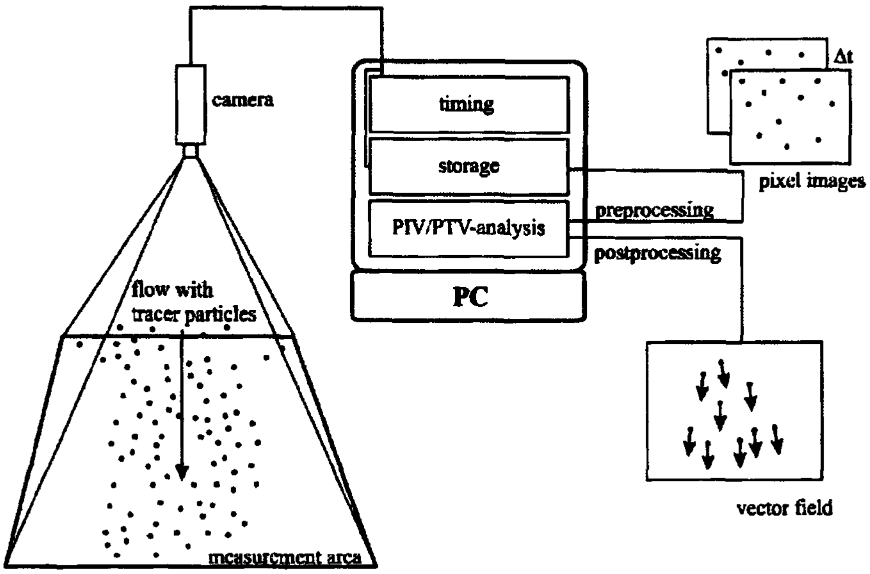

Figure 2.4 Schematic sketch of a PIV system (Weitbrecht et al., 2002).

The essential aspect of any PTV / PIV method is the image analysis algorithm, used to determine the displacements of the surface tracers between successive video frames (Ettema et al., 1997). While PTV algorithms attempt to track the movement of every particle (up to 16000 particles per frame for most commercially available systems) PIV utilises a parabolic fitting to establish the deviation between consecutive interrogation areas based on previous knowledge of persistent flow conditions.

The most common form of PIV image analysis algorithm utilises central difference interrogation of multiple, single exposed frames. The algorithm finds the correlation between the interrogation area (IA) – specific feature present within the flow field - centred on a point (a ij) in the image recorded at time (t), and the IA centred at point b ij in the image recorded at time t + *d*t (Figure 2.5). The correlation coefficient R (a ij, b ij) is a similarity index for images enclosed in the two compared IAs through the creation of a search area (SA) calculated from prior knowledge of the direction and magnitude of mean flow conditions. The correlation coefficient is then applied to the IA (a ij) to establish the most likely location of IA (b ij). Velocity vectors can then be derived from these displacements by dividing them by *dt*,, the time between successive frames (Creutin et al., 2003).

Figure 2.5 depict flow patterns on two successive video frames separated by a time interval *dt*. The interrogation area (solid square) defines the size of the flow area taken into account to identify the displacements. The search area (dotted square) defines the area that is investigated for possible displacements. The arrow from a ij to b ij represents the identified displacement.

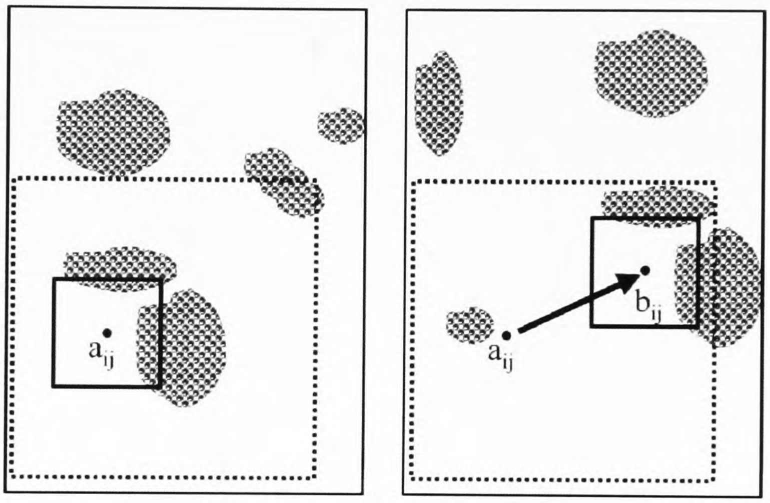

Figure 2.5 Sketch taken from Creutin et al., (2003) illustrating the algorithm used to identify the flow tracer displacement.

2.1.2.5 Large Scale Particle Image Velocimetry (LSPIV)

LSPIV differs from standard PIV and PTV approaches in both scale and technical set-up. LSPIV is an image-based technique that provides surface velocity measurement for open-channel research applications. Velocities are obtained by measuring the displacement of floating fluid-markers between successive digital images (Fox et al., 2008). The use of LSPIV is now widespread in the water resources community to facilitate investigations of surface flow velocities in both laboratory and field environments.

The majority of LSPIV applications utilise natural light for illumination and observations of surface flow features and / or deviations. The use of natural light however limits flow investigation to surface flows as opposed to the full flow field measurements possible with artificially illuminated PIV approaches. In high flow conditions, the increased abundance of surface debris and turbulence driven, aerated flow features such as boils or ripples can be utilised as natural references for image analysis (Jodeau et al., 2008). In the absence of sufficient surface material, artificial seeding can again be utilised as with traditional PIV techniques.

One of the simplest approaches was utilised by Ergenzinger et al., (1996) who released groups of florescent ping-pong balls into a natural gravel-bed river in Squaw Creek, Missouri, to act as marker buoys to monitor surface flow patterns. Measurements of deviation in position were conducted using paired cameras to record the marker's progress downstream.

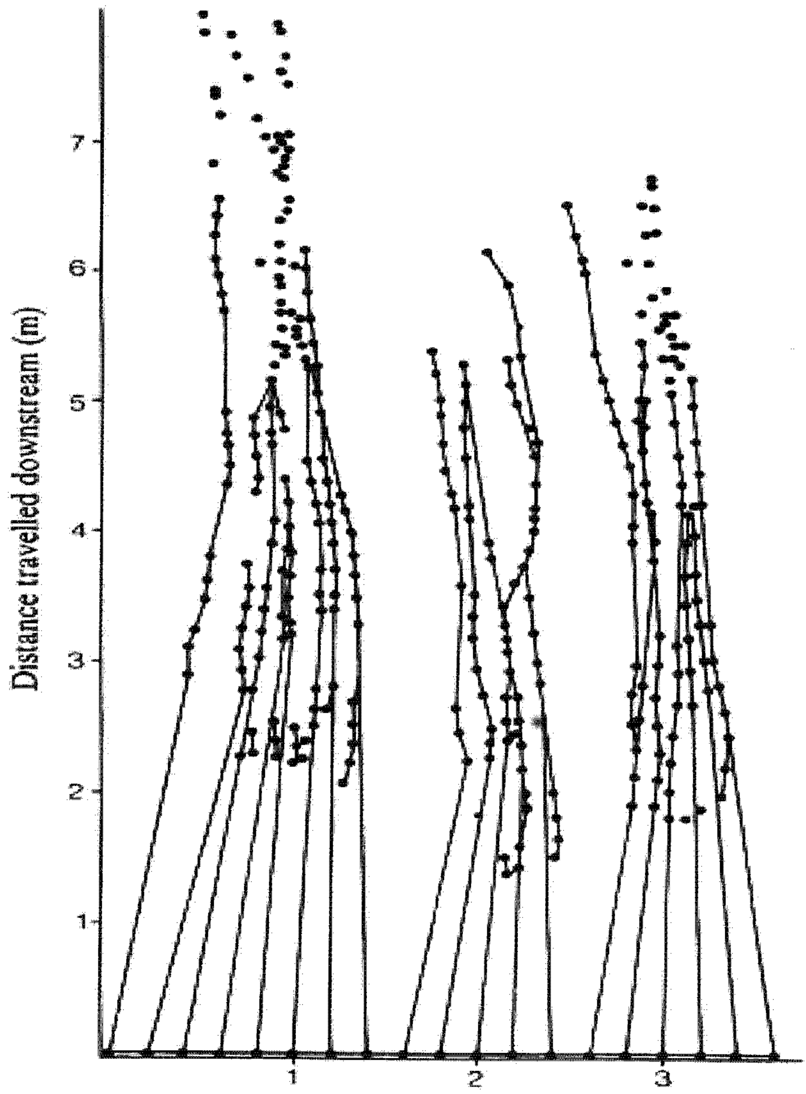

Figure 2.6 Distribution pattern of ping-pong balls utilised to monitor surface flow dynamics (Ergenzinger et al., 1996).

All LSPIV installations require the mounting of a digital video camera on a raised platform or mast to provide a sufficiently large field of view. Specified Ground Reference Points (GRP) are also required to rectify collected images and perform geometrical corrections to pictures. An example installation schematic is provided by Jodeau et al., (2008). Jodeau et al., (2008) utilised an artificial seeding device to supply the flow with Ecofoam chips, water soluble, foam filled material created from cornstarch (Figure 2.7).

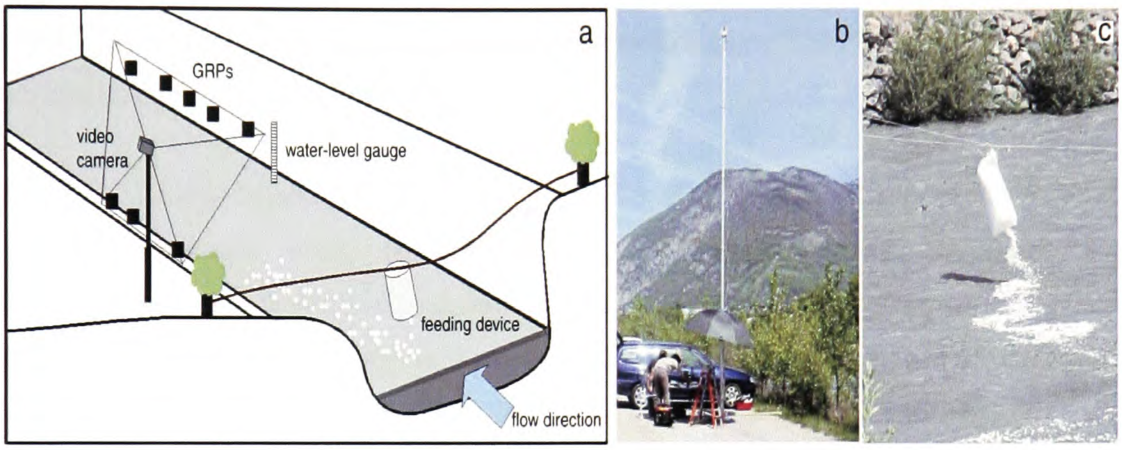

Figure 2.7 (a) Diagram of LS-PIV installations: mast, video camera and view field. Ground Reference Points (GRPs), tracer feeding device and water level gauge. (b) Photograph of the mobile lightweight telescopic mast. (c) Picture of the feeding device providing seeding material to the channel (Jodeau et al., 2008).

Following image collection, a standard central difference interrogation method was utilised, which as previously described calculates the correlation between the interrogation area (IA) centred on a point a ij in the first image and the IA centred on a point b ij in the second image recorded with a time interval of *dt*. Utilising the correlation coefficient (calculated as described previously) it is assumed that the most probable displacement of the fluid from point a ij during period *dt* is the one corresponding to the maximum correlation coefficient. Jodeau et al., (2008) specified an interrogation area of 2 x 2 m^2 as small enough to preserve the scale of interest and large enough to encompass recognisable tracer patterns (Figure 2.8). According to Jodeau et al., (2008) LSPIV measurement of surface flow velocities were underestimated by 0.7 ms^{-1} on average for the majority of the sequence through discharges ranging from 10 m^3s^{-1} to 150 m^3s^{-1}.

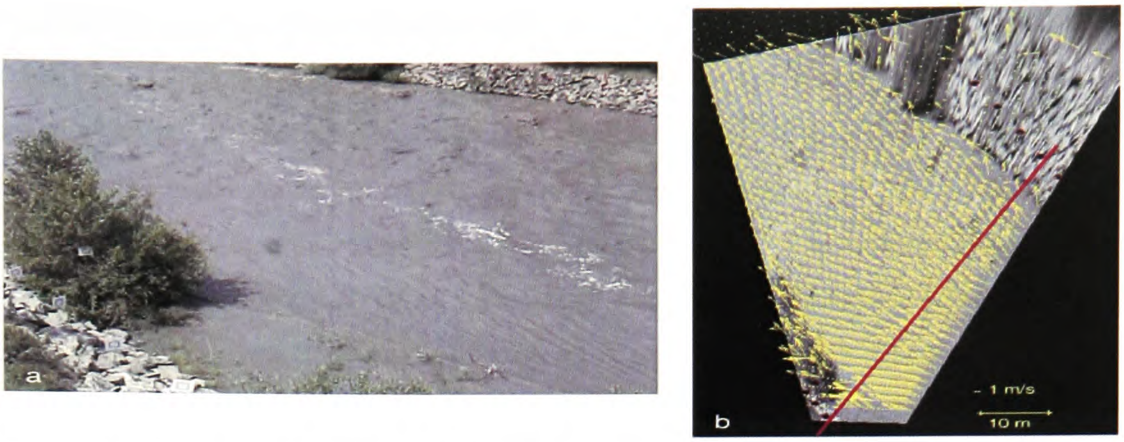

Figure 2.8 Typical flow images before and after rectification. LSPIV time-averaged surface velocity fields (Jodeau et al., 2008).

Fox et al., (2008) investigated the use of LSPIV to make measurements of macro scale turbulence features using the resultant surface velocity fields. Based on the identification of areas of faster and slower velocity in the data, the stream wise length of the large-scale eddies was approximated utilising specified time steps. Feature length was measured as the distance from the frontal edge of a fast velocity region to the backside extent of the slow velocity area, and the approximation of this technique is shown in Figure 2.9. Fox et al., (2008) utilised a number of techniques to remove inaccuracies from the LSPIV results to ensure surface feature could be measured. Data points were removed if agglomeration or inadequate tracer particles occurred in the image area. Post-processing removed images where poor light resulted in unreasonable low velocities and all velocities below a boundary tolerance (0.2 ms^{-1}) were removed. This resulted in losses of around 15% of each series of images.

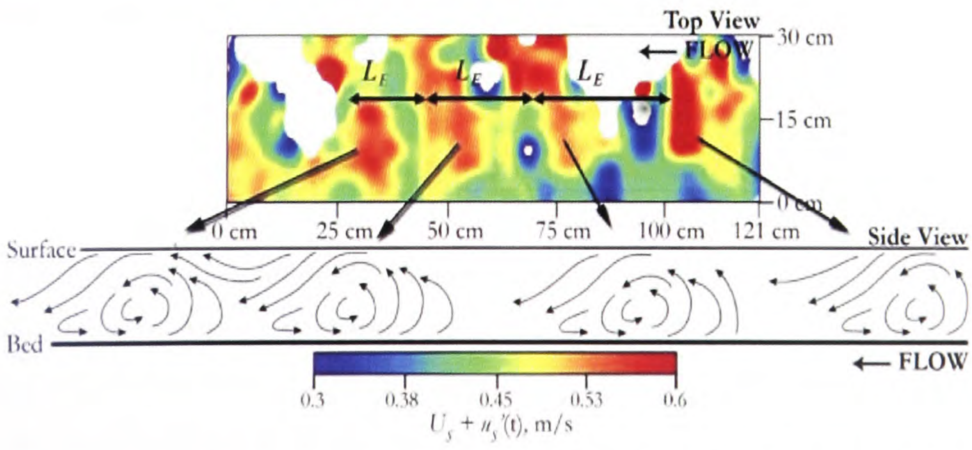

Figure 2.9 Description sketch of how the decomposed LSPIV data was used to approximate the length of large-scale eddies that are manifested at the free-surface (Fox et al., 2008).

As described previously, the potential exists to utilise natural "tracers" such as foams or other surface disturbances (waves, ripples or boils) at the free surface as reference material to allow velocity measurements. Muste et al., (2005) investigated the use of concentric surface waves as natural flow tracers (though artificially generated in this case). This technique is classified as Controlled Surface Wave Image Velocimetry (CSWIV) and sits aside LSPIV as a technique potentially suitable for application in a variety of natural river systems. The waves were generated by a fan directed towards the channel free surface and were scaled to be large enough to be distinguishable in video recordings and small enough to have negligible influence on the channel flow being measured (Muste et al., 2005). According to Muste et al., (2005) the potential of the CSWIC concept is proven by the "good agreement" between CSWIV measurements and those obtained with alternative experimental means (LSPIV).

2.1.2.6 Summary of Non-Invasive Measurement Methods

Non-intrusive velocity measurements are required when natural conditions do not permit the use of conventional techniques (Jodeau et al., 2008). A solution to these difficulties potentially lies in the use of LSPIV for surface velocity measurement which was first tested successfully by Costa et al., (2000) at the River Skagit, Washington. According to Creutin et al., (2003) the clear advantage of the approach, as seen during the Iowa River experiments, was the ability to make repeated measurements quickly. Additionally, Muste et al., (2005) highlighted that non-intrusive LSPIV has the advantage of performing measurements during bankfull conditions in a gravel-bed river, which typically are not wadeable under such conditions. Velocity measurements can also be made in heavily sediment laden flows which could cause equipment malfunction if ADCP or propeller meter measurements were attempted (Muste et al., 2005). The intrinsic advantages of both PIV and LSPIV approaches are that entry into the channel is not required for the performance of measurements, increasing the speed of the procedure and providing improved safety in addition to allowing measurements in a wider range of flow conditions and river environments. Fox et al., (2008) consider an extension of existing techniques by utilising LSPIV to measure length scales associated with macroturbulence in open channels. It however remains to be established whether other velocity measurement techniques could be utilised to make similar measurement of surface flow structures.

The unique advantage of PIV and LSPIV techniques are the ability to measure surface flow velocities, particularly in shallow water flows, as demonstrated by Weitbrecht et al., (2002) and Jodeau et al., (2007). According to Weitbrecht et al., (2002) shallow water phenomena can be found in river flows where the dominant processes are two-dimensional necessitating the need for genuine surface velocity measurements which can be provided by increasingly accurate "off the shelf" PIV packages. Additionally, the surface velocities measured by LSPIV and PIV techniques are not predetermined by sampling procedure and are therefore independently representative of flow in each specified area of the channel.

The use of PIV and LSPIV is not however without difficulties; according to Ettema et al., (1997) the main problems of applying PIV to natural river environments are the amount and uniformity of particle seeding and adequate lighting needed to create a useable set of grey-level images. Ettema et al., (1997) further discusses the difficulties associated with supplying an adequately large amount of seeding material to ensure that each interrogation area in the flow field contains enough visible particles.

Weibrecht et al., (2002) extends discussion of seeding difficulties to problems observed with homogeneity of particle seeding on the water surface and a tendency of most floating particles to agglomerate leading to a distorted particle distribution. Creutin et al., (2003) evaluated the limitations of spatial coverage when seeding flow, drawing particular attention to the difficulties associated with areas close to channel banks. As a results of these difficulties Creutin et al., (2003) warns that PIV algorithms do not compute velocities close to channel boundaries (a distance comparable to half the interrogation area size). According to Jodeau et al., (2008) estimation of surface velocities with limited tracers were underestimated by 0.7 ms^{-1} while large areas of flow can remain without calculated velocities.

The use of natural properties of flow as potential flow tracers has previously been discussed, however Fox et al., (2008) considers that further investigation is required to determine whether such natural tracers could be consistently utilised in other natural environments. This is principally due to the fact that in high flow conditions, although increased turbulence and aerated flow areas provide optical reference points, the resultant hydraulic jumps and stationary waves can adversely affects the representation of surface flow instabilities through elevated water surfaces and deviations in reflected light patterns (Jodeau et al., 2008).

In terms of adequate lighting, Creutin et al., (2003) considers that shadows and reflections from obstacles on or around the channel banks can introduce motionless patterns which disturb subsequent PIV calculations. Additionally, PIV in natural environments becomes increasingly difficult in adverse weather conditions where grey-scale contrasts, due to reflections within the river surface, make the identification of flow displacements almost impossible resulting in the loss of almost 50% of grid results (Creutin et al., 2003). Lighting issues can be addressed with additional artificial sources of light or by the use of appropriate camera filters (Creutin et al., 2003). However this introduces additional complexity, time and cost to the experimental procedure.

An additional problem arises with the use of image interpretation techniques. The majority of techniques use a probabilistic approach to determine particle displacements raising the potential of producing spurious velocity vectors. Though various post-processing routines are utilised to check for such vectors, additional investigation is required to validate these approaches relative to different river environments and how corrections would relate to insufficient / flawed seeding or lighting difficulties.

2.1.3 Drifter Buoy Technology

The term drifter buoy refers to any (often custom designed) floating platform upon which a series of environmental sensors can be mounted to collect and either store and / or transmit data. In existing literature the term has been utilised to include apparatus ranging from simple foam floats requiring visual recognition to highly complex, computerised data collection and relay platforms. The leading commercial manufacturer of surface drifter buoys, Clearwater, defines their surface drifters as sophisticated microprocessor-controlled oceanographic data collection instruments (Clearwater, 2007).

One of the simplest forms of surface drifter buoys featured cruciform buoys combining two perpendicular interlocking plexiglass plates with a 2m fibre-glass tip and a large triangular flag (for improved visibility) to investigate particulate transfer at the River

Rhone Plume (Naudin et al., 1997). The floating buoy was balanced using four polystyrene cubes attached to each upper corner of the plexiglass plates. This unique design allowed for rapid adjustment to floating depths whilst minimizing the effect of wind on the drifter and reducing the amplitude of buoy movements due to turbulence and waves (Figure 2.10).

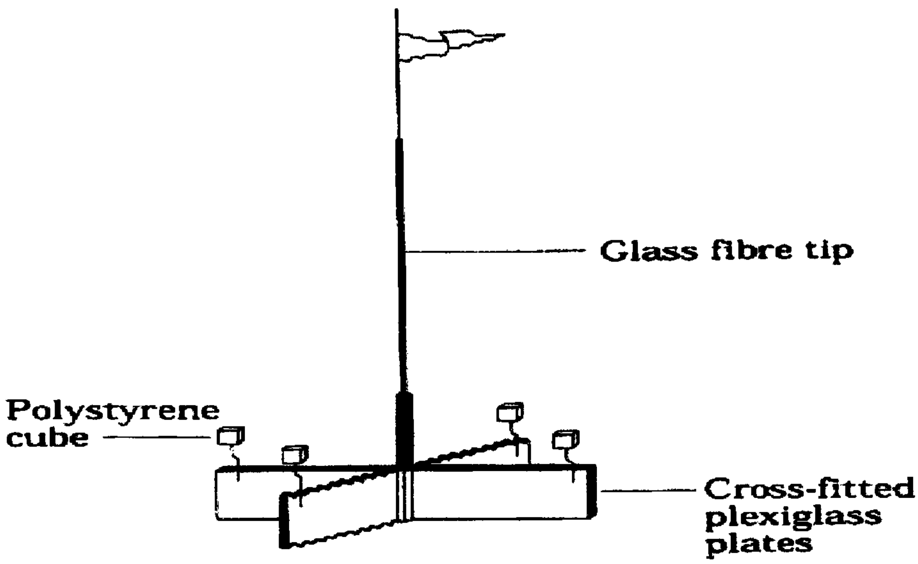

Figure 2.10 Schematic of the design of the drifter buoy utilised in the Rhone River (Naudin et al., 1997).

These drifters had no additional sensors meaning that after release they were followed using a motorboat with positions assessed visually and movements plotted relative to previous positions. According to Naudin et al., (1997) the drifter behaved in a similar manner to pieces of debris floating on the water thereby replicating the surface flow patterns. This simple cruciform design was however not ideal since it was noted that many anomalous results occurred (divergent and varied drifter flow patterns) due to highly varied discharges and wind surges affecting the integrity of drifter paths.

The use of simple floating drifters provided a unique approach for monitoring individual flow patterns at specific locations such as a river inlet or estuary but is limited in terms of requiring human interaction to monitor movements and deviations in positions. As described by Naudin et al., (1997) simplified surface drifters, particular of this type, suffer from difficulties associated with wind surges and responses to highly changeable discharges. To overcome these difficulties and allow investigations of larger environments and flow patterns more robust and technologically advanced drifters are required.

The largest worldwide user of surface drifters is the Global Drifter Program (GDP); a joint venture by the National Oceanic & Atmospheric Administration and the Atlantic Oceanographic & Meteorological Laboratory. The GDP recognises five commercial manufactures of surface drifter buoys – Clearwater (California, USA), Marlin-Yug Ltd (Sevastopol, Ukraine), Pacific Gyre (California, USA), Technocean (California, USA), Metocean (Canada) - each of which offers a variety of surface drifters engineered to meet specific remote sensing requirements (GDP Website, 2009). The majority of surface drifters are based around a universal design structure and component arrangement with customised alterations made to make each unit suitable for its specified purpose. Each drifter comprises a surface float (often spherical) tethered to a drogue that insures horizontal stability. The surface float houses all electrical components - a microprocessor that controls the collection and transmission of data from the incorporated environmental sensors, the power supply and an integrated antenna to transmit data to relay satellites. The environmental sensors contained within each unit are selected based upon the intended use of drifters however these most commonly include a thermistor for sea surface temperature, a barometer to measure pressure and sensors to measure salinity, irradiance and wind speed (Figure 2.11 and Figure 2.12).

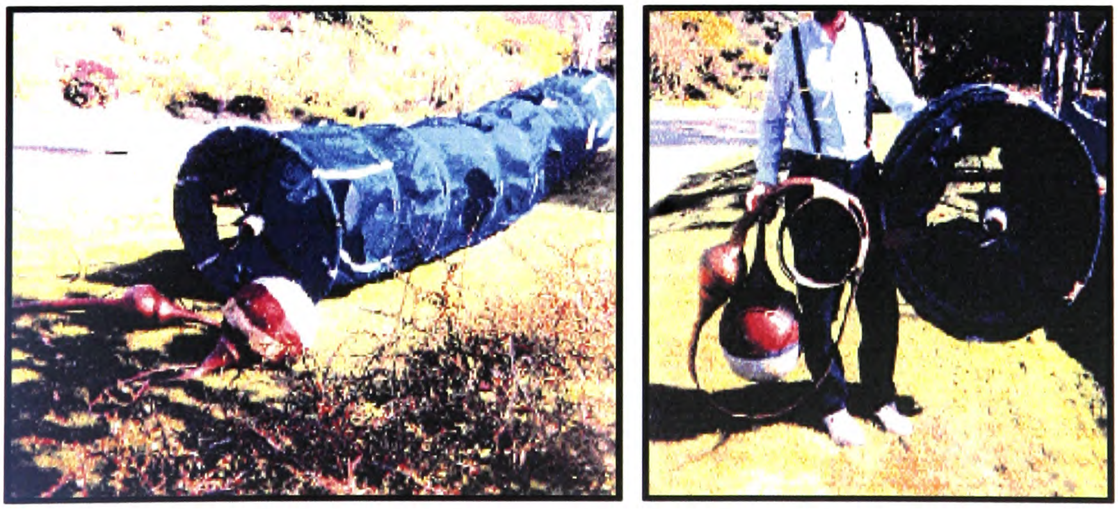

Figure 2.11 Photograph of Clearsat 15 GLD including drogue arrangement (Meteo 2009).

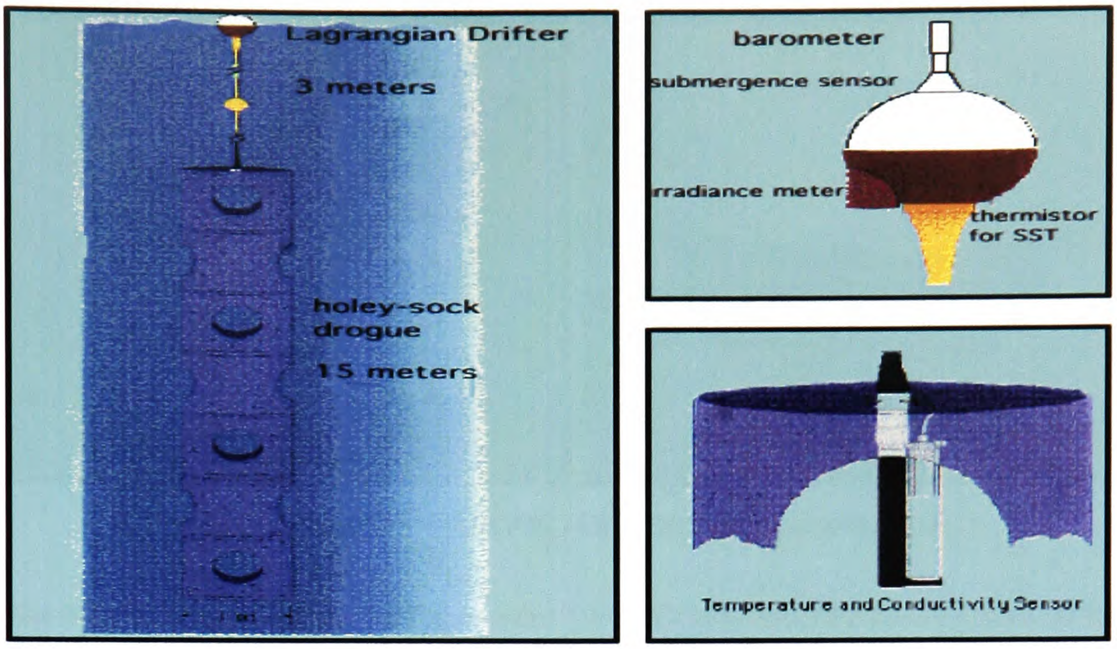

Figure 2.12 Schematic of Clearsat 15 GLD including drogue arrangement. (Meteo 2009).

The positioning element and data relay system within the majority of older surface drifters is provided by the ARGOS satellite system. This system utilises the Doppler Effect for position recognition to accuracies of 150-1000 metres, which is considered acceptable when dealing with entire oceans and seas (Grudlingh, 1998). The ARGOS system has the advantages that its components are small, relatively cheap and have an extremely low energy consumption allowing for the operational lives of surface drifters to extend to several year at intermittent operational periods (Clearwater, 2007).

Increasingly, GPS receivers are incorporated into surface drifter buoys to increase the accuracy with which positions can be measured, flow paths can be identified and velocity calculations can be made. This approach has been adopted in some form by virtually all commercial manufactures. Clearwater (Clearwater, 2007) provides commercially available drifter buoys built strictly to the specifications of the World Ocean Circulation Experiment (WOCE) and recently extended their available models to include the WOCE/GPS unit. The WOCE/GPS incorporates all the features of the standard spherical buoys carrying sea surface temperature sensors and indicators of submergence but with the addition of the GPS to allow significantly improved positioning (Figure 2.13).

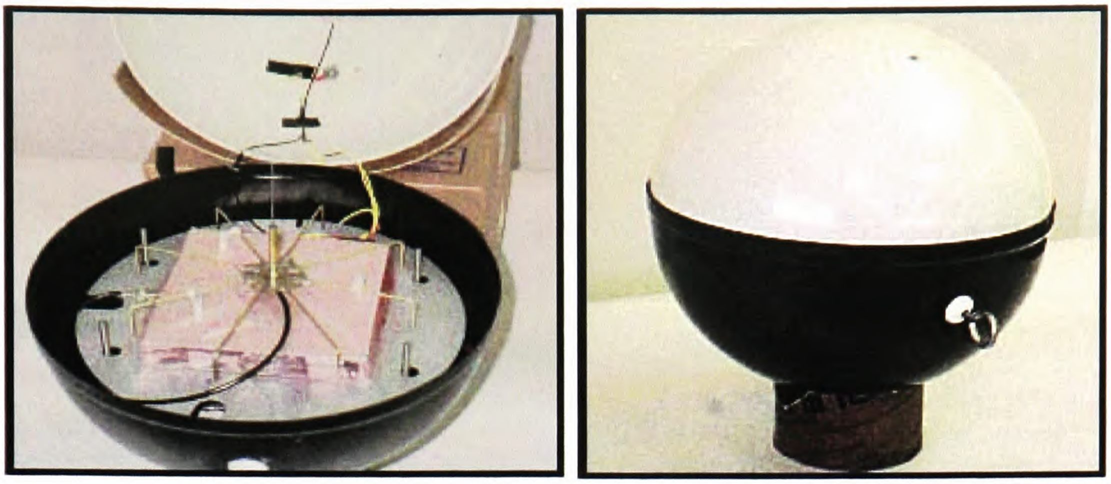

Figure 2.13 ClearSat-15 ARGOS / GPS Drifter (Clearwater, 2007).

The World Ocean Circulation Experiment (WOCE) was initially a component of the World Climate Research Program (WCRP) aimed at establishing the role of the oceans in the earth's climate and to obtain a baseline dataset against which future climatic change could be assessed. Sophisticated numerical ocean models were supplemented with extensive surface drifter datasets provided by the global drifter programme to facilitate the interpretation of observations and for the prediction of the future ocean conditions (WOCE website 2007). There are currently over 1200 Global Lagrangian Drifters deployed in the oceans and seas of the globe with the majority of these recording and transmitting data to the Global Drifter Centre (Miami - USA) (Figure 2.15) for the National Oceanic & Atmospheric Administration (NOAA) and the Atlantic Oceanographic & Meteorological Laboratory (AOML) (Figure 2.14).

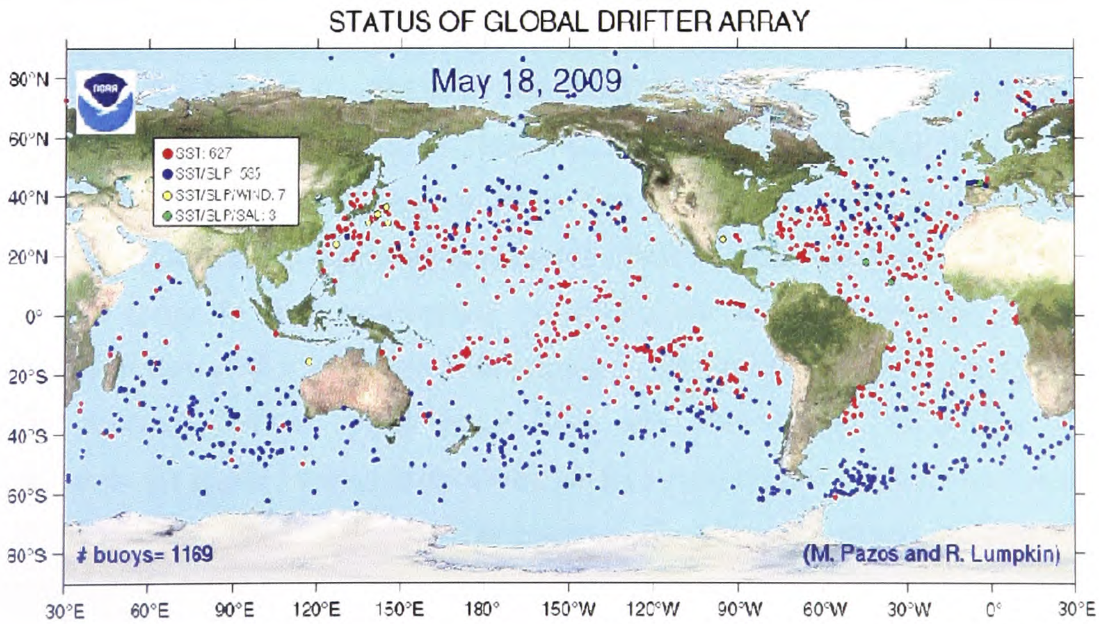

Figure 2.14 Status of Global Drifter Array - May 18 2009 (GDP, 2009).

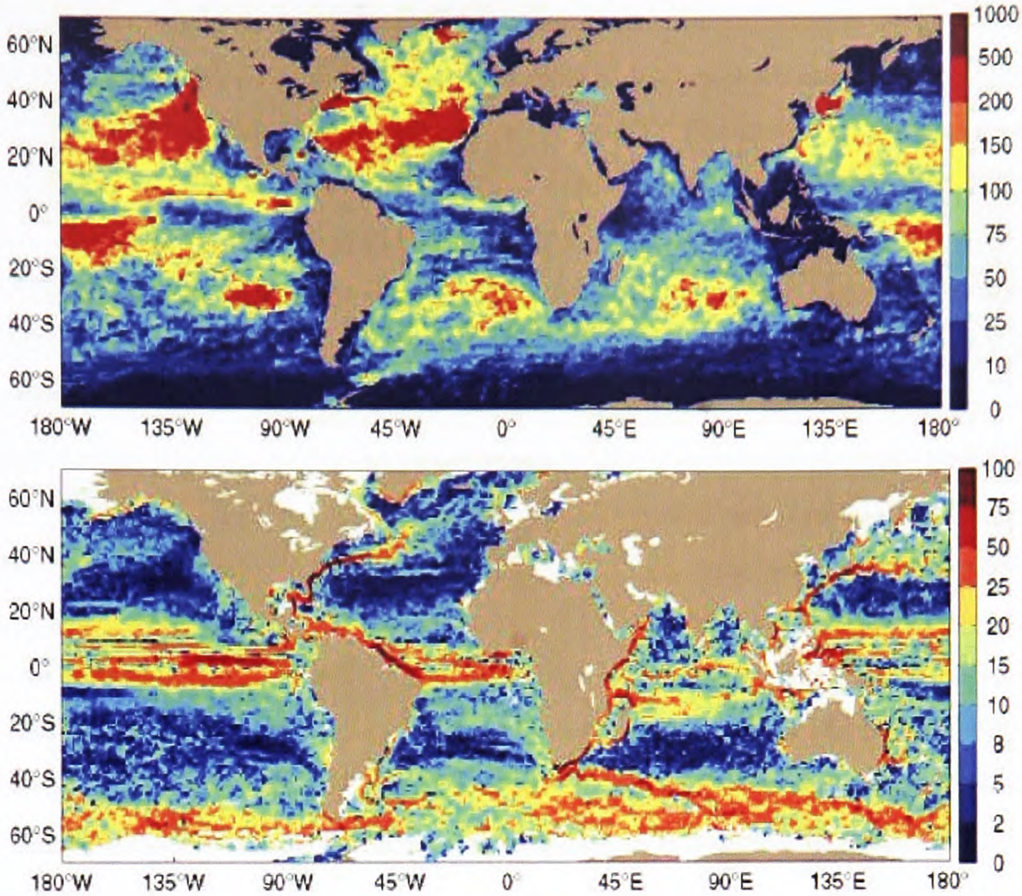

Figure 2.15 The figure is taken from the Global Drifter Buoy Centre (2005) and shows the density of drifter observations (top) and time-averaged surface currents (bottom) taken from current GLDB deployments.

In addition to their fundamental role in world-wide meteorological and climatological investigations, commercially available surface drifters are now widely utilised in a more specific academic research. Grudlingh (1998), Bogard et al., (1999), Grodsky et al., (2002) and Jakobsen et al., (2003) all utilised standard ARGOS drifters to investigate surface flow patterns off the coast of Namibia, in the Equatorial Atlantic Cold Tongue, in the northern North Atlantic and the North East Pacific respectively. Bushnell (1998) and Tseng et al., (2002) both adapted standard ARGOS surface drifters to include GPS receivers (prior to their commercial availability) to achieve increased positional accuracy in their studies of surface flow patterns in the vicinity of Taiwan and the North Brazil Current. Surface drifter buoys have also been utilised to produce flow simulations for applied management strategies for environmental hazards and disasters, such as chemical or oil spills, and the presence of underwater mines and explosives (Roland et al., 1998).

The manner with which drifter flow investigations are conducted is as diverse as their global distribution. Several of the most extensive studies were conducted by Bograd et al., (1999), Barth (2003) and Jakobsen et al., (2002). The investigation of near surface circulation patterns in the North East Pacific by Bograd et al., (1999) was based upon positions and velocities characterizing surface flow conditions over a five year period provided by 100 individual drifter trajectories. Results were taken at 10 randomly allocated time points throughout each 24 hour period with drifters utilizing alternative periods of 24 hours activity and 48 hours of inactivity. The utilised drifters had an approximate life span of one year before replacement was required. Barth's (2003) work on the southern advection of the Northern California Current also comprised five years of drifter data with individual tracks spanning April to June, with each drifter providing positional fixes between 9 and 12 times daily. In the investigation of near-surface currents in the northern North Atlantic, Jakobsen et al., (2002) used 387 units providing 81000 drifter tracks with each track spanning a minimum of 30 days. Tseng et al., (2002) utilised only two GPS customized drifters to investigate the surface flow patterns in the vicinity of Taiwan. Positions were reported at 30 minute intervals for twenty days by the first drifter and fifty three days by the second. Bushnell (1998) utilized similarly adapted drifters but based his research upon the results from four units.

The range of different sampling strategies utilised throughout these investigations highlights the potential applications and flexibility of drifter approaches and their ability to return informative results from a wide variety of environments and conditions. The selection of appropriate surface drifters combined with suitable sampling strategies ensures that it is possible to structure approaches to meet the demands of virtually all investigations and environments.

2.1.3.1 Adaptations and Developments

In recent years the use of surface drifters has been extended to cover the investigation of lakes, estuaries and the surf-zone. Deployment in such environments has required both structural and technical alterations to currently available drifter designs. Ohlmann et al., (2005) developed a customised drifter for observing small spatial and temporal scales of motion in the coastal zone off Santa Barbara, California. The new style drifter again comprises a spherical surface hull (housing electronic components) and subsurface drogue to ensure vertical stability and the integrity of water following capabilities. The size of each component has been reduced allowing for use in a wider variety of flow conditions and environments and improving transportability for ease of deployment and recovery. Additionally, a corner-radar-reflector drogue was used since it was collapsible to conserve space in transport. The need to observe smaller scale movements / flow patterns has also necessitated the incorporation of GPS receivers within each drifter since this dramatically improves positioning accuracy and recently the size of internal components. Ohlmann et al., (2005) integrated a combined GPS receiver and cellular phone to provide data recording and transmission potential. The use of a cellular phone based GPS further allows for reduced drifter dimensions since GPS, data logger and power source are contained within a single unit. A cellular based GPS drifter allows for data transmission by the Mobitex terrestrial communication system (custom designed telecommunication system designed to process short burst data) which offers rapid, reliable and cheap data relay and recording. Increasing the speed of GPS data collection has the additional advantage of improving the potential of making unit recovery and redeployments which makes the approach more cost efficient (Ohlmann et al., 2005; Manda et al., (2000). The surface drifters described by Ohlmann et al., 2005) are now commercially available through Pacific Gyre Inc as the "Microstar" (Figure 2.16).

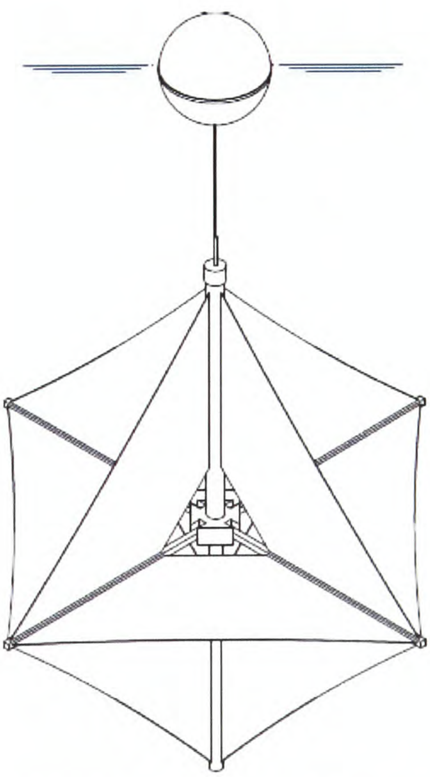

Figure 2.16 Pacific Gyre (2008) Microstar drifter.

The accuracy of surface drifters for the measurement of flow velocities requires both the performance of the positioning element (GPS) and water following capability of the drifter itself to be assessed. Manda et al., (2002) attempted a combined assessment method by comparing drifter-derived velocities with those measured by an ADCP mounted on the seabed. Though theoretically possible, the method failed since the pressure gauge present on the ADCP malfunctioned and failed to provide accurate depth assessments meaning the near surface flow velocities could not be measured accurately. Manda et al., (2002) also highlighted that difficulties often emerge when direct comparisons are attempted between Lagrangian (drifter) and Eulerian (ADCP) velocities. Ultimately however, utilising estimated tidal depths, it was determined that the drifter-derived velocity is consistent with the velocity profile of the ADCP. Manda et al., (2002) however concluded that is would be better to assess the slip of water past the drifter itself utilising current meters attached the drogue of the drifter.

Ohlmann et al., (2005) measured both the accuracy of GPS positioning and drifter slip. Utilising 14 stationary drifters, recording positions intermittently for 48 hours, returned 269 positions per unit and provided a standard deviation in positioning from the mean of 4.06 m. A single drifter was then combined with a pair of current meters to assess the slip of flow around the drifter, the measurement of positive or negative flow values would represent deviation from the true flow velocity. During a 20 minute lake deployment, intended to assess the ability of the drifters to measure near-zero velocities, slip was found to be on average 0.32 cms^{-1} with 0.1 cms^{-1} attributable to instrument noise. A second set of deployments, in notably rougher waters and at higher winds occurred 5 km off the coast of Santa Barbara and returned an average slip of 1.72 cm^{-1}.

Extensive research has also been conducted by the University of Western Australia using customised surface drifters for the measurement of flow irregularities and rip tides in the near-shore zone. Johnson et al., (2003) describes the construction of a small, simple, low-cost surface drifter. Based on the universal structure of a surface float (housing all electronic components) and subsurface drogue (adapted dependent upon selected environment) these drifters are constructed using low cost components. The exterior casing of Johnson et al's (2003) drifters are provided by 100-mm PVC sewage pipe whilst the positioning element was provided by standard marine GPS units (Garmin GPS 36 receiver) wired directly to DGPS-XM data loggers through an RS232 connection (providing, positions, times and dates at upon 1 Hz). Data are recorded internally to a capacity of 95200 data points equivalent to 26 hours continuous operation with battery power for 40 hours of continuous operation. (Johnson et al., 2003) (Figure 2.17).

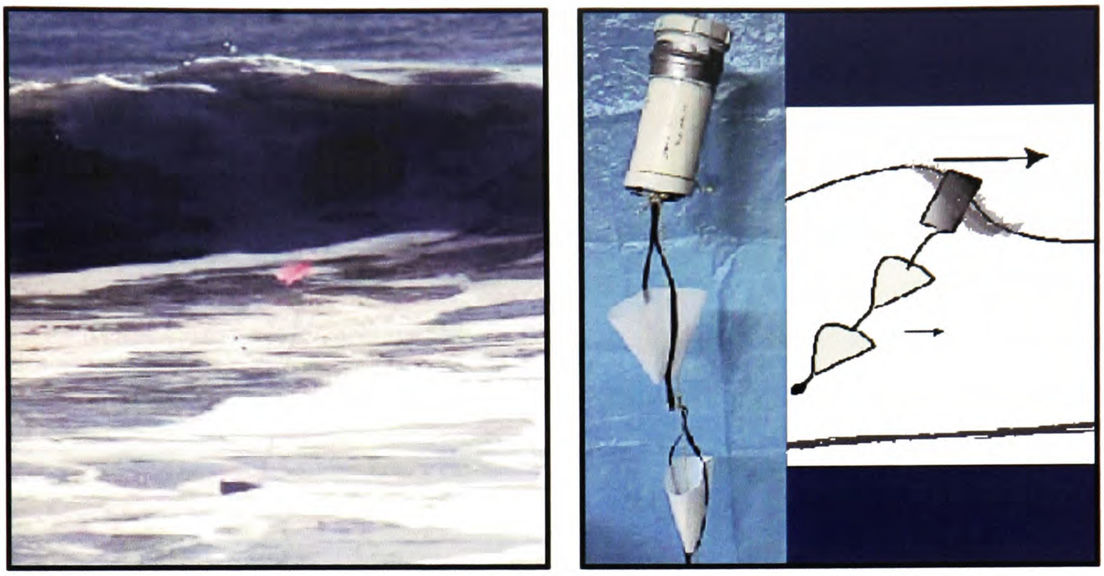

Figure 2.17 Initial trials, construction and schematics of the University of Western Australia's surf zone drifters (Johnson and Pattiaratchi, 2004).

When utilised in the surf-zone Johnson et al., (2003) fitted the drifters with a parachute-type drogue arrangement. Upon the initiation of movement the drogue opens and dramatically increases drag when there is a difference between velocity in the upper and lower part of the water column, the parachute drogue also stabilizes the drifter and prevents it from rolling or surfing in breaking waves. To aid recovery and allow redeployment, the floats were equipped with a two-stage waterproof radio transmitter (25 mm by 15 mm). A direction-finding antenna fixes the location of the drifter to within 100 m, within which a visible fix can be established (the drifters were also painted fluorescent orange to improve visibility). According to Johnson et al., (2003) the telemetry systems for 6 drifters costs below $1500 and allows for a retrieval time of approximately 3 hours for the 6 drifters.

Johnson et al., (2003) considered the performance of the drifters describing that they performed well in rip-current experiments, following the fast offshore flow resolving large circular motions in the rip head (eddies). Additionally, despite the drifters being completely submerged occasionally, the data acquisition rate remained 99% successful with data gaps rarely exceeding 10 s.

The environment into which Johnson et al., (2003) surf-zone drifters were deployed prohibited the assessment of their water following capabilities, since there were no directly comparable surface flow measurement methods. As a result of this inability to perform such comparisons, only GPS performance assessments were made. Johnson et al., (2003) activated a stationary drifter for 45 minutes to establish the limitations of GPS performance. Results demonstrated standard deviation from the mean position of 1.3 m in the east direction and 1.6 m in the north direction with maximum displacements of 4.2 m and 5.2 m respectively. The difference in the observed performance of GPS positioning in the tests conducted by Ohlmann et al., (2005) and Johnson et al., (2003) can be attributed to the structure of experimentation. Tests were designed to assess drifter performance with respect to the requirements of the intended application environments. Ohlmann et al., (2005) investigated the accuracy of intermittent GPS measurements for use in seas and oceans whilst Johnson et al., (2003) considered the precision of positioning for deployment within the near shore surface-zone.

2.1.3.2 Drifter Summary

The use of drifter buoys is widespread for data acquisition in seas and oceans. It has also been highlighted that drifter buoys can be customised to meet the specific requirements of varied environments and investigations. Structurally; the size, shape and material of the surface housing and subsurface drogue can be changed dependent upon the environment within which the drifter is to be deployed. Additionally, the type of positioning, data recording and transmission equipment must be selected specifically dependent upon the intended deployment environment, investigation specifics and subsequent structural constraints. Moreover, the sampling strategy utilised determines both the structure of data acquisition and the power requirements of the integrated equipment. Through the combination of each of these elements it is possible to construct a drifter suitable for deployment in a wide variety of fluid environments. This fact is highlighted by the development of drifter buoys for use in lakes, estuaries and surf-zone areas.

Johnson et al., (2003) highlighted the potential of constructing low cost drifters from "off-the-shelf" components. The use of customised drifters could therefore reduce the individual unit cost of equipment and therefore field investigation. By selecting suitably small components and adopting a restricted component arrangement it is also possible to reduce the size of equipment which simplifies transportation, further reducing costs and improves the ease of deployment, recovery and potential redeployment.

Drifter buoys have the added advantage that they can be utilised in a variety of flow environments which would be unsuitable for traditional velocity measurement methods. Furthermore, the use of bridges / banks for deployment and recovery would allow measurements in environments which have previous been inaccessible. Drifters can also be used in high velocity and high sediment flows where traditional measurement methods would potentially be compromised. The use of drifter buoys also removes the potential of user error in the performance of measurements since there is no user intervention prior to the processing and interpretation of collected measurements. The accuracy of velocity measurements made using surface drifters is therefore only dependent upon the performance of the GPS or other positioning / velocity measurement devices and cannot be degraded by poor human performance at the point of measurement.

2.2 Riffle-Pool Sequences

2.2.1 Definition and Description

Riffle-pool sequences are common, meso-scale, quasi-regular bedform features present in many upland, low-gradient gravel or mixed bed streams (Leopold et al., 1964; Richards, 1976a and Keller and Florsheim, 1993). Common to all riffle-pool sequences is the oscillation in mean bed elevation along the longitudinal flow profile (Wilkinson et al. 2004); riffles occur as topographic highs (shallows) whilst pools occur as intervening lows (deeps) (Richards, 1976a; Clifford, 1993a, 1993b; Cao et al., 2003, Sawyer et al., (in press) (Figure 2.18).

Figure 2.18 Photograph (by author) of a riffle-pool sequence at the Middle Derwent, UK 2005.

According to Harrison and Keller (2007) the most widely utilised approach to studying pool-riffle sequences has focused on the analysis of hydraulic parameters. Riffles and pools are marked by discharge dependent contrasts in flow velocity, water surface slope, channel morphology and bed sedimentology. Over low to moderate flows riffles are shallower, more divergent, faster zones, with steeper water surface slopes and coarser, better-sorted or more interlocking bed material than intervening pools (Bhowmik, 1982;

Clifford, 1993a, 1993b). According to Cao et al., (2003), reference to hydraulic parameters has most commonly focused on the velocity-reversal hypothesis, following the work of Keller (1971). Additional references pertaining to the velocity reversal hypothesis include Lisle (1979), Carling (1991), Keller and Florsheim (1993), Carling and Wood (1994), Miller (1994), Sear (1996), Thompson et al., (1998, 1999), Booker et al., (2001), Wilkinson et al., (2004), MacWilliams et al., (2006), and Harrison and Keller (2007).

The velocity-reversal hypothesis states that a hierarchical reversal exists in the magnitude of velocity over a riffle-pool sequence that acts to maintain the bed morphology (Harrison and Keller, 2007). At lower discharges, the velocity in the riffle exceeds that in the pool mobilising small bed material from the riffle and depositing it in the adjacent pool. At higher flows (at or above bankfull) the velocity of the pool exceeds that of the riffle creating contrasting periods of scouring in the pool at high flow and fill during low flow (Harrison and Keller, 2007). The existence and operation of the velocity-reversal hypothesis has and continues to attract much debate (Cao et al., 2003).

Riffle-pool sequences and their corresponding surface flow patterns are generally thought to occur periodically; (Wilkinson et al., 2004) being spatially related in the order of five to seven times the channel width (Keller, 1971; Richards, 1976b, 1982; Clifford, 1993) (Figure 2.19) with riffles appearing wider at the majority of flow conditions (Milan et al., 2001).

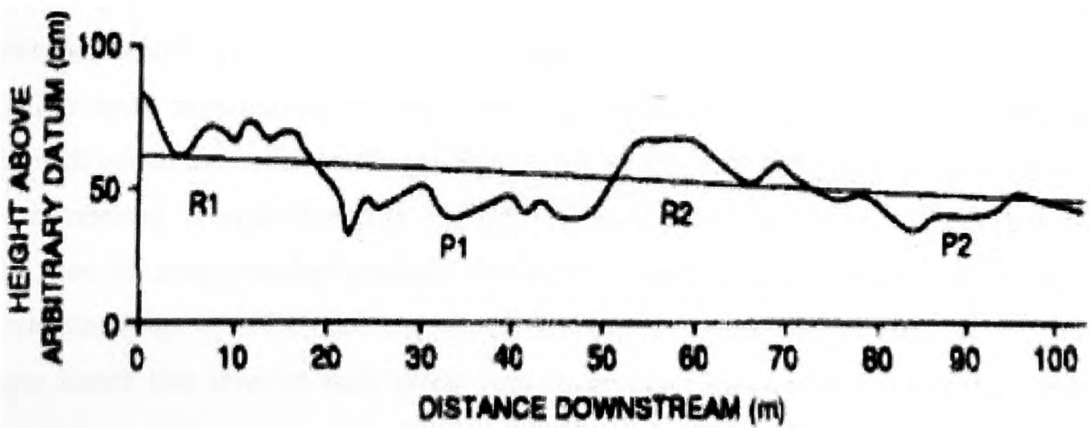

Figure 2.19 Longitudinal bed profile from which riffles can be identified as topographic highs whilst pools occur as intervening lows (Robert, 1997). Vertical exaggeration is 25 times the horizontal distance.

Geomorphologically, riffle-pool sequences feature distinctive sediment composition, with pools generally found to contain finer material, smoother bed surface profiles and more poorly sorted material. Heritage et al., (2004) identified significantly coarser surface armouring on riffles than in consecutive pools whilst Keller (1971), specifying bed roughness as a ratio of particle size to water depth, found that bed roughness was 0.04 for the pool and 0.42 for the riffle. Additionally, Clifford and Richards (1992) considered how riffles possess more structured sediments than pools due to sorting initiated by greater turbulence over riffles (Figure 2.20).

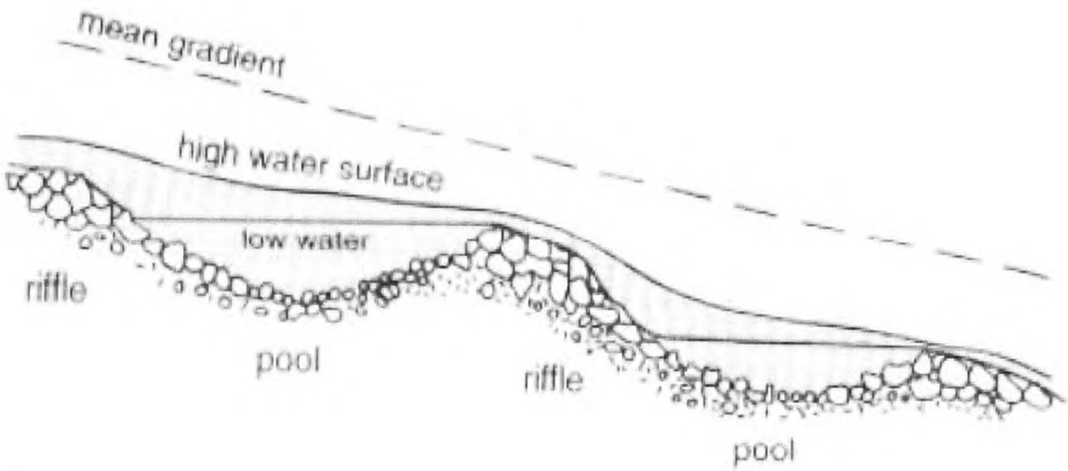

Figure 2.20 Definition sketch showing a riffle-pool sequences relative to the mean channel gradient with the approximate formation of the water surface slope at low and high flows (Knighton, 1998).

As described previously the understanding of large-scale flow dynamics, particular in upland gravel-bed rivers is limited by the inability to perform the required flow measurements (Sawyer et al., in press). These difficulties were considered by Richards (1976) when highlighting the need for closer attention to aspects of flow geometry, through which the understanding of these bedform features (riffle-pool sequences) could be developed. Despite Richards' (1976) observations, Booker et al., (2000) reiterated the need for more detailed spatially distributed hydraulic data, to expand upon current understandings of riffle-pool sequences. The spatial limitations of field investigation have meant that theories such as the velocity-reversal hypothesis can only be verified through comparison with hydraulic measurements along a cross-section (Booker et al., 2001) or through numerical modelling (Wilkinson et al., 2004; Harrison and Keller, 2007) which to date cannot be validated with natural flow measurements.

Riffle-pool sequences and the dynamics of flow over these subsurface bedforms in open channels provide a fluid problem of significant interest as it is critical to the understanding of sediment transport, morphological evolution processes and therefore is fundamental to many aspects of river management, rehabilitation and environmental engineering (Cao et al., 2003). Therefore alternative research methods and subsequent analysis is required to facilitate expanding understandings of the flow over these unique subsurface bedform features.

2.2.2 Development and Maintenance of Riffle-Pool Sequences

The processes responsible for the development and maintenance of riffle-pool sequences are an area of large-scale fluid dynamics that has attracted significant debate (Keller, 1971; Yang, 1971; Carling 1991; Clifford and Richards, 1992; Clifford, 1993a; Lofthouse and Robert, 2007, Sawyer et al., in press). Yang (1971) highlighted the need for explanation of these processes when stating that the hydraulic characteristics of natural streams could not be fully understood without knowledge of the basic principles that governs the formation of riffles and pools. More recently, Wilkinson et al., (2004) considered that, how and under what conditions, these ubiquitous, periodic bedforms are maintained is one of the fundamental questions of fluvial geomorphology. Existing literature however, fails to provide a clear consensus or single governing hypothesis for the mechanisms controlling riffle-pool development and maintenance (MacWilliams et al., 2006). As a result, a number of hypotheses, presented as uniquely different, but in many ways fundamentally similar, exist to potentially explain the development and maintenance of these subsurface bedform structures.

The five most prominent theories are considered below; the law of least time rate energy expenditure (Yang, 1971), the initiation of large-scale flow instabilities (Richards, 1976; Clifford, 1993), the velocity-reversal hypothesis (Gilbert, 1914; Keller, 1971), the flow constriction model (Thompson et al., 1998, 1999) and the hypothesis of flow convergence routing (MacWilliams et al., 2006)

2.2.2.1 The Law of Least Time Rate Energy Expenditure

One of the seminal works regarding the development of riffle-pool sequences was presented by Yang (1971) applying the law of least time rate of energy expenditure to the development of undulating deeps and shallows (riffle-pool sequences).Yang (1971) considered that during the evolution of a channel bed a river chooses the easiest route towards equilibrium. Illustrating Yang's (1971) theory by way of a theoretical example; if one assumes that a uniform flow is exerted over a channel bed composed of grains ranging in size from fine sand to large gravel (Figure 2.21) then according to the law of least time rate of energy expenditure the smallest material would be eroded first. This initial erosion would therefore produce small concavities and resultant convexities in the bed morphology. These initial convexities then experience steeper water surface slopes and higher near bed velocities which combine with the increased mobility of recently eroded material to develop pools and corresponding riffles. This process continues until the depth above the riffle is so shallow and the velocity so high that a further rise in bed elevation would cause the bed material, which is insufficiently stable to sustain shear stress, to be eroded (Yang 1971). Considering the sediment sorting patterns present in riffles and pools, Yang (1971) details that when grains of mixed size are sheared together the larger grains tend to drift towards the surface and because of the higher riffle velocity smaller grains are washed out and deposited within the pool. This produces the characteristic sediment patterns present in riffle-pool sequences. As the processes of erosion, dispersion and sorting continue, the difference between the water surface slope of a riffle and that of its adjacent pool increases eventually reaching a condition of dynamic equilibrium (Figure 2.21B) (Yang 1971).

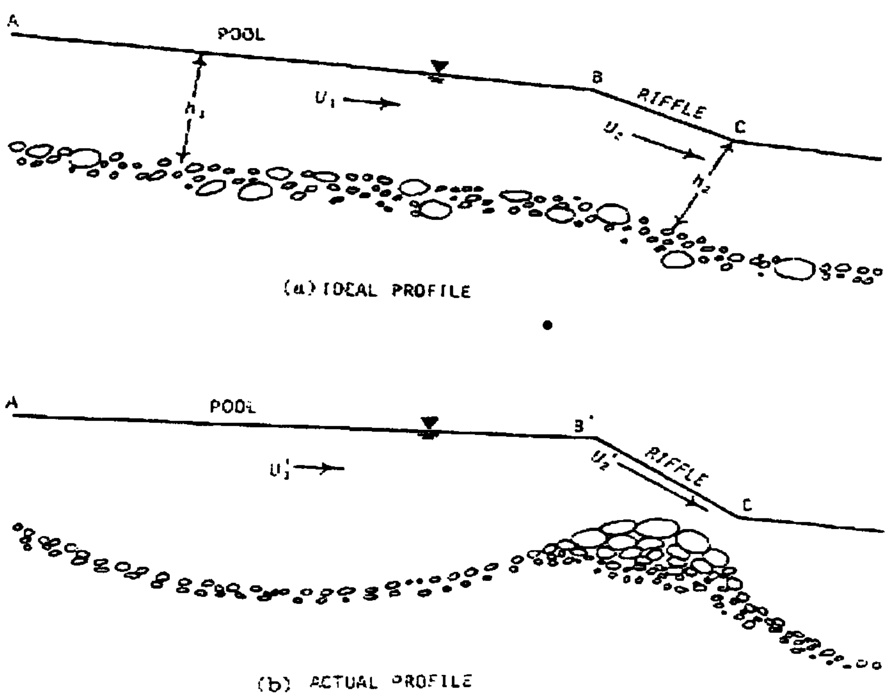

Figure 2.21 Schematic diagram of the water surface and bed profiles for a typical pool-riffle sequence presented by Yang (1971).

2.2.2.2 The Initiation of Flow Instabilities

The initial concept of flow instabilities generating riffle-pool sequences was introduced by Richards (1976). Richards (1976) suggests that riffles and pools form as a response to alternating patterns of scour and fill, sculpting the channel bed, through the development of full-boundary vortices and flow separations, either vertical, or horizontal with the primary role being accorded to 'fast-bottom rollers'. The motion of these eddies both occupied and caused the over-deepening of sections of the channel bed creating pools, which simultaneously mobilised sediment which would accumulate downstream to form raised riffles.

Clifford (1992) reinterpreted Richards (1976) findings describing that the formation of riffle-pool sequences can be understood by considering the initiation and propagation of flow instabilities during high flow conditions. Clifford (1992) primarily focuses upon the flow patterns and scour associated with the generation of roller eddies upstream and downstream from a major flow obstacles or obstruction.

Clifford's (1992) theory of development is summarised in Figure 2.22 and comprises three distinct stages; (a) randomly located bed material / obstacles creates upstream and downstream scour pools (b) continued erosion removes the obstacles leaving two depositional areas (riffles) separated by the scoured pool (c) the riffle itself then becomes a flow obstacles creating additional cycles of scour and deposition. (Clifford and Richards, 1992). As a result, Clifford (1992) concluded that riffle-pool sequences are initiated and maintained in a semi-autogenic manner.

Acknowledging that most pools in riffle-pool sequences cannot immediately be associated with specific flow obstructions, Clifford (1992) considers the generation of periodic wake vortices. Clifford (1992) hypothesised that these vortices would be shed downstream from initial obstacles thereby generating additional instabilities, scour and subsequent bedform undulations. Vortices of this type would experience rapid damping however the generation of each riffle-pool pairing would generate the next flow instability through jetting. Jetting occurs when flow converges and accelerates on the exit slope of riffles creating additional bed scour and the development of the next instability. Therefore the creation of a jet produces a riffle and the presence of a riffle produces a subsequent jet in a mutually dependent feedback mechanism.

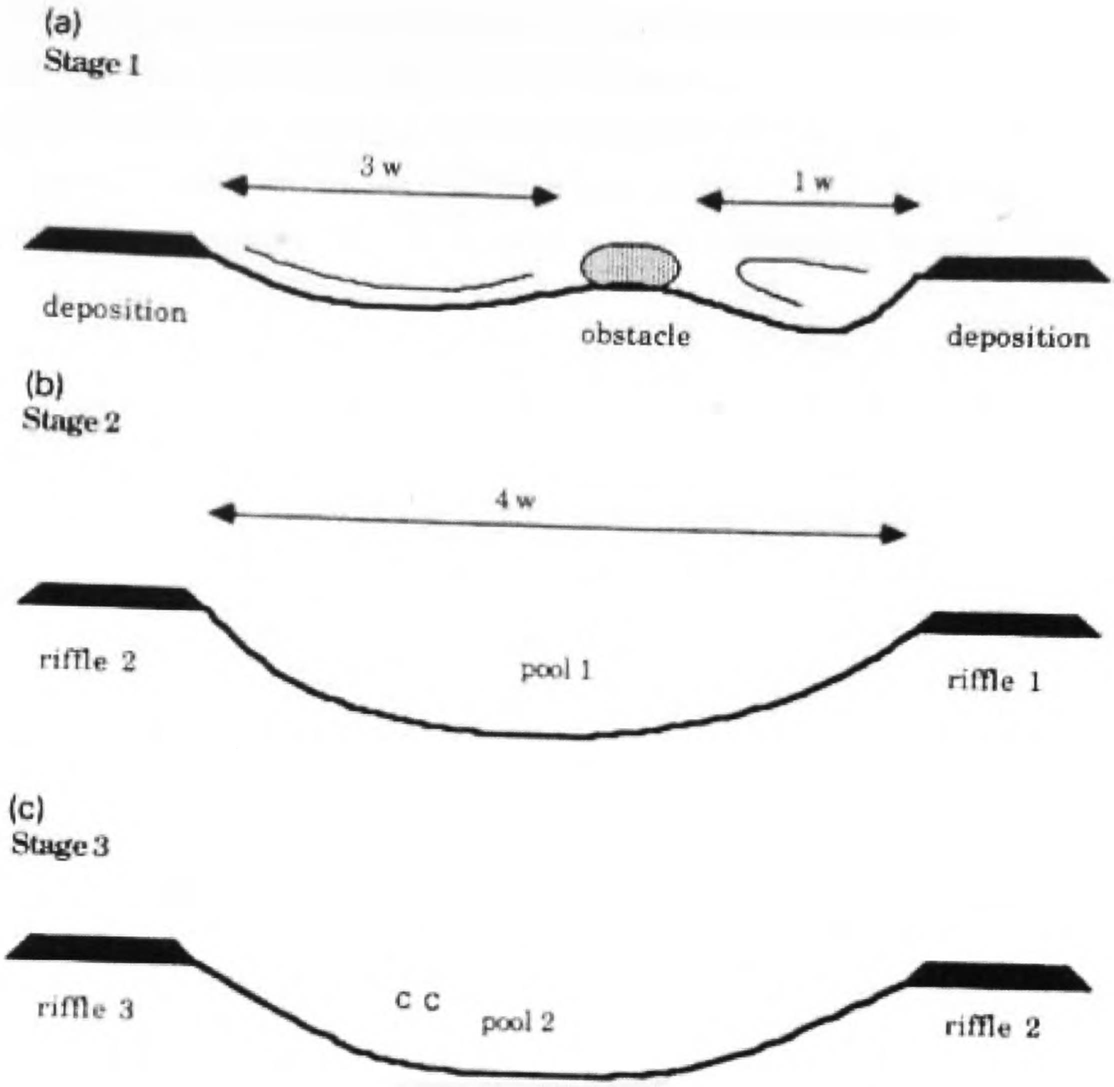

Figure 2.22 Schematic describing the development of riffle-pool sequences through the initiation of flow instabilities (Clifford (1992).

Clifford (1993a) explains the maintenance of riffle-pool sequences during the majority of flow-conditions through spatially differentiated turbulence and bed sediment interactions. Greater turbulent intensities in riffle locations restrict sediment movement causing accumulating of smaller material in the pools preserving the structure of the larger, coarser material on the riffle. This follows logically since coarse-bedded environments and zones of high relative roughness possess greater turbulent intensities (Clifford, 1993a).

Clifford (1993a) concludes that the development (high flow) and maintenance (majority of flow conditions) of riffle-pool sequences occurs as two process-form feedbacks (Figure 2.23). The sequence is initiated by the presence of a bedform obstacle producing turbulent flow instabilities which determines sediment transport rates and patterns (anticlockwise - outer circuit). Differences in the transport rate produce zones of erosion and deposition, generating bedforms which then perpetuate those flow differentials. In low to moderate flow conditions, the inner ring describes the maintenance of riffle-pool sequences. Varied turbulence over riffle and pool results in structured sediment sorting and particle organisation which itself produces turbulent differentials (Figure 2.23).

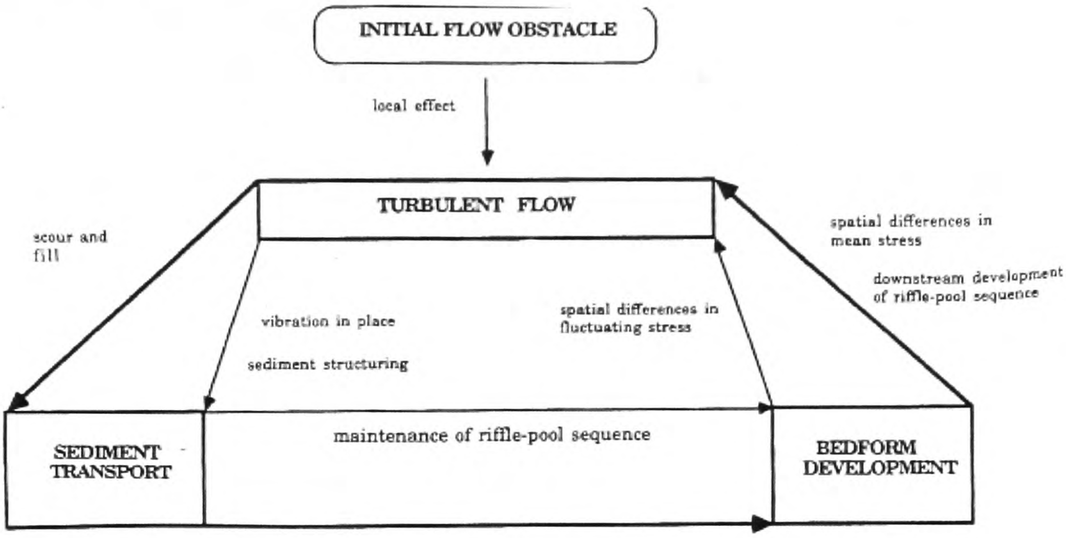

Figure 2.23. Function diagram which describes the development (anticlockwise outer circle) and maintenance of riffle-pool sequences (clockwise inner circle) (Clifford, 1993a).

2.2.2.3 The Reversal Hypothesis

According to Clifford and Richards (1992) the most widely accepted account of riffle-pool development and maintenance is provided by the hydraulic reversal hypothesis. Booker et al, (2001) highlights that various forms of hydraulic reversal have been suggested, including water surface slope (Keller, 1971), mean velocity (Lane and Borland, 1954; Keller and Florsheim, 1993), near-bed velocity (Keller, 1971; Carling, 1991; Carling and Wood, 1994) and shear stress (Lisle, 1979).

The most commonly referenced reversed parameters concern near-bed and mean cross-sectional flow velocities (MacWilliams et al., 2006). The velocity reversal hypothesis states that at low flow the distribution of some measure of sediment transport capacity, such as near-bed velocity or mean cross-sectional velocity is maximum at riffle crests and minimum in pool centres or troughs (Wilkinson et al., (2004). This distribution is then 'reversed' at high flow, becoming maximum in pools and minimum in riffles (Wilkinson et al., (2004).

The concept of a reversal in flow conditions between riffle and pool was initially introduced by Gilbert (1914), however the relationship was first quantified from field-based measurements by Keller (1971) formally presenting the velocity reversal hypothesis as the mechanism responsible for the maintenance of riffle-pool sequences at Dry Creek, California.

The velocity reversal hypothesis describes a hierarchical reversal in the magnitude of velocity over a riffle-pool sequence with increasing discharge (Harrison and Keller 2007). According to Keller (1971) as discharge initially increases (below the reversal velocity) fine material begins to be transported within the channel with the bottom velocity of the pool remaining less than that of the riffle ensuring that the largest material is trapped in the pool. As discharge increases further a "transitional point" is reached where the bottom velocity of the pools equals that of the riffle ensuring equal mobility of sediments through riffle and pool. Above the reversal velocity, the bottom velocity of the pool exceeds that of the riffle ensuring that any and all bed material can be transported onto the corresponding riffle (this only happens at bank full / flood stage). At the highest flows, the only stable area is on the riffle where lower tractive forces ensure the presence of larger bed material is maintained. With decreasing discharge the largest bed-material is stranded on the riffle whilst smaller material is returned to the pool by the (once again) higher riffle velocities. Below the reversal velocity, material moving across a riffle could not be moved through the pool. The relative size of material present in each area of the riffle-pool sequence is therefore determined by the magnitude at which the reversal velocity occurs. The higher the reversal velocity, the larger the material that is left in the pool with decreasing discharge and velocity (Keller, 1971).

According to Wilkinson et al., (2004) the velocity reversal hypothesis has been widely used as an explanation for observed scour of pools, and deposition on riffles at high flow conditions. Continuity would then dictate that for riffle-pool sequences to be maintained a reversal in flow competence must occur; resulting in the scouring of pools and deposition on riffles at low flow conditions. The occurrence of a reversal in flow parameters is clearly needed to facilitate many theories of the maintenance of riffle-pool sequences and is therefore perhaps more a convenient element of explanation rather than a measured phenomenon. MacWilliams et al., (2006) speculates that although the literature suggests that a velocity reversal does occur in some cases, it is unclear whether such a reversal is a requisite for pool maintenance or whether the reversal hypothesis is applicable for all pool-riffle sequences. Furthermore, following three-dimensional flow simulations MacWilliams et al., (2006) concludes that while simulations support a reversal in mean velocity (and other flow parameters) a reversal in mean parameters is not, in or of itself sufficient to explain the geomorphic processes that are necessary to maintain the riffle-pool sequence.

2.2.2.3 Constriction Forced Riffle-Pool Sequences

Thompson et al, (1999) considered that a distinction should be drawn between riffle-pool sequences and forced riffle-pool sequences located in close proximity to a channel constriction. According to Harrison and Keller (2007) in gravel-bed upland rivers, pools are often forced to develop by local obstructions such as boulders, bedrocks protrusions or debris jams (Keller and Swanson, 1979; Lisle, 1986; Montgomery et al., 1995; Montgomery and Buffington, 1997; Thompson et al., 1999). This view was supported by Buffington et al., (2002) highlighting that in coarse-grained upland rivers, pools formed by obstructions are the rule rather than the exception. According to MacWilliams (2006); Lisle (1986) found that 85% of pools were next to large obstructions or bends and that 92% of large obstructions on bends had pools. The theory of forced riffle-pool sequences overlaps the initiation of flow instabilities formulated by Clifford (1993a) who described an autogenic process whereby the deposition of material creates a riffle which generates the next downstream flow irregularity.

Thompson et al., (1999) proposed a model for the maintenance of riffle-pool sequences in gravel-bed river systems based upon an upstream channel constriction causing rapid flow convergence and high velocity jetting through into the resultant pool. This high velocity jet initiates the previously observed reversal in mean flow parameters across riffles and pools with increasing discharges. This model proposes that forced riffle-pool sequences are maintained by flows at or near bankfull discharge because of stage dependent variability in flow competence and the effective channel width (Harrison and Keller, 2007).

According to MacWilliams et al., (2006), Booker et al, (2001) noted that this concept links the velocity reversal hypothesis with the work by Keller (1971) and also overlaps with the generation of flow instabilities offered by Clifford (1992) who referenced large channel obstacles as opposed to constrictions. Cao et al., (2003) however warns that although a channel constriction can cause a flow competence reversal, the occurrence of a reversal is dependent upon channel geometry, discharge and sediment properties.

2.2.2.4 Flow Convergence Routing

Whilst investigating near-bed velocity patterns, Booker et al., (2001) observed that irrespective of a velocity reversal, it was the direction of near-bed flow that was the unique feature of flow in riffle-pool sequences with respect to discharge. At high flow conditions, sediment is routed around / away from the deepest parts of the pool thus maintaining the unique structure of these bedform features as opposed to the increased erodibility of material based on flow converging into the pool (MacWilliams et al., 2006).

MacWilliams et al., (2006) extends this discussion presenting the hypothesis of flow convergence routing for the development and maintenance of riffle-pool sequences in natural gravel-bed rivers. The hypothesis of flow convergence routing depends on the presence of an upstream flow constriction producing a convergence and acceleration of flow at the head of the pool. This convergence generates a jet of flow into the downstream pool; with the magnitude of the jet increasing at higher discharges, resulting in the development of a defined zone of increased velocity and shear stress (MacWilliams et al., 2006). Near-bed flow is routed through this high velocity zone creating increased shear stress and the primary pathway for sediment movement though the pool (MacWilliams et al., 2006). Depending upon the channel geometry, flow and sediment composition, the zone of flow routing can act to route the coarsest sediment away from the deepest part of the pool. Flow exiting the pool diverges leading to deposition on the riffle and the maintenance of a topographic high at the pool tail (Figure 2.24).

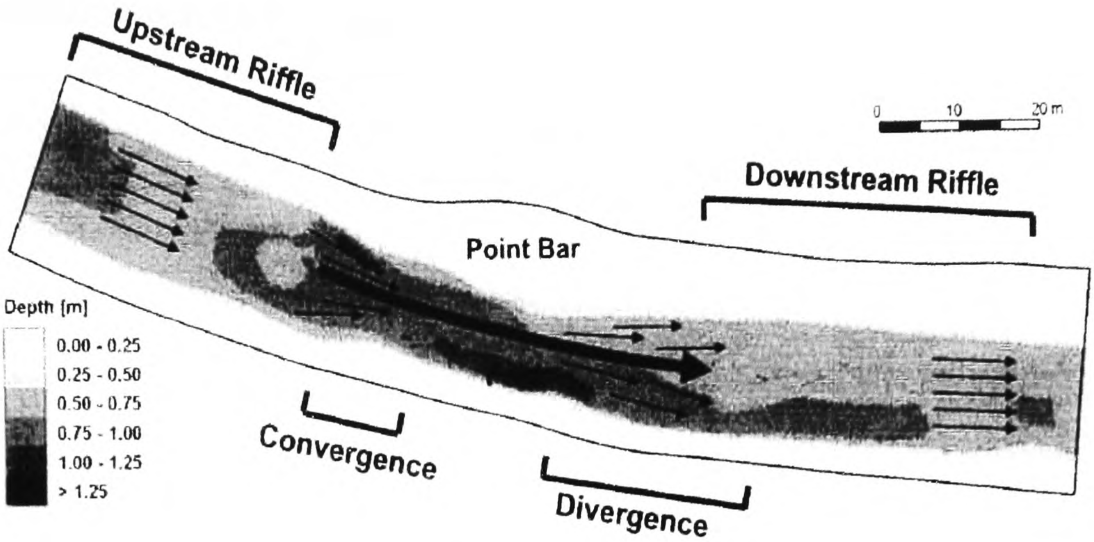

Figure 2.24. A conceptual model of the flow convergence routing mechanism during high flows on Dry Creek (MacWilliams et al., 2006)

MacWilliams et al., (2006) considers that the flow convergence routing hypothesis is not a rejection of previously published explanations, but an extension of the existing development and maintenance hypotheses. This is based on the recognition that cross-sectional average parameters are not sufficient to explain the complex flow interactions occurring in riffle-pool sequences. According to MacWilliams et al., (2006) many of the primary references pertaining to the velocity reversal hypothesis reference flow constrictions and / or convergences thereby providing implied support for the flow convergence routing hypothesis. The theory offered by MacWilliams et al., (2006) differs from the mechanism proposed by Thompson et al., (1998) in three ways. The first is the degree to which flow is constricted upstream of the developing riffle-pool sequence; Thompson et al., (1998) identified a more complete flow obstruction as opposed to MacWilliams et al's., (2006) more subtle narrowing of flow. Secondly, Thompson et al., (1998) incorporates the development of recirculating eddies feeding flow into the downstream jet. Finally, Thompson et al., (1998) determined that the jetted flow forces material through the deepest part of the channel as opposed to round the deepest part of the pool (MacWilliams et al., 2006).

MacWilliams et al., (2006) quantified the flow convergence routing hypothesis through three-dimensional simulation of the flow processes operating within Dry Creek, California; the same field site utilised by Keller (1971). It is therefore significant that MacWilliams et al., (2006) was able to demonstrate simulation results that agree well with the previous predictions of a reversal of near-bed velocity by Keller (1971) and a reversal in mean velocity by Keller and Floresheim (1993). The convergence routing hypothesis is unique amongst theories pertaining to the development and maintenance of riffle-pool sequences in that it incorporates elements of each of the other outlined theories. MacWilliams et al., (2006) considered that the new hypothesis is significant in its ability to explain the differences in previous investigations of the operation of the velocity reversal hypothesis and for highlighting the inadequacies of cross-sectional averaged measurement to represent complex flow interactions (Sawyer et al., in press).

2.2.3 The Structure and Periodicity of Riffle-Pool Sequences

The bedform morphology of riffle-pool sequences is thought to possess a degree of regularity / periodicity; having an average wavelength of several channel widths (Leopold and Wolman, 1957; Keller and Melhorn, 1978) whilst individual riffles and pools may be distinguish by structural differences in terms of width, depth, cross-sectional area and sediment composition.

2.2.3.1 Longitudinal Structure and Periodicity

According to Clifford (1993) most attention concerning the structure of riffle-pool sequences has focused on the correlation between macro-scale flow structure and mean inter-riffle spacing. It is widely accepted that the wavelength of inter-riffle spacing is 5 to 7 times the mean channel width (Melton, 1962; Church, 1972; Keller, 1971; Richards, 1976; Clifford and Richards, 1992). Thompson et al., (2001) similarly considered that researchers have documented average pool-to-pool spacing between five and seven channel widths in gravel-bed rivers (Leopold et al., 1964; Keller and Melhorn, 1978; Sear, 1996). Thompson et al., (2001) also referenced the work of Lisle (1986) and Carling and Orr (2000) who found that the average riffle length lies between 1.31 and 4.5 channel widths. Thompson et al., (2001) however warns that these findings have limited theoretical justification in gravel-bed river systems since it is difficult to quantify a spatial periodicity to a bedform arrangement which develops from irregularly distributed channel constrictions. Furthermore, Thompson et al., (2001) concludes that little progress has been made in determining why pools tend to approximate this five to seven bankfull-width spacing.

Clifford (1993) considers that if there is a consistent relationship between eddy size (pool length) and riffle spacing the model inter-riffle spacing is a more appropriate scaling relationship providing evidence that this value would be closer to three times the channel width. This highlights the influence that the selection of appropriate statistical methods and hydraulic definitions can have upon the measured wavelength of riffle-pool sequences.. Thompson et al., (2001) supported this view when writing that the definitions and methods used to define these features seem to be at least partly responsible for variation within measurement of riffle-pool sequences.

Tinkler (1970) interpreted the spacing of every second pool or riffle in straight channels finding that they have approximately the same wavelength with respect to mean channel width as the wavelength of meanders. The correlation of meander and riffle periodicity appears sensible since the development of meander trains and riffle-pool sequences are analogous being respectively horizontal and vertical transformations of channel form. Richards (1976) however contends that the fundamental velocity perturbations produced by riffle-pool sequences lags behind the 2π x width wavelength of consecutive meanders.

Considering the relationship between channel curvature and longitudinal bedform composition in gravel-bed rivers, Lofthouse and Robert (2007) found that overall curvature increased pool length relative to riffle length. This demonstrates that the bedform composition of straight and curved reaches should be distinguished and considered separately.

Thompson et al., (2001) concluded that dominant discharge could be viewed as the primary control on all geometric characteristics of channels including pool dimensions, bankfull width and spacing. Carling and Orr (2000) added that pool and riffle length increases in the downstream direction becoming longer and flatter further downstream with Thompson (2004) assessing that pools elongate at a rate of 10 times the rate at which they deepen. Lofthouse and Robert (2007) highlighted that in addition to dominant discharge conditions, bank and bed material structure and size, and bank vegetation characteristics are influential factors in the controlling the spacing of riffle-pool sequences. Lofthouse and Robert (2007) however concluded that extensive data sets provide average riffle-pool sequence length of 5 to 6 channel widths (in the lower part of the 5 - 7 channel widths, often quoted).

2.2.3.2 Lateral Structure and Cross-Section Area

Wilkinson et al., (2004) identified systematic variation in channel width, with riffles typically being 15-33% wider than pools (Lane and Borland, 1954; Richards, 1976b; Keller and Melhorn, 1978, Andrews, 1979; Carling, 1991). According to Richards (1976b) the tendency for riffle widths to exceed those of pools occurs due to the accumulation of sediment over the riffle deflecting flow towards one or both channel banks causing undercutting and channel widening. The degree of undercutting is determined by the composition of the channel bed and banks and dominant flow characteristics.

Carling (1991) disputed that riffles remain wider throughout all flow conditions finding that riffles were 25% narrower than pool at the lowest flow conditions whilst across a range of higher flows the riffle is 33% wider than the pool. MacWilliams et al., (2006) identified contradictory results at Dry Creek, California finding that at low flow the riffle is around 50% wider than the pool and slightly narrower than the pool at high discharges. The contradictory nature of these finding can potentially be explained by bank stability, sediment structure and vegetation composition limiting channel development for different investigations and field-sites (Richards, 1976a).

The dispute regarding the relationship between channel width through riffles and pools relative to discharge may in part stem for the lack of an appropriate definition of channel width. Cherkauer (1973) acknowledging this difficulty considered that the most useful approach would be to consider the 'effective width', which corresponds to the active zone of flow (Clifford and Richards, 1992). In riffles, the effective width is nearly the entire width of flow whilst in pools it may be considerable narrower albeit deeper than its riffle counterpart.

The definition of effective width was reinterpreted after the work of Thompson (2004) to include forced riffle-pool sequences, the implication being that effective channel width is the area of flow that will convey the flow capable of scouring bed material (Harrison and Keller, 2007). Harrison and Keller (2007) incorporated the concept of effective width into their modelling of forced riffle-pool sequences by specifying that it is represented by 90% of the highest modelled flow velocities (Figure 2.25). High-resolution, two-dimensional flow simulations demonstrated that the ratio of effective width to riffle and pool was 1:1 for low flows and 3:1 for high flows (Harrison and Keller, 2007).

Wilkinson et al., (2004) identified that variation in channel width lags behind the longitudinal depth oscillation. The maximum channel width occurs downstream of the riffle crests and minimum channel width occurs upstream of the riffle crest. Wilkinson et al., (2004) explains these findings by citing the original explanation offered by Richards (1976b) that diversion of flow over riffles at low flow conditions can cause undercutting of the channel banks.

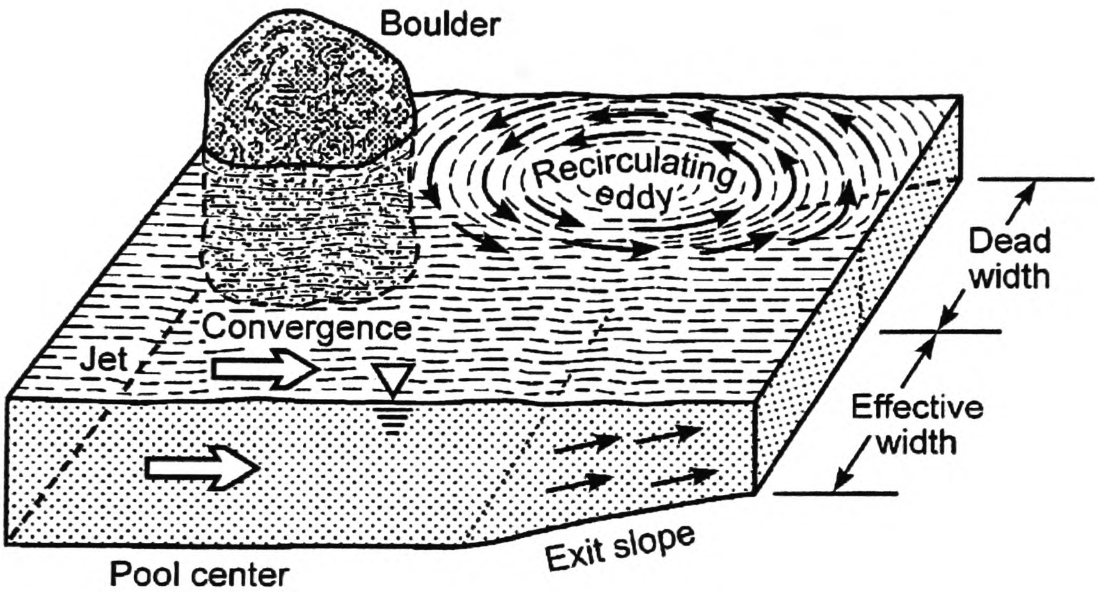

Figure 2.25 Conceptual diagram showing effective width in a forced pool (modified after Thompson, 2004). Dead width represents areas of low flow velocity and potential deposition. Arrows represent the direction of flow.

According to Thompson et al., (1999) several researchers have shown that during most stages, pools have a larger cross-sectional area of flow, and should therefore, exhibit lower cross-section averaged velocities than riffles (Richards, 1978; Schmidt, 1990; Carling, 1991; Carling and Wood, 1994; Thompson et al., 1996). Considering the relationship between flow-depth and discharge Carling (1991) found that although the absolute differences in depth remains constant (with pools inherently always being deeper than riffles) as discharge increases, the relative difference decreases towards a convergence at bankfull flow levels. Carling (1991) is therefore providing evidence towards a reversal in width, depth and cross-sectional area with increasing discharge.

Similarly, Keller (1993) identified a reversal in the size of the cross-sectional area relative to increasing discharges. Keller (1993) considering the work of Lane and Borland (1954) described that since channel geometry in the pool is asymmetric (triangular) and the riffle is symmetric (rectangular) at low flow conditions the cross-sectional area is greater in the pool resulting in lower mean velocities. However, during higher discharges the cross-sectional area of the riffle exceeds that of the pool resulting in the mean pool velocity exceeding that of the riffle (Keller and Florsheim, 1993) (Figure 2.26).

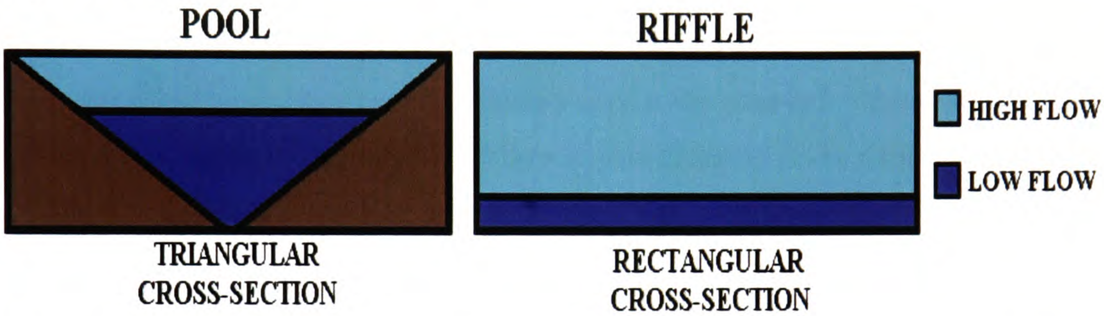

Figure 2.26 Diagram demonstrating the effect of increasing discharge upon the different cross-section areas / shapes of pools and riffles.

The reversal in channel structure of riffles and pools with increasing discharge as presented by Keller (1993) is fundamental to the widespread debate concerning the reversal hypothesis. Without a reversal in cross-sectional area the channel would be unable to accommodate a reversal in flow competence (Keller and Florsheim, 1993). Therefore, even if the convergence in relative depth, as observed by Carling (1991) does occur then there must also be a marked change in relative width for the potential of a velocity reversal to arise.

2.2.4 Large-Scale Flow Structures

In addition to the structured regularity identified in the formation of riffles and pools; the large-scale flow structures which occur over these bedform features exhibit equally unique lateral and longitudinal patterns.

According to Clifford (1992) flow over riffle-pool sequences possess distinctive longitudinal and lateral flow patterns; at low flow conditions longitudinal shallows (riffles) feature divergent flows whilst longitudinal deeps (pools) contain convergent flows. Clifford (1992) further describes that the lowest velocities are observed at the pool midpoint and the highest at the riffles crest with pool tail and riffle midpoint areas having almost identical mean velocities. These patterns are fundamental important to the existence and structure of channel morphology, driving the previously described-feedback mechanism that build and preserve these unique bedform structures (Knighton, 1998).

2.2.4.1 Lateral Flow Structures

Harrison and Keller's (2007) findings supported the work of Thompson et al., (1999) which described how velocity is dissipated across the pool-exit slope creating rapid flow divergence through riffles, whilst flow is constricted over the riffle tail producing rapid flow convergences entering corresponding pools.

Cao et al., (2003) highlighted the importance of channel plan geometry in addition to bed topography to the development and distribution of lateral flow patterns. Clifford and Richards (1992) similarly agreed that the flow patterns produced through a riffle-pool sequence occurs at a result of the interaction of channel form and channel flow (both upstream and downstream of the element in question). Clifford and Richards (1992) utilized these finds to stress that explanations relying on cross-sectional averages are inadequate to describe or explain the flow processes and patterns and therefore complicate as opposed to clarify the characteristics of the flow and form interaction. (Clifford and Richards in MacWilliams et al., 2006).

Keller (1969) determined that the highest bottom velocities occurred on the point-bar side of the pool as opposed to through the pool centre. These findings described an asymmetric structure to the lateral velocity patterns with Keller (1969) suggesting that at higher discharges the migration of higher velocities towards the point-bar increases. Applying both two and three-dimensional models to the same Dry Creek field site utilized by Keller (1969); MacWilliams et al, (2006) found that the presence of a flow constriction at the head of the pool results in flow convergence which produced the maximum velocities on the point bar of the pool rather than through the deepest part of the channel. MacWilliams et al., (2006) additionally determined that whilst the routing of higher velocity flow across the point-bar produced unique sediment flow patterns it also generated a secondary circulation in the deepest part of the pool which had the potential to mobilize the trapped finer sediment.

2.2.4.2 Longitudinal Flow Patterns

Harrison and Keller (2007) identified that at low discharges, a peak velocity zone occurs over the riffle, whilst at or near bankfull discharge, the peak can be found at the pool head due to the strong flow convergence created by large roughness elements. Additionally, as discharge increases the strength of the flow convergence intensifies resulting in a narrower, higher velocity core which runs through the pool head and centre.

To quantify the relationship between discharge and velocity, Harrison and Keller (2007) modelled flow at three distinct stages; low flow (0.5 m^3s^{-1}), bankfull discharge (5.0 m^3s^{-1}) and an estimated five-year flood (10.0 m^3s^{-1}). At low flow, the maximum velocities are observed over the riffle (1.2 ms^{-1}) as opposed to the pool (0.7 ms^{-1}). At bankfull discharge the peak velocities in the pool (2.8 ms^{-1}) exceed those observed over the riffle (2.5 ms^{-1}). According to Harrison and Keller (2007), flow convergence created by the constriction is concentrated through the pool, creating maximum velocities at the pool head with this jet being maintained by the recirculating eddy that develops below the constriction. Strong flow divergence occurs on the pool exit slope as demonstrated by divergent highly variable velocity contours on the riffle, which occur as a response to coarse and irregular local topography. At the highest discharge an equalization in the magnitudes of maximum riffle and pool velocities were observed (around 3.0 ms^{-1}); with velocities appearing more evenly distributed over both the riffle and pool as the relative prominence of the roughness element is reduced (Figure 2.27).

Booker et al., (2001) explained this changing pattern of the location of relative maxima across riffles and pools through the occurrence of a migration / phase-shift in longitudinal flow patterns. Wilkinson et al., (2004) similarly argued that instead of being reversed, maxima and minima velocities are phase-shifted with respect to the location of riffles and pools so that maximums occur upstream of the riffle crests at high flow and downstream at low flow.

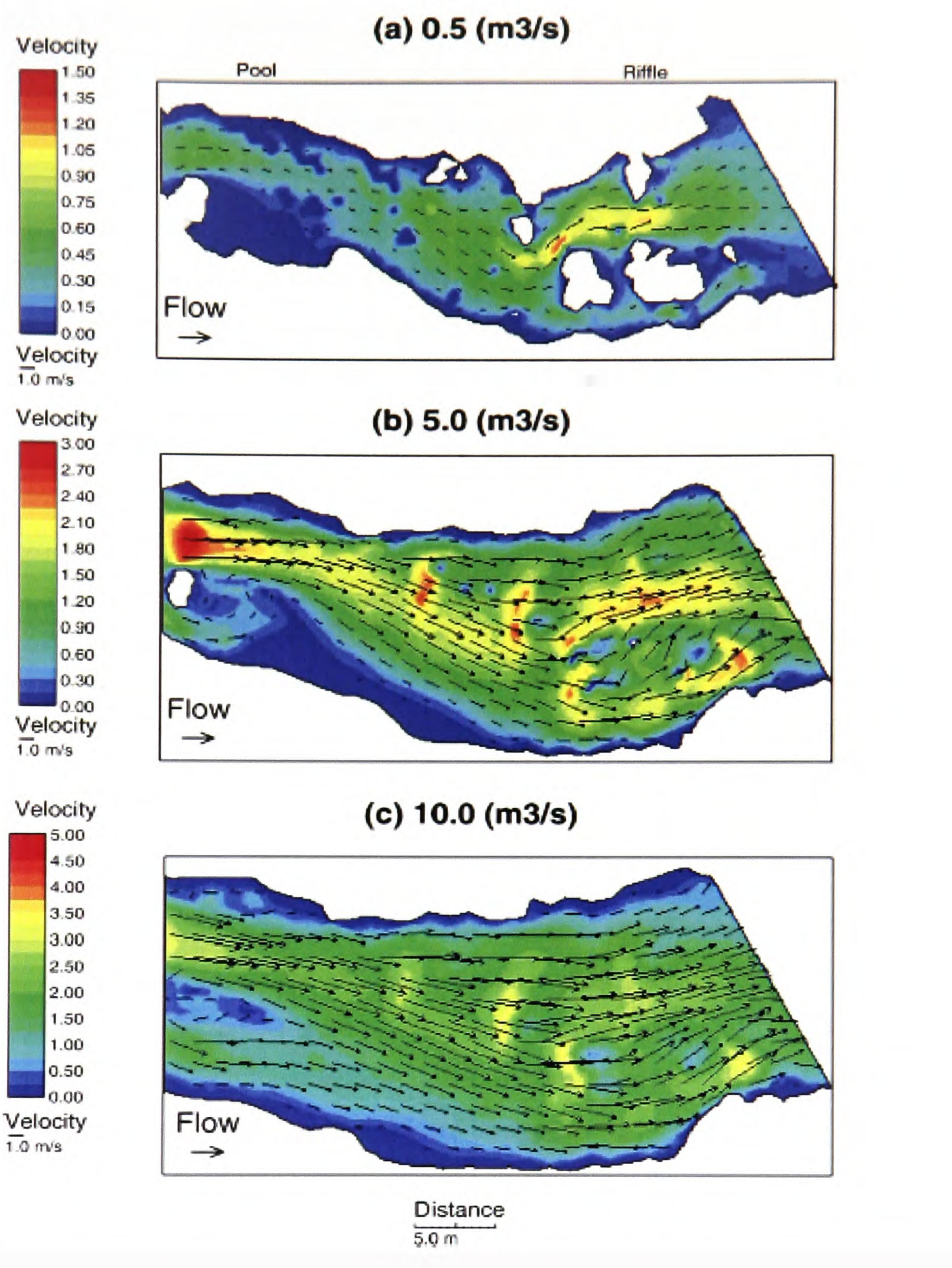

Figure 2.27. Modelled velocity overlain on velocity contour plots at discharges of: (a) 0.5 m^3s^{-1} (approximately 10% of bankfull discharge), (b) 5.0 m^3s^{-1} (approximately bankfull discharge), and (c) 10.0 m^3s^{-1} (approximate five-year flood discharge) (Harrison and Keller, 2007).

2.2.4.3 The Velocity Reversal Hypothesis

According to Harrison and Keller (2007) the most widely utilized approach to the study of riffle-pool sequences has been based on analysis of hydraulic parameters with the velocity reversal hypothesis receiving considerable attention. The velocity reversal hypothesis is based primarily on the measured observations that, with increasing discharge, the average bottom velocity of a pool increases faster than that of a riffle until at relatively high flow the average bottom velocity of the pool exceeds that of a riffle (Keller, 1971).

The concept of a reversal in bottom velocity was introduced by Gilbert (1914) finding that at low flows, the deeps previously formed at high flows, become pools interspaced by shoals (riffles) whilst the relative velocities remain diversified but have exchanged places (Milan et al., 2001; MacWilliams et al., 2006). Leopold and others (1964) concluded that bottom shear, which is proportional to the velocity squared, increased more rapidly with discharge over a pool than over a riffle, but did not further explore the phenomenon (Keller, 1971). It was not until Keller (1971) that the term velocity reversal was introduced and both observations and quantative data were formulated into a theoretical framework (MacWilliams et al., 2006). Keller (1971) used near-bed velocity as a surrogate for tractive force or stream power, and was able to demonstrate an equalization in velocity between pools and riffles at high stage flows (Milan et al., 2001).

By way of quantification Keller (1971) measured mean bottom velocities at four stages spaced at 3-ft intervals across the channel and demonstrated a convergence to equality at a discharge of 160 cfs (Figure 2.28). According to Keller (1971) "extremely hazardous conditions" prohibited velocity measurements at greater discharges meaning that a velocity reversal was only ever predicted as opposed to measured.

A similar review of reversals in different flow parameters as presented by Booker et al., (2001) was provided by MacWilliams et al., (2006) and concluded that the velocity reversal hypothesis should be extended to a suite of multiple working hypotheses, rather than a single ruling hypothesis since different mechanism will operate in different riffle-pool sequences.

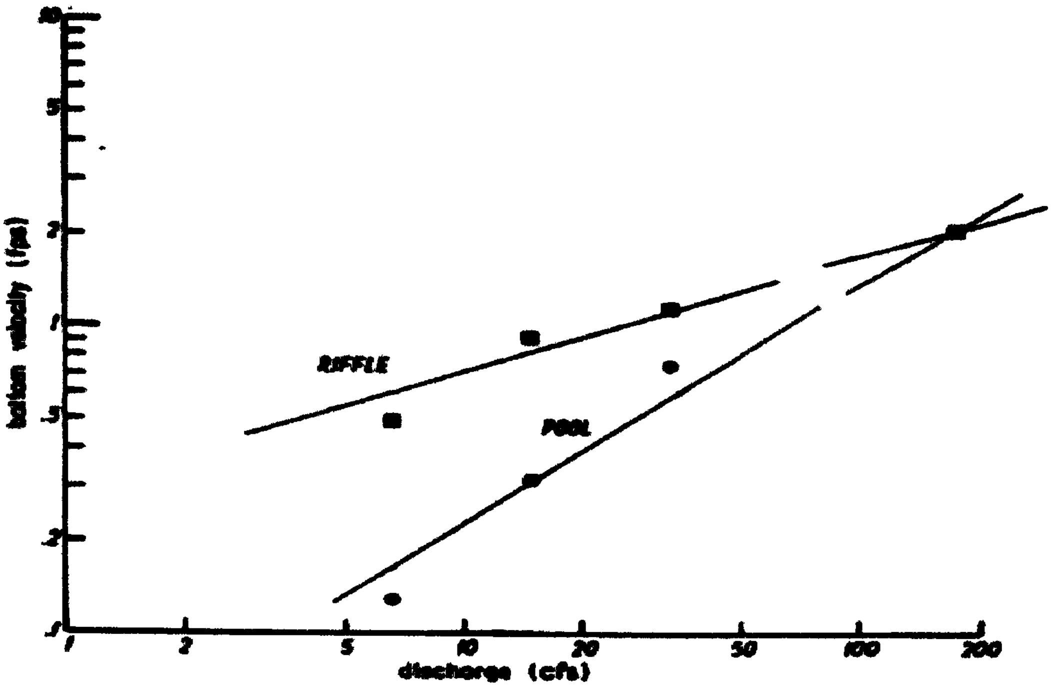

Figure 2.28. Mean bottom velocities for a pool and riffle pairing against discharge which Keller (1971) described as demonstrating the occurrence of a velocity reversal with increasing discharge.

The existence and operation of the velocity reversal hypothesis is widely disputed (Cao et al., 2003). According to Harrison and Keller (2007) many studies have investigated the velocity reversal hypothesis including, Lisle (1979) O'Connor et al., (1986), Clifford and Richards (1992), Keller and Florsheim (1993), Carling and Wood (1994), Sear (1996), Thompson et al., (1998, 1999), Booker et al., (2001), Milan et al., (2001), Cao et al., (2003), MacWilliams (2004) and MacWilliams et al., (2006). Despite these many investigations, Wilkinson (2004) reported that only four studies actually observed the occurrence of a velocity reversal; Lisle (1979), Andrews (1982), Booker et al., (2001) and Milan et al., (2001).

Reinterpreting Keller's (1971) work Richards (1978) stated that within physically realistic limits a reversal would not be observed and utilised additional experimental findings to demonstrate that as flow increased although mean cross-sectional pool and riffle velocities became less differentiated equalization seemed remote (Richards, 1978) (Figure 2.29).

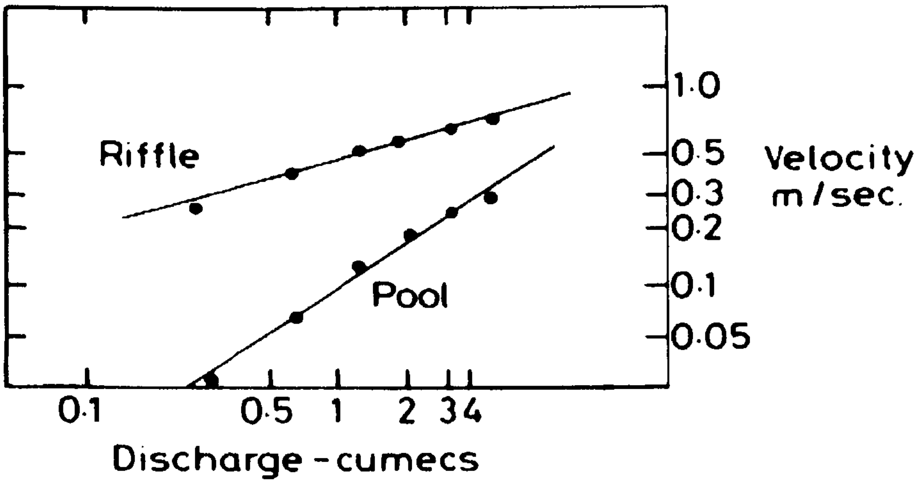

Figure 2.29 Simulated hydraulic geometry relations for adjacent riffle and pool cross-sections provided by Richards (1976). The figure demonstrates the convergence of riffle and pool velocities with increasing discharge however, as described by Richards (1976) a reversal in velocities failed to occur.

Further criticism was offered by Heritage et al., (2004) highlighting that Keller (1971) was only able to demonstrate a convergence in velocity at high flow conditions. Keller and Florsheim (1993) acknowledged this as a limitation of the 1971 work when stating that near-bed velocities were only measured to the point of equalization with a reversal in velocities inferred at still higher discharges (Figure 2.30).

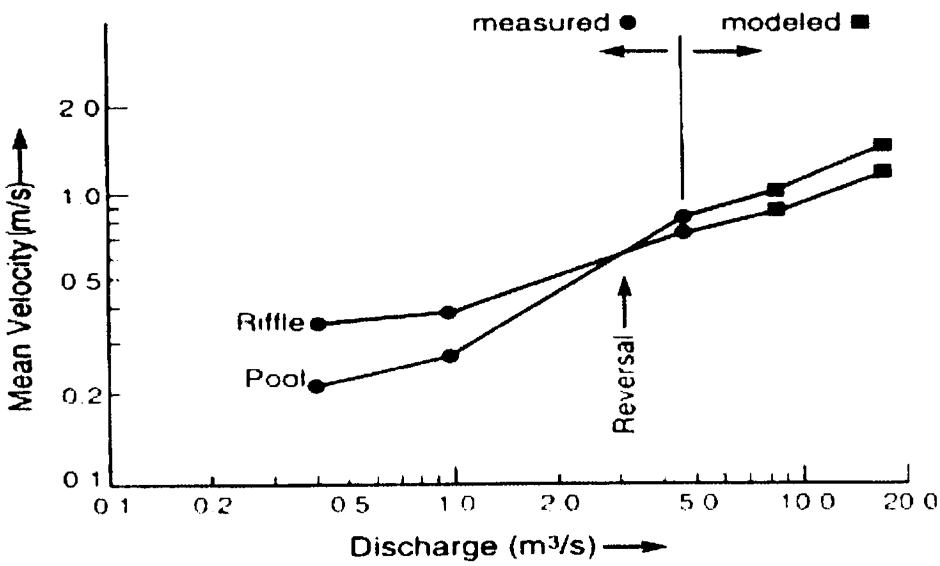

Figure 2.30. The relation between mean velocity and discharge for adjacent riffle and pool. The figure demonstrates that Keller (1971) was never able to demonstrate a reversal in the velocities present in natural river channels with the reversal being inferred from modelled values (Keller and Florsheim, 1993).

MacWilliams et al., (2006) applied both two- and three-dimensional models to Dry Creek, California, the field site originally utilised by Keller (1971) for the formulation of the velocity reversal hypothesis. Simulations predicted a reversal in mean cross-section bed velocity at a slightly lower discharge than was predicted by Keller (1971), however these results support Keller's (1971) original prediction that a reversal in near-bed velocity would occur at Dry Creek at higher discharges (MacWilliams et al., 2006). Support for the existence of the velocity reversal hypothesis has not however been universal across modelled riffle-pool sequences. Booker et al., (2001) utilised three-dimensional computational fluid dynamics to investigate the flow occurring throughout Highland Water (New Forest, Hampshire). Booker et al., (2001) observed a reversal in only three out of eight riffle-pool pairings. Additionally, where a reversal was observed the difference in the magnitude of riffle and pool velocities was 10% of less (Cao et al., 2003).

Clifford and Richards, (1992) criticized previous investigations for performing comparisons of the flow properties between non-consecutive riffles and pools. With reference to the velocity reversal hypothesis, Andrews' (1979) considered that there are no contiguous riffle and pool sections that demonstrate the occurrence of a reversal in mean velocity.

Heritage et al., (2004) also challenged the generally accepted view that a reversal in hydraulic parameters (when observed) must always occurs at bank full flow conditions (Keller, 1971; Carling, 1991) observing that reversals in hydraulic parameters may occur at different stages on the flood hydrograph for different riffle-pool units through different reaches.

Carling (1991) found a convergence in mean velocity in consecutive riffles and pools but concluded that the riffles in his study were not sufficiently wide at high flows to accommodate the discharge necessary to develop a velocity reversal (MacWilliams et al., 2006). Keller and Florsheim (1993) considered this issue, citing the work of Lane and Borland (1954) who found that a reversal of cross-sectional areas between pools and riffles simultaneously occurred when a velocity reversal was found. Wilkinson et al., (2004) also identified that reversals of mean or near-bed velocity generally occurred where riffle width was sufficiently larger than pool width to produce the larger cross-sectional area in the riffle with increasing discharge. Utilising a numerical simulation of shear stress through an idealized riffle-pool sequence, Carling and Wood, (1994) found that a reversal at high flow is only possible where riffles are at least 50% wider than pools (Wilkinson et al., 2004). These findings demonstrate the fundamental role that cross-sectional channel structure plays in the development of longitudinal flow patterns in gravel-bed river systems. Carling (1991) acknowledged this importance highlighting the need for further consideration to be given to bank strength and channel plan geometry before a reversal in velocity can be accommodated. More recently, MacWilliams et al., (2006) described channel widening as the geometric mechanism responsible for determining whether a velocity reversal could occur.

Milne (1982) considered lateral channel form geometry when stating that the results from meandering and straight channels should be considered separately. Keller (1993) similarly determined that the findings relating to the velocity reversal hypothesis were only applicable to straight channels and that further work was required to determine whether a reversal is likely in meandering channels containing riffle-pool sequences.

According to Wilkinson et al., (2004) the velocity reversal has rarely been recorded in field measurements. This is largely due to the limited spatial and temporal resolution of field evidence used to test reversal theories (Thompson, 2001). Thompson et al., (2001) considered that even the most detailed data sets (Clifford and Richards, 1992) consisted of only two pairs of velocity cross-sections in corresponding riffles and pools measured at seven discharge conditions. MacWilliams et al., (2006) highlighted that there is a growing recognition that section averaged data are not sufficient to explain the complex flow interactions that occur throughout riffle-pool sequences. The collection of more detailed spatial and temporal data at the full range of discharge conditions may not prove feasible, especially, when synchronous measurements of the whole field are required (Cao et al., 2003).

2.2.4.4 Froude Numbers

According to Carling (1991) and Clifford and Richards (1992) the observed reversal of hydraulic parameters with increasing discharge (which has principally been focused upon mean cross-channel velocity) has been extended to include reversals of other flow characteristics including stream power (O'Connor et al., 1986) and shear stress (Lisle, 1979). This is also true of the Froude number (Bhowmik, 1982, Cao et al., 2003) and water surface slope (Carling, 1991) which is often used as a proxy for the energy gradient throughout a riffle-pool sequences.

Bhowmik (1982) determined that under low to medium flow conditions, the Froude number is highest at the riffle and lowest at the pool due to the relative flow depths. With increasing discharge Bhowmik (1982) described that the equalization of flow depths in addition to the water surface gradient would correspond to a reduction in the difference between riffle and pool Froude numbers as the relative depth differential decreased.

Clifford et al., (1992) added that despite Froude numbers providing a dimensionless representation of flow parameters, comparable over the entire range of discharge conditions the relationships between riffle-pool sequences and Froude numbers has essentially been ignored (Richards, 1976; Clifford et al., 1992).

Harrison and Keller (2007) considered Froude number across a modelled riffle-pool sequence at three distinct flow conditions; 0.5 m^3s^{-1} (approximately 10% of bankfull discharge), 5.0 m^3s^{-1} (approximately bankfull discharge), and 10.0 m^3s^{-1} (approximate five-year flood discharge). It was initially highlighted that Froude numbers increased throughout the channel with increased discharges. Specifically, for simulations at low discharges, flow is subcritical through the reach yet Froude values are highest and flow is the most varied over the riffle. At bankfull flow conditions super critical flow is predicted at the pool head and downstream into the riffle. Model simulations for the five-year peak discharge predict super critical flow over the pool and riffle with the greatest values observed over the riffle (Figure 2.31). Despite the addition to the literature of Harrison and Keller's (2007) work, further investigation of the relationship between relative Froude numbers and discharge over a riffle-pool sequence is required based upon genuine flow measurement to potentially expand our current understandings of flow over these bed form features.

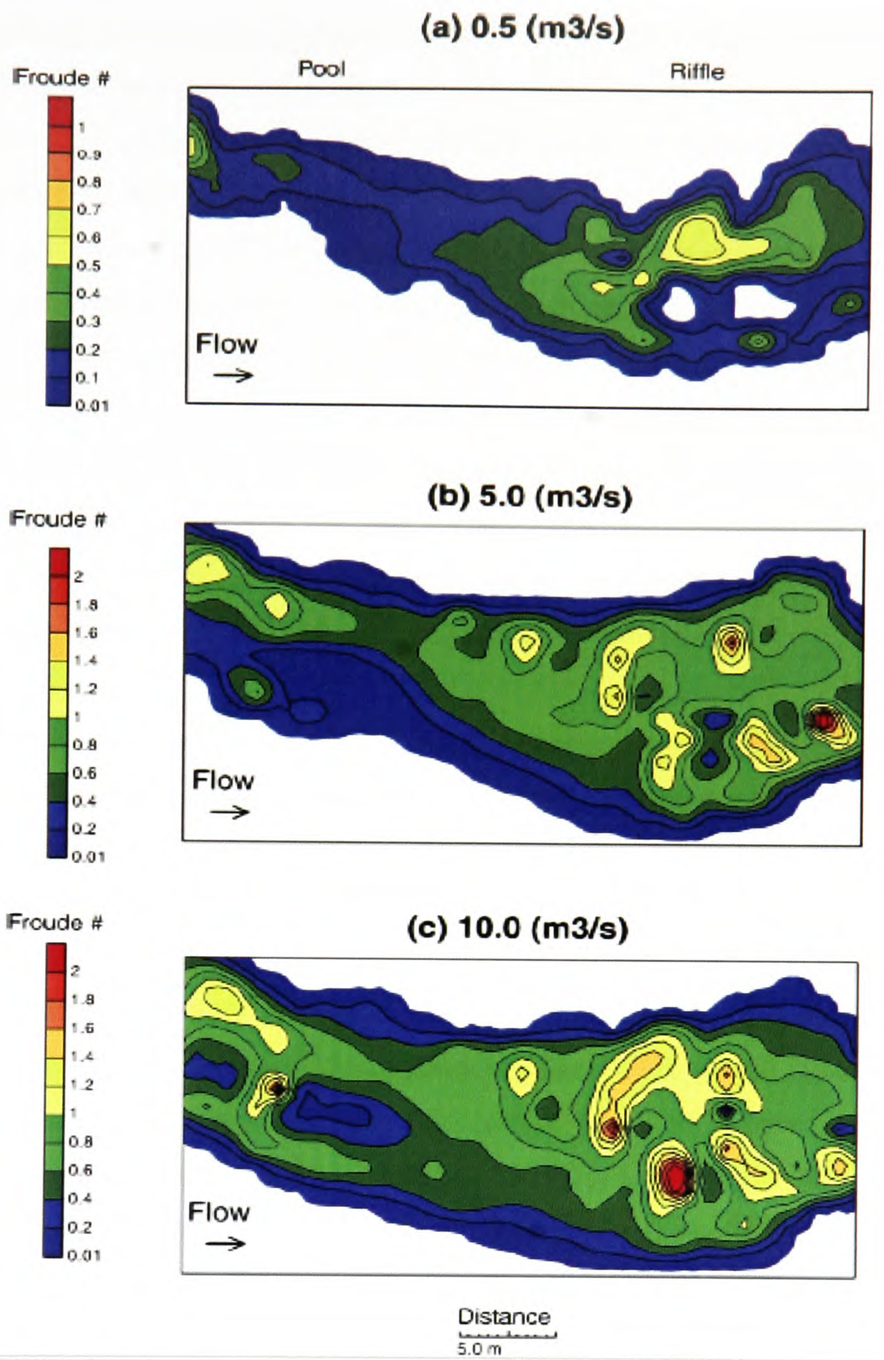

Figure 2.31. Contour plot illustrating the spatial trends in the Froude number, based on model output for discharges of: (a) 0.5 m^3s^{-1} (approximately 10% of bankfull discharge), (b) 5.0 m^3s^{-1} (approximately bankfull discharge), and (c) 10.0 m^3s^{-1} (approximate five-year flood discharge).

2.2.5 Riffle-Pool Summary

It is widely reported within existing literature that riffle-pool sequences generate distinctive longitudinal and lateral flow patterns with the individual flow structures of riffles and pools possessing a degree of regularity. At low flow conditions riffles feature higher, divergent velocities whilst pools contain lower velocity converging flows. The longitudinal flow patterns are generally thought to mirror the bedform topography providing a periodicity of 5-7 times the mean channel width. The point of maximum velocity throughout a reach, theoretically located at the riffle midpoint is thought to migrate with changes in discharge producing a phase-shift in any wavelength or periodicity. With increasing discharge the difference between riffle and pool flow patterns is believed to narrow towards equality or as reported by several authors a reversal in flow parameters. Despite the existing literature providing a widely agreed upon criteria and explanation for the classification and operation of riffle-pool sequences, there are areas of continued debate, methodological criticism and fundamentally important questions remaining to be addressed.

According to MacWilliams et al., (2006) existing literature has failed to provide a clear consensus or a single governing hypothesis to describe the mechanism controlling the development and maintenance of riffle-pool sequences. This remains problematic due to the fundamental importance of riffle-pool sequences to the understanding of all flow processes operating in natural gravel-bed river systems (Yang, 1971). Wilkinson et al., (2004) considered that how and under what conditions, these ubiquitous, periodic bedforms, are maintained is one of the fundamental questions in fluvial geomorphology. There has been a recent move towards constriction focused development and maintenance hypotheses (Thompson, 2001 and MacWilliams et al., 2006) attributing reversals in relative flow parameters to high velocity jets exiting riffles and entering pools. According to MacWilliams et al., (2006) the flow convergence routing hypothesis is an extension of existing development and maintenance hypotheses which includes elements of many of the previously published theories (Keller, 1971, Clifford and Richards, 1992; Thompson, 2001). Moreover, MacWilliams et al., (2006) claims that many of the primary references pertaining to the velocity reversal hypothesis feature flow constriction and / or convergence thereby providing implied support for the hypothesis. The requirement of a channel construction to produce a high velocity jet through the pool elements of a sequence however presupposes that all riffle-pool sequences are forced sequences as opposed to those formed without the presence of an upstream constriction. The distinction between forced and free formed riffle-pool sequences has yet to be adequately explored in existing literature specifically with reference to the respective development and maintenance processes.

An additional criticism is that the principal focus of investigations relating to the development and maintenance of riffle-pool sequences has concentrated on section averaged flow parameters and has therefore failed to consider the unique features of individual riffle-pool sequences (longitudinal and lateral channel structure, discharge regime, bank stability, vegetation and the ability of the channel to migrate vertically and horizontally). This has provided research that has sought to standardise many riffle-pool sequences returning often contradictory results and over-simplified explanations of development and maintenance processes.

Acceptance of this periodicity is not however universal, Thompson et al., (2001) for example warns that these findings have limited theoretical justification in gravel-bed river systems since it is difficult to quantify a spatial periodicity to a bedform arrangement which develops from irregularly distributed channel constrictions. Lofthouse and Robert (2007) determined that overall channel curvature increased pool length relative to riffle length demonstrating that additional research is required which examines riffle-pool sequences periodicity in meandering and straight channels separately. Clifford (1993) considered the relevance of statistical methods utilised to describe any identified periodicity in large-scale flow structures suggesting that the model inter-riffle spacing is a more appropriate scaling relationship. Thompson et al., (2001) supported this view when writing that the definitions and methods used to define these features seem to be at least partly responsible for variation within measurement of riffle-pool sequences.

The lack of consistent definition is also evident in the measurement of channel width. Cherkauer (1973) acknowledging this limitation introduced the concept of 'effective width', which corresponds to only the active zone of flow (Clifford and Richards, 1992). The definition of effective width was reinterpreted after the work of Thompson (2004) to include forced riffle-pool sequences, the implication being that effective channel width is the area of flow that will convey the flow capable of scouring bed material (Harrison and Keller (2007). Harrison and Keller (2007) incorporated effective width into two-dimensional flow modelling by specifying that it is represented by 90% of the highest modelled flow velocities. A genuine independent method for the measurement of effective flow width is yet to be established however as a concept, effective width offers the potential to standardise the description of channel width, cross-sectional area and periodicity in riffle-pool sequences.

According to Harrison and Keller (2007) the most widely utilized approach to the study of riffle-pool sequences has been based on analysis of hydraulic parameters with the reversal hypothesis receiving considerable attention (Lane and Borland, 1954; Keller, 1971; Lisle, 1979; Andrews, 1982; Carling, 1991; Keller and Florsheim, 1993; Carling and Wood, 1994; Thompson et al., 1996; Booker et al., 2001; Milan et al., 2001). Wilkinson (2004) however reported that only four studies actually observed the occurrence of a velocity reversal; Lisle (1979), Andrews (1982), Booker et al., (2001) and Milan et al., (2001). This is largely due to the limited spatial and temporal resolution of field evidence used to test reversal theories (Thompson, 2001). MacWilliams et al., (2006) also highlighted the growing recognition that section averaged data are not sufficient to explain the complex flow interactions that occur throughout riffle-pool sequences. The collection of more detailed spatial and temporal data at the full range of discharge conditions would improve the current understandings of riffle-pool sequences, however it may not prove feasible, especially, when synchronous measurements of the whole field are required (Cao et al., 2003).

The limitations of traditionally acquired point measurements were considered by Clifford and Richards (1992) when stating that the interpretation of hydraulic contrasts between riffles and pools obtained at a single point will not be meaningful. Since the flow distribution changes with discharge at all sections, measurements taken at a single fixed point should be interpreted in different ways at different sections and at different times (Clifford and Richards, 1992). Clifford and Richards (1992) also determined that additional difficulties arise with inferences based upon mean cross-section velocities. A reversal or absence can be demonstrated simultaneously depending upon the cross-section chosen for comparison between riffles and pools, the kind of measurement made, and the point within the section at which the measurement is made. Similarly, Richards (1976) highlighted that quantative measures for defining riffle and pools sections are lacking, largely because most attempts to develop a criterion rely on mean flow parameters. It is perhaps the pre-determined whilst often random (based on access / safety issues) data acquisition patterns that lead Carling (1991) to conclude that the use and extrapolation of conventional hydraulic geometry relationships is inappropriate for describing the flow behaviour through riffle and pool sections, especially at higher discharges where appropriate measurements are lacking.

According to Milan et al., (2001) comparisons of the results of different studies are complicated by varied sampling strategies and methodologies. Problems arise particularly because; (a) the majority of investigations consist of measurements performed in low to medium flow conditions with virtually no measurements at high discharges (b) there is often poor consistency between reach sizes and the number of riffle and pools considered (with many studies focused on either single riffle-pool pairings or non-consecutive riffles and pools) (Clifford and Richards, 1992) (c) a range of measurements techniques and values have been used to characterise the flow.

2.3 Global Positioning System (GPS)

It is clear from the review of literature referencing riffle-pool sequences that several fundamental questions remain to be addressed and that these questions have not, or cannot, be answered with existing data acquisition methods and therefore currently available data. Similarly evident from the literature relating to currently utilised flow measurements methods, has been the inadequacies of measurement techniques, particularly those used in gravel-bed environments and at higher discharge conditions. Concurrently there has been a recent move towards data acquired utilising remote sensing methods, particularly in fluid environments through the use of drifter buoys.

The potential therefore remains that if a drifter buoy could be engineered and applied to natural river environments, greater spatially distributed data from a wider range of environments and discharge conditions could be gathered. Drifters however, could only be applied to natural river environments if they can be made sufficiently small to allow passage through the channel, sufficiently robust to accommodate submergences and collisions, and sufficiently accurate to provide detailed position and velocity measurements. The movement towards drifter acquired data in oceanography and climatology has been in part facilitated by the incorporation of GPS receivers in drifter buoys. The incorporation of a GPS receiver into a river drifter presents the only viable option for the measurement of sufficiently accurate position and velocity data. The question therefore remains; is a GPS receiver suitable to be used to measure positions and velocities in a natural river environment?

2.3.1 Description

The Global Positioning System (GPS) is a satellite based navigation system which provides three-dimensional positioning to a limitless number of receiver units positioned anywhere on or above the earth's surface. The GPS performs triangulation between satellites and the receiver unit to calculate positions. The GPS incorporates three elements, the space segment, the operational system and the receiver unit. The space segment comprises a network of 24 orbital satellites to provide continuous global coverage with four to eight simultaneously observable satellites above 15° elevation (Hofmann-Wellenhof et al., 2001). The functionality of the system is controlled by a series of five relay / base-stations providing operational information and correction date for the position, internal configuration and most importantly the atomic timing of each orbital satellite (Hofmann-Wellenhof et al., 2001). Access to the system is then provided through the use of a variety of commercially available GPS antennas and receivers.

2.3.2 Operation

In order to calculate position, GPS receivers measure the length of time that an emitted satellite signal takes to arrive at its location. Based on knowing that the signal travels at the speed of light, the distance between a satellite and the receiver can be calculated, generating a sphere of possible locations. Acquiring the same information from a second satellite provides an additional sphere that intersects the first at a plane (DePriest, 2003). Repeating this process for a third satellite generates another sphere and provides three unknowns, (latitude, longitude, and altitude) each of which must be resolved through range equations, to calculate the true location of the GPS receiver (Hofmann-Wellenhof et al., 2001). As a result of the differences in the accuracy of the true GPS atomic time and the internal clock of each GPS receiver a series of pseudoranges develop in the three unknown dimensions. Therefore, four simultaneously measured pseudoranges (and therefore satellites) are required to calculate the three components and address the offset from GPS timing (El-Rabbany, 2002). With each additional satellite used for positioning, the more accurate the solution to these pseudoranges will be. Geometrically, the solution to these pseudoranges is returned by a single smaller sphere whose centre lies at the exact unknown position (Hofmann-Wellenhof et al., 2001). These calculations are achieved by utilizing the ephemeris and almanac data contained and constantly transmitted in the GPS satellite signals. The ephemeris data provides information about the status of the satellite; the current date and time, whilst the almanac data defines the location of each satellite relative to each other at any given time (Hofmann-Wellenhof et al., 2001).

2.3.3 Velocity Calculation Methods

The determination of instantaneous velocity from a GPS system is achieved through the use of the Doppler Effect which refers to the phase shift that occurs between the position of the receiver at the time when the signal is emitted from the satellite and ultimately received (Witte et al., 2004). According to Hofmann-Wellenhof et al., (2001) this phase shift is proportional to the relative radial velocity of both the receiver and a satellite and since the radial velocity of the satellite is known the velocity of the receiver can be calculated. Equations utilizing four Doppler effects are required to solve the three dimensional components and time pseudoranges. The precise methods of data processing utilised to return Doppler calculated velocities are unique to each GPS provider and unknown since they are protected due to commercial confidentiality and intellectual property rights.

Adrados et al., (2002) describes how no independent attempt had been made to assess the ability of a non-differential GPS system for determining the velocity of a moving body. Although manufactures quote achievable accuracies around 0.1-0.2 ms^{-1} this cannot easily be assessed since commercial confidentiality prohibits the release of the relevant calculation algorithms. From experimental work with the movement of bicycles, Witte et al., (2004) demonstrated that speed determined by a GPS receiver was within 0.2 ms^{-1} of the true speed for 45% of the data with a further 19% of values within 0.4 ms^{-1}. It was also found that a general underestimation of the true velocities was noted. In terms of movement around a curve an initial overestimation of speed was frequently found followed by an underestimation for subsequent movements. This is due to the Kalman filter employed to remove the effects of corresponding satellite orbital velocity in all Doppler velocity calculations, which predicts an observation from previous measurements and corrects its prediction parameters by comparing it to the actual observations (Witte et al., 2004). Although filtering of this type is very effective in improving the quality of positioning it is likely responsible for the "overshoot" phenomenon which is often a feature of GPS navigation when rapid course deviations occur or satellite signal is lost. Witte et al., (2004) concluded that the GPS is an accurate means of determining speed over ground when moving at relatively constant speeds in straight lines and is competent at determining speed on curved paths, although there are occurrences of overestimations during transitions between straights and bends. It is further described that absolute error increases slightly at higher speeds (Witte et al., 2004).

In addition to measuring the Doppler shift for the calculation of velocity, it is possible to utilise changes in GPS assessed positions to independently calculate velocity based on specified time periods. Though the integrity of these values is based upon the precision of each position, the methods utilised to calculate velocity can be independently assessed unlike the commercially sensitive and highly protected Doppler calculation approaches. Accessing the NEMA code (the language in which GPS signal is transmitted) in its initial form, provides the potential for such independent velocity calculations (v_t) based upon the two perpendicular horizontal components at time t (u_{Nt} and u_{Et})

$$u_{Nt} = \frac{N_{t+\frac{\Delta t}{2}} - N_{t-\frac{\Delta t}{2}}}{\Delta t} \qquad \text{Equation 1}$$

$$u_{Et} = \frac{E_{t+\frac{\Delta t}{2}} - E_{t-\frac{\Delta t}{2}}}{\Delta t} \qquad \text{Equation 2}$$

$$v_t = \sqrt{u_{Et}^{\;2} + u_{Et}^{\;2}} \qquad \text{Equation 3}$$

where N_t and E_t are the GPS positions in the northerly and easterly directions respectively at a given time t and Δt is the time difference between position measurements (Stockdale et al., 2007).

2.3.4 Indicators of the Quality of GPS Measurements

The accuracy of the GPS for both positioning and velocity measurement is determined by four factors; the number of visible satellites from which theoretical spheres can be generated, the geometric arrangement of the orbital satellites relative to each other and the receiver units (this is quantified by an internally calculated value – dilution of position (DOP)), the configuration of the environment in which the receiver is utilised and the atmospheric and climatic conditions which occur between the satellites and the receiver.

Two indicators of the quality of GPS measurements are internally calculated. The first is the number of visible satellites which provides the key component to the operation of the global positioning system. Without the minimum required four visible satellites the GPS will fail to return a complete position or velocity measurement. With each additional visible satellite the accuracy of the global positioning system improves, therefore any external factor which limits the number of visible satellites will inherently be detrimental to the operation of the GPS (El-Rabbany, 2002). An additional indicator of the integrity of GPS measurement is provided by the geometry of the overhead satellite constellation. According to El-Rabbany (2002), with improving satellite geometry, the positions and velocities obtained by the GPS are increasingly accurate. The quality of satellite geometry is measured by a single dimensionless number called the dilution of precision (DOP). The DOP number is computed based on the relative receiver-satellite geometry calculated from the coordinates of both the receiver and the satellites allocated to each receiver channel. The lower the DOP value the greater the integrity of GPS positioning and velocity measurement. A measure of the integrity of positioning (easting and northing) is provided by the Horizontal Dilution of Precision (HDOP) (Fig 2.32). According to El-Rabbany, 2002, DOP values below five are generally sufficient to provide accurate results, however optimal conditions occur with DOPs below two.

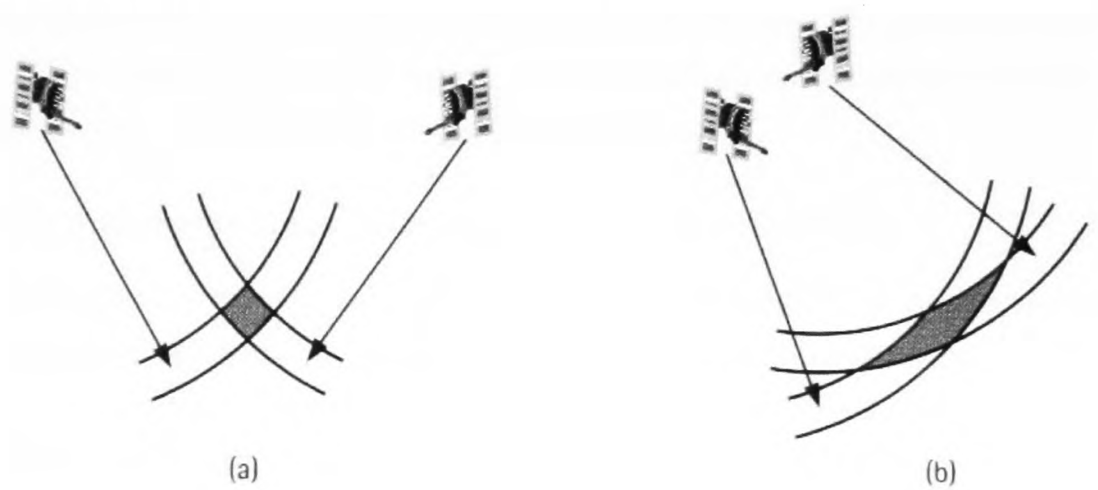

Figure 2.32 Graphical explanation of the effect of satellite geometry using two satellites. The shaded areas represent the area of uncertainty within which the GPS receiver can lie, due to the geometry of the satellites. If the two satellites are positioned wider-apart then the area of uncertain becomes smaller returning a lower HDOP values (a) while the reverse is true of more tightly distributed satellites (b).

Witte et al., (2004) acknowledged that satellite geometry is regarded as having a major influence on the accuracy of GPS positional data and hence speed determination. However, under the conditions of experimentation Witte et al., (2004) found that satellite geometry had only minor effects on the accuracy of speed determination. Similarly, despite increasing HDOP values occurring with reducing satellite numbers, there was no significant effect on speed accuracy (Witte et al., 2004). The deviation from the theoretically expected relationships observed in Witte et al., (2004) can potentially be attributed to the insufficient number of visible satellites failing to allow the manifestation of difference in accuracy (maximum number of satellites was six) and insufficient sensitivity to HDOP values since the minimum category was <= 5. Therefore, the results provided by Witte et al., (2004) fail to provide definitive explanation of whether satellite number and / or HDOP values could be used to filter data for the improvement of positioning and velocity measurement.

2.3.5 Sources of GPS Error

In the investigation of GPS provided positioning and velocity measurements a series of experimental and processing errors can occur which are detrimental to the integrity of the emitted results. These errors can be broadly classified into three groups; (i) errors that can be avoided, removed or reduced, (ii) errors that can be measured and accounted for, and (iii) errors that are beyond control or measurement.

2.3.5.1 Errors that can be Avoided, Removed or Reduced

The position of the receiver unit relative to the configuration of its surrounding environment influences the number of visible satellites from which the receiver can calculate position. Additionally, the clarity of the path between the receiver unit and the orbital satellites is highly important to the integrity of GPS performance.

The presence of large buildings, varied terrain and dense vegetation can block or effect signal reception (Garmin, 2000). The clearer the view of the sky, the larger the satellite mask (the angle below which the receiver antenna can view satellites) and the greater the number of satellites which can be utilised for position and velocity calculations. As previously described, GPS performance improves with increasing numbers of visible satellites. In addition to the number of visible satellites their orientation with respect to the receiver unit determines the quality of GPS performance. A widespread distribution across the sky improves triangulations and therefore the accuracy of position and velocity measurements and is represented by a lower internally calculated HDOP value. In addition to limiting the passage of emitted satellite signals, large buildings and other obstacles (particular metallic or reflective) can cause signal multipathing. This occurs when the incoming satellite signal rebound from external surfaces thereby altering the relative geometry of the emitting satellite to the receiver unit and falsifying the position results produced (Leick, 2004).

Signal blockage, loss and / or multipathing are all examples of error which can be avoided or reduced through the selection of suitable environments prior to testing or removed through the selective filtering of data during analysis. The potential of improving the performance of the GPS through post-process data filtering using either the number of visible satellite or HDOP values will be considered later.

2.3.5.2 Errors that can be Measured

A variety of errors may occur in the process of calculating GPS positions and velocities. The principal error and one that is itself utilised as a mechanism for calculating position is the deviation between satellite (atomic) time and the time measured by the internal clock of each GPS receiver. Though corrected through pseudorange equations, if minor timing errors occur at the satellite they become magnified due to the distances covered by the emitted satellite signals on their path towards the receiver (Pace et al., 1995). Additional errors can occur by virtue of the discrepancies in the satellite's orbital paths. These ephemeris errors can cause the receiver to falsify the location of the origin of the coded signal it receives and miscalculate the location of the satellite and inherently the position and velocity of the receiver unit (Pace et al., 1995). These errors can and are constantly measured by the GPS control base station and frequently corrected in order to improve GPS performance.

Additional errors occur as the result of ionosphere and troposphere delays. These errors occur as the satellite signals slow as they pass through the earth's atmosphere, a phenomenon intensified by precipitation, and though the satellite and receiver units both make modelled adjustment to the results, inaccuracies often remain (Garmin, 2000).

The magnitude of each of these errors is temporally and spatially specific so cannot be accessed relative to the performance of a moving GPS receiver. However, through the use of a stationary GPS receiver it is potentially possible to determine how likely a particular period of time, at a particular location is to allow "good" or "bad" GPS performance. Identification of periods of degraded GPS performance could again potentially be utilised as a filtering mechanism for improving overall GPS performance.

2.3.5.3 Errors that are Beyond Control or Measurement

The operation and accessibility of the GPS prohibits direct measurements of the effects of individual sources of error emanating from ionosphere and troposphere delays, offsets in receiver and atomic timings, ephemeris deviations and signal multipathing. Though it is possible, as previously described, to assess the collective effect of these errors upon the precision of positioning from the use of a stationary unit, the intended use of GPS receivers in this research requires the assessment of positions and velocities from a moving receiver. This further complicates the assessment of errors since the location and therefore satellite conditions and environmental configuration are constantly changing. Further, the effects of turbulence upon GPS performance cannot directly be measured. Therefore additional research will be presented which assess the operational limitations of the GPS for both positioning and velocity measurement to establish parameters within which the large-scale flow dynamics in natural river systems can be measured.

2.3.6 Extensions to the Global Positioning System

2.3.6.1 Differential Global Positioning System (DGPS)

When initially introduced the GPS was designed solely for military use and as a result the American Government applied "selective availability" to the system whereby it was only available to the public with limited precision, degrading the accuracy of position and velocity measurements. The enforcement of selective availability on civilian GPS necessitated the need for a means of improving the operation of standard GPS receivers – the solution was provided by differential GPS (dGPS). Differential GPS (dGPS) enhances the positional accuracy of GPS receivers based upon the calculation and transmission of error correction signals from base stations located at known positions (Witte et al., 2005). With the addition of a local beacon and carrier-wave phase differentiation, dGPS can improve positioning to within centimetres (Schutz et al., 2000). The cost, size and complexity of dGPS however prohibit the use of such systems in the majority of field investigations, specifically in adverse or remote environments. Despite offering potentially improved performance these properties would clearly prohibit the use of dGPS in drifter buoys. Following the removal of selective availability on May 1st 2000 the potential of utilising a satellite based approach to dGPS was introduced through the creation of the wide area augmentation system (WAAS).

2.3.6.2 Wide-Area Augmentation System

The Wide-Area Augmentation System is a satellite-based dGPS, potentially providing dramatic improvements in positioning and velocity measurements, within the same simple, cheap and lightweight GPS receivers (Witte et al., 2005). The Wide-Area Augmentation System is a group of unique geostationary satellites, which relay correction data collected by a set of ground stations positioned across the globe (Witte et al., 2005). Each ground station collects clock, ephemeris (satellite position), and ionosphere corrections (upper atmosphere) and formulates this information relaying it to a series of additional GPS satellites. Each of the WAAS enabled satellites provides this information through two automatically allocated receiver channels (11 and 12) present within WAAS enabled GPS receivers (GPS, 2006). The WAAS satellites therefore act in the same way as the base station of a dGPS, correcting the receiver errors which have occurred in the timing of emitted satellite signals.

Witte et al., (2005) quantified the use of WAAS-enablement for the assessment of speed over ground finding that 57% of results were within $0.2ms^{-1}$ and 82% of values were within $0.4ms^{-1}$ of the actual observed speed (Witte et al., 2005). These values represent dramatic improvements from those observed when utilising non-WAAS enabled GPS receivers. Despite the addition to the literature offered by Witte et al., (2004 and 2005) the accuracy with which GPS can be utilised to measure both positions and velocities within natural river systems remains to be addressed, as does the effect of WAAS-activation upon the relative accuracy of these measurements. Additional research is necessary since no similar validation has been attempted on the performance of GPS for the measurement of positions and velocities in natural river environments and not at the significantly lower velocities likely to be observed within the study of river flow dynamics ($0.0 - 3.0\ ms^{-1}$).

2.3.7 Summary

The use of a GPS receiver provides the potential to measure accurate positions and velocities anywhere on the earth's surface. The selection of a WAAS-enabled receiver theoretically offers dramatically improved positioning within the same cheap, lightweight GPS receivers. There however remain several potential difficulties associated with the use of GPS receivers within natural river environments. The steep slopes and channel banks present in the majority of upland river environment would dramatically increase the angle of the satellite mask, therefore limiting the number of visible satellites and the quality of over-head satellite geometry relative to the GPS receiver. Additionally, signal blockage and multipathing would be a likely result of dense bank vegetation or channel crossing bridges which would again be detrimental to the quality of GPS measurements.

The performance of GPS for the measurement of positions and velocities in natural river environments could potentially be improved through the use of post-data-capture filtering. Filtering the collected data based on the previously outlined quality indicators (satellite number and hdop value) provides the potential of minimising or removing the effects of the previously outlined errors. The precise relationships between the accuracy of positioning and velocity measurements and satellite number and HDOP value do however require further independent consideration. Additionally, the ability of GPS (and WAAS-activation) must be considered relative to the significantly lower velocities likely to be observed in the investigation of surface flow patterns in natural river environments.

3 Method

Chapter three comprising seven linear sections spanning the initial concept and development of the GRiFTer, introduces the concept of cellular flow representation, determines the appropriate approach to position and velocity measurement, establishes confidence intervals for GPS performance and validates GRiFTer performance against a comparable velocity measurement method.

3.1 The Concept and Development of a GPS River Flow Tracer

The use of traditional invasive flow measurements is limited in a number of different flow environments, particularly in extremely high or low discharge conditions (Carling, 1991). For example, at high discharges there can be difficulty gaining access to the channel safely. The use of invasive methods is also limited in high sediment, high vegetation and high velocity flows (Ferguson et al., 1989, Carling, 1991). Invasive methods typically provide point measurements which are detached from the dynamic nature of river flow and there can be difficulties performing measurements close to channel boundaries.

Large Scale Particle Image Velocimetry (LSPIV) has the potential to address many of these difficulties (Costa et al., 2000; Creutin et al., 2003; Muste et al., 2005) but can only be used where sufficient natural light permits the capture of complete images (Ettema et al., 1997) and where the reach is suitable to allow adequate particulate seeding of the water surface (Ettema et al., 1997). Irrespective of these issues, equipment installation and measurement procedures remain complex and costly, especially where reach scale measurements are desired.

The inadequacies of current measurement methods have left significant gaps in the available data pertaining to large-scale flow phenomenon in natural formed gravel-bed river systems, particularly with reference to riffle-pool sequences where the majority of investigations have focused on low to medium discharge conditions. In addition to the inadequacies highlighted in the range of discharge conditions investigated, existing literature has also highlighted that the interpretation of hydraulic contrasts obtained at a single point will not be meaningful (Clifford and Richards, 1992) and that section averaged data are insufficient to explain the complex flow interactions that occur throughout riffle-pool sequences.

The growth in the use of drifter buoys for remotely sensed data acquisition and recent developments and adaptations of drifter principles to lakes, estuaries and the surf zone highlighted the potential of creating a drifter suitable for deployment in natural gravel-bed river environments (Johnson et al., 2003). Improvements in GPS technology and commercially available integrated GPS receivers and data recording units allowed for the development of a GPS river flow tracer (GRiFTer) (Stockdale et al., 2007). A GRiFTer provides the potential to solve many of the issues / limitation of data acquisition in natural river environments and therefore the understandings of large-scale flow phenomena and specifically riffle-pool sequences. The following section explains the development, testing and modification of the GRiFTer towards the model of the device utilised to acquire the desired experimental data.

3.1.1 Development of the GPS River Flow Tracer

3.1.1.1 GRiFTer v1.0

The initial design of the GPS river flow tracer combined a hardened nylon cylindrical outer casing that would protect the internal components, both from impact and from submergence, whilst allowing the unit to rotate and spin over submerged obstacles and around larger boulders. The internal components consisted of a GPS mounted inside the cylinder to provide positions and velocities (Garmin N17 GPS), a recording and transmitting device (Mobile Phone) and a power supply (PP9 battery) (Figure 3.1). The Windows CE mobile phone (Orange SPV E200 Windows CE Mobile) provided a platform for recording and storing data and gave the potential of data transmissions. Custom designed software contained within the mobile phone performed real-time calculations of GPS emitted NEMA code, returning times and positions in British National Grid co-ordinates. To ensure that the GRiFTer v1.0 behaved as close as possible to the body of water that its presence displaced, the cylinder had 1 kg additional weight added to achieve neutral buoyancy.

Figure 3.1. The GRiFTer v1.0 comprised a cylindrical nylon outer casing housing a GPS antenna, Windows CE mobile phone utilised for data collection and transmitting, additional weight and a power supply.

To test the GRiFTer v1.0, it was deployed on the River Hull (Figure 3.2a) using a floating rope tether to allow ease of recovery and ensure the unit was not lost (Figure 3.2 b). This initial field test was designed to consider the water-following capabilities of the GRiFTer v1.0, the ease of recovery, and the operation of the calculation software.

The GRiFTer v1.0 was initially deployed from a road bridge crossing the river, then further downstream from a lower part of the channel bank. The successful return of results from such deployment methods highlights the potential for the use of the GRiFTer v1.0 in hazardous and inaccessible environments (Figure 3.2). Upon entry into the channel the GRiFTer v1.0 migrated laterally across the channel orientating itself within the thalweg of the channel flow and appeared to flow at velocities close to those observed through the movement of surface debris. This is further supported by the lack of wake appearing in front or behind the GRiFTer v1.0 (Figure 3.2a) suggesting that the tracer was accurately tracking the flow.

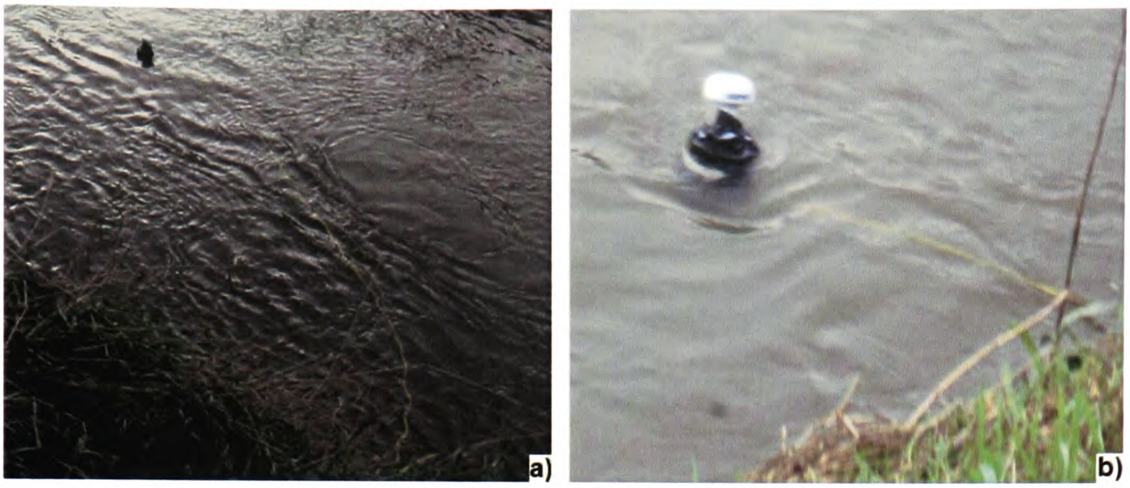

Figure 3.2 Images taken during the initial river deployments of the GRiFTer v1.0. River Hull 01.12.05. a) Movement of the GRiFTer v1.0 in the channel b) Recovery of the GRiFTer v1.0 using a rope tether.

Two difficulties were highlighted from this initial test. The first was that the unit was difficult to seal resulting in the internal components becoming waterlogged. Secondly, the customised software performed real-time calculations from NEMA coding during data collection. This produced a situation whereby any loss of connection between the satellite constellation and GPS receiver (either due to submergence, overturning or by the units passage under overhead obstacles such as bridges) resulted in the failure of the calculation software. Additionally, the software only allowed for the acquisition of position and time data meaning that many potentially informative NEMA messages could not accessed. This information could potentially be used to further explore surface flow patterns and / or define the quality of the calculated GPS data.

3.1.1.2 GRiFTer v2.0

From initial testing, the relative ease of making multiple deployments and recoveries of the GPS river flow tracer meant that the ability to transmit recorded data would not be necessary. Therefore the Windows CE mobile phone was replaced with an AntiLog serial recording device. The AntiLog downloaded all NEMA code emitted by visible GPS satellites providing access to the full range of NEMA messages and also provided a significantly greater recording capacity which would extend potential field applications (Figure 3.3). GPS information was then accessed following recovery utilising customised NEMA extraction software ensuring there was no data loss as experienced with the earlier version. Additionally, the sealing procedure was adapted to ensure the unit remained water tight when submerged.

Figure 3.3 The GRiFTer v2.0 comprised a cylindrical nylon outer casing housing a GPS antenna, AntiLog recording device utilised for data collection, additional weight and a power supply.

Initial testing of the GRiFTer v2.0 was conducted at Buckden Bridge on the River Wharfe. Testing consisted of three repeated deployments on a short meander section (Figure 3.4). Deployment was conducted by lowering the GRiFTer into the channel whilst recovery was achieved through the use of a large telescopic landing net positioned at a downstream channel constriction.

The incorporation of the AntiLog recording device in the GRiFTer v2.0 ensured that submergence or overturning of the unit only produced gaps in the data with recording recommencing once the required four satellites were again visible. Two difficulties were identified in the use of the GRiFTer v2.0; the first concerned the occurrence of grounding on the channel bed and banks whilst the second was the effects of wind steering the unit, resulting in falsified surface flow patterns. Grounding is an inherent problem with any flow tracer deployment in shallow gravel-bed rivers but was worsened due to the exterior casing measuring 0.3m in length. Although it was apparent that the cylindrical shape meant that the GRiFTer v2.0 rotated away from larger boulders when pinned, groundings frequently occurred. The effects of wind steering the GRiFTer v2.0 caused migration of the lateral flow patterns towards the outside of the meander resulting in further groundings / entanglements and disrupting the integrity of the measured flow paths. In terms of the flow following capability of the GRiFTer v2.0, no visible wake formed either in front of behind the unit demonstrating that the tracer appeared to follow the surface flow. The GRiFTer v2.0 also appeared to navigate laterally across the channel, in sheltered areas, following the dominant flow path along the reach.

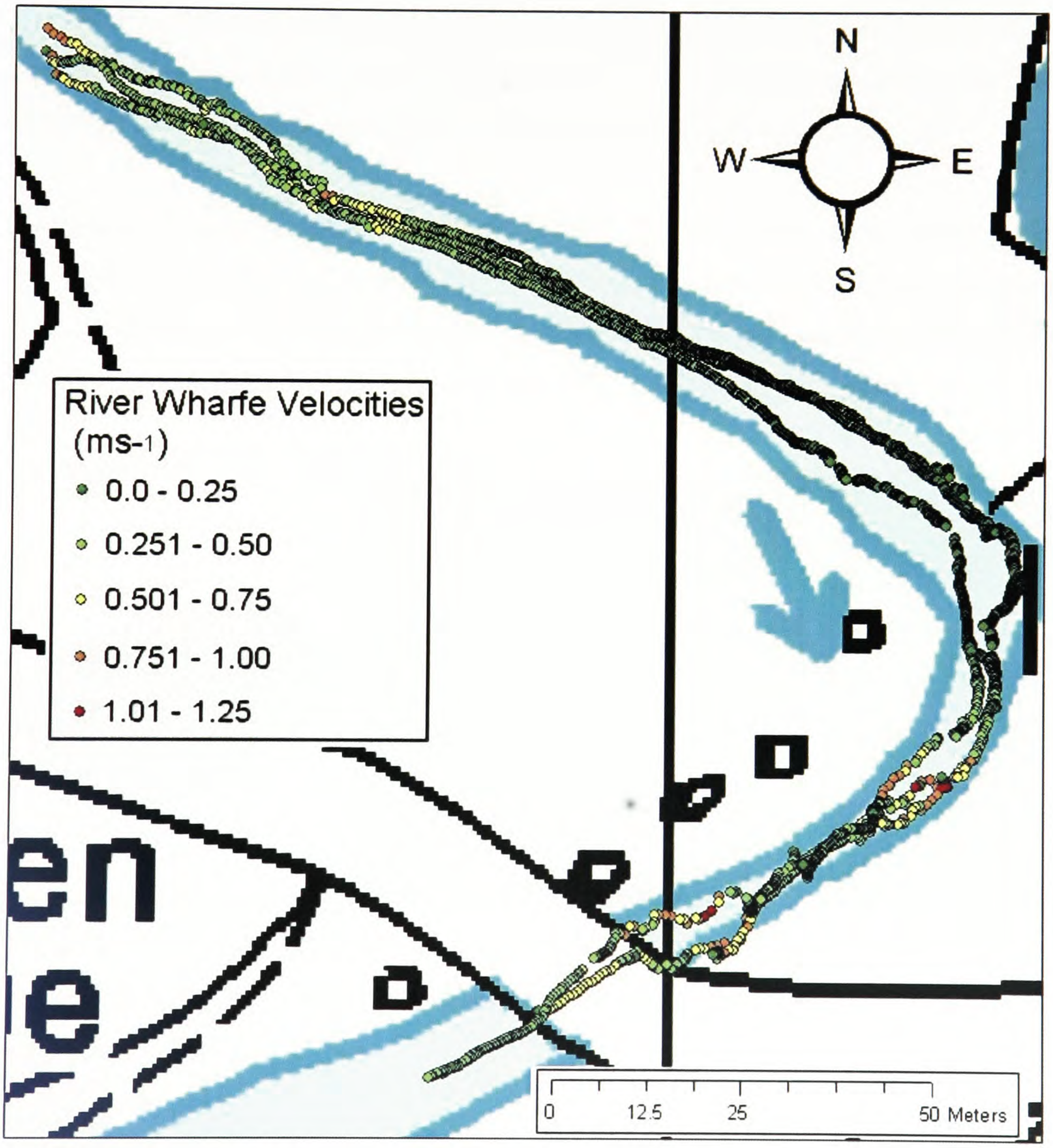

Figure 3.4 Spatial distributions of velocities from three short deployments at Buckden Bridge on River Wharfe 26/02/06 (Map from Edina, 2006).

3.1.1.3 GRiFTer v3.0

The internal components within the GRiFTer v2.0 were restrictive in terms of determining the structure and dimensions of the tracer. Therefore, in order to reduce size of the flow tracer and improve its applicability to shallow river environments an alternative component arrangement was sought. Advancing technologies allowed for the incorporation of the RoyalTek GPS Bluelogger (RGB). The RGB combines a GPS receiver and data logger with an inbuilt power supply that was configured and controlled through a Bluetooth connection. Measuring 0.1 m x 0.05 m x 0.25 m the RGB could be incorporated into a significantly smaller outer casing. The outer casing of the GRiFTer v3.0 was provided by a circular plastic container with a diameter of 0.2 m and extending to a depth of only 0.1 m. The shallower outer casing remained cylindrical to ensure it would continue to rotate away from channel obstacles (Figure 3.5).

Weighting to achieve neutral buoyancy resulted in the surface of the device being almost fully submerged, thereby removing the potential for wind effecting flow paths. The integration of the RGB also provided the most cost-effective approach to GRiFTer construction and raised the potential of introducing a flotilla of many units.

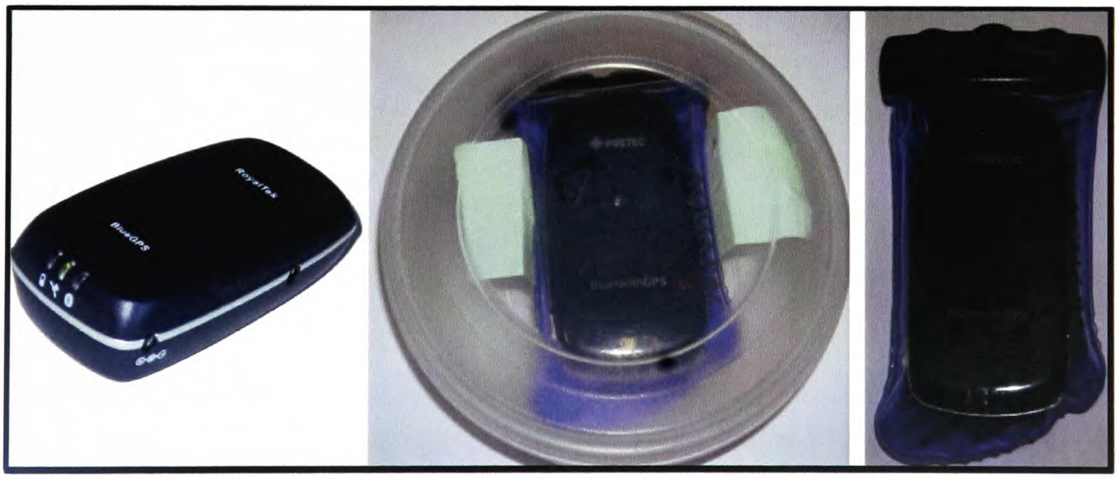

Figure 3.5 GRiFTer v3.0 components and design. The RoyalTek GPS Bluelogger was housed in a 1 litre cylindrical container with base ballasting to provide neutral buoyancy.

A flotilla of GRiFTer v3.0 was first released at Buckden Bridge on the River Wharfe (270206). Three deployment waves were conducted with the individual GRiFTers v3.0 released equally spaced across the width of the channel, upstream of the short meander section. Recovery was once again conducted on a lower part of the channel bank using a telescopic landing net (Figure 3.6).

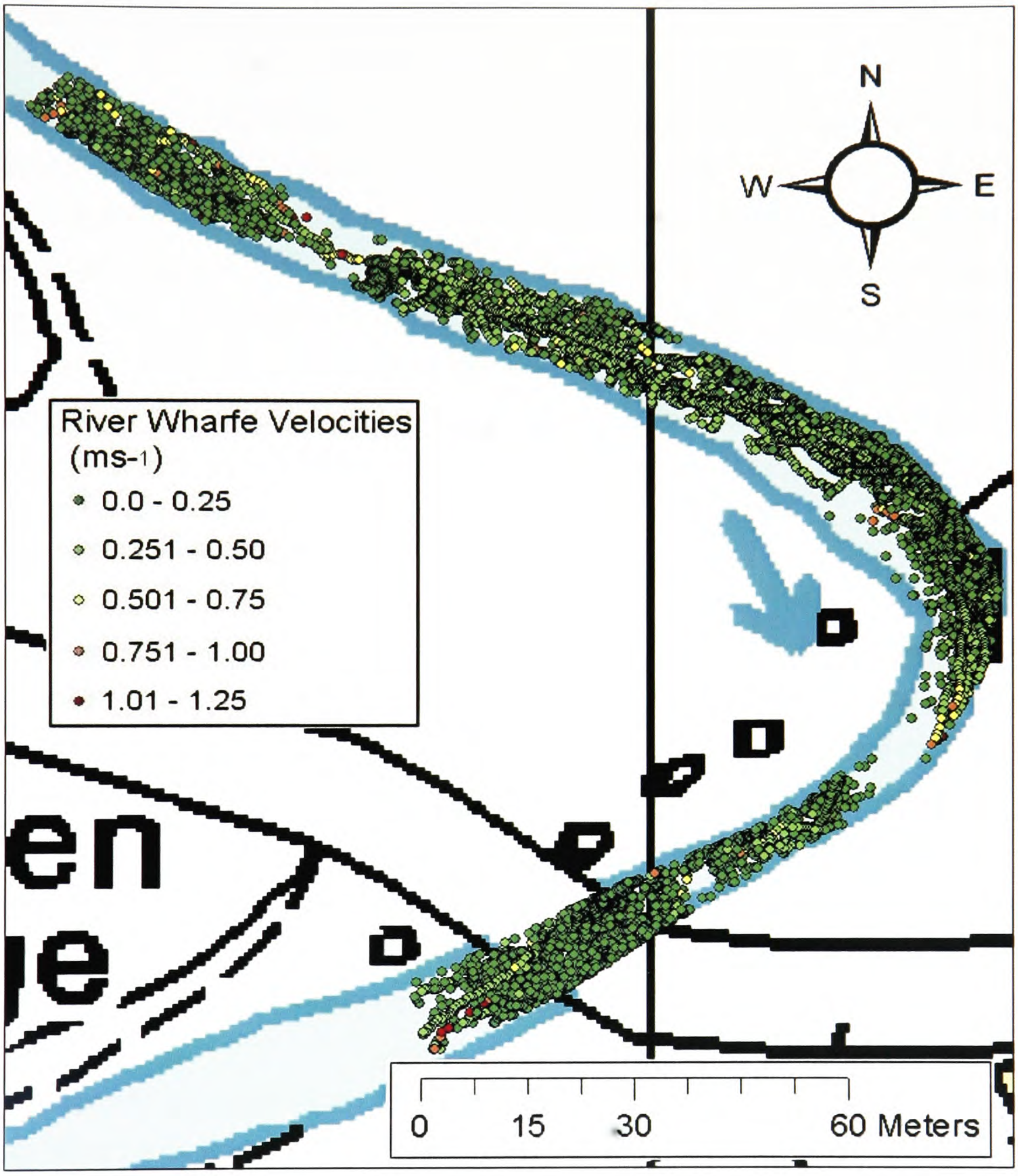

Figure 3.6 Spatial distributions of individual data points returned from three deployment waves of the flotilla of GRiFTers V3.0 – Buckden Bridge, River Wharfe 131006 (Map from Edina, 2006).

Deployment of the flotilla of GRiFTer v3.0 achieved significantly higher numbers of individual velocity results across the reach (Figure 3.6). Passage through the test reach was improved by the reduction in the depth of the GRiFTer v3.0 providing more complete flow tracks. The lower profile of the GRiFTer V3.0 also reduced the effects of wind on the integrity of measured flow patterns. The release of the flotilla of tracers highlighted that the lateral distribution of data points can be utilised to identify convergences and divergences in flow, potentially expanding the current understandings of surface flow patterns.

Two prominent difficulties remained in the use of GRiFTers for flow measurement; grounding events still occurred and the individual units were hard to identify particularly in more turbulent areas of the channel. Additionally, the size and weight of each individual GRiFTer v3.0 produced logistical problems in recovering the flotilla of devices from the channel. As a result of these limitations it was clear that a further reduction in the size and weight of individual units was required. Additionally, any future GRiFTer needed to be significantly more visible, particular in the more turbulent areas of the channel, when close to vegetation or during periods of limited visibility.

3.1.1.4 GRiFTer v4.0

The current version of the GRiFTer v4.0, comprises a RGB device incorporated within a waterproof AquaPac bag and overlaid with luminous yellow card improving visibility and detailing individual unit numbers to simplify the inventory of recovered units. Each individual GRiFTer also features a Loc8tor chip, a commercially available radio tracking device. The simplification of the structure of the GRiFTer allowed for each individual unit to measure only 0.125 m x 0.075 m x 0.35 m. The reduced size and weight of the GRiFTer v 4.0 decreased grounding events and entanglements in addition to making recovery and redeployment easier (Figure 3.7).

Widespread field testing of the flotilla of GRiFTers has been conducted at Low Roe on the River Swale (Figure 3.8). Multiple deployments have been conducted with flotillas of GRiFTers released across the channel. Specific deployment strategies are considered in section (3.2.2). Units were again recovered by a telescopic landing net but this time from within the channel. The reduced size and weight of each GRiFTer meant that the entire flotilla could be easily collected, removed and redeployed.

Figure 3.7 GRiFTer v4.0 components and construction. The GRiFTer v4.0 comprised a RGB device, AquaPac waterproof bag, luminous coloured inserts and Loc8tor tracking device.

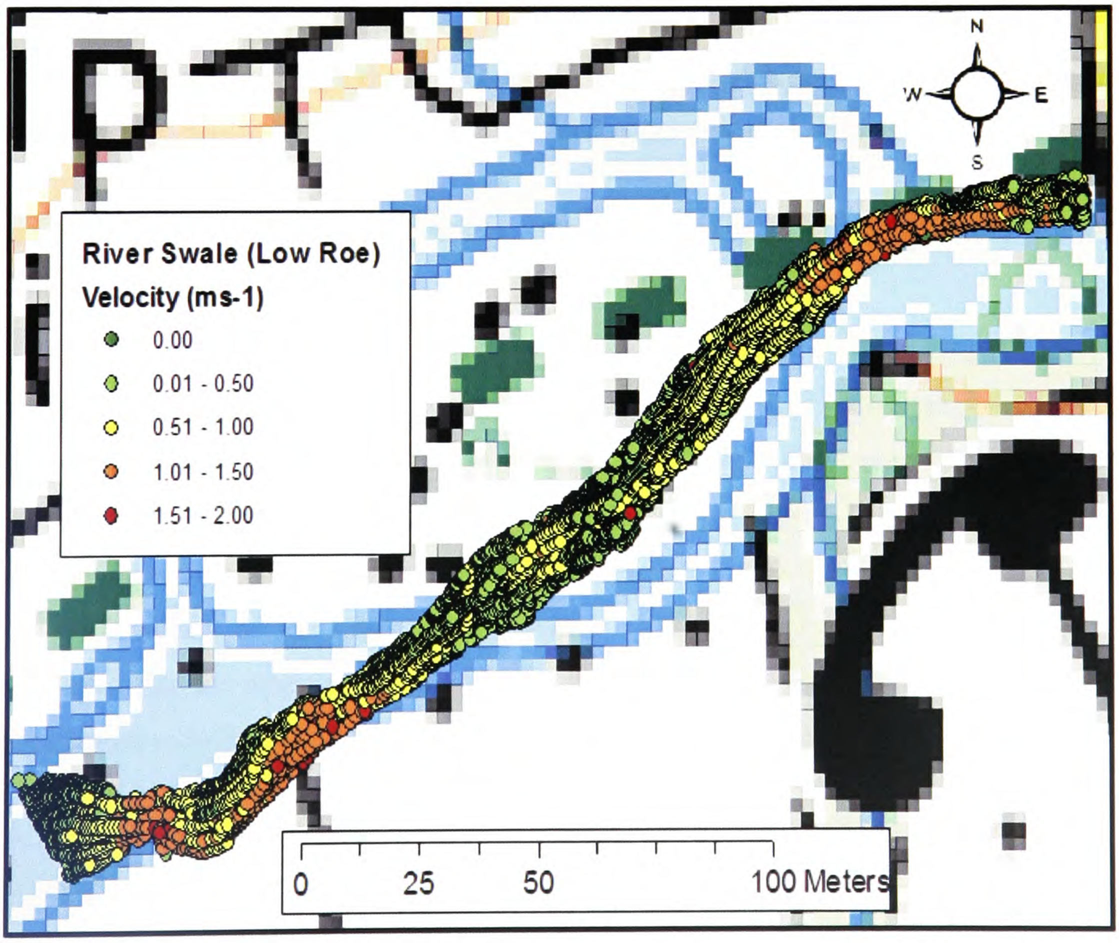

Figure 3.8 Distribution of data points throughout a 400m reach of the River Swale at Low Roe (090807) (Map from Edina, 2006).

The results presented in Figure 3.8 feature the individual data points collected from the River Swale at Low Roe on 090807. In excess of 90000 individual measurements (positions and velocities) were made within approximately 5 hours. The lower profile of the GRiFTers again reduced the occurrence of grounding and significantly aided recovery and redeployment allowing a more time efficient measurement procedure. Velocities were measured between 0.0 – 2.0 ms^{-1} with prominent areas of higher velocities observed on the outside of gentle meanders and lower velocity areas in the middle of the long straight.

The results presented in Figure 3.8 clearly demonstrates that GRiFTers can be used to provided detailed information relating to spatially distributed surface velocity patterns. Furthermore, measurements can be made through longer reaches and at significantly higher abundance and frequency than possible with earlier prototypes. Despite the structural and technical improvements made to the initial GRiFTer design, the approach still inherently suffers from submergence in highly turbulent areas of channel, grounding in the extreme shallows and entanglements in vegetation or channel banks. The potential however remains through optimal deployment strategies, GPS configuration and through the use of selective data capture and post-capture filtering techniques to maximise the results from GRiFTer flow investigations.

3.2 The Logistics of Performing a GRiFTer Based Flow Investigation

Throughout the development of the flotilla of GRiFTers, deployments were made within a variety of natural river environments. These initial tests highlighted the potential of using GRiFTers to acquire detailed information relating to spatially distributed surface flow velocities. As described previously, several factors influence the performance of the GPS receiver within each GRiFTer. These can be broadly classified into the selection of appropriate field sites, determining the appropriate field application techniques and GPS configuration and data acquisition strategy.

3.2.1 Issues Affecting the Selection of Appropriate Field Sites

The use of GRiFTers provides the potential to perform surface flow measurement in virtually all natural fluid environments and locations. The procedural ease of making measurements and the relative quality of GPS performance will however depend upon the configuration of the environment selected for measurement. The selection of ideal field sites, for the use of GRiFTers, requires consideration of the environment surrounding the channel, the structure of the channel itself and the flow regime.

- Optimal GPS performance would occur where the surrounding environment has a low topographic profile to allow for a higher number of visible satellites (optimum is an angle within 10° of the horizon).
- An absence of dense vegetation, buildings, bridges or other large obstacles would remove potential sources of signal shadowing and multipathing surfaces.
- The channel itself would ideally possess low banks to minimise signal shadowing and maximise the number of visible satellites whilst providing suitable deployment and recovery positions.
- The channel, including banks should be free from vegetation and debris which could cause unit entanglement or loss and therefore erroneous data or incomplete flow paths.
- The flow regime would ideally allow for slower / shallower sections of the channel, which could be utilised to make unit recoveries either from within the channel or from channel banks.
- Where entry into the channel is not possible an alternative recovery point, such as a bridge should be located.

Each element of the configuration of the field site must be considered prior to the selection of appropriate locations with the relative importance of each being different dependent upon the site and the aims of the specific research being conducted.

3.2.2 Deployment Strategies

Precise deployment, recovery and redeployment strategies will depend on the flow regime, discharge levels and the configuration of the test site at the specific time of investigation. Any successful deployment strategy must however provide maximum lateral and longitudinal flow coverage. In order to establish which deployment strategy most closely meets these needs, a series of field trials was conducted at Sinnington on the River Seven (Fig 3.9).

This reach was selected since it provided complex flow conditions and channel structures, and would therefore present a wide variety of channel characteristics likely to be observed in future field investigations. The principal channel feature was a large mid-channel bar located downstream from the point of deployment which produced two major flow paths. Additional complications were produced by over hanging vegetation on the channel banks and floating debris within the channel which would cause unit entanglements and the return of incomplete flow tracks. Measurements were also conducted during low flow conditions which increased the potential of grounding events.

Four different deployment strategies were tested during field investigation (Figure 3.9) with 21 GRiFTers released in each deployment. The cluster approach (Figure 3.9a and 3.14a) featured the units deployed in a single large group in the centre of the channel (Figure 3.10), the wave approach (Figure 3.9b and 3.14b) utilised 3 groups of 7 GRiFTers spaced evenly across the entire width of the channel and interspaced at 1 minute intervals (Figure 3.11), the chain deployment (Figure 3.9c and 3.14c) featured a continuous longitudinal line of GRiFTers deployed at the channel thalweg (Figure 3.12) and the line approach (Figure 3.9d and 3.14d) which consisted of a single line of GRiFTers tightly spaced across the channel (Figure 3.13).

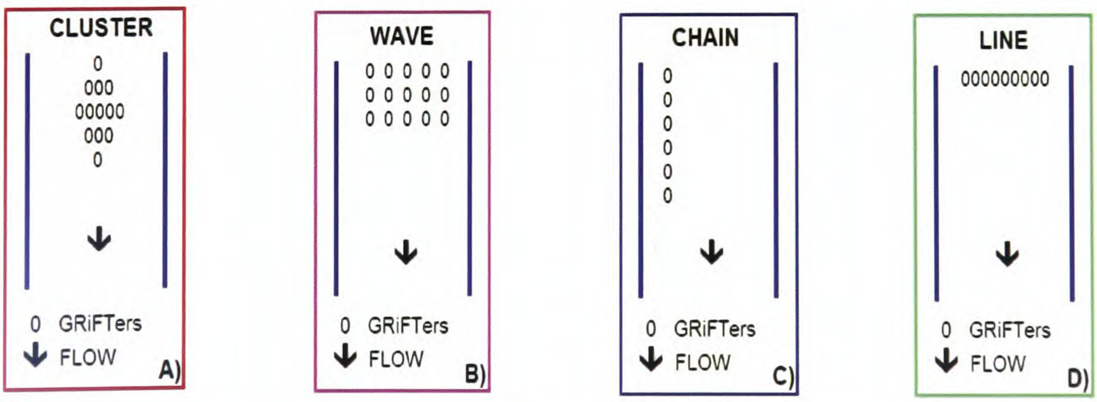

Figure 3.9 Schematic of drifter deployment strategies.

Figure 3.10 GRiFTers deployed at Sinnington (River Seven) in Cluster formation.

Figure 3.11 GRiFTers deployed at Sinnington (River Seven) in Wave formation.

Figure 3.12 GRiFTers deployed at Sinnington (River Seven) in Chain formation.

Figure 3.13 GRiFTers deployed at Sinnington (River Seven) in Line formation.

Figure 3.14 demonstrates that full longitudinal flow coverage was returned by all deployment techniques however significant differences occurred with the degree of lateral coverage. The cluster and chain deployment strategies provided limited lateral flow coverage, with improvements made by the line approach; however the best lateral coverage was achieved by the wave approach (Figure 3.14). The difference between lateral flow coverage returned by the wave and line approach can potentially be explained by the increased sensitivity to fluctuations in flow velocities when using a time staggered approach. Furthermore, both the wave and chain approaches have the advantage that, by spanning a greater time period over which deployment occurs they provide a more complete temporal representation of the surface flow dynamics of a particular reach. The greatest density of data points was provided by the chain approach however, lateral coverage was minimised suggesting that deployment in the thalweg would provide excellent coverage of this line of flow but fail to respond to lateral migrations or movement between flow paths. The specific method of GRiFTer deployment will depend on the requirements of specific field investigations. For entire reach scale investigations, as required for this research, the wave approach provides the best method for maximising longitudinal and lateral data coverage.

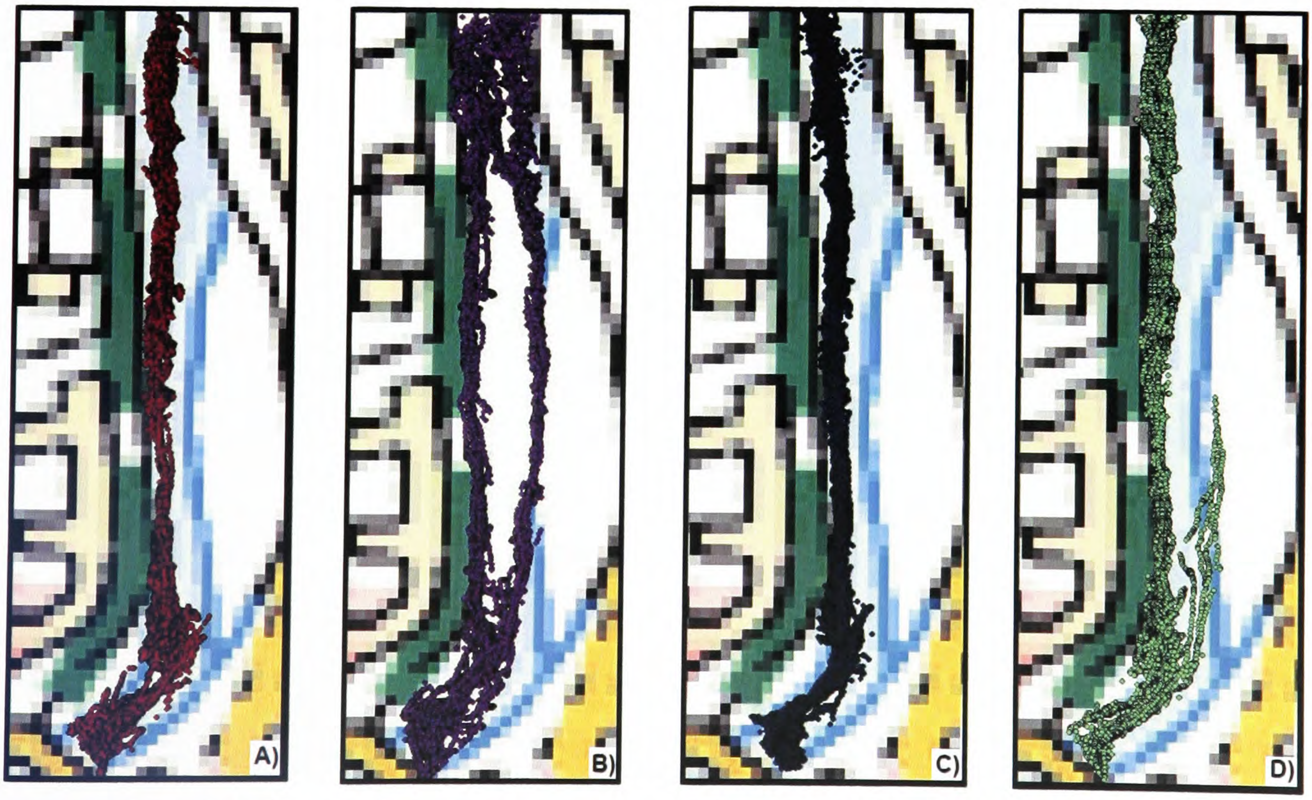

Figure 3.14 Distribution of positions returned from each GRiFTer deployment strategy. (A - Cluster, B - Wave, C - Chain, D - Line).

3.2.3 Recovery Techniques

Having determined that the "wave" deployment strategy provides the best approach to maximising data coverage, it remained to be established how best to recover GRiFTers from the channel. The simplest approach is to use a telescopic landing net positioned either on a low channel bank (Fig 3.15) or within the channel itself (Figure 3.16). Recovery from the channel downstream of the reach of interest ensures that the presence of individuals or equipment within the channel does not affect individual data points or resultant flow patterns within the reach being observed. Netted methods of recovery become difficult in flood events or in extremely large, fast or deep parts of the channel. To overcome these difficulties, recoveries have been conducted from channel spanning bridges (Figure 3.17) or by using kayaks within the channel.

The potential to net entire widths of the channel was also explored for suitable locations how this was not required at the site / conditions utilised for data aqusition in this research. Upon recovery of the GRiFTer units, each is deactivated and stored until the entire flotilla is collected then returned to the start of the channel, reactivated and then redeployed. On occasion where units cannot be netted and are lost downstream, the loc8tor chips within each GRiFTer can be activated and searched for independently utilising a unique unit reference number.

Figure 3.15 Recovering GRiFTers from low platform at Sinnington using a telescopic net.

Figure 3.16 Recovering GRiFTers from within the channel using a telescopic net at the River Swale.

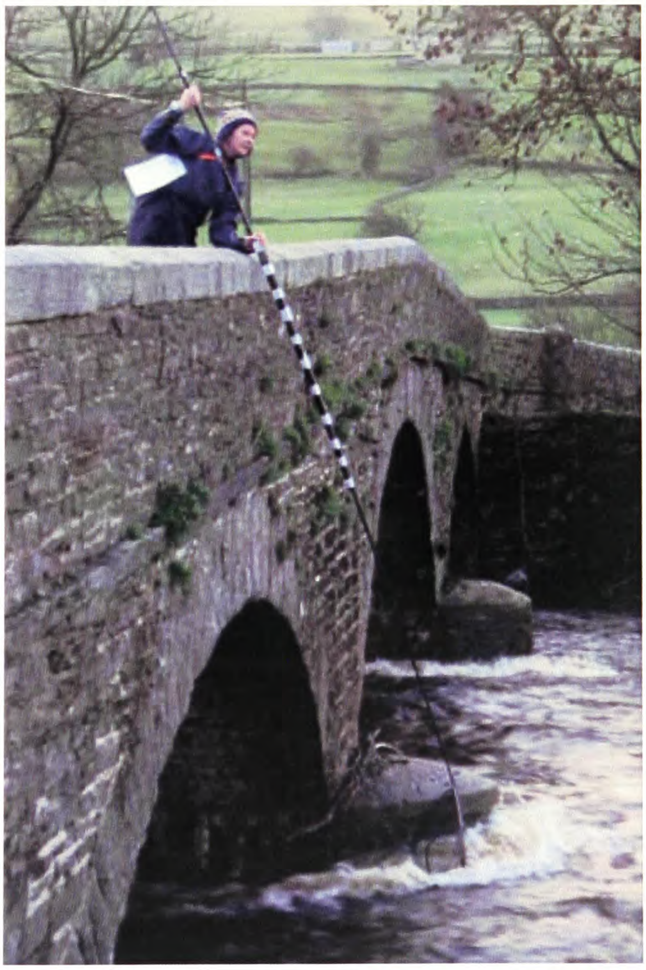

Figure 3.17 Recovering GRiFTers from channel spanning bridge using an extended telescopic net.

3.2.4 Issues Affecting the Use of GRiFTers for Surface Flow Investigation

Having established the appropriate methods of GRiFTer deployment and recovery, several issues remain to be addressed regarding the use of GRiFTers for surface flow investigations. The passage of GRiFTers through the channel is subject to three potential sources of interruption; grounding, submergence and entanglement. Grounding refers to individual units becoming pinned on subsurface material in shallower parts of the channel (Figure 3.18) and falsely representing slower areas of flow in measured flow patterns. Submergences occur when GRiFTers pass through turbulent sections of the channel, most notably at hydraulic jumps or where large boulder causes flow obstructions. Entanglements are disruptions in downstream movement caused by channel debris (Figure 3.19) or vegetation and by overhanging bank vegetation (Figure 3.20). Entanglements and submergence can falsify velocity measurements by returning lower velocities in rapidly flowing sections of the channel or by producing gaps in data coverage where satellite signal are lost. The potential exists to utilise post-capture data filtering to remove occurrences of signal interruption - this is explored in greater detail in Section 3.3.4.

In addition to potential source of interruption, data can also be affected by GRiFTer collisions. Whilst the potential of collision is reduced through the selection of the "wave" deployment strategy they remain inevitable in any attempt to maximise flow coverage. Currently, collisions are not isolated or removed from existing data since the effects of these are unlikely to be significant within the magnitude of measured changes in velocity. Further, the majority of collisions are likely to occur in slower areas of the channel and as such are likely accounted for in post-oapture data filtering.

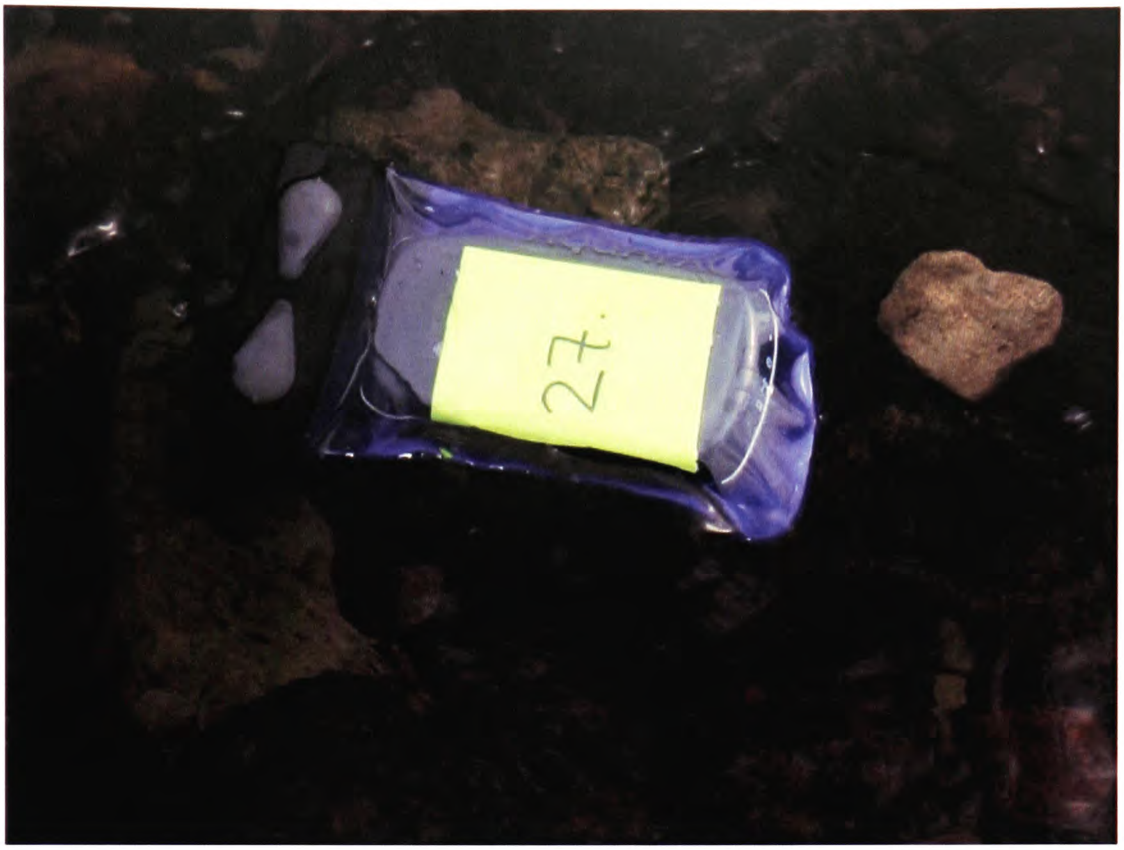

Figure 3.18 Grounding of GRiFTer on channel bed due to low flow levels.

Figure 3.19 Entanglement of GRiFTer in channel debris.

Figure 3.20 Entanglement of GRiFTers in overhanging vegetation.

3.2.5 Management of Issues Affecting the Use of GRiFTers for Surface Flow Investigation

In order to account for the issues highlighted that affect the application of GRiFTers for surface flow investigations, a series of control measures are implemented. Groundings or entanglements are accounted for within the channel by the recovery and deactivation of redundant GRiFTers. These are then returned to the flotilla for subsequent deployments. The results returned whilst GRiFTers remained stationary in the channel are removed through a post-capture data processing system ("minimum velocity" filter). The filter removes measured velocities of magnitudes below the previously defined GPS operational limitations (considered in Section 3.3.4). This control removes all velocities which cannot reasonably be determined as actual measurement of movement and not merely errors associated with the operation of the GPS. The occurrence of data gaps caused by submergence or large-scale entanglements require no additional attention since no incorrect information is introduced into the dataset that requires removing and the presence of the gaps in data itself is potentially informative about structures of flow and the presence of hydraulic features.

As discussed previously, in Section 2.3, the operation of the GPS requires a time period between receiver initiation and full operational access to the orbital satellites and therefore positioning and velocity measurements. In the first instance, this period is referred to as a "cold start" since each receiver maintains information regarding its last known location and without the necessary information the time period required to make the position fix is significantly longer. Following GRiFTer initiation for subsequent deployments this time period is significantly reduced and referred to as a "hot start". To ensure sufficient time is afforded to maximise GPS performance each unit is activated then remains stationary for 600 s prior to initial deployment and subsequent redeployments. These periods are then removed from the data before additional calculations are made and results are presented.

3.26 Example Field Investigation Procedure

3.2.6.1 Minimum Equipment and Personnel Requirements

- Flotilla of GRiFTers.
- 2 X Telescopic landing net (or alternative means of recovery).
- Loc8tors Tracker or other form of radio tracking device.
- Propeller meter and measuring stick or other form of discharge measurement device.
- Field-bag to collect deactivated GRiFTers.
- Suitable clothing and footwear.
- Personal Flotation Devices (Life-Jackets) for all individuals.
- Minimum of four individuals.
    - Deployment and unit tracking.
    - Recovery and deactivation.
    - DGPS surveying and bank person (with safety line).
    - Discharge measurement.

3.2.6.2 Step-By Step Guide to Field Investigation

1. Identify suitable / desired reach for field investigation.
2. Scout field site for potential deployment and recovery areas.
3. Scout for potential causes of grounding and entanglement.
4. Survey reach to provide channel outline for data analysis.

5. Establish discharge to classify flow paths and velocities produced.
6. Initiate units above the release area.
7. Perform first deployment. Flotilla of GRiFTers to be deployed in wave formation (total number of units divided into two of more groups, spaced across the channel and then release allowing sufficient time to avoid collisions).
8. Track GRiFTers down the channel, preferable along the bank, collecting and deactivated redundant units.
9. Recover and deactivated GRiFTers beyond the conclusion of data collection – returning redundant GRiFTers to the flotilla.
10. Return GRiFTers upstream and reactivate.
11. Repeat steps 5 – 9 as required.
12. After final recovery and deactivation, upload data.

3.3 Data Acquisition, Calculation, and Processing

3.3.1 The Concept of Cellular Flow Representation

The inherent nature and a unique advantage of the GRiFTer approach is the return of almost limitless numbers of data points from flow investigations. Therefore, in order to utilise the results generated from large-scale surface flow investigations, it is necessary to provide a standardised approach to data presentation, analysis and comparison. Since each reach may be completely unique and change rapidly (specifically in dynamic flow conditions) any approach to data presentation must be flexible in its application and have the potential to both represent and weight areas of the channel appropriately, relative to significant inequalities in spatial data coverage. As a result of these requirements a cellular representation is to be utilised.

Each cellular grid will be structured dependent upon the size and extent of the selected reach or area, the relative size of each cell, the dynamics of flow observed throughout field testing and the number of velocity measurements. Although the smaller the grid cells, the more sensitive they are to changes in flow, if cells are too small (relative to mean flow velocity) flow coverage will be comprised. For example, initial field testing at the River Swale has repeatedly returned velocities in excess of 1.0 ms^{-1} therefore (sampling at 1 Hz) a cell must be greater than 1 m in length to avoid GRiFTers bypassing entire cells, and therefore loosing continuity of flow through the grid. The use of larger cells also allows for the collection of a greater number of measurements providing a more accurate / complete representation of the flow within each cell. The flexibility of a cellular approach is highlighted by the ability to determine the requirements of specific representations following data capture.

The quality of cellular flow representation is determined by two components, the ability to precisely position individual results within the correct cell and the accuracy of each individual velocity measurement. The most directly comparable flow measurement approach to the GRiFTer technique is provided by the use of LSPIV methods. Within LSPIV investigation, interrogation areas, as opposed to cellular representations are utilised however literature provides for areas of 2 m x 2m (Section 2.1.2.5). Commercial GPS manufacturers quote positional accuracies between 1-3 m, therefore if similar field-based performances can be observed then grid cells measuring 2 m x 2 m would present the most appropriate / achievable approach to reach scale flow investigations.

In order to use 2 m x 2 m grid cells the achievable precision of a single measurement must be determined, as must the ability to make repeated measurements (percentage of results) within 2 m deviations of the true position. In addition to the precision and accuracy of positioning, the accuracy with which the GPS can measure velocity is fundamentally important to the successful investigation of surface flow phenomena in natural river environments. Velocities can be measured by the GPS at theoretical sub-millimetre accuracies; however such accuracies have yet to be demonstrated in academic publications. Additionally, the use and therefore potential accuracy of GPS measurements made in natural river environments has yet to be considered. Therefore it is necessary to determine the accuracy of velocity measurements within natural river environments to validate the use of GRiFTers to investigate surface flow phenomena. Further, within the use of the GPS for position and velocity measurement the optimum equipment configurations and position and velocities calculation methods must also be determined.

3.3.1.1 Factors Affecting the Operation of GPS for Flow Investigation

As described previously, the ability of the GPS to determine position and measure velocity is controlled by four factors: the number of visible satellites from which theoretical spheres can be generated; the geometric arrangement of the orbital satellites relative to each other and the receiver unit (represented by DOP values); the configuration of the environment in which the receiver is positioned (which may give rise to multipathing or signal shadowing); and the atmospheric and climatic conditions which exist between the satellites and the receiver (Witte et al., 2004).

The integrity of GPS positioning and velocity measurement is related directly to the number of visible satellites and the DOP (dilution of precision); with higher numbers of visible satellites and lower DOP values providing improved GPS performance. These values determine and can therefore be used to describe the quality of GPS measurements. As a result, examining the number of visible satellites and DOP values provides the potential to improve GPS performance through post-process data filtering. Post-process data filtering refers to the selective use of data based on a determined criterion, referring to either the number of visible satellite or the horizontal dilution of precision as indicators of the quality of GPS performance.

In addition to the potential of filtering data to improve positioning and velocity measurement, the most appropriate method of velocity calculation must be determined. Velocities can be provided by Doppler measurements or by independent calculations made directly from changes in position (Section 2.3.3). If calculated velocities are to be utilised the correct time period (t) over which calculations are made must also be established.

Initially however, it is necessary to establish the optimal approach to data collection. Data collection consists of two elements; the deployment strategy of GRiFTers within the river environment (see Section 3.2.2) and the configuration of the GPS receiver within each GRiFTer. As detailed in section (Section 2.3.6.2) the GPS receivers integrated within each GRiFTer provides the potential of capturing data from standard GPS satellites or from both standard and WAAS-Enabled (Wide Area Augmentation System) satellites, with the theoretical potential of improving precision and accuracy. The effect of WAAS enablement must therefore be considered relative to the effect it has upon both positioning and velocity measurement.

3.3.2 GPS Configuration - Establishing the Optimal Approach to Data Acquisition

A series of tests were performed to investigate the following issues associated with the use of GPS for surface flow investigation in natural gravel-bed river environments.

1. The optimal approach to data acquisition.
2. The correct methods of velocity calculation.
3. The precision and accuracy of positioning.
4. The accuracy of velocity measurements.
5. The effect of GPS configuration (WAAS enablement) on each of these variables.
6. The potential of performing post-process data filtering utilising the number of visible satellites and HDOP values as indicators of data quality.

3.3.2.1 Stationary Tests

Two types of test were conducted to validate GPS performance; stationary and dynamic. Stationary testing comprised a pair of GPS receiver fixed in position ensuring that any detected / measured movement would be known to be an error in positioning and / or velocity measurement. The true position of each unit was established from the mean position of each GPS, with the magnitude of deviation from this position calculated accordingly. Stationary tests were performed on a raised area located at Paull Holme Strays, which was chosen since it provided the best environmental configuration for optimising GPS performance; an open area free from overhead obstacles and potential sources of signal shadowing and multipathing. Both units were positioned in close proximity and configured identically except that one unit was activated to utilise both standard and WAAS enabled satellites.

In order to establish the precision and accuracy of GPS positioning four statistical tests were conducted on the stationary data. These tests considered the effects of filtering data using the number of visible satellites and the HDOP value, both with and without access to WAAS-enabled satellites to determine whether data filtering improves the quality of positioning and velocity measurements. The determination of the appropriate approach to data filtering will ultimately be made based on a cost-benefit analysis weighting the achievable improvements in GPS performance and therefore the quality of acquired data against the quantity of data lost through the filtering process. Stationary tests will also be used to evaluate errors in Doppler velocity measurements against those observed in velocities calculated from measurements of deviation in position. In order to make comparisons of error in velocity measurements, the appropriate averaging time over which velocities are calculated will initially be established.

3.3.2.2 Dynamic Tests

Two groups of five GPS units (one group of which was enabled to access WAAS satellites) were mounted on a trolley drawn by a pulley system along a 30 m course. The speed of the pulley system was varied using different cog arrangements to control the rate of the trolley's movement.

Three different speeds were used and each trial was repeated five times to produce a total of 15 sets of measurements for each GPS. Two sets of data are presented to consider the effects of alternative orbital satellite conditions; the first set of experiments was performed in optimal satellite conditions on a local airfield (Hibblestowe) whilst the second sets of tests were conducted in a less favourable urban environment (Barton Upon Humber). GPS velocity measurements are compared against independently timed velocities and then considered relative to the effects of data filtering (Figure 3.21).

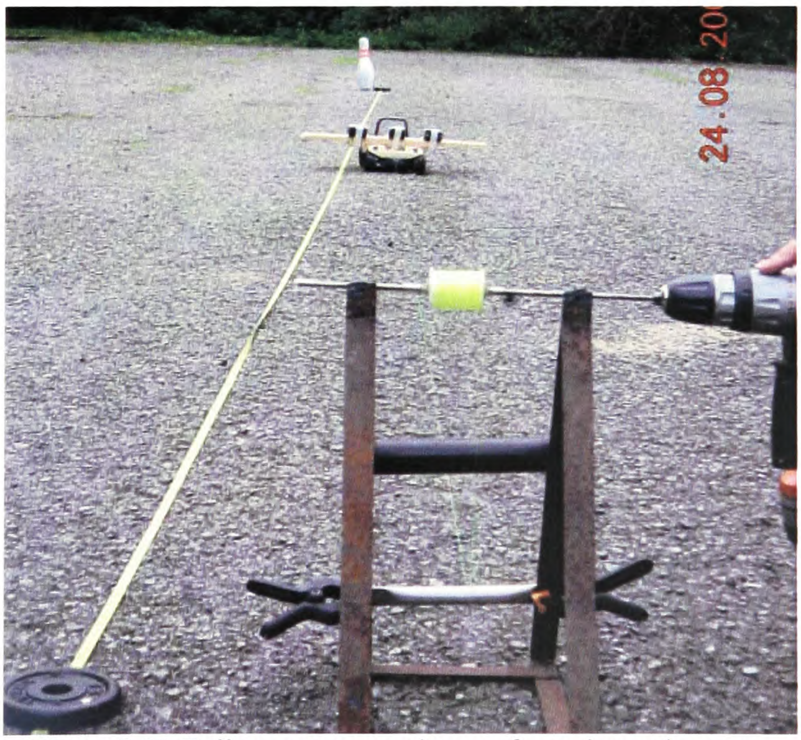

Figure 3.21 Pulley system used to perform dynamics tests.

3.3.3 Establishing the Optimal Approach to Data Acquisition - Results

3.3.3.1 Stationary Tests and the Precision of Positioning

Over 30000 data points were returned from eight hours of stationary testing at Paull Holme Strays. Each data point represents the apparent position of the GPS receiver at a specific point in time with the true position being provided by the mean point from the entire testing period. Paull Holme Strays was selected as the test site to provide conditions conducive to the optimal performance of the GPS. The site was located on a raised area extending into the Humber Estuary which could only be reached by crossing a mud flat, providing a clear view of the sky and therefore access to the maximum number of visible satellites. The site was also free from obstructions or overhead obstacles which would potentially cause signal shadowing or multipathing. Additionally, the use of this area ensured that the stationary GPS receivers could not be tampered with or stolen.

To standardise analysis of the results generated through different filtering approaches and unit configurations a series of density distribution plots (DDP), probability distribution functions (PDF) and statistical tables will be presented using normalised positions (the deviation of each individual value from the mean GPS position).

3.3.3.2 The Effect of the Number of Visible Satellites (WAAS)

Figure 3.22 provides DDPs (density distribution plots) corresponding to filtering using specified numbers of visible satellites. The minimum number of satellites observed throughout testing was 5 therefore the result for 5+ satellites is representative of the complete unedited dataset (Figure 3.22 A).

Figure 3.22 A demonstrates a central cluster of deviations; measuring around 3 m in each of the north and south directions and in excess of 2 m in both the east and west directions. Around the central cluster is evidence of a wandering / drift in positions away from the know position of the unit. Drift occurs in all but the western direction with greater occurrence to the east and south west of the region. Up to 15000 values were observed within the main part of the central cluster with the greatest number of values occur around 1m south of the true position. The drift away from the central cluster never exceeds the 1 - 1000 data points category however the range of area covered by the drift suggest that it is significantly albeit not at consistent magnitudes or occupying similar locations. The occurrence of drift is significant to the integrity of surface flow investigation since without the ability to precisely and accurate locate the position of a velocity measurement it will be impossible to measure genuine flow phenomena.

Filtering by 7+ satellites (Figure 3.22c) reduces the occurrence of drift away from the central cluster, only preserving that which occurs to the east and north east of the region. The size of the central cluster reduced further; extending to around 2m in all directions. The first significant changes in the structure of measured positions occur when data is filtered by 8+ satellites (Figure 3.22d). There is a clear reduction in the number of values present within the central cluster, with maximum values within the 5001-10000 category but virtually the entire central cluster measuring below 5000 values, highlighted that 8+ satellite provides a much more rigorous filtering mechanism. Additionally it is clear that drift is removed from virtually the entire area and only preserved directly to the east of the central cluster.

Figures 3.22 e and 3.22 f provide the results of filtering based on +9 and +10 satellites respectively. The effect of filtering by +9 satellites produces a dramatic decrease in the size of the central cluster which extend to approximately 1 m in each direction except to the south where deviations upto 2 m remain. Filtering by +9 satellites also results in the removal of all drift away from the central cluster. Additionally clear is that the magnitude of observed values is significantly reduced from those previously presented. The results produced by data filtered using +10 satellite provide a further reduction in the size of the central cluster the maximum deviation from the known positioning occurring towards the south / south west of the region.

Figure 3.23 provides PDFs (probability distribution functions) produced by filtering data based on numbers of visible satellites; each PDF corresponds to a density distribution plot featured in Figure 3.22. Apparent throughout the majority of PDFs (Figure 3.23 a - d) is a consistent distribution structure that corresponds to the similarities observed in the DDPs. In excess of 90% of values are contained with the desired 2 m deviation from the mean position, with 37% and 29% of values falling within 1.0 m and 1.5 m deviations respectively. Additionally, 4% of values deviate by more than 3 m, highlighting the occurrence of drift away from the central cluster.

The first notable change in PDF structure occurs for 8+ satellites (Figure 3.23 d) with the percentage of values demonstrating deviations between 2 - 2.5 m from the mean value decreasing from 13% to 10%. Further the percentage of values with deviations greater than 3 m is also reduced from 4% to 2%. More significant changes occur in the structure of the +9 satellites results (Figure 3.23 e) with no observable results deviating by in excess of 2 m and deviations of 0.5 m and 1.0 m providing in excess of 90% of values. Filtering by +10 satellites (Figure 3.23 f) demonstrates an increase in the dominance of 0.5 m deviations with in excess of 70% of values accounted for within this category.

Statistically, Table 3.1 demonstrates that the mean deviation for the unedited dataset is 1.43 m with 93.1% of values within the desired 2 m deviation; with the first notable decrease in these value occurring for +8 satellites producing a mean deviation of 1.07 m with 96.9% of values occurring with the desired 2 m deviation. These improvements in precision and accuracy are however achieved at a cost of 33.5 % of data. Large-scale improvements are observed in the data when filtered by +9 satellites. The mean deviation is reduced to 0.5 m and the percentage of values within the desired 2 m deviation is increased to 99.66%. These improvements however occur at the costs of 82.28% of data which is clearly prohibitive to the collection of data representing complete river reaches.

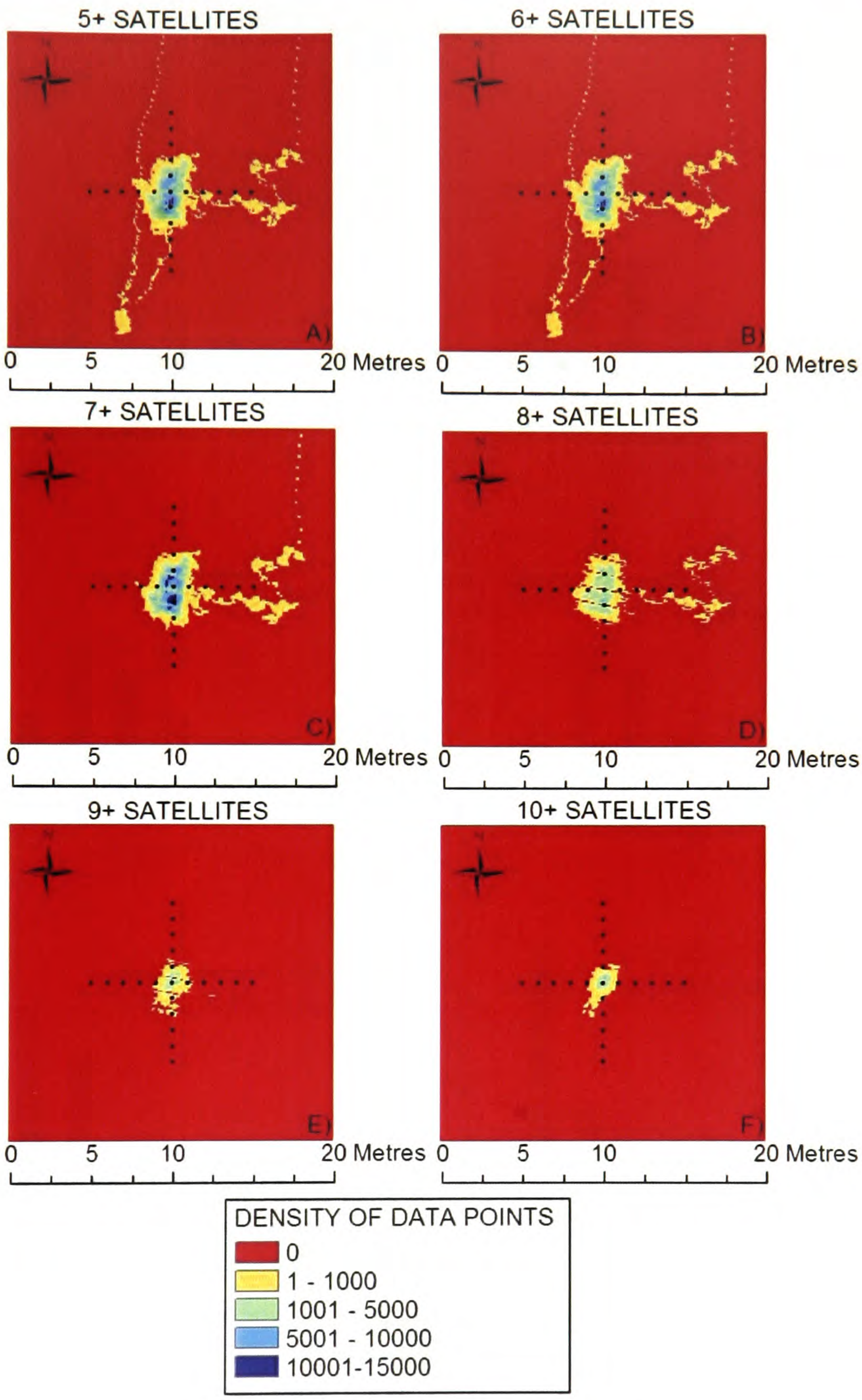

Figure 3.22 Density distribution plots (DDP) of normalised data points from the mean position of each stationary base-station. Each DDP features marker points extending in 1 metre spacing away from the mean position of each dataset and utilises the same graduated colouring and scale. Clear from the distributions provided is improved positional accuracy with increasing satellite numbers. The results presented are generated from the processing of data acquired utilising WAAS-activated GPS receivers.

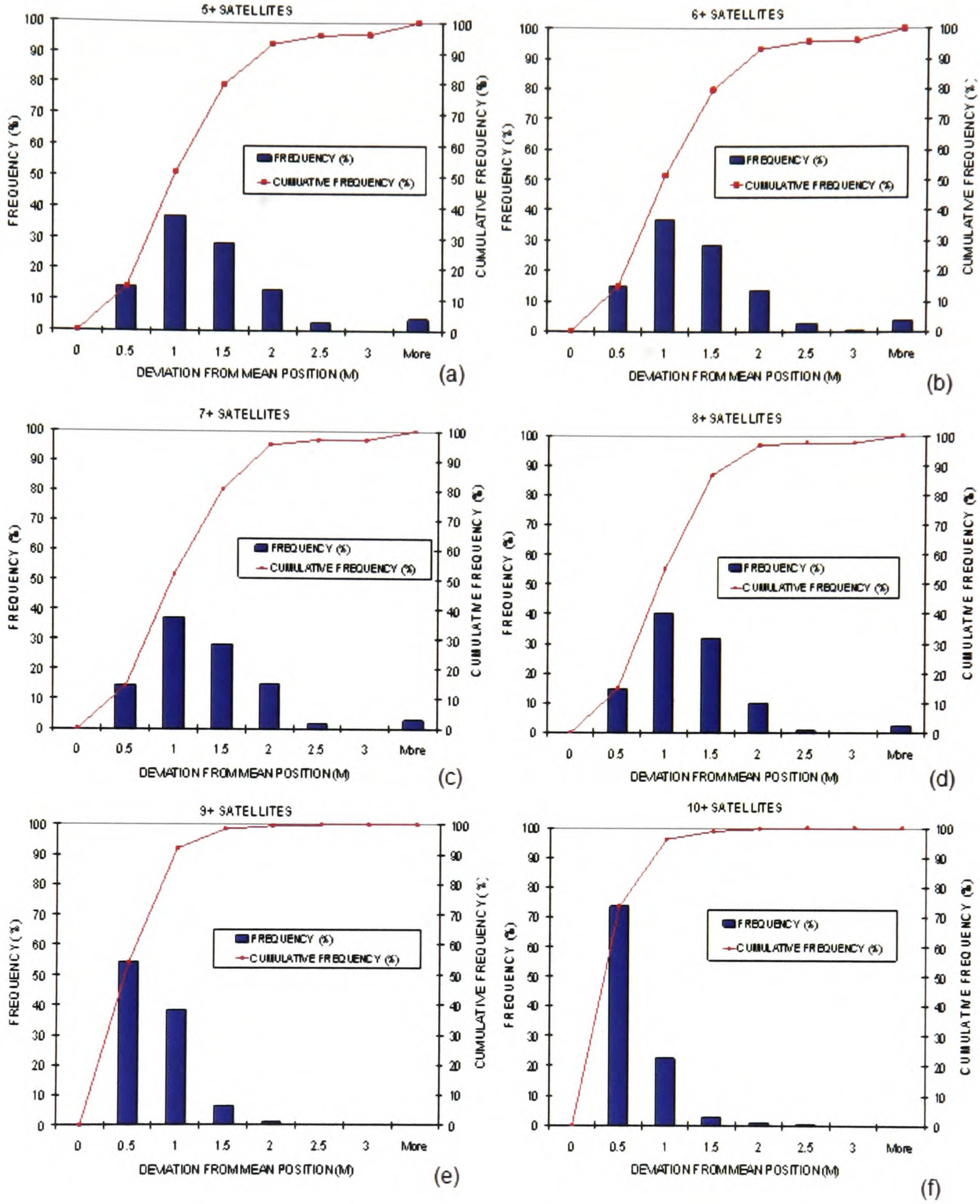

Figure 3.23 Probability Distribution Functions (PDF) of the deviation in position of each individual value from the mean position of the GPS receiver. Each PDF is representative of the results observed when filtered to a specified number of visible satellites and scaled 0 – 3+m to allow ease of comparison.

Satellites (WAAS)	Number of Results	Remaining (%)	Mean Deviation (m)	Within 2m (%)
5	30237	100.00	1.43	93.15
6	30214	99.92	1.43	93.15
7	27613	91.32	1.35	95.38
8	20099	66.47	1.07	96.93
9	5358	17.72	0.52	99.66
10	2475	8.19	0.41	99.64

Table 3.1 Summary of the effects upon the precision of positioning when data are filtered using the number of visible satellites.

3.3.3.3 The Effect of the Horizontal Dilution of Precision (WAAS)

Figure 3.24 provides DDPs for filtering based on HDOP values. The highest HDOP values observed throughout testing were 5.0, however to consider the effects of data filtering, HDOP values of 2.0 - 0.9 are considered. The structure of the density distribution plots produced by filtering based on HDOP values of 2.0 and 1.9 (Figure 3.24 j and k) mirrors those produced by filtering based on 5+ and 6+ satellites (Figure 3.23 a and b). The first observable change in distribution structure occurs when data is filtered by HDOP 1.8 demonstrating the removal of drift to the north and south / south west areas of the region. Filtering based on HDOP values between 1.7 and 1.2 preserve the same structure to the central cluster and the occurrence of drifter towards the east and north east of the test region (Figure 3.24 d - i). Filtering by HDOP 1.2 all produces a clear reduction in the size of the remaining dataset. Figure 3.24 b provides the results of filtering based on a HDOP value of 1.1 and demonstrates the removal of drift in all but an eastern direction. Filtering based on HDOP 1.0 produces additional structural changes to the distribution of position deviations (Figure 3.24 b). The size of the central cluster is reduced in a horizontal direction extending to 1 m east and west of the known position, whilst the magnitude of deviations is maintained in both the north and south directions. The maximum possible level of filtering is achieved by utilising a HDOP value of 0.9. Figure 3.24 returns results that closely resemble those produced by filtering based on 10+ satellites (Figure 3.23 f); the removal of all drift away from the central cluster and a significant reduction in both the lateral and longitudinal extent of the cluster, with the furthest extent extending to the south / southwest.

Figure 3.25 provides PDFs (probability distribution functions) produced by filtering data based on HDOP values; each PDF corresponds to a density distribution plot featured in Figure 3.24. The majority of PDFs (Figure 3.25 b - l) provided by filtering based on HDOP 1.0 - HDOP 2.0 produce the same broad structure as observed from the complete unedited datasets (Figure 3.23 a). The first clear structural change occurs when data is filtered based on a HDOP value of 1.0; demonstrating a reduction in the size of the 2.5 m and 2.0 m deviation from 3% and 14% to 0.5% and 5% respectively. These reductions occur concurrently with a growth in the 0.5 m deviation category from 14.5% to 23%. Increasingly dramatic structural changes occur when data is filtered utilising a HDOP value of 0.9 with 87.5% of values falling with 1 m deviation of the true position. Additionally, the largest categories become deviations of 0.5 m and 1.0 m containing 49% and 38.5% of values respectively.

As observed throughout DDPs and PDFs, filtering by HDOP 2.0 – 1.9 provides virtually no improvement in precision (Table 2). Statistically, HDOP 1.8 – 1.3 provides negligible improvement in deviation from the mean position (0.08 – 0.11 m) resulting in a minimum mean deviation of 1.33m (Table 2). Improvements of this magnitude occur at a cost of 6.08 – 11.91% of data values.

Table 3.2 demonstrates gradual increases in both precision and accuracy with lower HDOP values (HDOP 2.0 - 1.3). The first notable increases occur between HDOP 1.3 and HDOP 1.2 with mean deviation of 1.33 m and 1.02 m respectively. The improvement in the percentage of values within the desired 2 m deviation is less distinct however filtering by HDOP 1.2 provides 4.28% more values that the complete unedited dataset. The relative data costs of improvement dramatically increases between HDOP values of 1.2 and 1.1 with a further 10% of data lost (85% remaining down to 75% remaining). These losses increase further between HDOP 1.1 and 1.0 where a further 18.26% of data is lost and more so to HDOP 0.9 where only 4.58% of values remain following filtering.

As observed throughout DDPs and PDFs filtering by HDOP 2.0 – 1.9 provides virtually no improvement in precision (Table 2). Statistically, HDOP 1.8 – 1.3 provides negligible improvement in deviation from the mean position (0.08 – 0.11 m) resulting in a minimum mean deviation of 1.33m (Table 2). Improvements of this magnitude occur at a cost of 6.08 – 11.91% of data values.

Cross-comparison of filtering based on 7+ satellites and HDOP 1.8 provides an equal mean deviation (1.35m) however filtering based on HDOP preserves 2.6% more data. Interestingly however, filtering by 7+ satellites returns 0.61% more values with the desired 2 m deviation from the true position. This demonstrates that the desire for improvements in precision and accuracy in positioning may not occur simultaneously and the relative importance of each may need to be considered dependent upon the specific investigation requirements.

Filtering by HDOP 1.2 returned an improvement in mean deviation of 1.02 m (0.05 m more than the equivalent 8+ satellite based filtering) for a loss of 15.72% of data (17.81% less data lost than filtering by 8+ satellites). This pattern of HDOP based filtering preserving a higher percentage of data for similar improvements in precision and accuracy. This trend is not however universal as at the lowest HDOP values and highest number of visible satellites the satellite based approaches provide superior cost-benefit results. Filtering using HDOP 0.9 improves the mean deviation to 0.59 m and maintains 99.35% of values within 2 m for a loss of 95.3% whilst filtering based on 9+ satellites improves the mean deviation to 0.52 m, providing 99.66% of values within 2 m deviations for a loss of 13% less data than the HDOP approach.

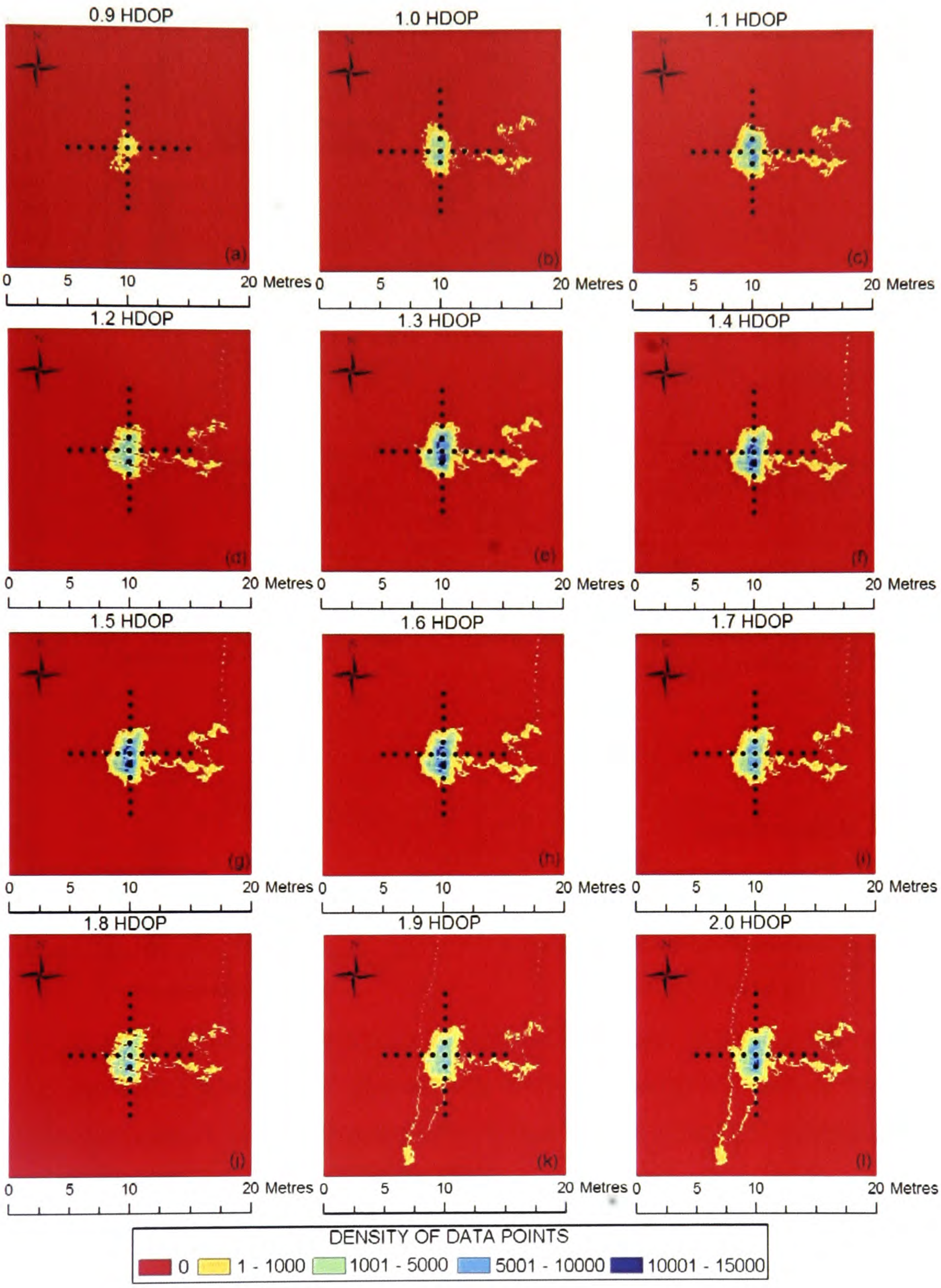

Figure 3.24 Density distribution plots (DDP) of normalised data points from the mean position of each stationary base-station. Each DDP features marker points extending in 1 metre spacing away from the mean position of each dataset and utilises the same graduated colouring and scale. Clear from the distributions provided is improved positional accuracy with decreasing HDOP value. The results presented are generated from the processing of data acquired utilising WAAS-activated GPS receivers.

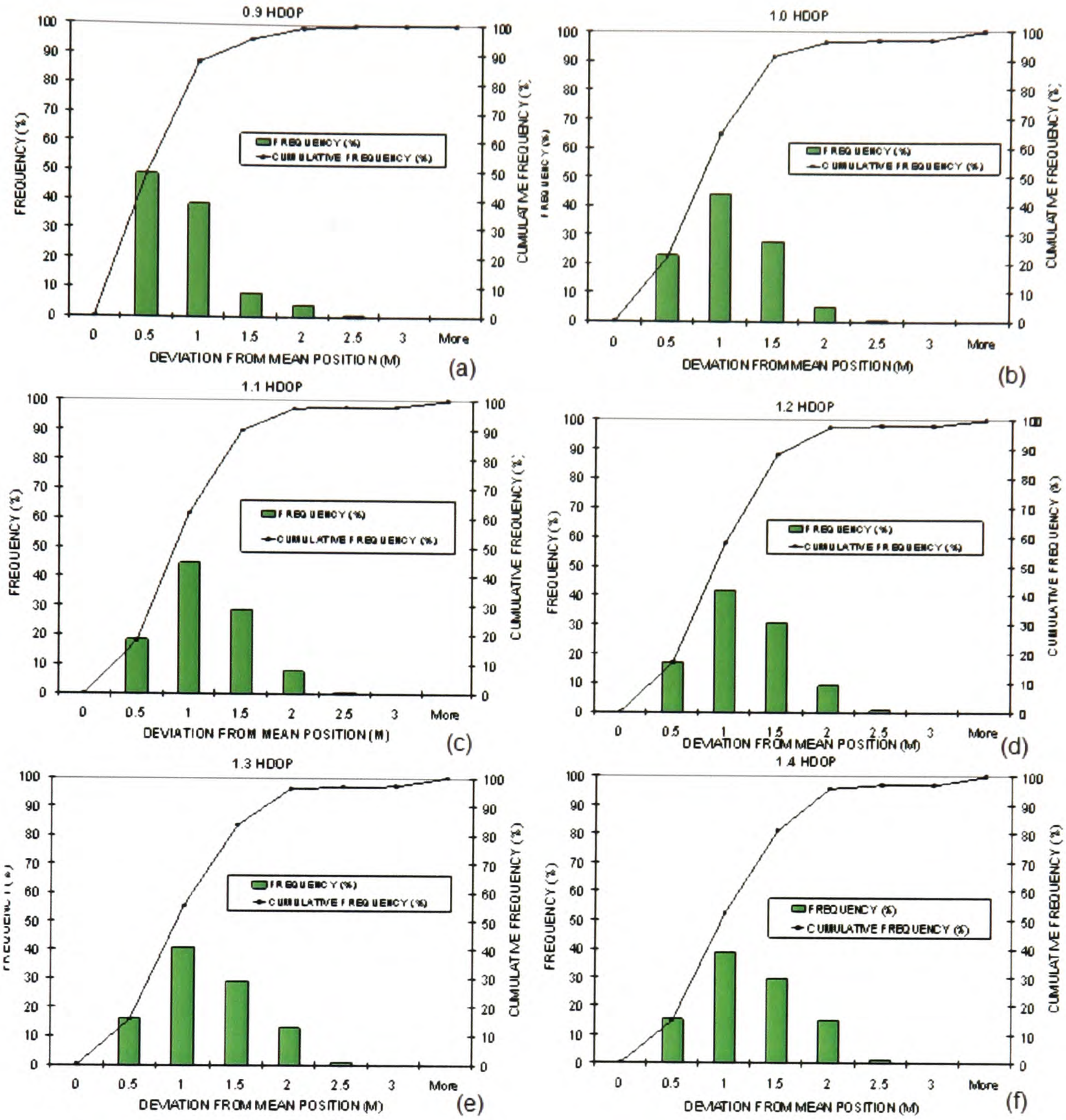

Figure 3.25 (Section 1).Probability Distribution Functions (PDF) of the deviation in position of each individual value from the mean position of GPS receiver. Each PDF is representative of the results observed when filtered to a specified number of visible satellites and scaled 0 – 3+m to allow ease of comparison.

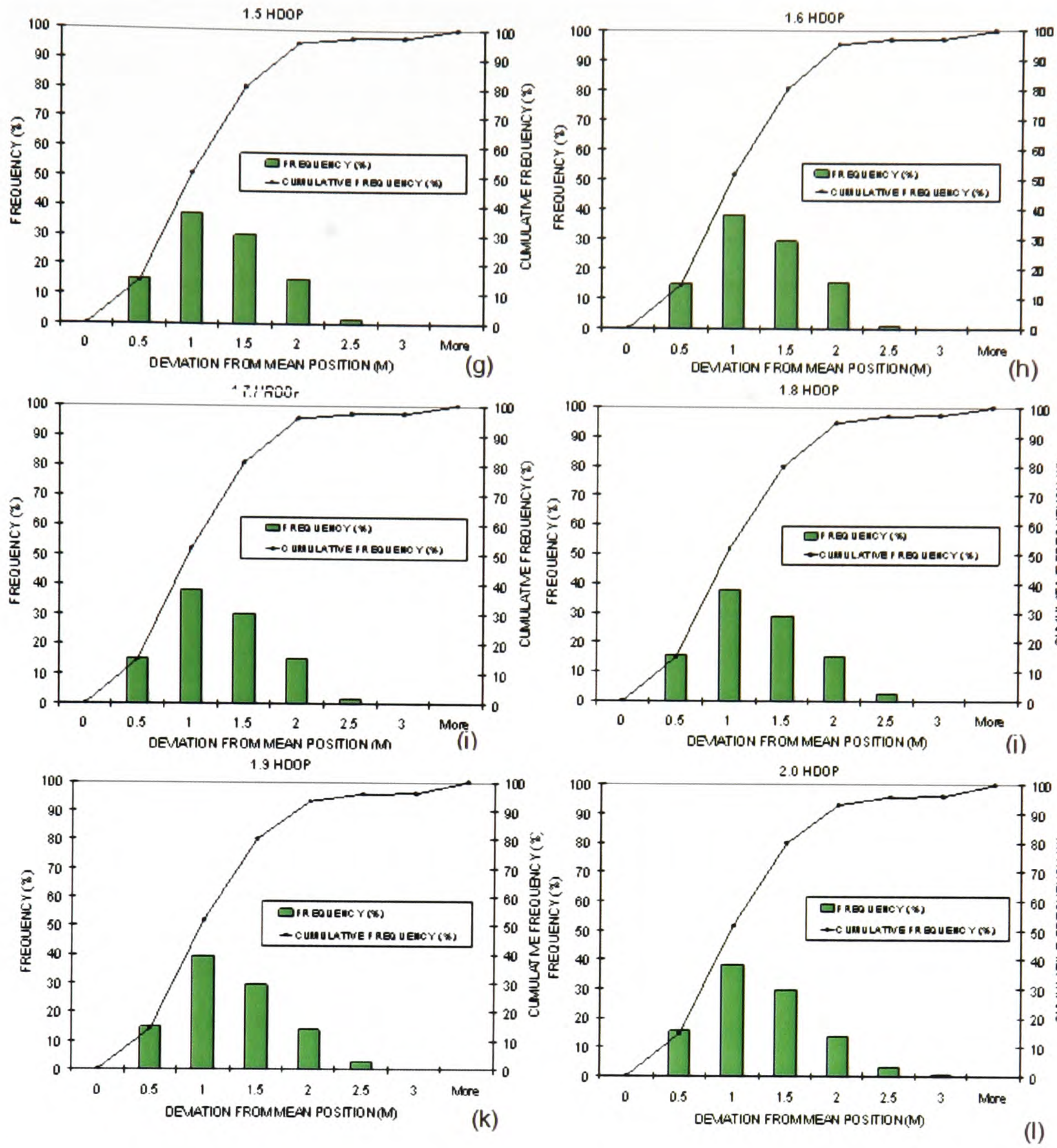

Figure 3.25 (Section 2).Probability Distribution Functions (PDF) of the deviation in position of each individual value from the mean position of GPS receiver. Each PDF is representative of the results observed when filtered to a specified number of visible satellites and scaled 0 – 3+m to allow ease of comparison.

HDOP (WAAS)	Number of Results	Percentage Remaining (%)	Mean Deviation (m)	Within 2m (%)
ALL	30237	100.00	1.43	93.15
2	30216	99.93	1.43	93.15
1.9	29465	97.45	1.44	93.15
1.8	28378	93.85	1.35	94.77
1.7	28036	92.72	1.35	95.56
1.6	27673	91.52	1.35	95.63
1.5	27475	90.87	1.35	95.57
1.4	27357	90.48	1.35	95.75
1.3	26615	88.02	1.33	96.11
1.2	25598	84.66	1.02	97.43
1.1	22576	74.66	1.00	97.292
1	15512	56.40	0.99	98.44
0.9	1384	4.58	0.59	99.35

Table 3.2. Summary of the effects upon the precision of positioning when data are filtered using the HDOP.

3.3.3.4 Summary - Filtering WAAS-Enabled Data

Cross-comparison of filtering based on a HDOP value of 1.2 returned an improvement in mean deviation of 1.02 m (0.05 m more than the equivalent 8+ satellite based filtering) for a loss of 15.72% of data (17.81% less data lost than filtering by 8+ satellites). This pattern of HDOP based filtering preserving a higher percentage of results for equal or superior improvements in precision and accuracy is not universal since at the most extreme filtering approaches satellite based approaches provide superior results in terms of cost-benefit comparisons. Filtering using HDOP 0.9 improves the mean deviation to 0.59 m and maintains 99.35% of values within 2 m for a loss of 95.3% of data whilst filtering based on 9+ satellites improves the mean deviation to 0.52 m, providing 99.66% of values within 2 m deviations for a loss of 13% less data than the HDOP approach.

It is clearly apparent that filtering based on the number of visible satellites and the HDOP can be used to improve WAAS enabled data; both in terms of precision as demonstrated by reducing the mean position deviation and accuracy by increasing the percentage of results within the desired 2.0 m deviation. These improvements are however achieved at a cost, since filtering inherently requires the removal of data to achieve the desired improvements. Additionally prominent is that at all but the most severe approaches to filtering, HDOP based approaches achieves equal or superior precision and accuracy improvements for smaller data losses and therefore would potentially provide the most profitable approach to filtering should WAAS-enabled data be designated as the most appropriate approach to data acquisition.

3.3.3.5 The Effect of the Number of Visible Satellites (WAAS-Disabled)

Figure 3.26 provides DDPs for data acquired using GPS receiver access only standard satellites (WAAS-disabled). Each DDP corresponding to data filtered using specified numbers of visible satellites. The minimum number of satellites observed throughout testing was again 5 therefore the result for 5+ satellites is representative of the complete unedited dataset (Figure 3.26 A). The structure of the density distribution plots returned from unedited WAAS-disabled data is significantly different from that produced by WAAS-enabled data collection.

The unedited WAAS-disabled dataset (Figure 3.26 a) features a central cluster, more uniformly structured in terms of horizontal and vertical deviations measuring below 2 m in all axis from the known position. The occurrence of drift away from the central cluster is significantly reduced and only occurs to the north-east and north-west of the test region at significantly lower magnitudes than observed in the unedited WAAS-enabled data (Figure 3.22 a). An additional circular cluster occurs at the furthest extent of the north-western drift measuring around 1 m in diameter; this additional cluster contains cells with up to 10000 values. The occurrence of the additional cluster demonstrates that WAAS-disabled data is more precise but less accurate than WAAS-enabled data since the magnitude of the greatest deviations are significantly smaller however the reoccurrence of small scale deviations are more frequent.

Filtering based on 8+ satellites reduces the size and structure of the central cluster specifically in the north-south direction and completely removes the emergent data cluster; however drift is preserved to the northwest and northeast of the test area (Figure 3.26 d) whilst a clear reduction occurs in the size of the remaining dataset.

Filtering by 9+ satellites (Figure 3.26 e) changes the structure of the central cluster with the deviations being greater in an east-west direction as opposed to in the north-south axis as observed throughout all other WAAS-disabled distributions. Filtering based on 10+ and 11+ satellites (Figure 3.26 f & g) further reduces the size of the central cluster, removes all drift and increases uniformity in the distribution of deviations. Uniquely, the maximum number of observed satellites throughout WAAS-disabled data was 11 satellites as opposed to 10 in the WAAS-enabled data.

Figure 3.27 provides PDFs (probability distribution functions) produced by filtering data based on numbers of visible satellites; each PDF corresponds to a density distribution plot featured in Figure 3.26. Apparent from the PDFs produced by filtering based on 5+, 6+ and 7+ satellites (Figure 3.23 a - c) is a consistent distribution structure that corresponds to the similarities observed in the DDPs. In excess of 92% of values are contained with the desired 2 m deviation from the mean position, with 40% and 39% of values contained within 1.0 m and 1.5 m deviations respectively. Unlike the unedited WAAS-enabled data, no values occurred of magnitude greater than 3 m.

Filtering by 8+ satellites (Figure 3.27 d) removes the occurrence of deviations beyond 2.5 m and provides 97.89% of values within the desired 2 m deviation whilst preserving the previously outline distribution structure. Figure 3.27 e demonstrates that filtering based on 9+ satellites significantly alters the structure of position deviations. The most common deviations are contained within the 1 m category (57%) whilst the second most common category becomes deviation below 0.5 m (25%). As a result of these changes 99.6% of values remain within the desired 2 m deviation from the known position. Increasing the number of satellites upon which data is filtered achieves in increasing the percentage of values contained within the 0.5 m deviations and reduces the magnitude of the largest deviations until for 11+ satellites 99.75% of values are contained with 1 m of the known position.

Table 3.3 provides the statistically summary of the effect of filtering WAAS-disabled data, based on the number of visible satellites. Again clear is that both the precision and accuracy of positioning increases when data is filtered based on higher numbers of visible satellites.

A significant division occurs between 7+ and 8+ visible satellites where the mean deviation improves form 1.15 m to 0.99 m and the accuracy of positioning increases by 5.33%. These improvements are however achieved at the cost of 26.35% of recorded data. Greater increases can be achieved by filtering based on higher numbers of visible satellites however with 9+ satellites only 24.59% of data is preserved and this figure worsens at higher satellite values, prohibiting their use as potential filtering mechanisms. This pattern again demonstrates that a compromise must be sought between desired improvements in precision and accuracy and acceptable losses in the collected data.

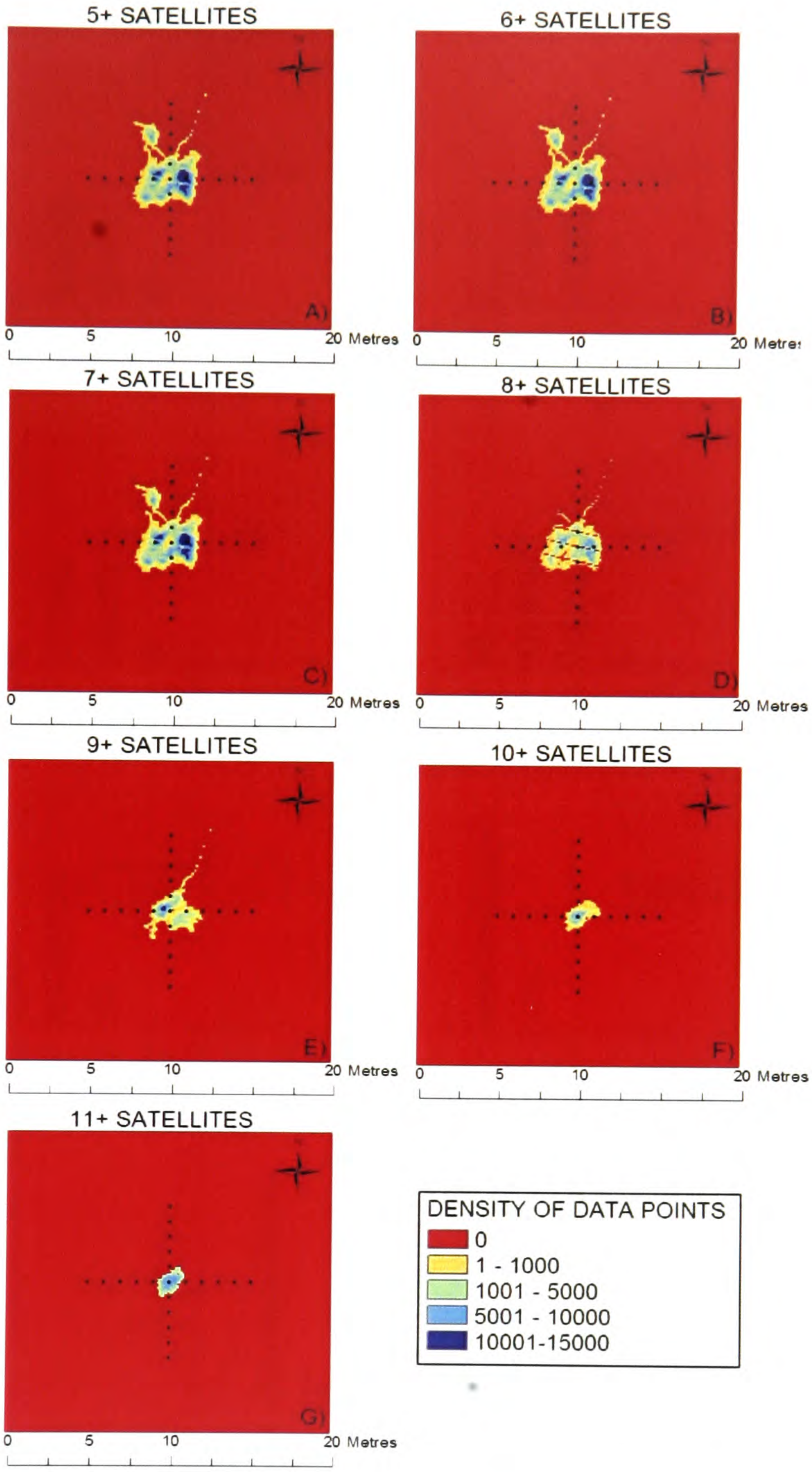

Figure 3.26 Density distribution plots (DDP) of normalised data points from the mean position of each stationary base-station. Each DDP features marker points extending in 1 metre spacing away from the mean position of each dataset and utilises the same graduated colouring and scale. Clear from the distributions provided is improved positional accuracy with increasing number of visible satellites. The results presented are generated from the processing of data acquired utilising WAAS-disabled GPS receivers.

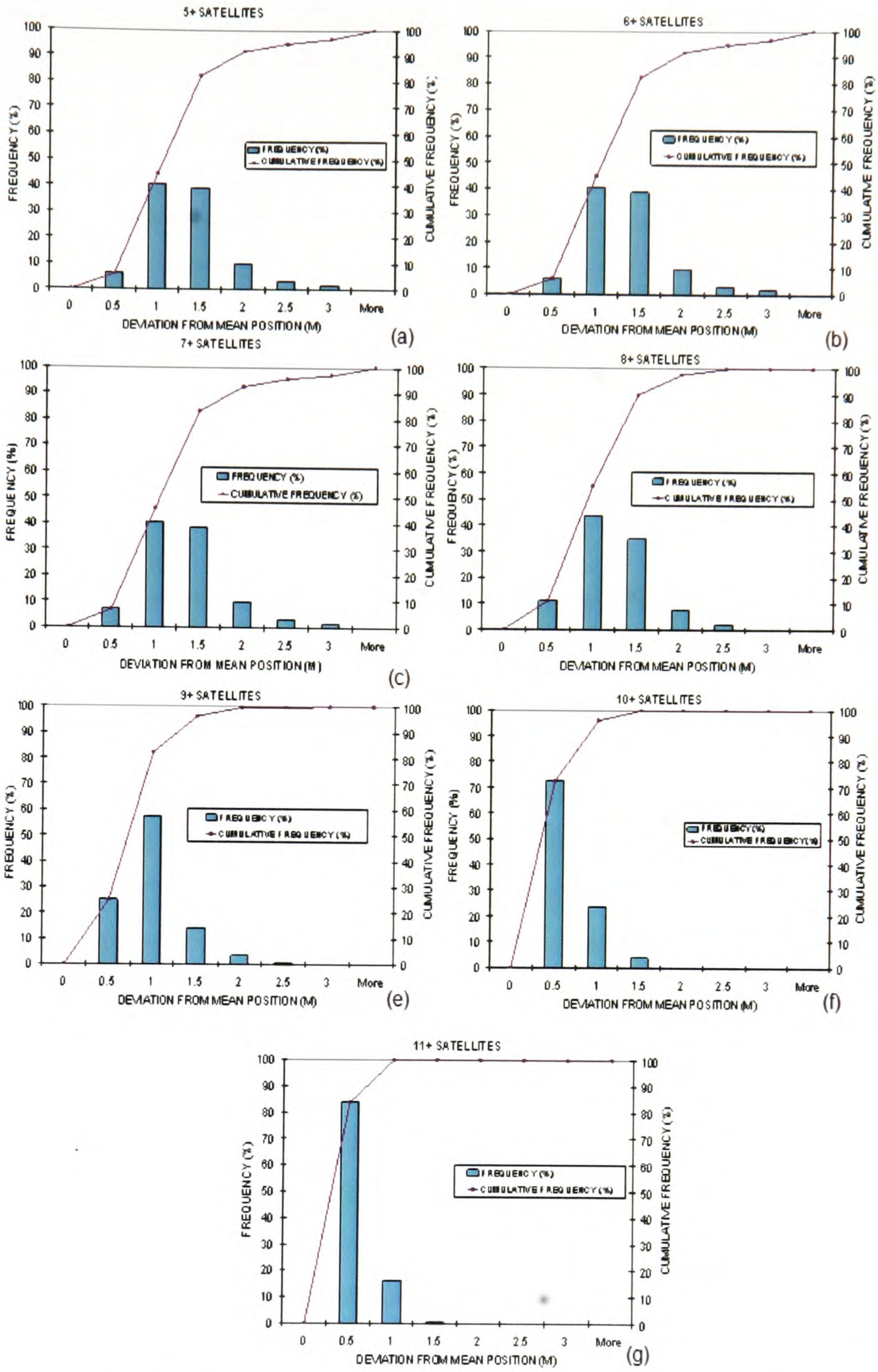

Figure 3.27 Density distribution plots (DDP) of normalised data points from the mean position of each stationary base-station. Each DDP features marker points extending in 1 metre spacing away from the mean position of each dataset and utilises the same graduated colouring and scale. Clear from the distributions provided is improved positional accuracy with increasing satellite numbers. The results presented are generated from the processing of data acquired utilising WAAS-disabled GPS receivers.

Satellites (NON WAAS)	Number of Results	Percentage Remaining (%)	Mean Deviation (m)	Within 2m (%)
ALL	30224	100.00	1.19	96.43
5	30195	99.90	1.17	91.84
6	30194	99.90	1.17	91.84
7	29923	99.00	1.15	92.56
8	23075	76.35	0.99	97.89
9	7432	24.59	0.73	99.61
10	4471	14.79	0.40	100
11	2476	8.19	0.33	100

Table 3.3 Summary of the effects upon the precision of positioning when data are filtered using the number of visible satellites.

3.3.3.6 The Effect of the Horizontal Dilution of Precision (WAAS-Disabled)

Figure 3.28 provides individual DDPs for filtering of WAAS-disabled data based on HDOP values. Filtering based on HDOP values creates three distinct structures to the data; HDOP 2.0 - 1.7 (Figure 3.28 l - i) has little effect on the distribution of data points; HDOP 1.6 - 1.1 (3.29 h - c) achieves in removing the occurrence of the additional cluster although preserving minor drift away from the central cluster. The highest intensity approaches (HDOP 1.0 and 0.9) to filtering achieves in removing all drift away from and reducing the size of the central cluster (3.28 b and a).

The PDFs presented in Figure 3.29 correspond to filtering based on specified HDOP values outlined in Figure 3.28. Initially clear is that the standard PDF structure for the complete data; positional deviations in all categories but dominated by 39.1% and 37.5% in the 1.0 m and 1.5 m deviations respectively, remains essentially unaffected by filtering based on HDOP values of 2.0 - 1.7 (Figure 3.29 l - j). Figure 3.29 h - c provides the results of filtering based on HDOP 1.6 - 1.1. Initially clear is a reduction in the number and magnitude of larger migrations; filtering by HDOP 1.6 removes deviations greater than 2.5 m. Filtering utilising lower HDOP values 1.6 - 1.1 achieves in reducing the magnitude of 2.5 m and 2 m deviations and increasing the percentage of values within the 1.5 m and 1 m deviations (41% and 40.5% at HDOP 1.1). Filtering by HDOP 1.0 demonstrates the first PDF where an increase in the 0.5 m and 1 m deviations occurs concurrently with a decrease in 1.5 m magnitude deviation, providing evidence of improving precision and accuracy with more server filtering approaches.

The only clear structural change occurs when filtered by HDOP 0.9 providing for 100% of values within 2 m deviation, nearly 60% of values within 1 m deviation and the percentage of 0.5 m deviations being greater than the 1.5 m category.

Table 3.4 provides the statistically summary of the effect of filtering based on HDOP values. Filtering by HDOP 2.0 – 1.8 demonstrate virtually no change in the filtered data. Filtering by HDOP 1.7 highlights a more distinct improvement in the mean deviation of 0.12 m at a cost of 4.12%. Within the HDOP 1.6 – 1.1 the mean deviation is improved from 1.04 m to 1.00 m returning in excess of 98% of values within 2 m deviation of the mean position for losses between 5.38% - 16.93% of data. Filtering by HDOP 1.0 and 0.9 has significantly greater effects on increasing the precision of position (mean deviations of 0.98 and 0.74 m respectively) and improving the repeatability of measurements (99.64% and 100% of values within 2 m deviation). Again, these improvements are made at a significant cost to the data, removing 37.71% and 85.65% of values respectively).

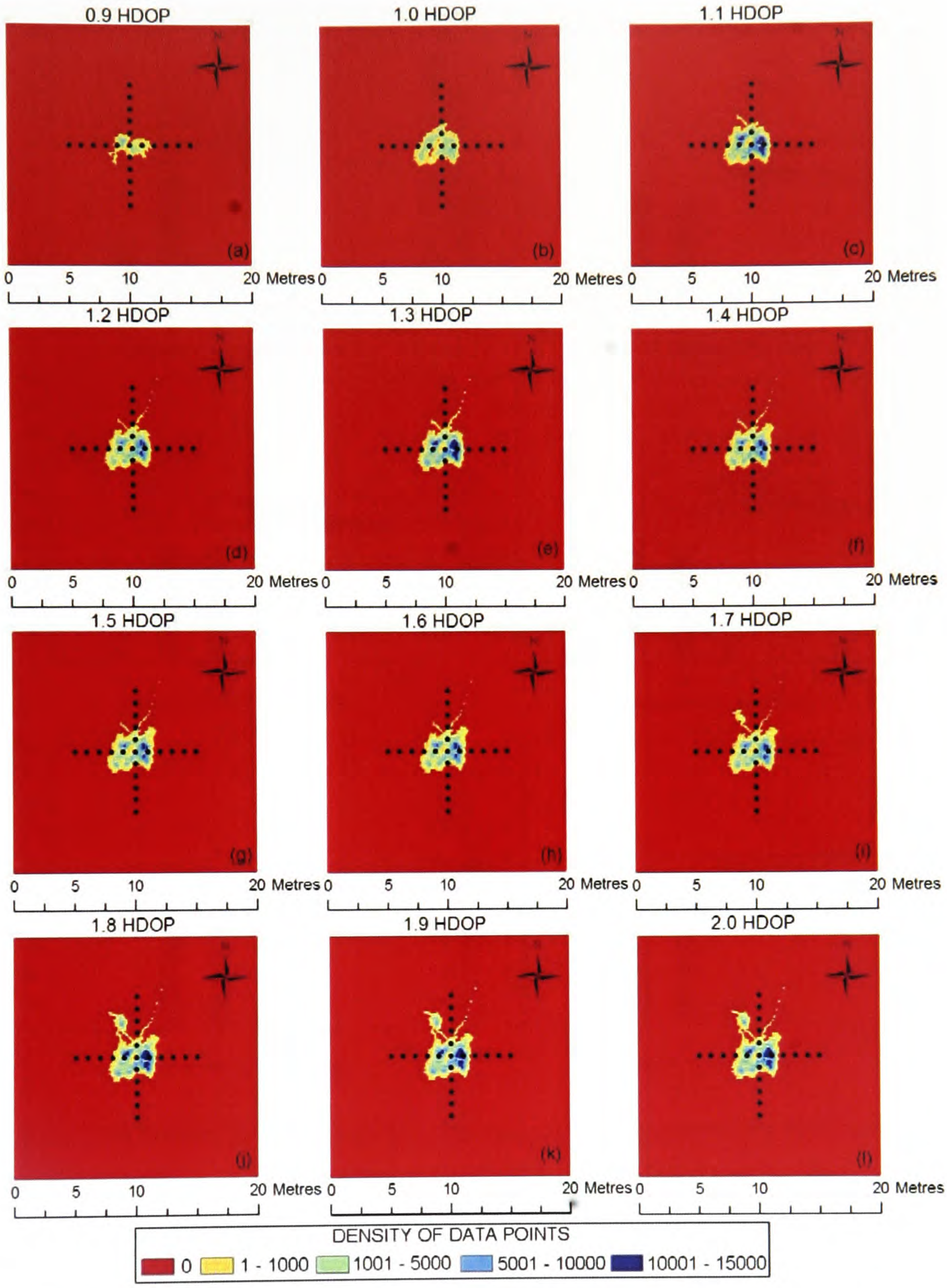

Figure 3.28 Density distribution plots (DDP) of normalised data points from the mean position of each stationary base-station. Each DDP features marker points extending in 1 metre spacing away from the mean position of each dataset and utilises the same graduated colouring and scale. Clear from the distributions provided is improved positional accuracy with decreasing HDOP values. The results presented are generated from the processing of data acquired utilising WAAS-disabled GPS receivers.

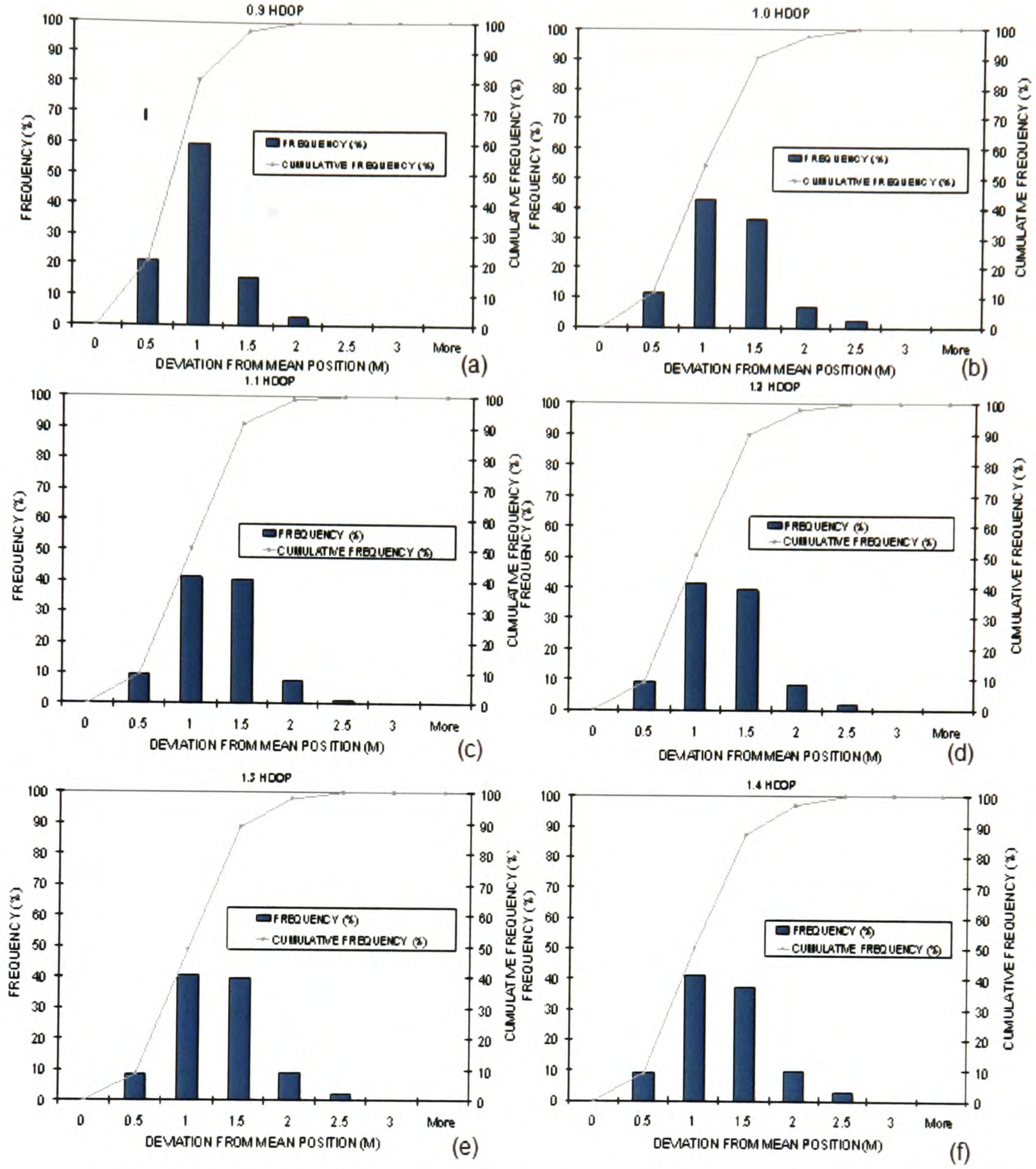

Figure 3.29(Section 1). Density distribution plots (DDP) of normalised data points from the mean position of each stationary base-station. Each DDP features marker points extending in 1 metre spacing away from the mean position of each dataset and utilises the same graduated colouring and scale. Clear from the distributions provided is improved positional accuracy with decreasing HDOP value. The results presented are generated from the processing of data acquired utilising WAAS-disabled GPS receivers.

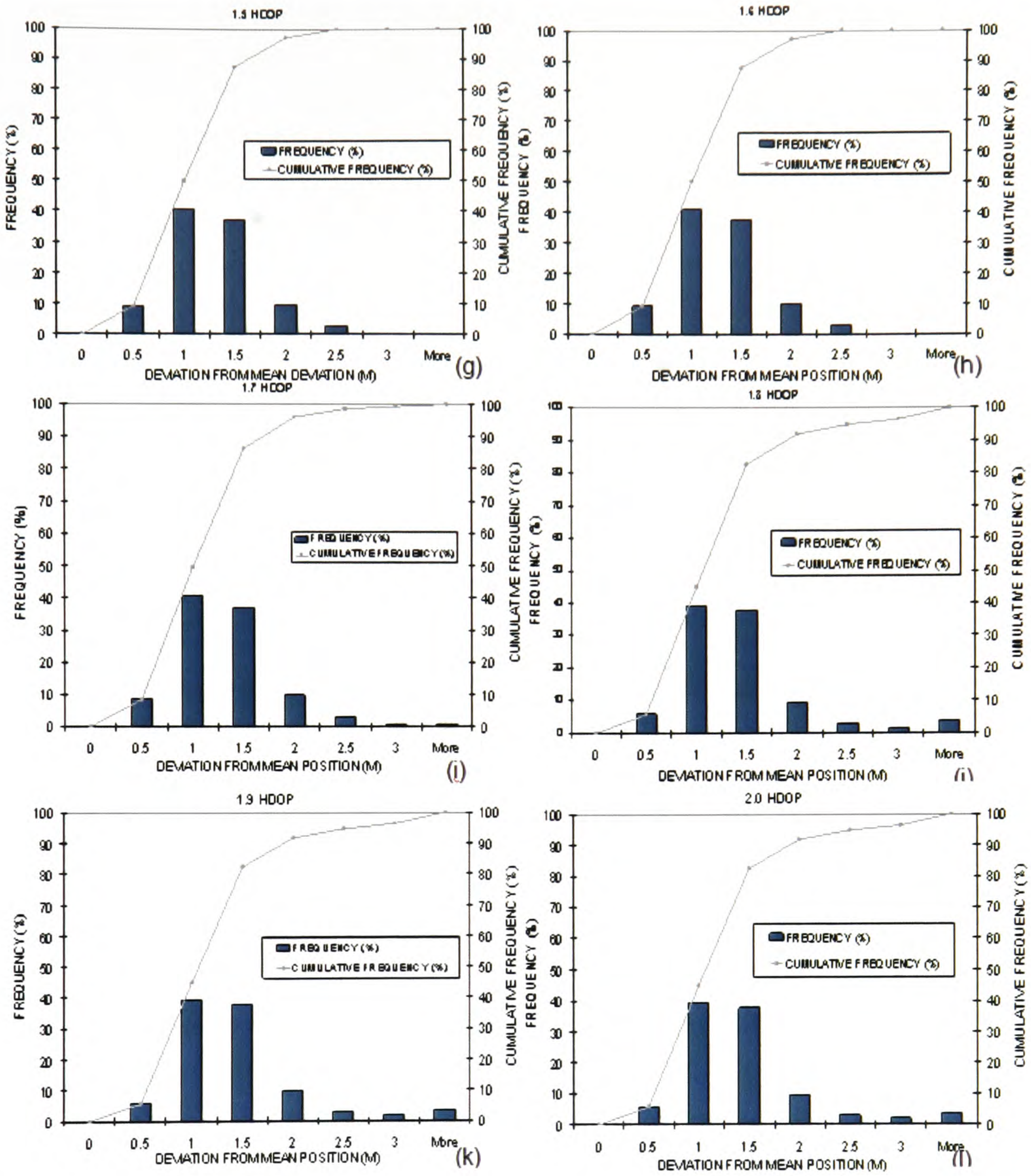

Figure 3.29 (Section 2). Density distribution plots (DDP) of normalised data points from the mean position of each stationary base-station. Each DDP features marker points extending in 1 metre spacing away from the mean position of each dataset and utilises the same graduated colouring and scale. Clear from the distributions provided is improved positional accuracy with decreasing HDOP value. The results presented are generated from the processing of data acquired utilising WAAS-disabled GPS receivers.

HDOP (NON WAAS)	Number of Results	Percentage Remaining (%)	Mean Deviation (m)	Within 2m (%)
ALL	30224	100	1.19	96.43
2	30194	99.90	1.17	91.84
1.9	30194	99.90	1.17	91.84
1.8	30155	99.77	1.17	91.96
1.7	28978	95.88	1.07	95.99
1.6	28599	94.62	1.04	97.2
1.5	28599	94.62	1.04	97.2
1.4	28599	94.62	1.04	97.2
1.3	27872	92.22	1.03	97.94
1.2	26916	89.06	1.02	97.99
1.1	25107	83.07	1.00	98.86
1	18825	62.29	0.98	99.64
0.9	4336	14.35	0.74	100

Table 3.4 Summary of the effects on the precision of positioning when data are filtered using the HDOP.

3.3.3.7 Summary - Filtering WAAS Disabled Data

Filtering based on the number of visible satellites and HDOP values can be used to improve both the precision and accuracy of WAAS-disabled data; however the improvements observed in the repeatability of positioning are again only achieved at a cost. Additionally clear is that the configuration of the GPS utilised for data acquisition (in terms of WAAS-enablement) clearly effects the precision and accuracy of measured positions. Cross-comparison of filtering based on a HDOP value of 1.2 and 8+ satellite for WAAS-disabled data again highlights the increasing sensitivity of HDOP based filtering through the preservation of significantly more data for similar precision and accuracy improvements. HDOP 1.2 preserves 12.71% more data than when data is filtered by 8+ satellites returning a mean that is 0.03 m less precise and 0.1% less values within the desire 2 m deviation.

3.3.4 Positioning Conclusions

3.3.4.1 The Effect of WAAS Enablement

The configuration of the GPS receivers present within each GRiFTer determines whether data is gathered from all orbital satellites (WAAS-enabled) or only standard GPS satellites (WAAS-disabled). The appropriate data acquisition configuration must therefore be determined to maximise accuracy and precision in positioning and velocity measurement.

It is initially apparent that the magnitude of drift observed in the WAAS-enabled data is not present within the WAAS-disabled results. There are two potential reasons for the differences in data structures. The first is that the activation of WAAS is detrimental to positioning (within this environment), whilst the second is that the results returned by the WAAS-enabled receiver throughout stationary tests are anomalous or subject to additional external interference. Throughout the acquisition of data from stationary testing, 8 GPS units were deployed in sequences (WAAS-enabled & WAAS-disabled) in order to ensure that a complete dataset was returned, even if individual units malfunctioned or otherwise failed to return data. This provision allowed for additional WAAS-enabled units to be compared, in order to establish whether the observed drift was in fact related to the operation of WAAS, as opposed to an anomaly in the recorded data.

Figure 3.31 demonstrates the corresponding drift which occurs with a pair of WAAS-enabled stationary units deployed simultaneously at Paull Holme Strays. Similar drift patterns have also been observed when WAAS-enabled GPS receivers have been deployed at other locations demonstrating that these data structures are not merely the result of poor performance with a particular set of environmental conditions. The example provided is taken from the River Swale where two GPS receivers were positioned at either end of the channel (400 m apart) returning similar drift patterns (Figure 3.32). The reoccurrence of similar drift patterns in two completly different locations demonstrates that the drift observed in the WAAS-enabled data (presented through Figures 3.31 and Figure 3.32) occurs as a result of WAAS-enablement in data acquisition.

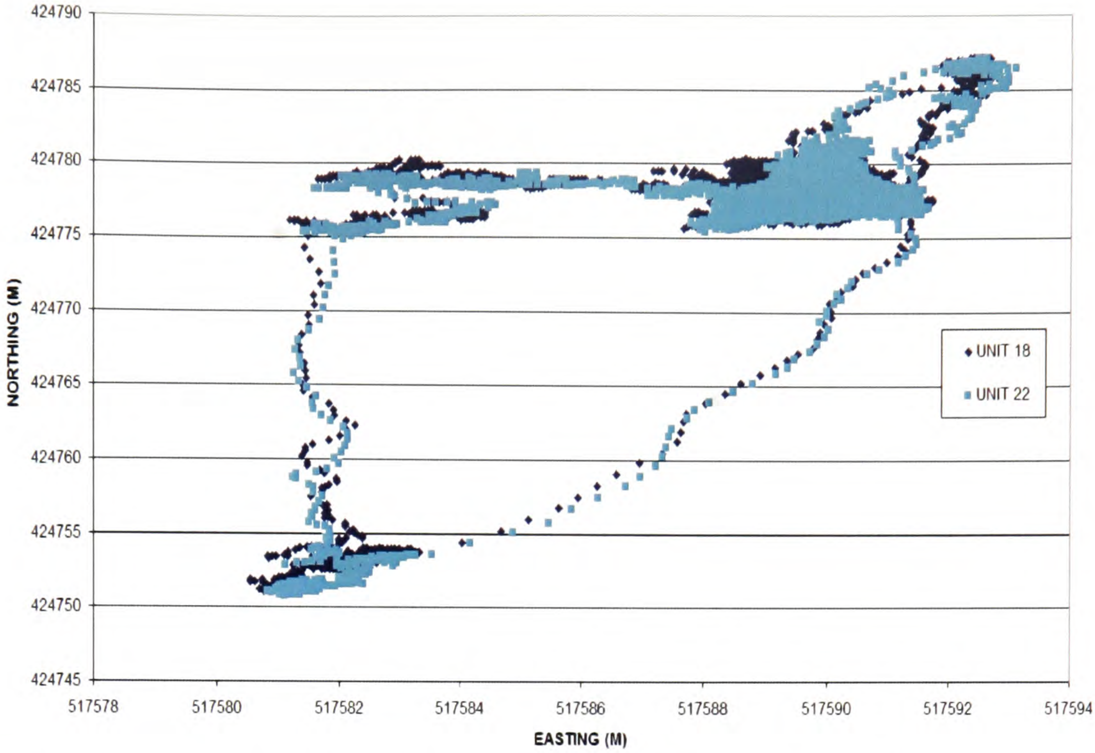

Figure 3.30 Distribution of OSGB positions provided by two SBAS enabled GPS receivers deployed for the same 8 hour period at Paull Holme Strays.

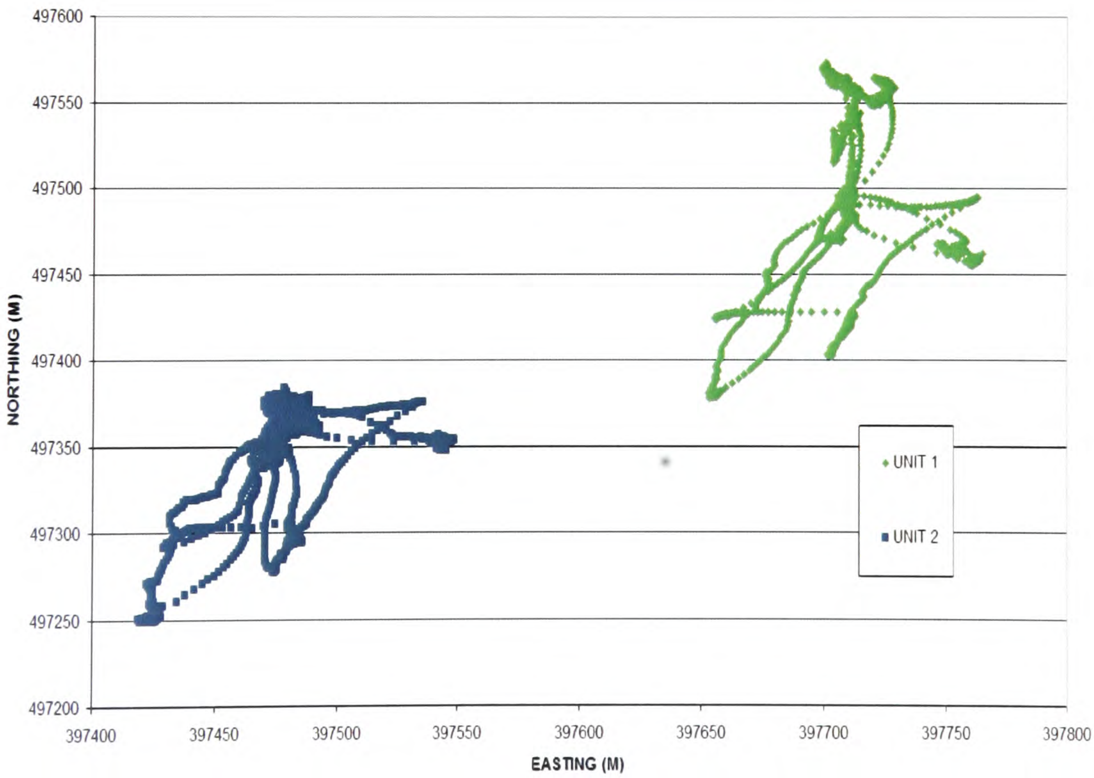

Figure 3.31 Distribution of OSGB positions provided by two SBAS enabled GPS receivers deployed at either extent of a survey reach of the River Swale for the same five hour sampling period.

The occurrence of widespread drift observed in WAAS-enabled data acquisition demonstrates that WAAS-enablement may be detrimental to the performance of GPS positioning over an extended time period. This is potentially due to WAAS activated GPS receivers prioritising data provided by WAAS allocated channels (channels 11 and 12 of the 12 channel receiver utilised). This would result in superior positioning when WAAS satellites are in clear view and inferior positioning when WAAS satellites are unavailable or in an inferior alignment. This can also potentially explain the form of drift in positions away from the central cluster observed in WAAS-enabled data as the GPS receiver searches for WAAS-enabled satellites. This explanation of the interaction between GPS receiver and WAAS satellites is also evidenced by the fact that the WAAS-enabled data is acquired from 10 satellites as opposed to the 11 satellites which provided the WAAS-disabled data when both datasets were drawn form the same environment. This would also mean that the 12 GPS channel capacity would be reduced to a capacity of 10 where WAAS-enabled satellites were unavailable.

In addition to variation in large-scale position deviations (drift), two further structural differences remain in the returned data. The first is the difference in the size and structure of the central cluster of position deviations. For the WAAS-enabled data, the central cluster is larger in the northing component by 1.4 m (unfiltered data), whilst for the WAAS-disabled data, the central cluster is larger in the easting component by 0.4 m (unfiltered data). The second structural issue concerns the resolution of emitted data and the resultant minimum changes in position.

Evident from the DDPs of both WAAS-enabled and WAAS-disabled data is the occurrence of gaps in the data. This is most clearly evident when data is filtered by 8+ satellites (Figure 3.24 D and Figure 3.26 D). In both forms of dataset the minimum change in position, provided by each directional component, is 0.1 m. This occurs as a result of the resolution of the satellite emitted numeric representation of positioning. Though these patterns have little impact upon the use of GPS for positioning at the accuracies required for river investigation, they highlight the complexity of internal calculations which are beyond end-user influence due to their inaccessibility and protection provided by commercial confidentiality. Therefore, interaction with a system where exact calculation methods, for positioning and values representing the quality of measurements (HDOP) are unknown, should be limited to the simplest form to maximise the integrity and repeatability in the results produced.

The structural findings demonstrate that if WAAS-enabled data acquisition is to be used, then although theoretically superior positioning can be achieved, the potential remains for sporadic widespread drift which would be detrimental to the integrity of any surface flow investigation. Therefore, unless the presence of WAAS-enabled satellites can be confirmed throughout the entire duration of testing, then WAAS-disabled data acquisition should be conducted since GPS performance will be more consistent and less prone to large-scale errors.

3.3.4.2 Determining the Appropriate Approach to Post Capture Data Filtering

The principal aim of post capture data filtering is to improve both the precision and accuracy of positioning. Precision is demonstrated by the mean deviation of positions from the true location of the GPS through data acquisition, whilst accuracy is determined by the repeatability of multiple measurements and is therefore described by the percentage of results within the desired 2.0 m deviation (the individual size of the intended cellular representation). Filtering data based on either the number of visible satellites or the HDOP value in addition to potential improving GPS performance inherently incurs losses of collected data. The appropriate approach to filtering must therefore provide the maximum improvement in the mean deviation and the highest percentage of results within 2.0 m deviation, relative to the percentage of results lost through filtering. For ease of comparisons, two relationships are considered; the first (x) is the function of percentage improvement in the mean deviation per percent of results lost through filtering, whilst the second (y) is the function of percentage improvement in the results within 2.0 m deviation of the true position per percent of results lost. The optimal approach to filtering will therefore be highlighted by relative maximum values in functions x and y.

Four figures are presented to highlight the effects of filtering both WAAS and WAAS-disabled data utilising the number of visible satellites and HDOP values (Figure 3.32 - Figure 3.35). Prior to discussing specific filtering values, it must be noted that specific function values can only be compared relative to the same parent population (e.g. WAAS or WAAS-disabled data) since improvements are based on changes to initial, full datasets. This is highlighted by the x and y values returned through filtering based on 8+ satellites; although the function (x) value is significantly larger for the WAAS-enabled results, the filtered mean deviation is 0.08m higher with 9.98% less results maintained than for the WAAS-disabled results. The inability to conducted cross-population comparisons between WAAS and WAAS-disabled results is not however detrimental to determining the most appropriate means of filtering since it has been determined that WAAS-enabled data acquisition should not be used due to the widespread and sporadic drift which occurs.

Initially apparent is that filtering WAAS-enabled results produces more precise results at the same magnitudes of filtering however WAAS-disabled results are more accurate when filtered by the same magnitude values. These results appear sensible when the intended use of WAAS-enablement is to increase the precision of positioning however as identified previously extended use of WAAS-enablement data capture can lead to widespread drift and deterioration of the accuracy of GPS positioning (Figure 3.32 - Figure 3.35).

The four function figures described previously are utilised to identify the most appropriate filtering values with respect to the optimising the precision and accuracy of GPS performance:

1. Figure 3.32 demonstrates that if filtering is to be conducted based on the number of visible satellites, then 8+ satellites provides the optimal approach for improving the mean deviation in position (precision) relative to the proportion of values lost.
2. Figure 3.33 highlights that for HDOP based filtering the best approach to maximising precision is provided by HDOP 1.2.
3. Figure 3.34 provides that if filtering is to be conducted based on the number of visible satellites, then 8+ satellites again provides the best approach for maximising the percentage of results within the desired 2.0 m deviation in position, relative to results lost.
4. Figure 3.35 demonstrates that filtering based on HDOP 1.1 provides the optimum result.

These results therefore highlight three potential approaches to filtering GPS data for improving the precision and accuracy of positioning, a summary of which is presented in Table 5.

Apparent from Table 3.5 is that the difference in precision (0.03 m) and difference in accuracy (0.97%) are both essentially negligible meaning that the percentage of results remaining following filtering provides the definitive argument to the selection of the best approach to filtering. Filtering based on HDOP 1.2 preserved 12.7% more data than filtering by 8+ satellites and 6% more data than filtering by HDOP 1.1. Though it has been discussed that the precise method of HDOP calculation is unknown due to commercial confidentially, the results demonstrated in Table 5 highlight that filtering by HDOP 1.2 provides a more robust and appropriate approach to filtering.

Figure 3.36 provides a comparison of the number of visible satellites against corresponding HDOP values. Though clearly related, the use of HDOP values allows for the use of data points provided by lower numbers of visible satellites that are in superior geometrically arrangements and is therefore more appropriate to described conditions likely to return more precise and increasingly accurate positioning.

In conclusion, the acquisition of WAAS-disabled data, filtered by HDOP 1.2 provides the optimal approach to maximising the precision and accuracy of positioning. It is however important to note that the optimal approach to post-capture filtering of WAAS-disabled data outlined here is temporally and spatially specific and therefore the parameters of which require determining at each new field test location, date and time.

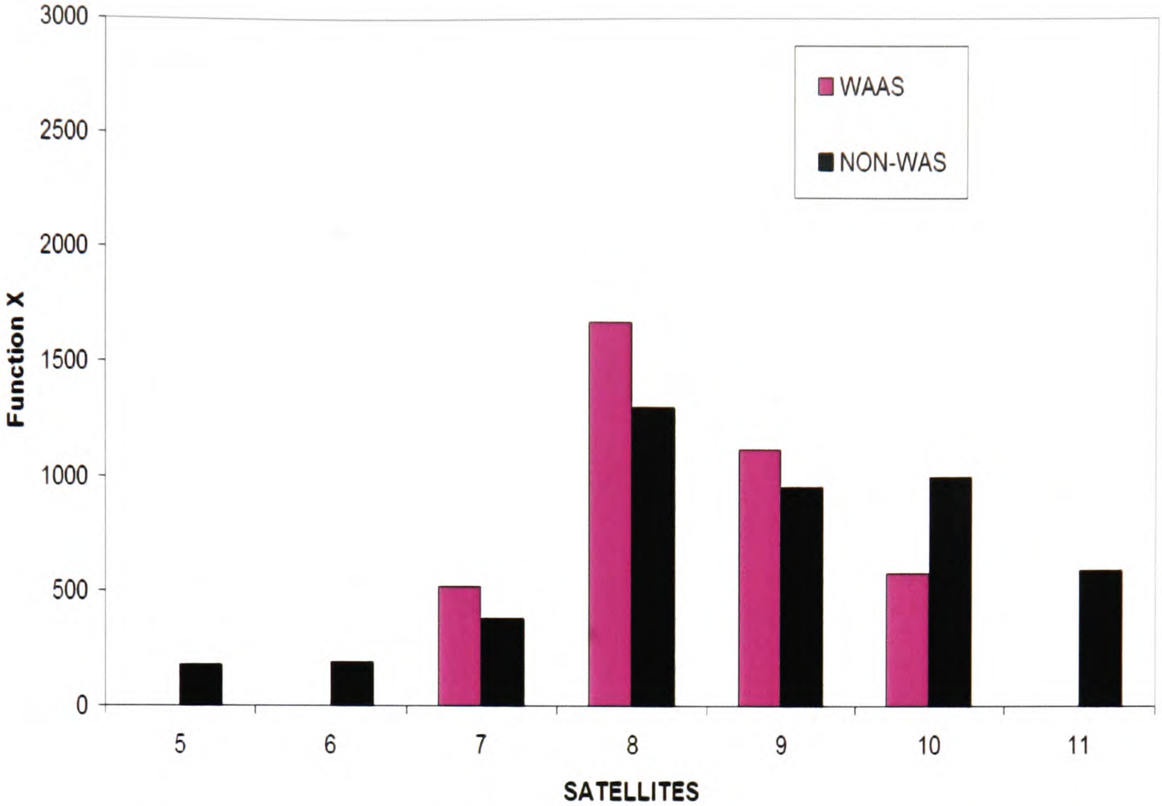

Figure 3.32. Column graph representing the Function X values relative to the number of visible satellites.

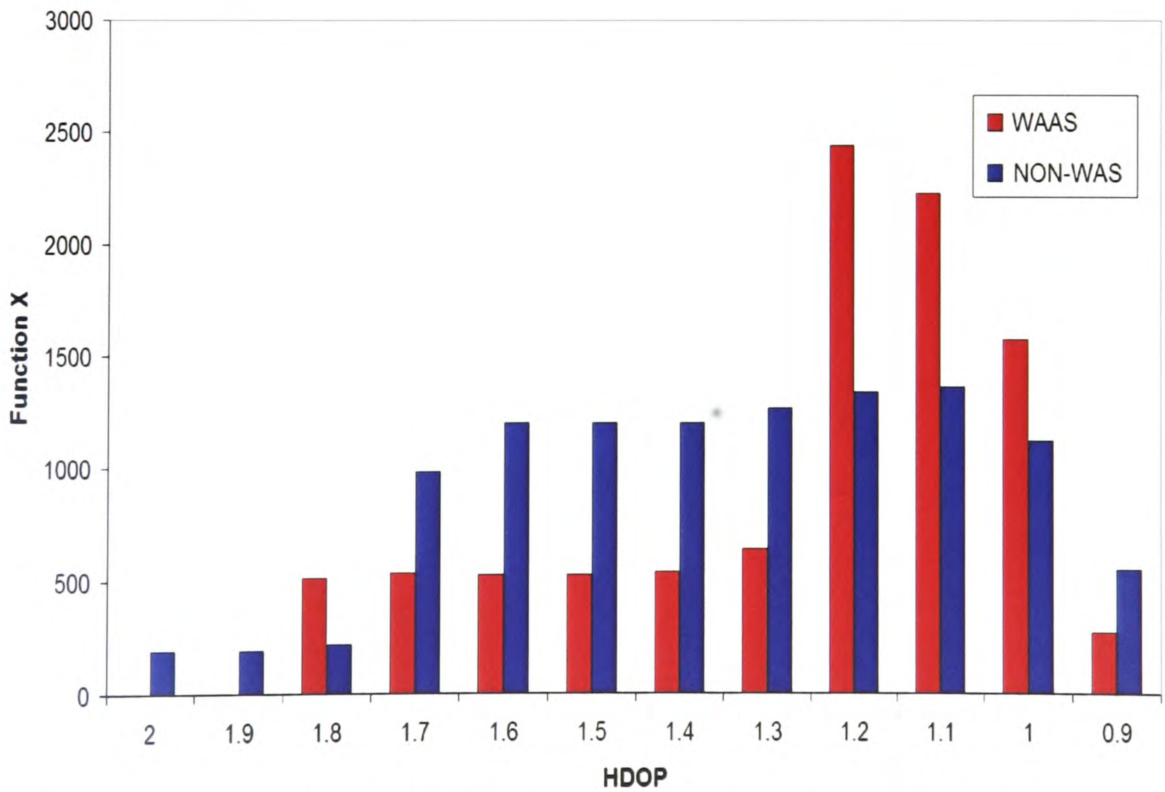

Figure 3.33 Column graph representing the Function X values relative to HDOP values.

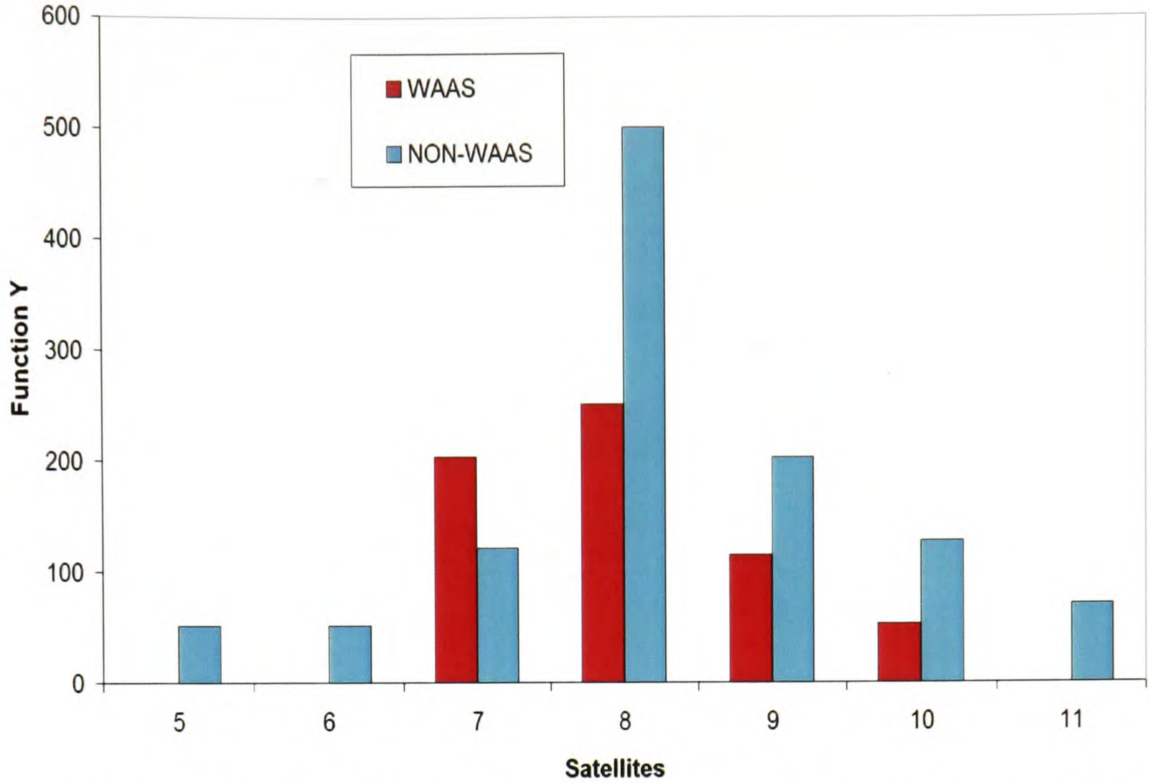

Figure 3.34 Column graph representing the Function Y values relative to the number of visible satellites.

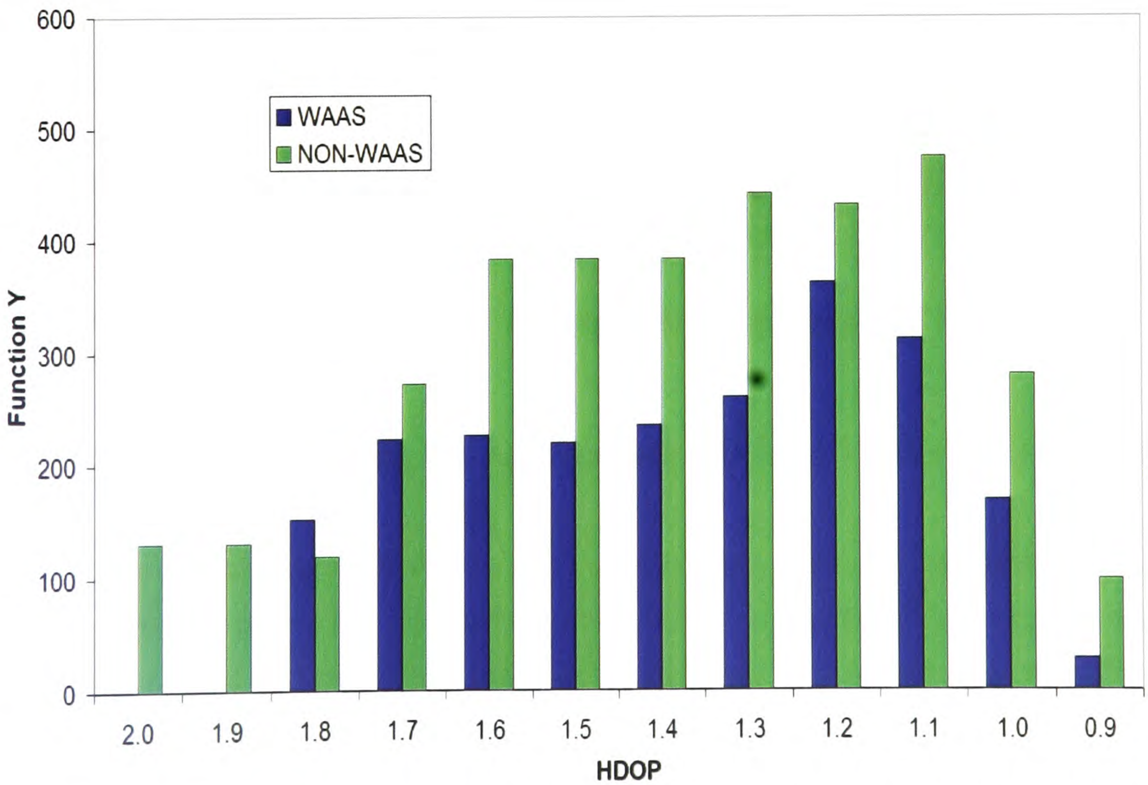

Figure 3.35 Column graph representing the Function Y values relative to HDOP values.

FILTERING MECHANISM		RESULTS REMAINING (%)	MEAN DEVIATION (M)	WITHIN 2m (%)	FUNCTION (X)	FUNCTION (Y)
HDOP	1.2	89.06	1.02	97.99	1335	431
HDOP	1.1	83.07	1.00	98.86	1359	474
Satellites	8	76.35	0.99	97.89	1307	501

Table 3.5. Summary of the short-listed approaches to filtering GPS data for improved precision and accuracy relative to results lost through filtering.

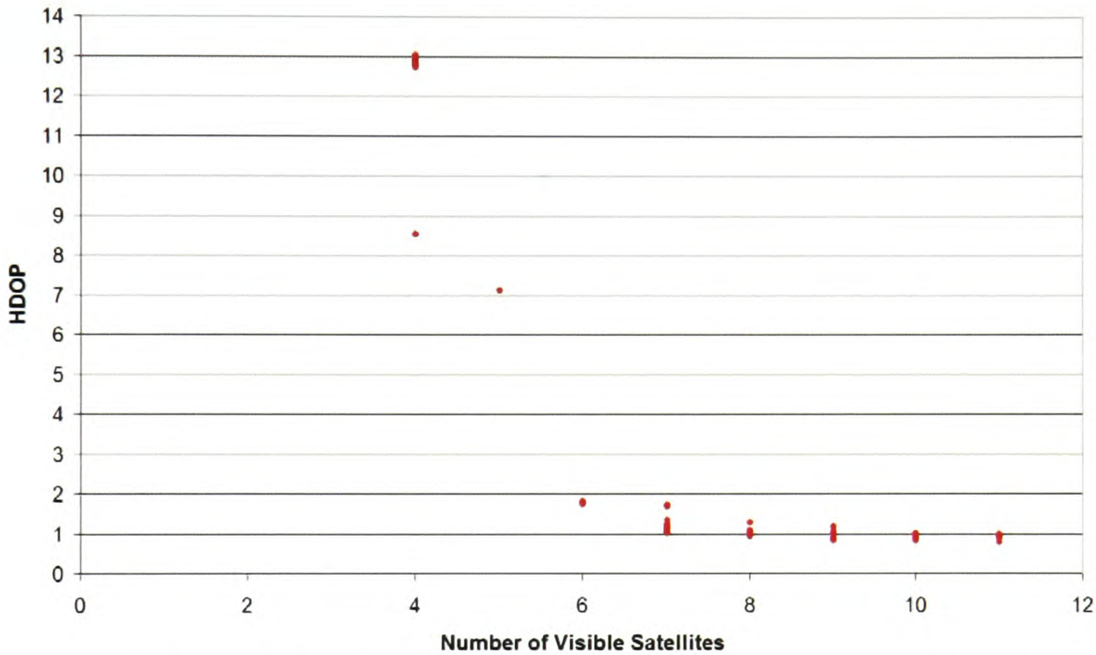

Figure 3.36 The relationship between the number of visible satellites and the corresponding HDOP value for each data point taken from a WAAS-disabled stationary base-station deployed for 8 hours – Paull Holme Strays.

3.3.5 Utilising the GPS for the Measurement of Velocity

3.3.5.1 Determining the Appropriate Method of Velocity Calculation

As previously described, the quality of cellular representation is determined by both the ability to precisely and repeatedly position individual results within the correct cell and the accuracy with which each individual velocity can be measured. Prior to establishing the achievable accuracy of velocity measurements, it is first necessary to determine the most appropriate method of velocity calculation. Velocity can be provided through Doppler measurement or by calculations made from changes in position over known time periods. To determine whether calculated or Doppler velocities provide the most accurate approach to velocity measurement, the appropriate time period over which comparisons should be made must be established.

To facilitate comparison of velocity measurements, stationary testing is utilised to identify any measured velocities as errors. Table 3.6 provides a statistical summary of apparent Doppler velocity results returned from a stationary WAAS-disabled GPS receiver filtered utilising the HDOP value. Having previously determined that HDOP 1.2 provides the most appropriate method of position calculation, the corresponding apparent Doppler velocity following filtering is 0.034 ms^{-1}.

Figure 3.37 demonstrates the decreasing mean apparent calculated velocity provided by increasing the period over which each velocity is calculated. Individual values feature error bars providing 99% confidence intervals for velocities calculated with each (t) value. The mean apparent Doppler velocity for HDOP 1.2 is marked on the Figure 3.37 by a continuous red line. Intersection of the mean apparent Doppler and mean apparent Calculated velocities occurs at t = 12 seconds. Therefore, in order to achieve the same level of accuracy in calculated velocities as Doppler velocities a (t) value of 12 s should be used.

When considering the potential application of calculated velocities, a sampling time of 12 seconds would fail to provide sufficient sensitivity to small scale fluctuations in flow. Surface velocities have commonly been observed within the range of 0.5 - 1.5 ms^{-1}, meaning that a single velocity measurement may be required to represent between 6 m and 18 m of flow. In order to provide results spatially comparable with those returned by Doppler velocities a 1 second averaging period would be required. Utilising a 1 second calculation period would however yield a mean deviation / error of 0.13ms^{-1}. Therefore, the use of Doppler velocities provides a more accurate and therefore appropriate method for the measurement of surface flow velocities using the GRiFTer technique.

HDOP (NON WAAS)	Number of Results	Percentage Remaining (%)	Mean Velocity (ms^{-1})
ALL	30224	100	
2	30194	99.90	0.035
1.9	30194	99.90	0.035
1.8	30155	99.77	0.035
1.7	28978	95.88	0.035
1.6	28599	94.62	0.035
1.5	28599	94.62	0.035
1.4	28599	94.62	0.035
6.4	27872	92.22	0.035
6.3	26916	89.06	0.034
1.1	25107	83.07	0.033
1	18825	62.29	0.032
0.9	4336	14.35	0.028

Table 3.6. Summary of the effects upon the apparent Doppler velocity when HDOP is utilised as a mechanism for filtering.

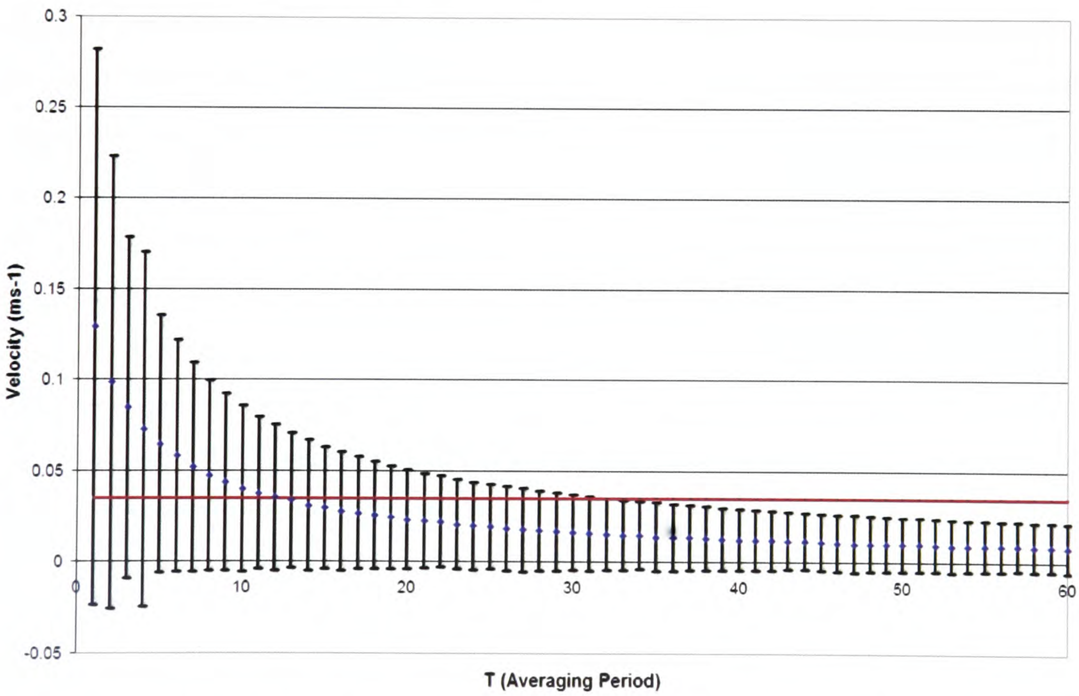

Figure 3.37 The relationship between mean apparent velocity error and the period over which each velocity was calculated. The error bars associated with each value represent 99% confidence intervals. The red line across all values represents the mean Doppler velocity returned when filtered to HDOP 6.3 with equal mean values for both Doppler and calculated approaches occurring at t = 12 seconds.

3.3.5.2 GPS Velocity Measurement Methods

An initial set of GPS velocity measurements were made in idealised satellite conditions at a local airfield free from potential overhead obstacles or signal multipathing surfaces. Velocity measurements were made utilising a set of 5 GPS units configured to be WAAS-disabled with results subsequently filtered using a HDOP value of 1.2.

The velocity comparison tests were conducted utilising a trolley (mounted with GPS units) drawn by a pulley arrangement fixed at the end of a 30 m course. The speed of the pulley system was determined by the size of the cog arrangement with rotation controlled by a geared electric drill to ensure consistent speed. The cog arrangements provided three speeds (0.3 ms^{-1}, 0.6 ms^{-1} and 1 ms^{-1}). 5 tracks were conducted at each speed and the GPS measured velocities were compared to independently stop-watch timed velocities (See Figure 3.21 a and b).

Figure 3.38 provides the unedited WAAS-disabled measurements of three independently timed velocities. The data is unedited since, in these conditions, all data points have values within HDOP 1.2. Regression analysis highlights that the rate of change is 1.03x representing a 3% error in velocity measurement, whilst the $R^2 = 0.99$ demonstrates an excellent degree of correlation. The magnitude of errors observed throughout field-testing, which sought to replicate the velocities likely to be observed throughout flow investigation, returned errors that would not be detrimental to the analysis of measured surface flow patterns. It is also important to note that the assessment of 3% error in GPS Doppler velocity measurements may be the result of human error in the measurement of timed velocities. Additionally, although the satellite conditions present throughout velocity comparisons were classifiable as ideal, the surface of the airfield was uneven and potentially gave rise to additional errors.

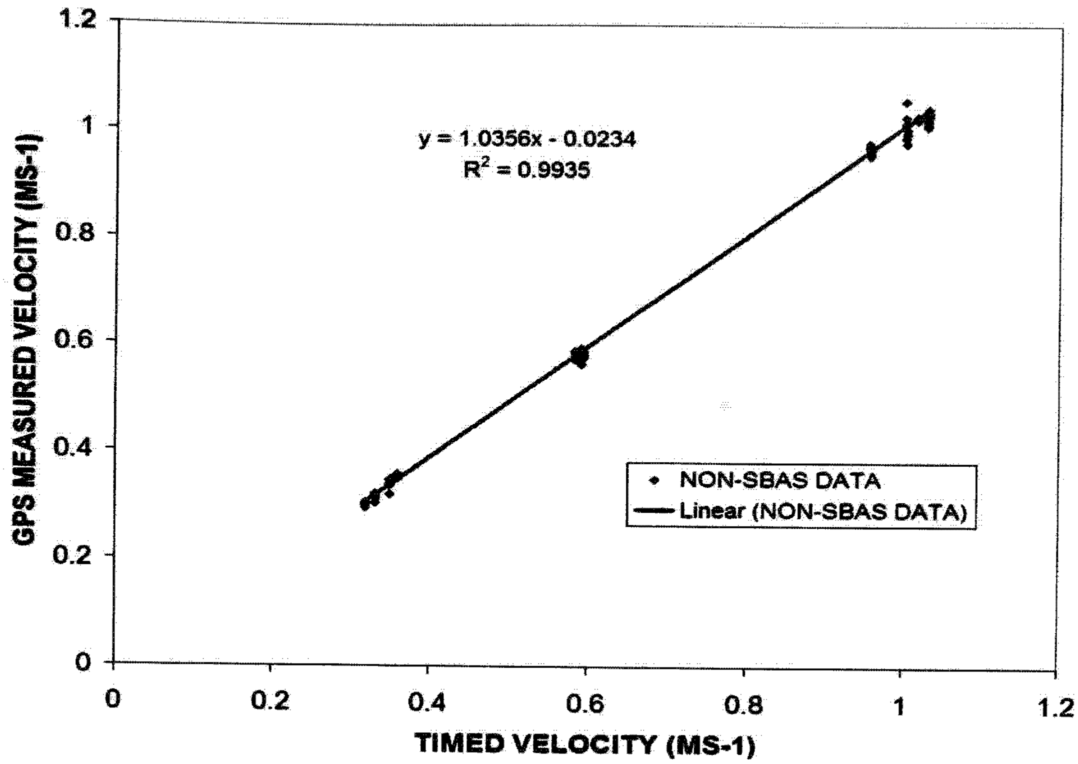

Figure 3.38 Regression analysis of the relationship between independently timed velocities and the unedited Doppler velocities provided in idealised conditions by WAAS-disabled GPS receivers.

A second set of velocity comparisons were made in an urban car park in Barton Upon Humber. The site was selected to provide intentionally degraded GPS performance and as such contained potential signal multipathing surface (cars, lamp posts and trees) and a shopping centre which would limit the number of visible satellites. The data acquired from this site also allowed for the effects of HDOP 1.2 filtering to be tested with reference to effect it has upon the accuracy of velocity measurements.

Figure 3.39 provides regression analysis of the unedited WAAS-disabled data. Regression analysis demonstrates 11% error in the measurement of velocity and an R^2 value of 0.97 providing an excellent fit of the relationship to the dataset. Following filtering based on HDOP 1.2, regression analysis demonstrates that error in the measurement of velocity is reduced to 3%, a figure below that observed in the unedited ideal conditions (Figure 3.40). Additionally, the $R^2 = 0.9988$ highlights that the linear relationship more accurately represents the entire dataset. The calculation of errors of lower magnitudes than those observed in ideal satellite conditions demonstrates the potential effect of filtering based on HDOP 1.2.

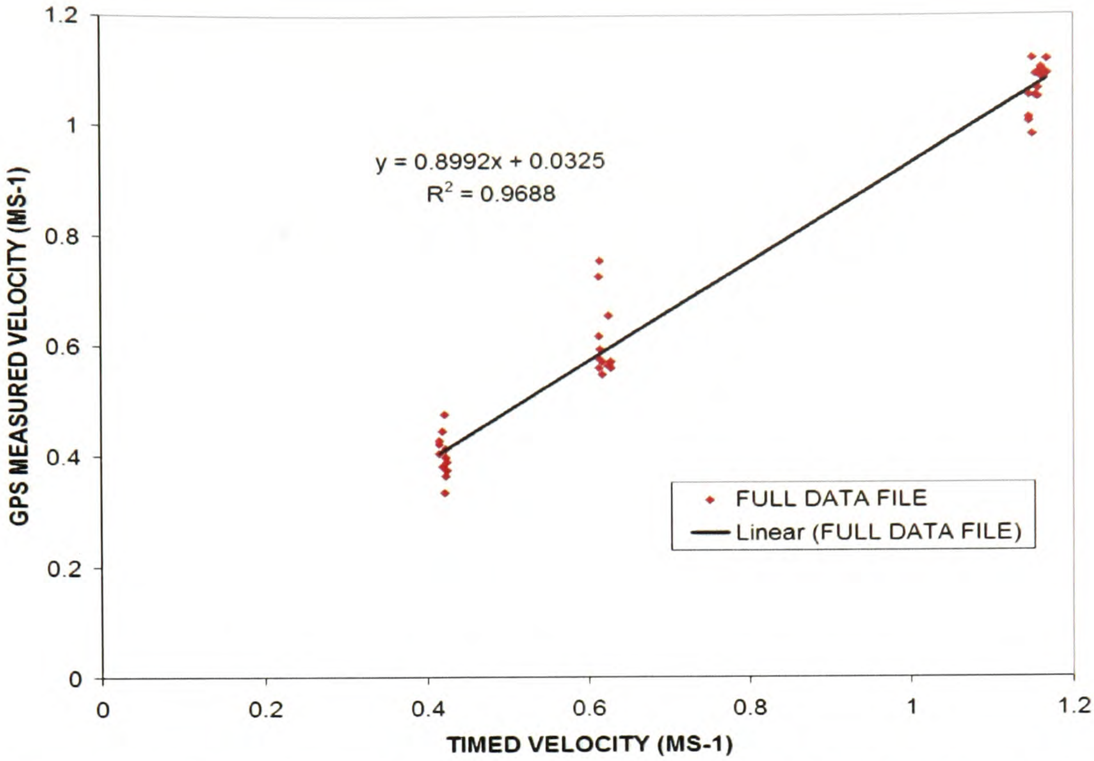

Figure 3.39 Regression analysis of the relationship between independently timed velocities and the unedited Doppler velocities provided by WAAS-disabled receivers.

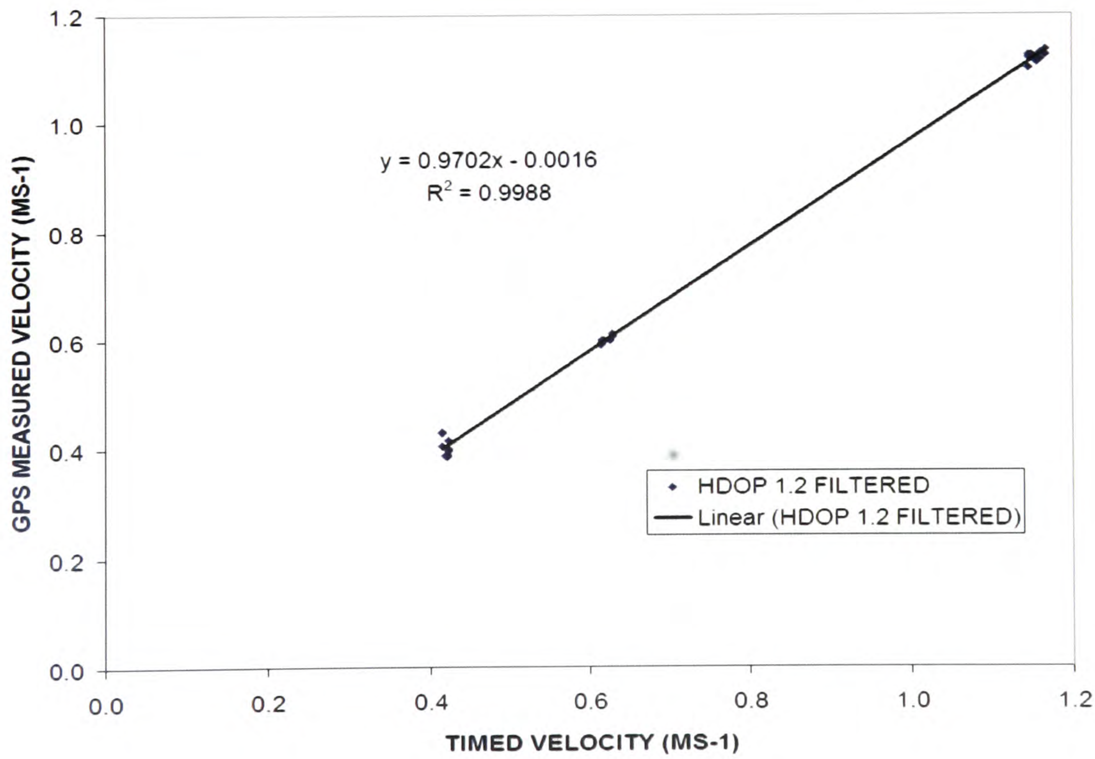

Figure 3.40 Regression analysis of the relationship between independently timed velocities and the Doppler velocities provided by filtering WAAS-disabled data by HDOP 1.2.

3.3.6 Determining the Correct Approach To GPS Course Calculation

Any attempt to investigate surface flow dynamics utilising GPS measurements requires analysis of the individual directions of flow. In order to present individual reaches as a series of grid cells, each containing representative summary statistics, it is necessary to establish the direction of flow which corresponds to each velocity measurement.

Figures 3.41 A and B both provide four theoretical velocity measurements within a single grid cell, each of which has a magnitude of 1 ms^{-1}, each arrow represents the direction of flow of each velocity measurement. Figure 3.41 A would return a mean velocity of 0 ms^{-1} due to two pairs of counteracting velocity vectors with equal magnitude and opposing directions. Figure 3.41 B would results in a mean velocity of 1.0 ms^{-1} due to four velocities of equal magnitudes and equal directions. Therefore without an accurate course calculation method both Figure 3.41 A and B would return identical velocities and therefore falsely represent the behaviour of surface flow dynamics within a specified area.

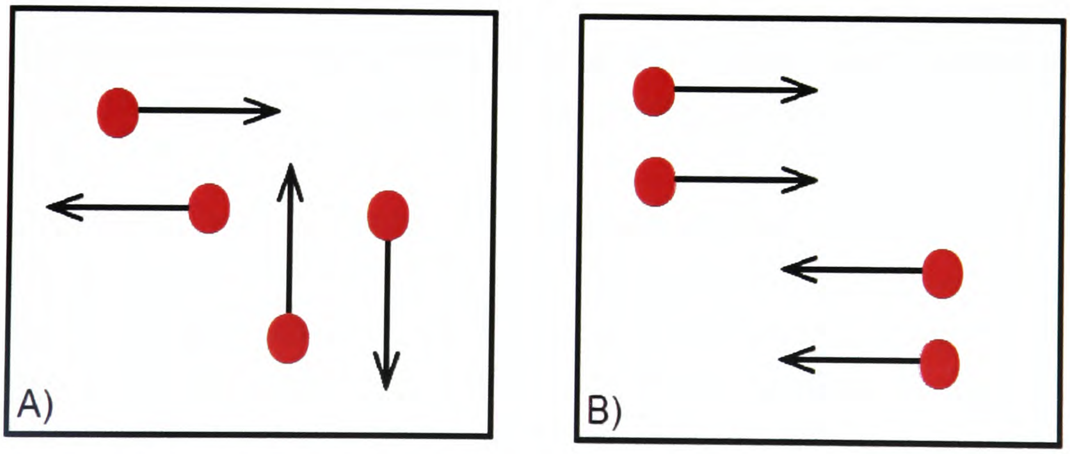

Figure 3.41 Individual velocity points that comprise a representative grid cell.

3.3.6.1 Course Calculation Methods

As demonstrated when considering the appropriate method of velocity measurement, there are two methods of extracting vector properties from GPS measurements; either directly from Doppler outputs or by calculations (*cCal*) made utilising changes in position (e_t and n_t) over specified time periods (t).

$$cCal = \tan^{-1}\frac{e_t - e_{t-1}}{n_t - n_{t-1}}$$

Equation 4 - Calculation method for course using changes in position over specified time periods.

In addition to the methods previously outlined for velocity calculations, the potential of engineering a hybrid approach which utilises independently calculated courses weighted relative to measured Doppler velocities (which have previously been demonstrated to be the more accurate approach to velocity measurement).

3.3.6.2 Validation Tests

In order to establish the appropriate course calculation method a series of tests were performed upon two sets of position data acquired using a WAAS disabled GPS receiver. The first set of control data was collected from a single lap of the Hull University Cricket Circle (Figure 3.42) to provide the full range of direction changes. The second control data set was taken from a single flow path following the deployment of a WAAS-disabled GPS receiver at the River Swale (Figure 3.43).

Following the collection of control position data (x, y positions), a series of theoretical courses were calculated utilising the three calculation methods then for comparison the deviation from each individual position was measured. For the calculated course method, time periods between 1s and 10s were investigated whilst for the hybrid approach averaging periods of 1s, 3s and 10s were tested. Each course calculation / measurement approach was then considered relative to the control course to measure the deviation in position of each individual measurement with the cumulative deviation in position provided to represent the accuracy of each approach over the entire testing period.

Figure 3.42 Aerial photograph of control course provided by walking a WAAS-disabled GPS around the Hull University Cricket Circle.

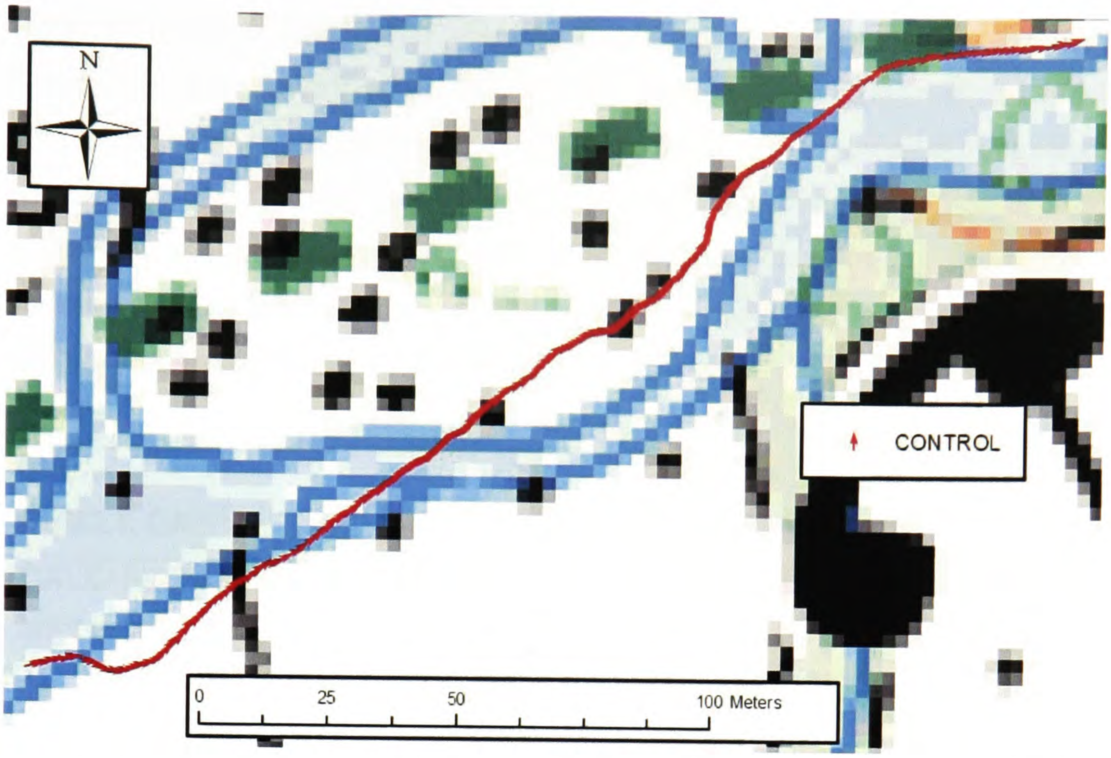

Figure 3.43 Schematic of control course provided by the release of a single WAAS-disabled GPS receiver at the River Swale.

3.3.6.3 Validation Test Results

The result of each approach to course calculation are presented in Table 1 A (corresponds to Figure 3.42) and Table 1 B (corresponds to Figure 3.43). By virtue of the parent population of each dataset comprising a different number of results it is not possible to make cross comparisons of the quality of course calculation methods. Therefore, the results of each approach are presented independently on two graphs with the optimal course calculation / measurement method provided by the lowest cumulative deviation (Figure 3.44 and Figure 3.45).

Figure 3.44 and 3.45 features the results produced from utilising t values of 1s, 3s, 5s and 10 s in calculated velocities in addition to the Doppler measurements and hybrid course provided by combining a 1s calculating period and Doppler velocity. Several patterns appear across both figures (3.44 and 3.45), the first is that with increasing time periods in calculated approaches the cumulative deviation increases, this is highlighted by the largest cumulative deviations occurs with the t = 10s calculated approaches in addition to the Doppler method. The smallest cumulative deviations occur in both field-tests using the independent course calculation method using t values of 3s (circle test) and 1s (flow test) respectively. The difference between the cumulative deviations for t values of 1s and 3s are however virtually insignificant and equated to a difference of 0.03m in the mean deviation from the controlled positions (2.33m for t = 3s and 2.36 for t = 1s). Therefore, when assessing the best approach for course calculation, the higher resolution of data provided by a value of t = 1s determines it as the optimal approach. The results of calculating courses based upon position deviations using a t value of 1s are presented in Figure 3.46 and Figure 3.47 and highlight the potential accuracy of utilising this form of course calculation.

(A) CIRCLE DATA	
CALCULATION METHOD	CUMULATIVE DEVIATION
1s	416
2s	623
3s	410
4s	614
5s	637
6s	830
7s	866
8s	1054
9s	1087
10s	1264
DOPPLER	1170
HYBRID1	734
HYBRID3	773
HYBRID 10	764

(B) FLOW PATH DATA	
CALCULATION METHOD	CUMULATIVE DEVIATION
1s	347
2s	380
3s	420
4s	456
5s	415
6s	430
7s	491
8s	483
9s	629
10s	606
DOPPLER	1472
HYBRID1	593
HYBRID3	673
HYBRID 10	1628

Table 3.7 Statistical summary of the cumulative deviation in position from the control position for each course calculation method. (A) Hull University Cricket Circle. (B) Flow path, River Swale.

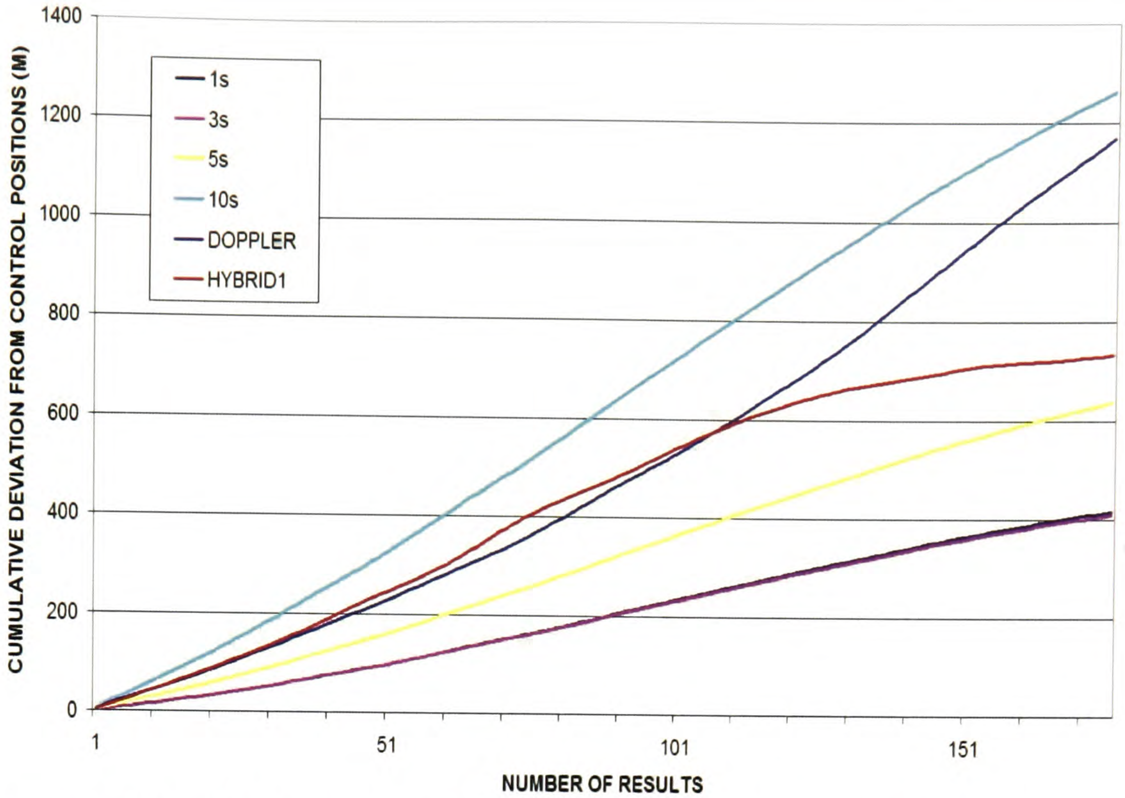

Figure 3.44 Graphical representation of the developing cumulative deviation from control position from each calculation / measurement approach (circle data).

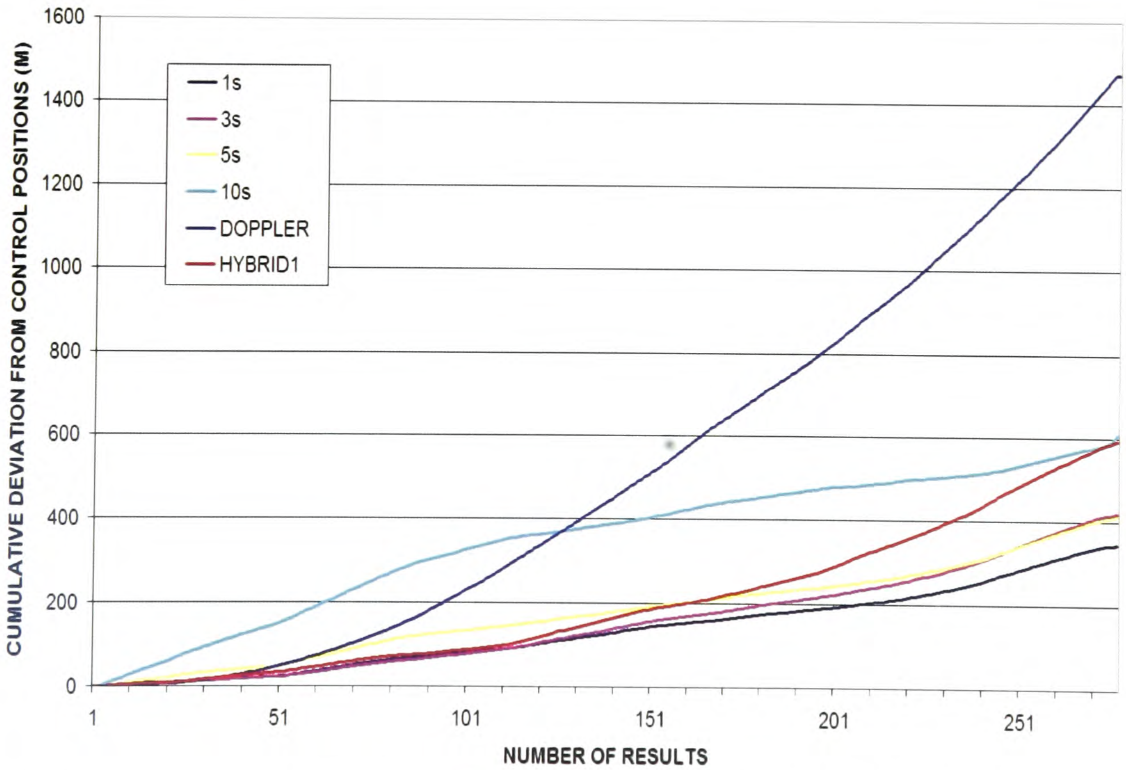

Figure 3.45 Graphical representation of the developing cumulative deviation from control position from each calculation / measurement approach (flow path data).

Figure 3.46 Schematic of control course and t = 1s calculated course provided by walking a WAAS-disabled GPS around the Hull University Cricket Circle.

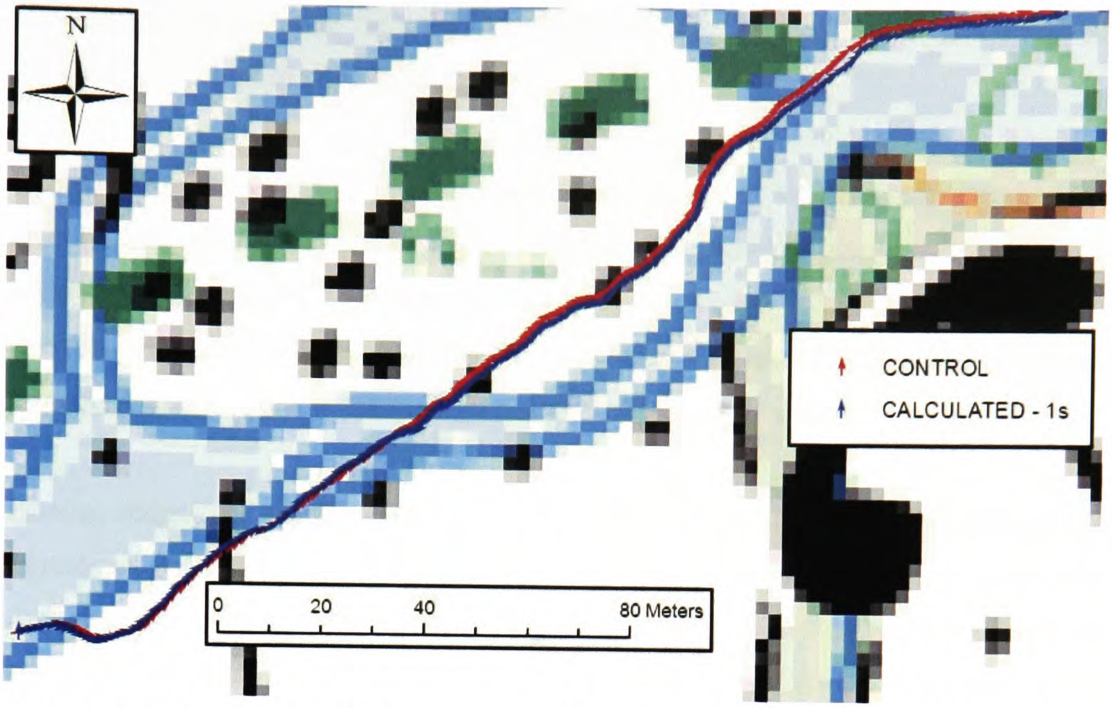

Figure 3.47 Schematic of control course and t = 1s calculated course provided by the release of a single WAAS-disabled GPS receiver at the River Swale.

3.4 Comparative Validation of GRiFTer Velocity Measurements

3.4.1 The Precision and Accuracy of GRiFTer Based Flow Investigations

Throughout chapter 3 the logistic of designing, engineering, and then performing GRiFTer based flow investigations were considered. Following the determination that it was possible to apply a GRiFTer based approach to natural formed river system it was vital to ascertain the precision and accuracy with which flow measurements could be made. It was initially determined that WAAS-disabled data acquisition should be utilised to provide more consistent results and that a HDOP value of 1.2 should be utilised in post-processing to optimise the precision and accuracy of positioning.

Following post-processing, the precision of positioning improves to a mean deviation of 1.02 m from the known positioning and accuracy improves with 98% of results within the desired 2 m deviation from the mean position. These improvements are achieved at the costs of 10% of the full dataset.

In addition to the precision of positioning, the accuracy of velocity measurements were also established. Tests performed in an environment known to posses degraded satellite conditions determined that velocity could be measured in the expected range of magnitudes within 11% of true known velocities. Post-process filtering of this data improved performance to within 3% error of the known velocities.

Having determined these confidence factors for the performance of GRiFTer based flow investigation, it remained to perform a comparative validation against a similar field measurement method. The simplest comparative approach was to utilise a propeller meter to perform measurement comparisons against GRiFTer calculated cellular velocities. Propeller meters present the simplest and most cost-comparable comparative approach in terms of flow velocity measurement. It is important to note that the relationship would not be perfect since, as previously highlighted the use of propeller meters is limited in natural river environments and cannot provide genuine surface velocity measurements.

3.4.2 GRiFTer Performance Validation

In excess of 200000 data points were acquired over an eight hours testing period at Low Row on the River Swale. These results were utilised to create a cellular representation of the reach. Simultaneously 49 propeller meter measurements were taken across the reach and are featured in Figure 3.48 marked by white circular points. Field data were then filtered based on a HDOP value of 1.2, with measurements removed where propeller meter velocities could not be compared to cellular values comprised of velocity with appropriate HDOP values. Filtering the results based on HDOP values of 1.2 results in the removal of 14 of 49 measurement points preserving 35 measurements. Filtered data is presented in Figure 3.49 with the location of propeller measurements marked with black circles.

Figure 3.50 provides the relationship between GRiFTer calculated cellular velocities and propeller meter velocities from the River Swale 121007. Figure 3.50 provides regression analysis of the propeller measurements made at the River Swale (Figure

3.48). Evident from Figure 3.50 is that unedited GRiFTer velocities are made within 23.5% of propeller meter measured velocities. However the R^2 value of 0.4851 highlights that the linear regression is relative poor for the dataset suggesting that this measure of deviation between velocities is flawed. Filtered data (Figure 3.51) highlights that the relative error of GRiFTer velocities to propeller meter velocities is less than 4%. Further the R^2 value improves to 0.84 demonstrating that the regression has a improved fit to the data and provide greater assurance as to the validity of the measure of error. Error bars feature on each data point in both Figure 3.50 and Figure 3.51 providing 11% errors for unedited data and 3% error for edited data in the x-axis and the standard deviation in velocities for the y-axis.

It is clearly apparent from Figure 3.51 that GRiFTers can be utilised to provide both precise and accurate measurement of surface flow velocities within natural river environments. Propeller meters are inherently unable to make genuine surface velocity measurements therefore and comparison to GRiFTer measured surface velocities is unlikely to be complete. Further, as previously described, propeller meters are prone to error particular in gravel-bed river environments. Therefore if the measurements returned by the propeller meter underestimate velocities then GRiFTer measurement are likely to be more precise then the errors represented here.

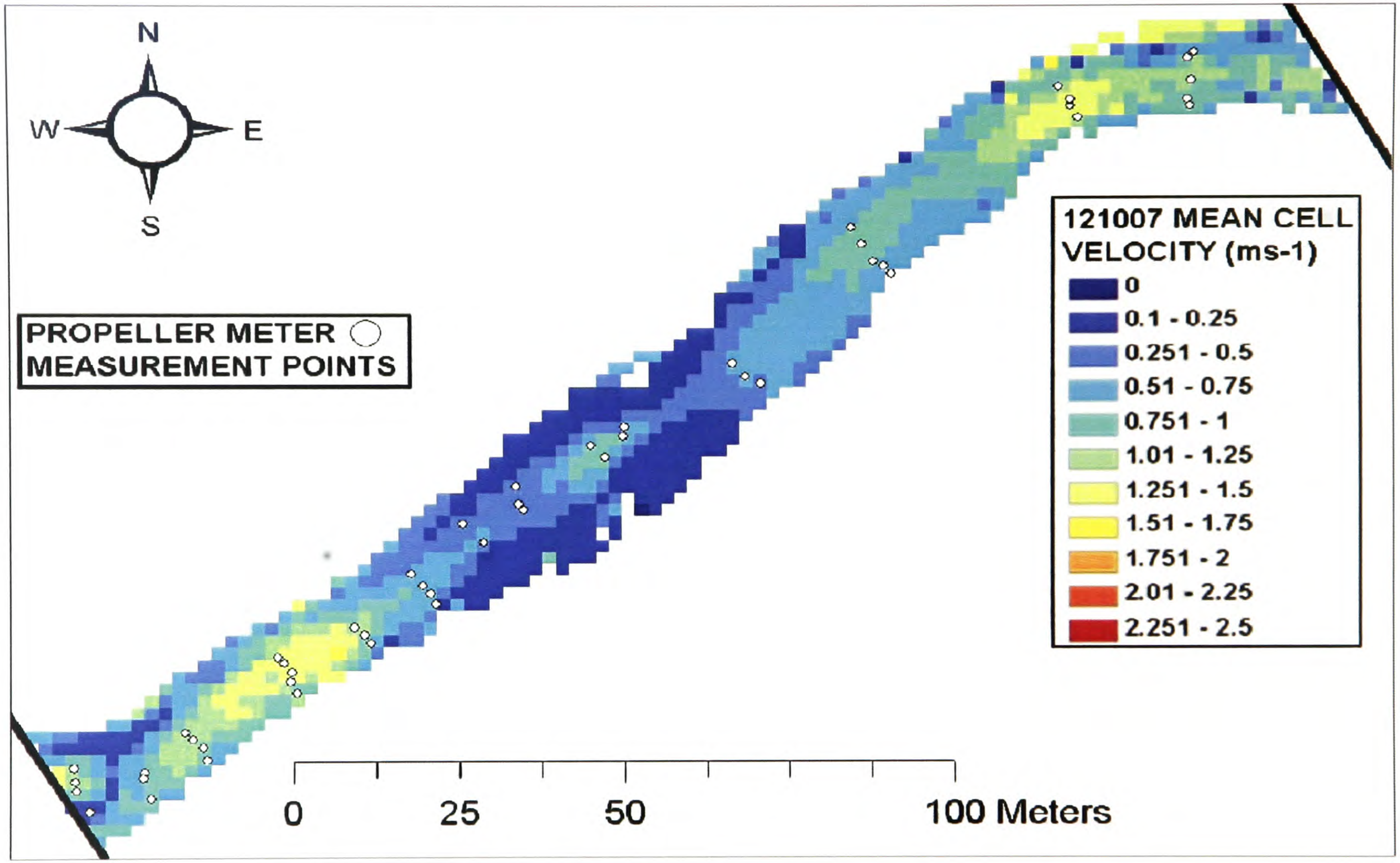

Figure 3.48 Location of propeller meter measurements taken on River Swale 121007

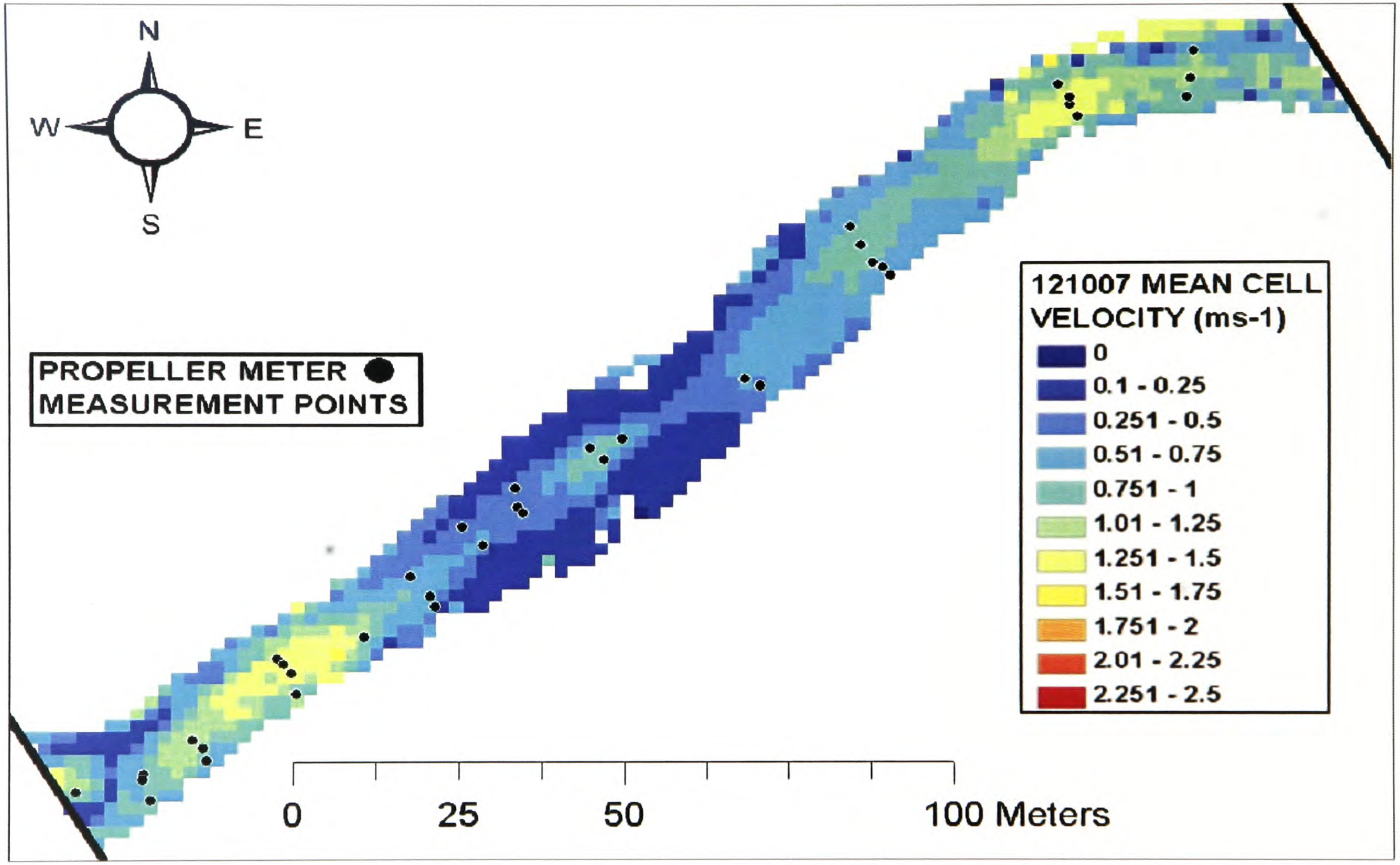

Figure 3.49 Location of propeller meter measurements taken on River Swale 121007 filtered based on HDOP values

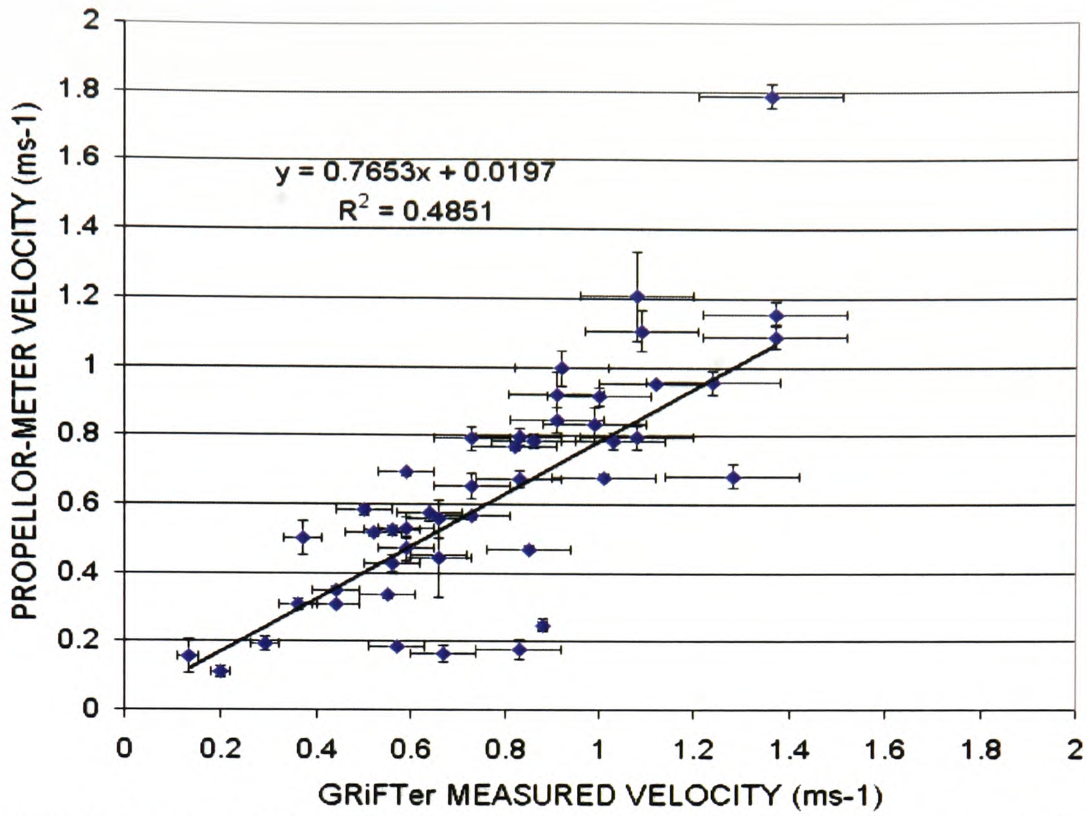

Figure 3.50 Comparison of GRiFTer measured and propeller meter measured velocity (complete data file) River Swale 12/10/07.

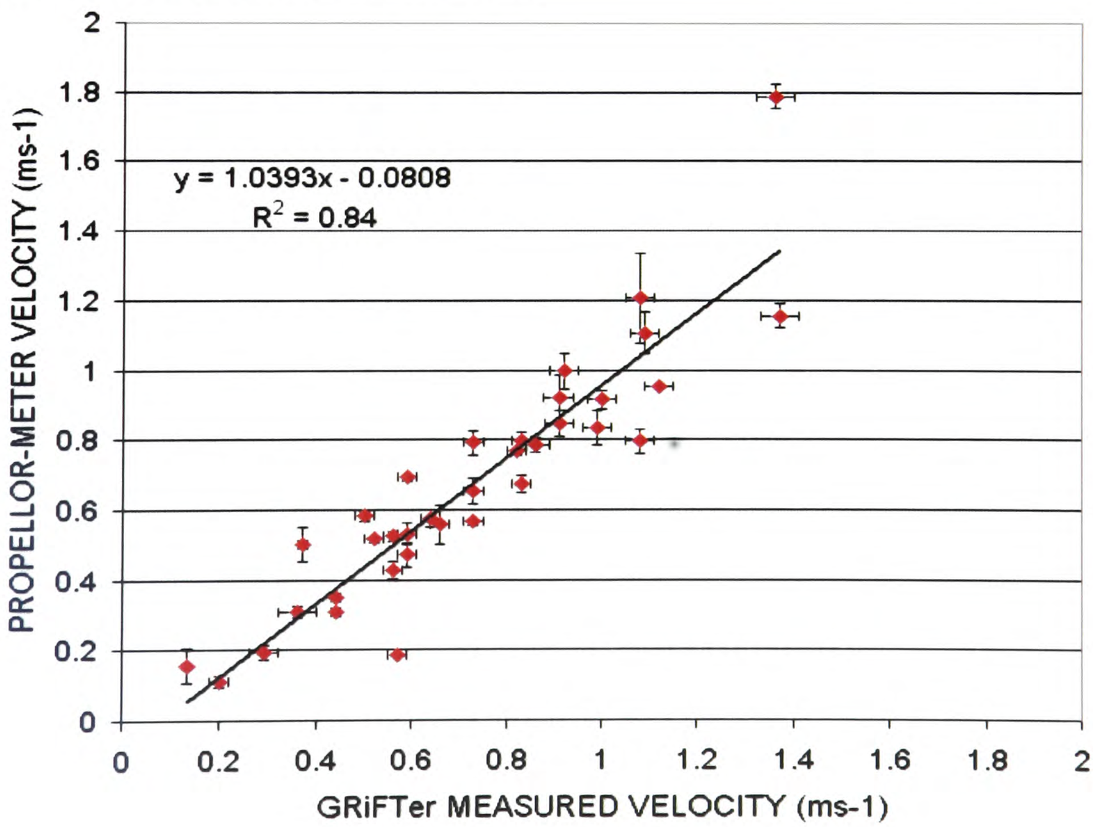

Figure 3.51 Comparison of GRiFTer measured and propeller meter measured velocity (edited data file) River Swale 12/10/07.

4 Results - New Developments in the Measurement of River Flow Phenomena

The development of a GPS River Flow Tracer (GRiFTer) has provided an innovative approach to the acquisition of surface velocity measurements from natural formed gravel-bed river systems (Figure 4.0). Within this research GRiFTers have performed two functions; the first is through the development of new techniques for the measurement and description of surface flow phenomena and the second is for the acquisition of reach scale velocity data from a wider range of discharge conditions and at a higher density than previously investigated.

Figure 4.0 Aerial photograph of field test site, Low Roe on the River Swale. Areas believed to contain riffles are marked with red squares and the pool area of the channel is believed to be located within the green square (Easimap, 2010).

4.1 Depth

In order to contextualise the surface velocity measurements provided through the GRiFTer method it is valuable to determine the relationships which exist with corresponding depth measurements. Additionally, determining the relative depth of each area of the channel highlights the occurrence of morphological change which provides the simplest criteria for a definitive identification of riffles and pools within the test reach.

Simultaneously, whilst conducting GRiFTers flow measurements under base flow conditions, experienced on 12/10/07 (4.39 m^3s^{-1}) depth measurements were made utilising a DGPS (Differential Global Position System). Measurements were taken of both the channel bed and water surface and a differencing method utilised to calculate the respective flow depths. Depth measurements were only possible at base flow conditions since any increase in discharge meant that the required entry into the channel would not be possible. The inability to enter the channel under higher discharges, in addition to providing one of the motivations for the development of the GRiFTer technique, again exists as a barrier to making the necessary depth measurements at the full range of flow conditions. Following data capture a cellular grid representation of the flow depths was produced and will subsequently be utilised to identify areas of the channel as possessing riffles and pools (Figure 4.1).

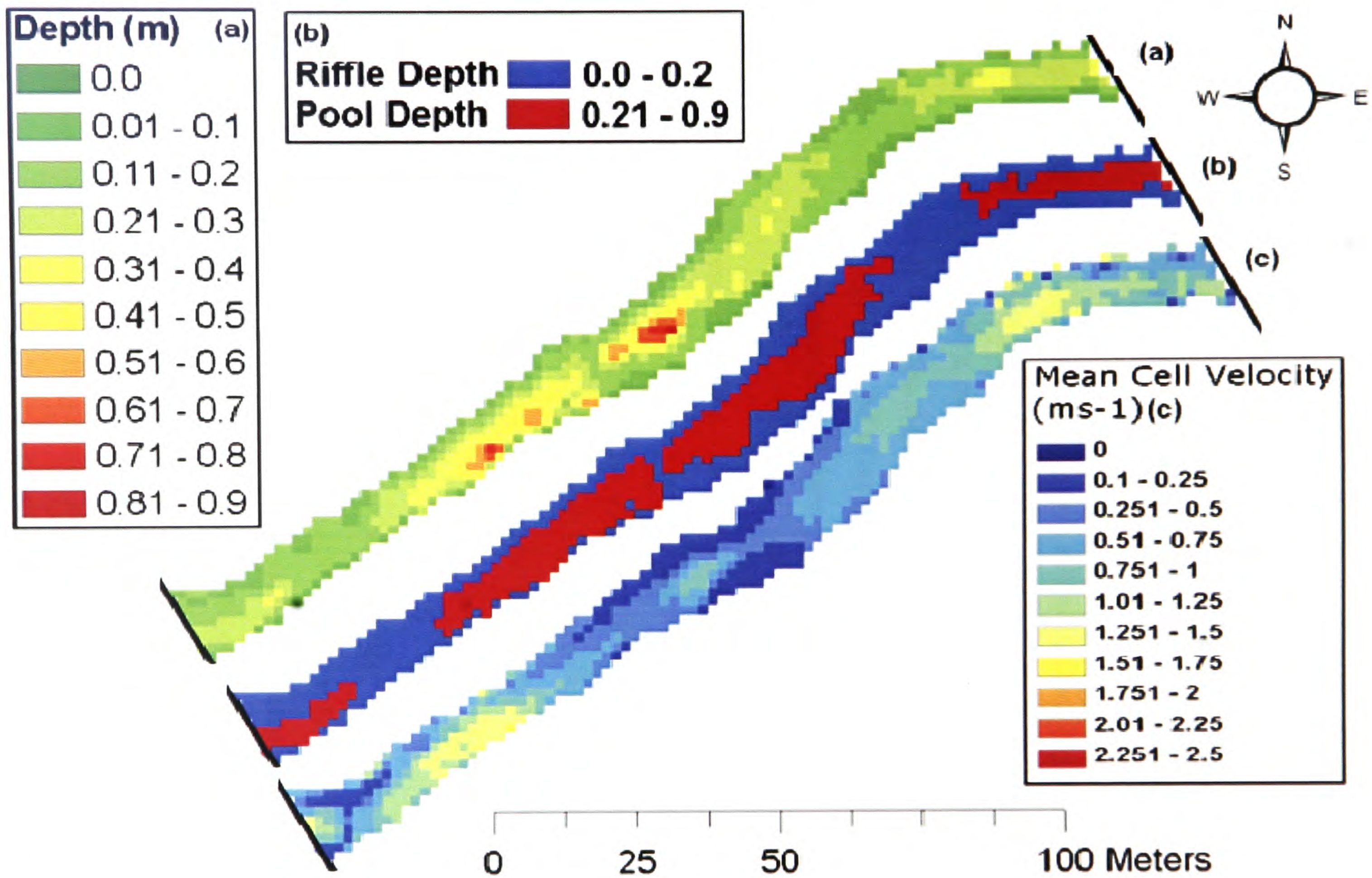

Figure 4.1 Reach scale depth patterns, corresponding velocity patterns and the location of individual riffles and pools at a discharge of 4.39 m^3s^{-1} (121007)

4.1.1 Depth Patterns

Flow throughout the majority of the reach has developed an asymmetric structure whereby flow is shallowest close to the lateral extent of data and increases in depth from left to right across the channel. The relative maximum depth occurs between the channel centreline and right channel side and measured 0.25 m. Additionally apparent is that depth also increases with distance downstream towards the junction between the first curve and the initiation of the long straight; reaching a maximum depth of 0.31 m.

Through the majority of the early straight part of the channel, depth remains relatively constant marking the location of the first riffle within the reach; throughout this area the cross-channel structure adopts a more symmetrical form with depth measuring around 0.15 - 0.2 m. Following the riffle, the same previously identified asymmetric structure returns as increasing depth can be observed through the development of a deeper channel running between centreline and right channel side.

Depth generally increases throughout the first part of the middle straight with the majority of the right channel side demonstrating depths greater than or equal to 0.35 m. Further downstream a deeper zone develops close to the right channel side with a localised maximum depth of 0.71 m. A relatively deeper channel continues to run close to the right side of the channel centreline measuring around 0.45 m towards the middle of the reach.

At the midpoint through the reach a shallow band develops across the channel dividing the two deeper areas running through the middle-straight region of the channel. From downstream of this band, demonstrates an additional deeper channel which runs through the centre of the region reaching a maximum depth of 0.81 m. From this maximum depth, flow shallows towards the initiation of the second curve through to the conclusion of the reach. Particularly prominent is an extremely shallow area close to the right channel side approaching the junction between the straight and curved areas.

Flow through the long downstream curve demonstrates a shallow area developing on either side of the channel with maximum depths of 0.05 m. The shallower area on the left channel side is shorter and wider than the area to the right channel side which is longer and more continuous but narrower. Through the middle of this area deeper channel progressively develops towards a maximum depth of 0.4 m. Following this localised maximum depth flow gently shallows towards the conclusion of the reach.

In terms of general trends it is apparent that depth displays an asymmetric structure through the curved and main straight area of the channel. Through the second half of the reach a deeper core runs closer to the centre of the channel. The deepest parts of the reach are located in the long straight sections of the channel and prominent shallow regions can be observed on both sides of the channel at the transition between straight and curved areas.

4.1.2 Utilising Depth Profiles to Identify Riffles and Pools

As described previously, all riffle-pool sequences have common oscillations in the mean bed elevation along the longitudinal flow profile (Wilkinson et al. 2004); with riffles occurring as topographic highs (shallows) and pools as intervening lows (deeps) (Richards, 1976; Clifford, 1993; Cao et al., 2003). Therefore by identifying the mean channel depth it is possible to determine a transitional point between shallows (riffles) and deeps (pools). The mean depth across the entire reach (on 12/10/07) is 0.2 m therefore any part of the channel deeper than 0.2 m can categorised as a pool and any area shallower than 0.2 m can be categorised as a riffle (Figure 4.2 a).

There are three prominent areas of the channel displaying mean depths in excess of 0.2 m and as such these are therefore classified as pools (red) in the longitudinal cross-section velocity patterns. The first region occupies an area close to the right side of the channel centreline measuring 24 m long with an area of 140 m^2. This area is surrounded by shallower areas particularly to the left channel side (again highlighting the asymmetric structure to the depth profiles). The second pool occurs through the main channel straight spanning 120m of the channel and has an area in excess of 1000m^2. This pool is divided by a narrow band of shallower flow (2.2 m long) located close to the centre of the reach at 102 m downstream. The third pool area of the channel occurs at 190 m downstream, is 42 m long and has an area of 282 m^2. As previously identified the deepest areas of the channel occur through the middle straight providing maximum depths of 0.71 m and 0.82 m in the first and second parts of the 2nd pool respectively.

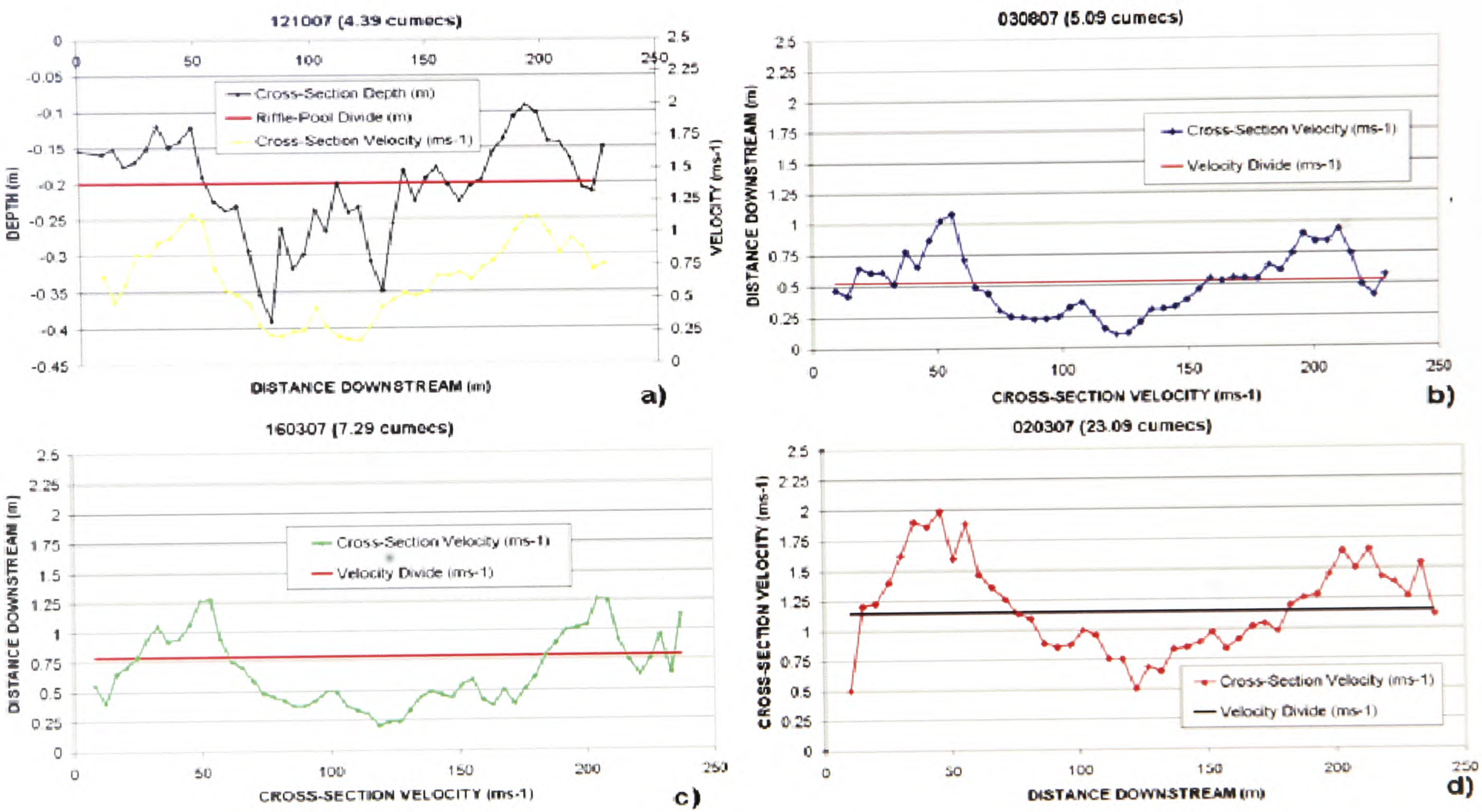

Figure 4.2 Longitudinal "cross-section" velocity patterns with the location of individual riffles and pools distinguished at 45% of the maximum observed velocity.

4.1.3 Calculation of Inter-Riffle Spacing Utilising Longitudinal Depth Profiles

Measuring cross-sections at 5 m intervals through the reach allows the construction of a longitudinal mean cross-section depth profile (Figure 4.2 a). Applying the previously determined transitional value (0.2 m) it is possible to distinguish between riffles and pools. Utilising this approach it is also possible to calculate an inter-riffle spacing. The inter-riffle spacing refers to the longitudinal distance between the conclusion of the first and beginning of the second riffle.

From the longitudinal depth profile for 12/10/07 it is possible to identify the conclusion of the first riffle at 53.1 m downstream and the beginning of the second riffle at 173.9 m downstream; this returns an inter-riffle spacing of 120.8 m. The existing literature determines that it is appropriate to characterise inter-riffle spacing in terms of channel width. It was previously determined that the mean effective width for the channel at a discharge of 4.39 m^3s^{-1} was 17.8 m (Table 4.1). Therefore the inter-riffle spacing is equal to 6.79ew (effective widths).

4.1.4 The Relationship between Depth and Surface Flow Velocity

Figure 4.2a features both the longitudinal cross-section depth profile and the longitudinal cross-section velocity pattern. It is clear that there is a degree of correlation between the depth profile and the velocity profile. Cross-section depth remains relatively consistent from the beginning of the reach to a minimum depth at 48.3 m downstream. The cross-section velocity, which increases from the beginning of the reach peaks concurrently around 48.3 m. Following this peak, cross-section depth increases to the first maximum depth at 82 m downstream. Simultaneously mean cross-section velocity decreases to a minimum velocity at 87 m downstream. Both cross-sectional depth and flow velocity rise to respective profile peaks at 101 m (velocity) and 111 m (depth) before falling again to minimum velocity at 120.7 m and max depth at 130.4 m. Depth decreases as velocities increase to subsequent peaks at 193.2 m (depth) and 198 m (velocity) downstream before both decreasing through to the conclusion of the reach.

It is clear from Figure 4.2a that despite the cross-section depth being more varied that cross-section velocity; as depth increases the mean cross-section surface velocity decreases and as the flow depth decreases the velocity increases.

4.1.5 Calculation of Inter-Riffle Spacing Utilising Longitudinal Surface Velocity Patterns

Figure 4.2a highlights the correlation between the longitudinal cross-section depth and cross-section velocity patterns. The potential therefore exists to utilise transitions in the surface velocity profiles as indicators for the location and dimensions of individual riffles and pools in the absence of available depth data. This would therefore provide a means of assessing the existence, location and dimensions of the individual elements of riffle-pool sequences where entry into the channel to measure depth data is not possible either due to increased discharge or other logistical constraints such as legal access or safe entry and egress sites.

From the 4.39 m^3s^{-1} discharge (12/10/07) it was possible to determine that transitions between riffles and pools occurred at approximately 45% of the maximum reach velocity value (mean cellular velocity from entire reach dataset). Table 4.1 provides the 45% maximum velocity values from which transitions between riffles and pools can be determined at each discharge. Initially clear is that the raw inter-riffle spacing displays a degree of variance at different discharges; ranging between 96.2 and 122.6 m irrespective of increases in discharge. Concurrently, the mean effective width decreases with increasing discharge (except for the 5.07 m^3s^{-1} data). These observations result in the inter-riffle spacing, expressed in terms of effective channel widths, increasing from 6.8 to 7.54 as discharge changes from 4.39 to 23.09 m^3s^{-1}.

DISCHARGE	MAX VELOCITY	45% VELOCITY	INTER-RIFFLE SPACING	MEAN EFFECTIVE WIDTH	SPACING
(m^3s^{-1})	(ms^{-1})	(ms^{-1})	(m)	(m)	(ew)
4.39	1.66	0.75	120.8	17.76	6.8
5.07	1.17	0.53	96.2	13.78	6.98
7.29	1.75	0.79	122.6	16.61	7.298
23.09	2.55	1.15	106.5	14.12	7.54

Table 4.1 Measurement of inter-riffle spacing.

4.1.6 Identifying the Location and Dimensions of Individual Riffles Utilising the 45% Maximum Velocity Criteria

It is also possible to utilise the transitional velocities, previously determined, to determine the location of riffles and pools from the reach scale surface velocity patterns. Figure 4.3 defines areas of the reach as either riffle or pool and will subsequently be utilised to determine the dimension of the two riffles contained within the reach.

As previously determined the results produced by a discharge of 5.07 m^3s^{-1} (03/08/07) exhibit different patterns to the progression of results observed under the other discharge increases. The deviation in results produced by the 5.07 m^3s^{-1} data is again present with respect to the dimensions of individual riffles and pools. There is clear variance in the location and dimensions of both riffles within the reach with respect to discharge. The initiation of the first riffle varies between 15.21 m and 24.5 m downstream. At discharges of 4.39 m^3s^{-1} and 7.29 m^3s^{-1} the first riffle occurs almost concurrently at 24.1 and 24.5 m respectively; however with the largest increase in discharge to 23.09 m^3s^{-1} the beginning of the first riffle migration upstream by 9.29 m to 15.21 m downstream. A clear pattern can be observed in the location of the conclusion of the first riffle with respect to discharge. With the exception of the 5.07 m^3s^{-1} results, with increasing discharge riffle one concluded further downstream to a maximum of 60.89 m at a discharge of 23.09 m^3s^{-1}. Additionally apparent is that the increases in distance downstream are greater with larger increases in discharge. This results in a clear relationship between the length of the first riffle and discharge. At higher discharges the length of riffle one increases, excluding the length of riffle one at 5.07 m^3s^{-1} which is longer than that observed at 7.29 m^3s^{-1}. The greatest increase in length occurs with the largest change in discharge; between 7.29 m^3s^{-1} and 23.09 m^3s^{-1}. There is also a clear relationship between the area of the first riffle and discharge. With all increases in discharge the area of riffle one grows accordingly reaching a maximum of 720.8 m^2 at a discharge of 23.09 m^3s^{-1}.

The location of the start of the second riffle also varies dependent upon discharge. There is a general trend that at higher discharges the initiation of riffle two occurs further downstream. At 4.39 m^3s^{-1} the second riffle starts at 173.90 m downstream, whilst at 7.29 m^3s^{-1} and 23.09 m^3s^{-1} riffle two begins at 183.90 m and 182.60 m downstream respectively. There is also an apparent downstream advancement of the conclusion of the second riffle with increased discharge. At 4.39 m^3s^{-1} riffle two concludes at 222.70 m whilst at 23.09 m^3s^{-1} the maximum downstream migration of the conclusion of R2 occurs to 238.40 m downstream. The location of the second riffle is complicated by the end of the test reach being positioned immediately upstream of a weir causing an artificial break in the development of subsurface flow features and therefore surface flow patterns. The observed spatial changes result in the length of the second riffle increasing at greater discharge excluding the results returned by a discharge of 5.07 m^3s^{-1}. Despite the observed increases in the length of the second riffle, with increased discharge, there is no clear pattern in the relationship between discharge and riffle area. The minimum area of 721.30 m^2 occurs at 7.29 m^3s^{-1} whilst the maximum area of 843.90 m^2 occurs at a discharge of 5.07 m^3s^{-1}.

	RIFFLE 1			
DISCHARGE	**START**	**END**	**LENGTH**	**AREA**
(m^3s^{-1})	**(m)**	**(m)**	**(m)**	**(m^2)**
4.39	24.1	53.1	29	499
5.07	18.7	62.54	43.84	578.1
7.29	24.5	61.3	36.8	609.1
23.09	15.21	76.1	60.89	720.8

Table 4.2a Measurement of riffle dimensions (Riffle 1).

	RIFFLE 2			
DISCHARGE	**START**	**END**	**LENGTH**	**AREA**
(m^3s^{-1})	**(m)**	**(m)**	**(m)**	**(m^2)**
4.39	173.9	222.7	48.8	770.5
5.07	158.74	220.1	61.36	843.9
7.29	183.9	237.1	53.2	721.3
23.09	182.6	238.4	55.8	833.4

Table 4.2b Measurement of riffle dimensions (Riffle 2).

4.1.7 The Relationship between Riffle Structure, Dimensions and Spacing with Respect to Discharge

At base flow conditions three distinct longitudinal zones can be observed through the test reach at the River Swale; two shallower, symmetrical riffle areas interspaced by deeper asymmetrical pools. In terms of the dimensional and structural deviations of individual bedform features relative to changes in discharge several prominent patterns develop. As previously described the results presented at a discharge of 5.07 m^3s^{-1} deviate significantly from the patterns observed across the other discharge conditions, therefore these conditions are momentarily removed from the analysis of depth and surface flow phenomena.

Table 4.1 demonstrates that with increasing discharge the inter-riffle spacing of consecutive riffles through the test reach demonstrates a degree variation in the pure inter-riffle spacing. However when considered with respect to the mean effective channel width, inter-riffle spacing increases from 6.8 widths at 4.39 m^3s^{-1} to 7.54 widths at 23.09 m^3s^{-1}.

In terms of individual riffle specifics, at the highest discharge, the first riffle occurs further upstream suggesting an upstream migration in the longitudinal flow patterns. Additionally, with increasing discharge, the first riffle concludes further downstream demonstrating an increase in the overall length of the feature. Similarly, despite the changes previously outlined in the effective channel width, the area of the first riffle increases with increasing discharge.

The patterns observed through the second riffle are significantly less ordered or formalised. The initiation of the second riffle occurs more consistently and less well structured relative to discharge, however the conclusion of the second riffle occurs further downstream with increasing discharge. Overall, changes in area are also less structured relative to discharge due to the effect of changing effective width. The development of spatial patterns, as they relate to the second riffle are less structured than those previously observed due to the occurrence of a reach terminating weir located at the further extend of the test reach prohibiting the downstream migration of bedform features.

The changes which occur in the structure of riffles and pools through the test reach with increasing discharge can be explained with reference to the changing nature of flow within and through the riffle-pool interface. At base flow conditions, the first riffle adopts an elongated oval shape producing narrow v-shaped ends, and the widest area of the riffle occurring 2/3 of the distance through the feature. With increased discharge the form of the riffle changes dramatically adopting a more rectangular shape as the greater flow volume occupies virtually the entire, narrowing effective width. This results in a more defined cross-channel boundary between riffle and pool, where previously at lower discharges a v-shaped flow pattern marked the initiation and conclusion of riffles and therefore provided slower transitions between each element of the overall bedform structure. At lower discharges, changes in velocity and therefore deposition occurred in a more structured manner, initial occurring close to the channel banks and extending into the channel centre further downstream. At the highest discharge the cross-channel margin observed at both the beginning and end of the riffle demonstrates immediate channel wide deposition upstream of the previous riffle initiation and subsequent downstream deposition of material into the pool.

This change in the structure of the riffle-pool margin is directly driven by increases in discharge. Higher discharge flow results in higher relative velocities and therefore a greater sediment carrying capacity. This flow enters the reach through an upstream pool, whereby in accord with the flow convergence routing, this sediment can be carried into the subsequent riffle since it would have been routed around the deepest part of the upstream pool. Upon entering the test reach sediment is deposited close to the right channel side due to locally reduced flow velocities (Figure 4.16 - 12 m downstream). This is evidenced by the occurrence of lower magnitude velocities close to the right channel side and results in upstream elongation of the first riffle. The effect of increased discharge maintains greater relative flow velocities over the riffle area mobilising and carry a greater volume of sediment further downstream which is deposited beyond the previous margin with the pool due to the increased flow momentum. This again has the effect of elongating the riffle further downstream. This is evidenced by a band of lower velocities (which appears as a localised trough in the cross-section longitudinal velocity pattern) following the first riffle where deposition of the carried material could occur (Figure 4.3 - 86 m downstream).

If this pattern of the interaction between pool and riffle continues to manifest within the next riffle-pool pairing then this would explain the observed relationship between discharge and inter-riffle spacing. In order to confirm the occurrence of this phenomenon several evidentiary elements are required. Initially the occurrence of routing around the deepest part of the pool must be observed, as much the development of a band or area of lower velocities entering the second riffle area where upstream deposition and therefore expansion can occur. Analysis of the primary flowline highlights sediment routing at around the deepest part of the pool at 7.29 and 23.09 m^3s^{-1} (Figure 4.3) further Figure 4.3 highlights the occurrence of reduction in the general increasing velocity pattern at 175 m downstream (23.09 m^3s^{-1}) highlighting the potential for sediment deposition causing an upstream expansion of the riffle. This pattern of riffle-pool development / migration serves to explain the reduction in the inter-riffle measurement at the highest discharge; with the expected pattern of decreases spacing with respect to channel width remaining due to significant reductions in the average effective width.

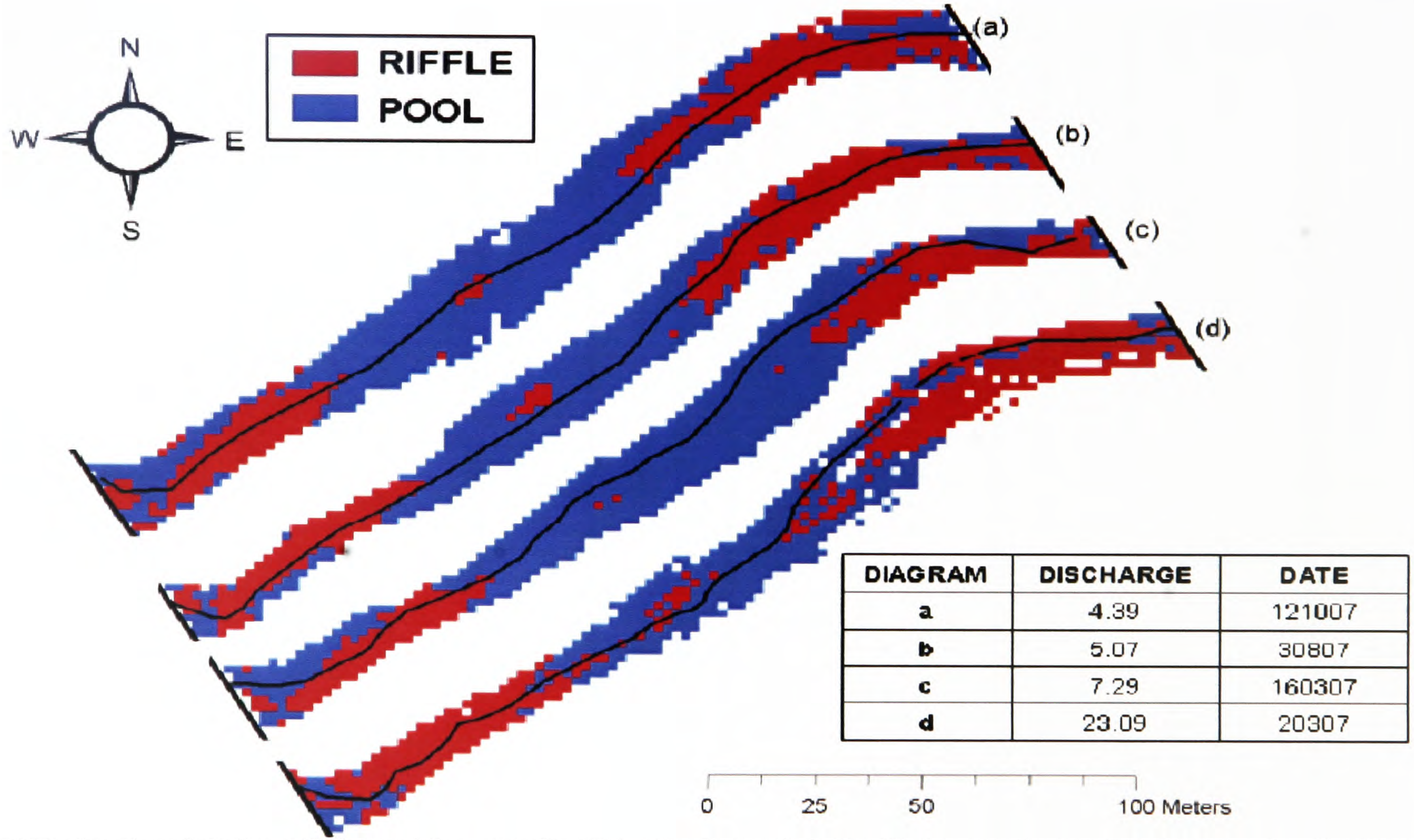

DIAGRAM	DISCHARGE	DATE
a	4.39	121007
b	5.07	30807
c	7.29	160307
d	23.09	20307

Figure 4.3 The location of shallows (riffles) and deeps (pool) utilising the observed relationship between flow depth and measured surface flow velocities.

4.2 Longitudinal Flow Patterns

4.2.1 Critique of Traditional Measurement Methods

The results of previous large-scale flow investigations have been based upon series of point or cross-sectional velocity measurements (Clifford and Richards, 1992). These data are then utilised to describe reach scale flow patterns, with the behaviour between measured values being inferred, predicted or modelled (Stockdale et al., 2007). Increasingly, flow investigations are conducted utilising interrogation areas. These specify particular regions of flow where a greater number of measurements can be made to improve the accuracy with which flow can be described (Ettema et al., 1997 and Creutin et al., 2003). The use of LSPIV (Large Scale Particle Image Velocimetry) can provide almost complete coverage of surface flow properties in these specified areas (Fox et al., 2008). This however again leaves the behaviour between these areas requiring further interpretation, prediction or modelling. In addition to the incomplete coverage of flow afforded by both traditional investigation methods and the use of interrogation area based approaches; the distribution and path of data acquisition is largely arbitrary and predetermined (Weitbrecht et al., 2002). This further exacerbates the fragmented and inadequate availability of detailed measurements for reach-scale flow patterns.

4.2.2 Reliance on the Role of the Thalweg

The path of data acquisition is often extremely simplified and focused on either the channel centreline or the thalweg as a reference frame from which point or cross-section measurements can be made (Carling, 1991; Thompson et al., 1999). Flow at the centreline or along the thalweg is often utilised as a proxy for the dominant path of flow and referenced as the driving force for change in the channel planform. The distribution of the thalweg is also qualatively assessed and therefore prone to error in positioning. Large-scale flow structures often fail to align with either the channel centreline or thalweg highlighting the need for a more flexible / informative reference frame. Whilst both the centreline and thalweg are informative regarding the physical structure of the channel; is this a good way to describe reach scale flow patterns?

The spatial distribution of riffles and pools for example has often been expressed based on the number of channel widths along the channel centreline. The periodicity of this longitudinal relationship demonstrates the limitations of current reach scale flow investigations. The channel centreline is an arbitrary reference frame from which cross-section channel measurements are often made, but provide an incomplete record of the flow across a specified area at an again arbitrarily determined series of locations. Additionally, the measurement of cross-sectional widths and subsequent cross-sectional flow velocities is theoretically a simple concept; however, the precise definition of width, the logistics of performing the required measurements and the appropriateness of utilising each approach requires additional consideration.

4.2.3 Introducing the Concept of the Primary Flowline

The use of the flotilla of GRiFTers allowed the first documented attempt to independently determine a single dominant flow path through a specific reach. In this section we describe how to determine the "primary flow line". The primary flowline describes the path of flow through which the majority of flow entering the channel would follow (the most frequently visited path of flow) and therefore the flow most readily responsible for determining the longitudinal and lateral composition of the channel.

4.2.4 How the Primary Flowline is Assessed and Measured

In order to calculate the primary flowline the flotilla of GRiFTers was deployed utilising a wave formation, whereby groups of units are released spaced across the entire width of the channel above a referenced start line. Upon entering the test reach, each GRiFTer followed a completely independent path as determined by the natural flow conditions. Multiple GRiFTer releases created a series of flow tracks, each with a unique reference number. Utilising a cellular based representation of the entire reach makes it possible to establish the number of unique flow tracks passing through each individual cell. Determining the cell or cells within each cross-section that feature the highest number of unique flow paths creates a point of intersection. Connecting each of these intersection points creates an independently determined primary flow line (Figure 4.4).

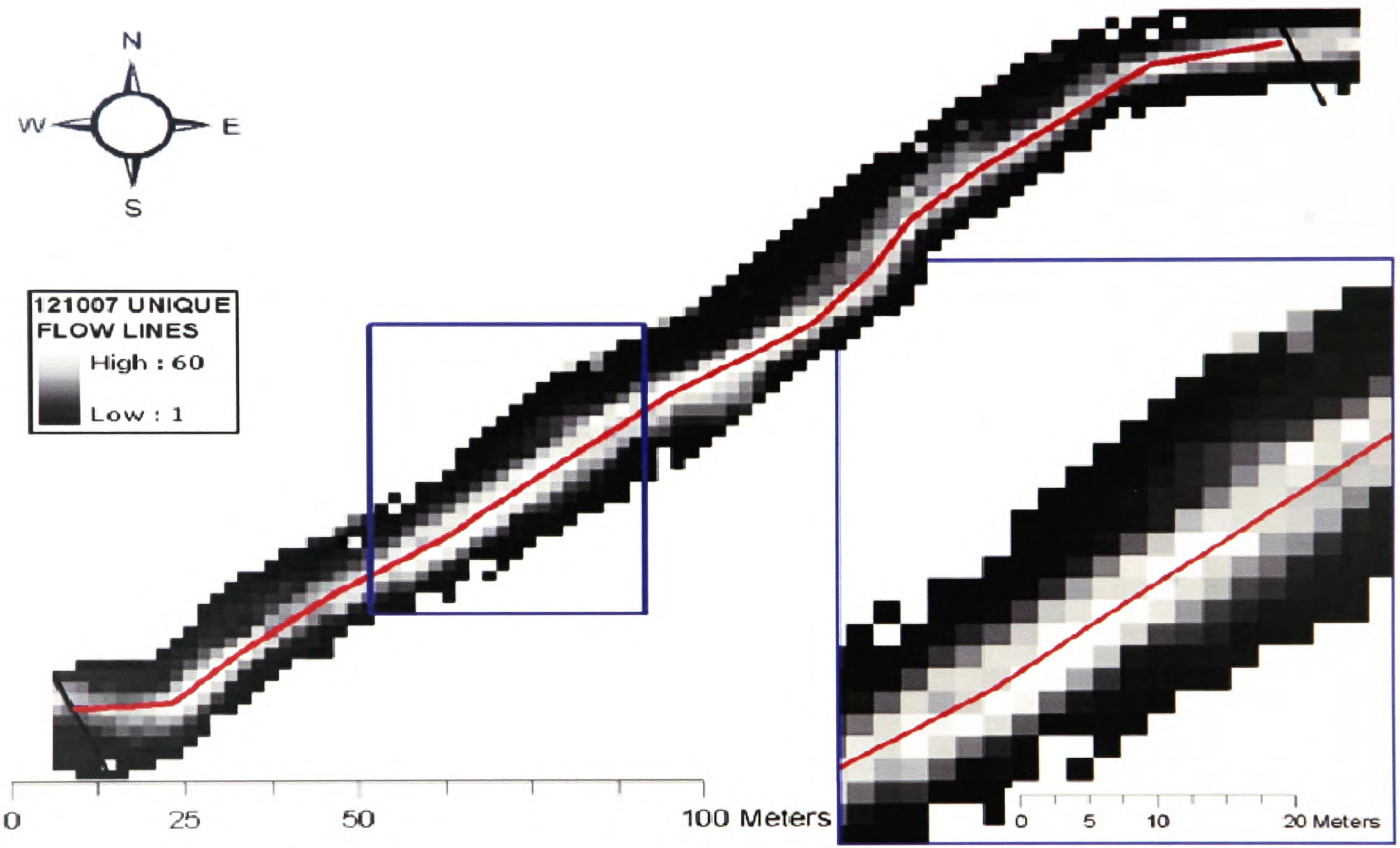

Figure 4.4 Example "primary flowline" produced through cellular investigation of River Swale 121007

A series of rules are utilised to determine the passage of the primary flow line (Figure 4.5).

Where a single primary cell in each cross-section occurs consecutively the primary flowline will follow a direct route either vertically or diagonally (Figure 4.5 A & B).

Where multiple primary cells occur in a cross-section (second order) the primary cell in the next order (third order) cross-section will determine the path through the second order cross-section (Figure 4.5 C & D & E).

Where multiple primary cells occur in multiple cross-sections, the primary flowline will pass centrally through the primary cells in each order cross-section before orientating towards a single primary cell (Figure 4.5 F).

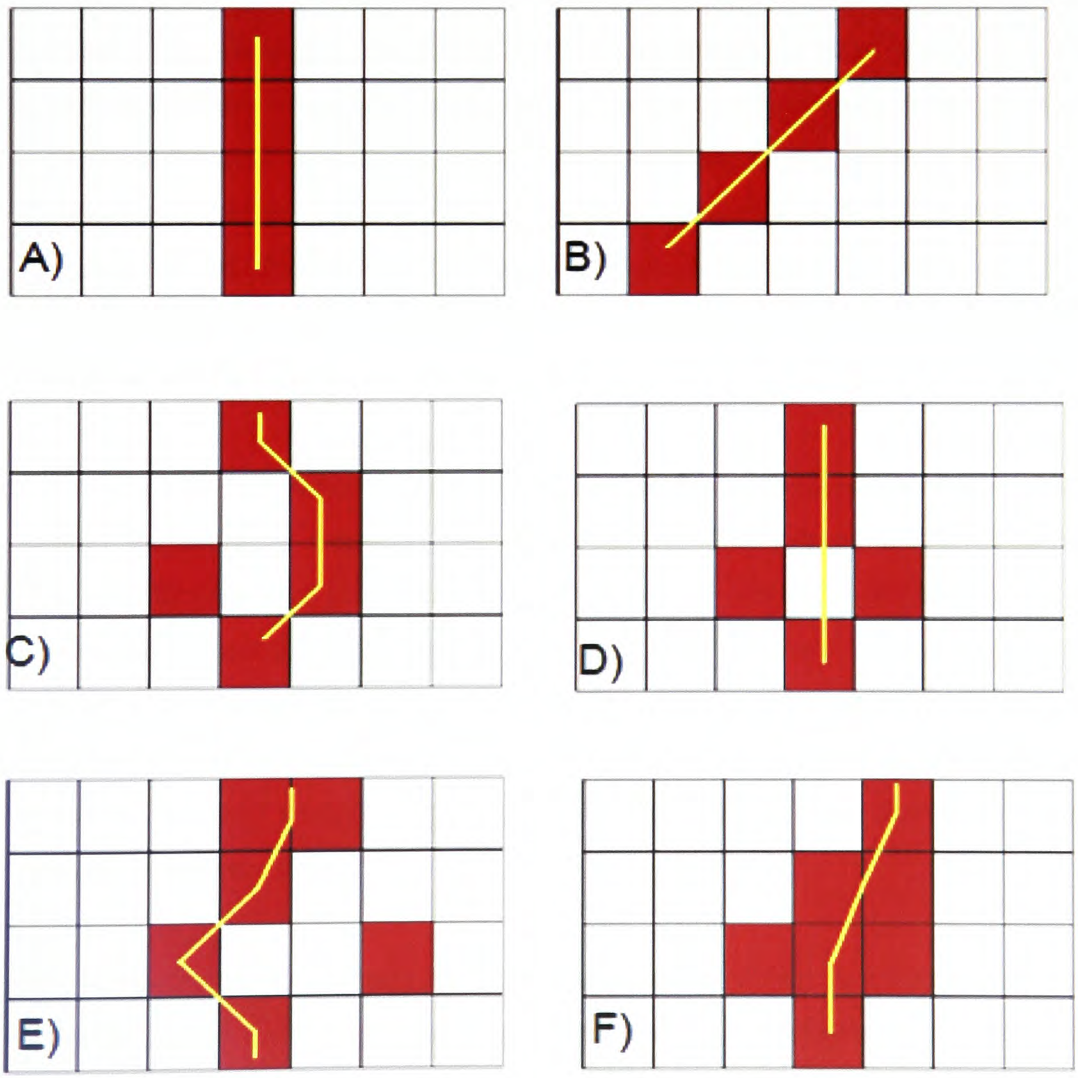

Figure 4.5 Example rules for the construction of the primary flowline.

4.2.5. The Behaviour of the Primary Flowline with Respect to Discharge.

Flow enters the reach through an initial right-hand curve spanning the first 20 m of the channel. The entry position into the reach of each primary flowline is determined by the development of large-scale flow structures further upstream (Figure 4.6 & 4.7). At the lowest discharges, primary flowlines (yellow (4.39 m^3s^{-1}) and blue (5.07 m^3s^{-1})) pass between the centre and outside bend of the channel whilst the higher discharge flowlines (green (7.29 m^3s^{-1}) and red (23.09 m^3s^{-1})) flow from the centre to the inside of the curve. This highlights that with increasing discharge there is a reorganisation of the channel geometry and large-scale flow features, as the primary flowline and therefore dominant flow migrates laterally across the channel throughout curved areas.

As the channel straightens all primary flowlines begin to demonstrate a convergence (around 35m). Throughout the first part of the long straight all flow lines become tightly clustered reaching a complete convergence around 65-68m downstream. This region represents the only area of the reach that is common to the primary flowline at all discharges therefore representing a complete convergence in flowlines and the minimum lateral distribution. This pattern demonstrates that the primary flowline is more consistent through the straight sections of the channel and more varied across the curved areas of the reach.

Following this complete convergence, the higher discharge flowlines begin to diverge around the straighter running lower discharge flowlines (around 100m). The highest discharge flowline (red (23.09 m^3s^{-1})) curves away towards the right channel side whilst the second highest discharge flowline (green (7.29 m^3s^{-1})) runs further towards the left channel side. This divergence continues as the green flowline uniquely follows a path close to the left hand channel side. The divergence of the two higher discharge flowlines produces the only straight section of the channel where clear lateral deviations in primary flowlines occur.

The behaviour of the primary flowline suggests that within this Swale reach; riffles occur in curved areas highlighted by wider flow line distributions. These appear to occur due to higher velocity flows being deflected over the riffle area widening the channel and allowing the observed primary flowline migration. Therefore, it follows that pools occur throughout the straight areas of the channel as demonstrated by the occurrence of converging primary flowlines and the only complete uniform primary flowline path. The observed deviation of the highest discharge flowlines from the converged path, through the straight elements of the channel, is fundamentally important in understanding the processes responsible for the development and maintenance of riffle-pool sequences. MacWilliams et al., (2006), introduced the concept of flow convergence routing which states that at high flow conditions, sediment is routed around / away from the deepest parts of the pool thus maintaining the unique quasi-regular structures of these bedform features as opposed to the increased erodibility of material based on flow directly converging into the pool (MacWilliams et al., 2006). Exiting the pool, flow diverges leading to deposition on the riffle and the maintenance of a topographic high at the pool tail. The fact that the lower discharge flowlines remains straight through this area of the channel further supports the concept of flow sediment routing developing pools through convergence jetting at lower flows.

At the end of the long mid-channel straight, all primary flowlines, excluding the green flowline (7.29 m^3s^{-1}) which continues to flow towards the left channel side again begin to converge towards the right hand channel side (113m). This reconvergence downstream of the deepest part of the pool again supports the operation of the flow convergence routing hypothesis.

Through the majority of the second curve, the lateral distribution of flow paths is significantly greater than through the initial upstream curve and the majority of the mid-channel straight. Between 160m and 180m downstream, the highest discharge flowline (23.09 m^3s^{-1}) arcs towards the outside of the curve before crossing the second order flowline (7.29 m^3s^{-1}). Beyond 180m downstream the flowlines align from left to right in discharge order from highest to lowest discharge, for approximately 10m. Around 185m the two lower discharge flowlines (4.39 m^3s^{-1} and 5.07 m^3s^{-1}) navigate towards the right channel side whilst the higher discharge flowlines (7.29 m^3s^{-1} and 23.09 m^3s^{-1}) continue towards the left channel side.

The behaviour of the primary flowlines through the second curve initially highlights the likely occurrence of an additional riffle where the lateral distribution of flowlines increase to the maximum observed throughout the reach. Additionally prominent is that through the second curve riffle, the higher discharge flow lines again follow a path towards the left side of the channel. Interestingly, through this riffle the left side of the channel is the outside as opposed to the inside of the curve observed previously. Flow reconverges around 210m as the channel begins to straight again and remain tightly grouped through the remained of the reach.

The relationship between discharge and the path of the primary flowlines presents several interesting findings. At lower discharges (4.39 m^3s^{-1} and 5.07 m^3s^{-1}), the primary flowlines are relative straight, flowing centrally and with the general curvature of the channel with minimal changes in their lateral distribution. At higher discharges (7.29 m^3s^{-1} and 23.09 m^3s^{-1}) the flow lines are significantly more varied laterally, changing direction more rapidly and frequently diverging away from the lower discharge flowlines through the channel centre. Important divergences occur throughout the downstream curve where higher discharge (7.29 m^3s^{-1} and 23.09 m^3s^{-1}) flowlines follow the outside of the curve whilst the lower discharge (4.39 m^3s^{-1} and 5.07 m^3s^{-1}) flowlines follow a path close to the inside of the curve. There is also a notable migration from right to left with increased discharge.

Additionally, through the channel midpoint, the higher discharge flowlines (7.29 m^3s^{-1} and 23.09 m^3s^{-1}) arc round the straighter lower discharge flowlines (4.39 m^3s^{-1} and 5.07 m^3s^{-1}), which has previously been highlighted as supporting the existence of flow convergence routing hypothesis. However, the highest discharge flowline transverses to right channel side whereas the second order flowline transverses to the left channel side. Furthermore, the type of divergence from the middle of the channel varies relatively to discharge conditions. At the highest discharge conditions, the divergence occurs later, is shorter and of a smaller lateral magnitude than for the second order divergence. Two clear convergences also occur around the mid-channel straight divergences.

The clear lateral and in this case longitudinal deviation in the primary flowlines highlights that at increased discharges the composition of the bed and therefore the location and spatial relationship between riffles and pools adjusts accordingly.

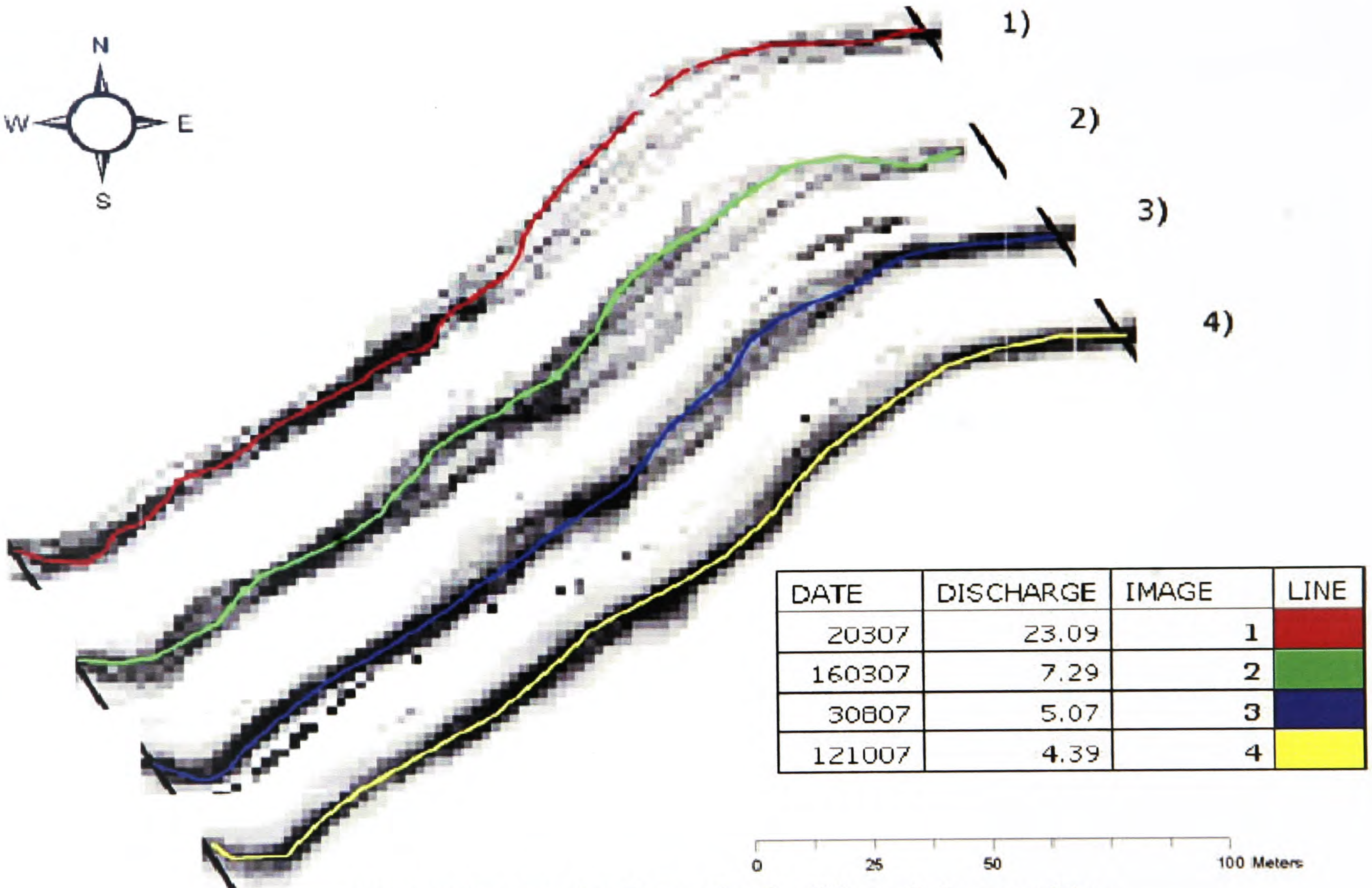

DATE	DISCHARGE	IMAGE	LINE
20307	23.09	1	
160307	7.29	2	
30807	5.07	3	
121007	4.39	4	

Figure 4.6 Example primary flowlines produced at different discharge conditions.

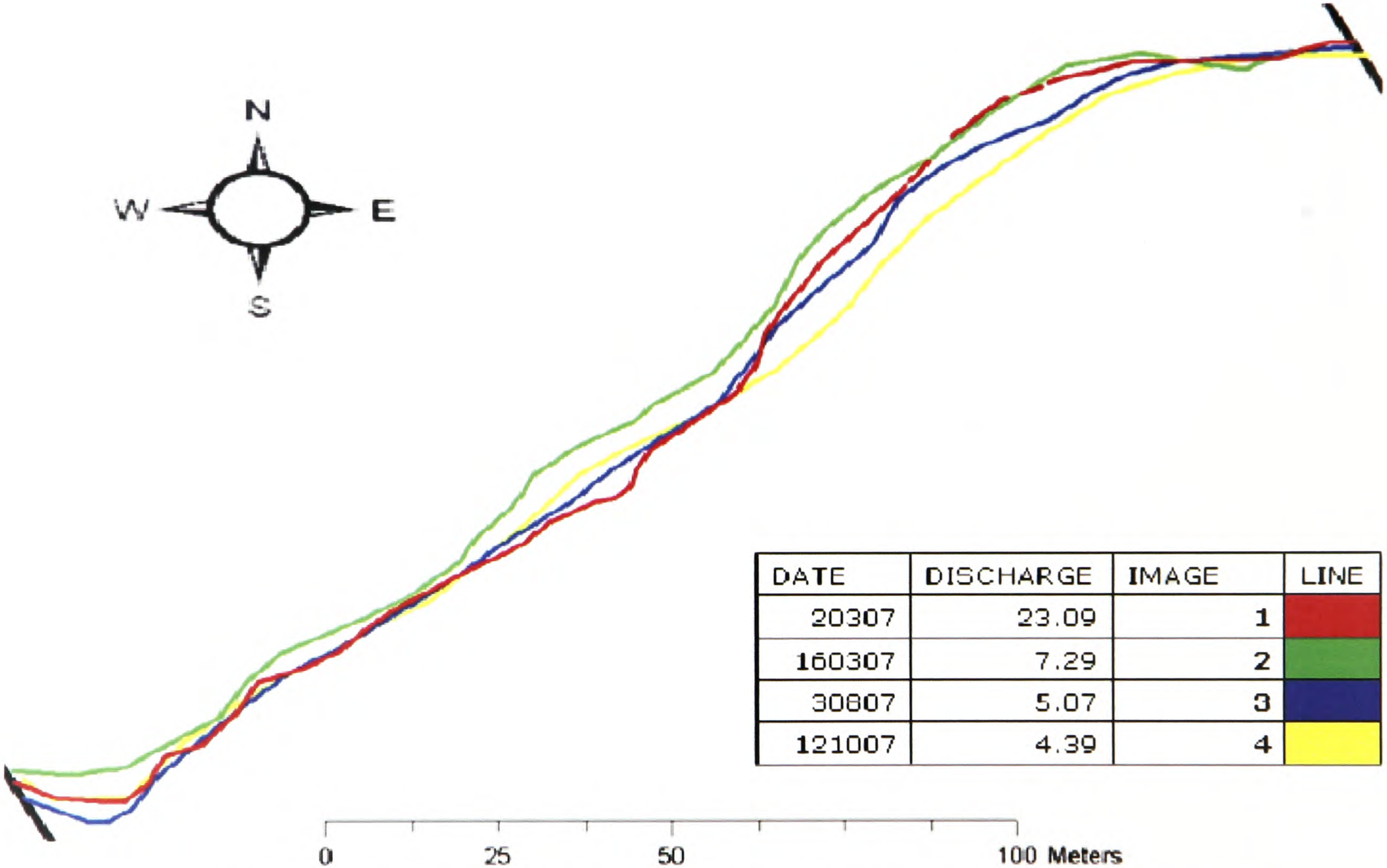

DATE	DISCHARGE	IMAGE	LINE
20307	23.09	1	
160307	7.29	2	
30807	5.07	3	
121007	4.39	4	

Figure 4.7 Comparative representation of primary flowlines produced at different discharge conditions

4.3 Flow Width

4.3.1 The Importance of Bankfull Flows

Flow experienced under bankfull conditions is often regarded as a condition for channel form and change. It is widely accepted that "bankfull width" provides the discharge through which the channel form is developed and large-scale sedimentary and flow structures are built and / or modified. Under such conditions it is deemed that since the entire channel is occupied the entire width of flow acts to determine the overall channel structure. The concept of bankfull depth is a qualative measure of flow condition and as such open to error. Similarly, the importance of bankfull width has yet to be quantified objectively and little is known as to relatively importance of different occupation levels / degrees of channel width.

4.3.2 Difficulties in Making Bankfull Flow Measurements

At bankfull conditions, the difficulties and limitations highlighted in the measurement of flow are exacerbated since entry into the channel becomes difficult. Additionally, although the measurement of the maximum visible extent of channel width is the simplest representation of flow width to observe and measure there has previously been no means of physically determining the area of flow which directly contributes to the development of the channel form and subsequent flow structures.

4.3.3 The Concept of Effective Width

The debate regarding the role and measurement of flow width is highlighted in the study of riffle-pool sequences. The longitudinal periodicity of riffle-pool sequences and the flow patterns over riffle-pool sequences are often characterised by ratios based on channel width (Keller, 1971; Richards, 1976b, 1982; Clifford, 1993b).

Cherkauer (1973) considered that the dispute regarding the relationship between channel width through riffles and pools may in part stem for the lack of an appropriate or consistent definition of channel width. Cherkauer (1973) acknowledging this difficulty considered that the most useful approach would be to consider the 'effective width', which corresponds to the active zone of flow (Clifford and Richards,1992). The definition of effective width was reinterpreted after the work of Thompson (2004) considering that the effective channel width is the area of flow that will convey the flow capable of scouring bed material (Harrison and Keller, 2007). The only published attempt to determine the physical extent of effective width was provided by Harrison and Keller (2007) specifying that modelled effective width is represented by 90% of the highest modelled flow velocities. Despite the important role effective width plays in the current understand and explanation of large-scale flow phenomena in natural gravel-bed river systems, a genuine method for measuring this flow property has yet to be development.

4.3.4 GRiFTer Measured Effective Width

The development of a GPS River Flow Tracer provides the first opportunity to measure the effective width of channel flow up to and beyond bankfull flow conditions. The flotilla of GRiFTers was deployed utilising a wave formation (groups of channel wide releases) whereby groups of units are released spaced across the entire width of the channel above a referenced start line. Upon entering the active area of the reach, each GRiFTer followed a completely independent path as determined by the natural flow conditions. Multiple GRiFTer releases create a series of flow tracks each with a unique reference number. The maximum horizontal distance between flow tracks can then be utilised to measure the effective width of channel flow across a particular cross-section. This analysis method would provide a genuine representation of effective width since only flow genuinely conveying water downstream throughout the entire reach would be represented by flow tracks and therefore included within the measurement.

4.3.5 The Relationship between Discharge and the Effective Width of Riffles and Pools

The literature pertaining to the lateral structure of riffle-pool sequences has provided much debate; Wilkinson et al., (2004) identified that riffles are typically 15-33% wider than pools (Lane and Borland, 1953; Richards, 1976b; Keller and Melhorn, 1978, Andrews, 1979; Carling, 1991), whilst Carling (1991) disputed that riffles remain wider throughout all flow conditions finding that riffles were 25% narrower than pool at the lowest flow conditions whilst across a range of high flow the riffle is 33% wider than the pool. MacWilliams et al., (2006) identified further contradictory results at Dry Creek, California finding that at low flow the riffle is around 50% wider than the pool and slightly narrower than the pool at high discharges.

4.3.6 Effective Width Flow Structures in the River Swale

Figure 4.8 provides GRiFTer calculated effective width structures for the River Swale, at the four unique discharge conditions previously identified. For ease of reference, riffles are approximately located through the middle of the curved regions of the channel whilst the inter-riffle pool occupies the long middle section of the reach.

Figure 4.8 highlights three key findings regarding the effective width of flow through riffle-pool sequences.

1. At base flow conditions (4.39 m^3s^{-1}) effective width is generally greater through the pool area (found through the long middle straight) than through the riffle areas of the channel (located within the curved sections).

2. With increasing discharge the effective width of the channel decreases through both the riffle and pool areas.

3. The rate of decrease is greater through the pool areas of the channel as opposed to the riffles thereby demonstrating the occurrence of a convergence in the relative effective width of riffles and pools with increasing discharge.

It is important to note that the results returned from a discharge of 5.07 m^3s^{-1} fail to correspond directly to many of the patterns outlined through the analysis of the other three discharge conditions. A possible explanation for this is that measurements were made soon after a large-discharge event allowing insufficient time for channel reorganisation to the persistent flow conditions following the retreat of higher discharge flows.

4.3.7 The Importance of the Relationship between Effective Width and Discharge for the Accommodation of a Velocity Reversal between Riffle and Pool.

The majority of research conducted into large-scale flow phenomena in riffle-pool sequences has focused on the existence of a reversal in hydraulic parameters with the velocity reversal hypothesis receiving considerable attention (Harrison and Keller, 2007). Thompson et al., (1999) described that several researchers have shown that during most stages, pools have a larger cross-sectional area of flow, and should therefore, exhibit lower cross-section averaged velocities than riffles (Richards, 1978; Schmidt, 1990; Carling, 1991; Carling and Wood, 1994; Thompson et al., 1996). The reversal in channel structure of riffles and pools with increasing discharge as presented by Keller and Florsheim (1993) is fundamental to the widespread debate concerning the reversal hypothesis. Similarly, Keller and Florsheim (1993) concluded that without a reversal in cross-sectional area the channel would be unable to accommodate a reversal in flow competence.

Considering the relationship between flow-depth and discharge Carling (1991) found that although the absolute differences in depth remains constant (with pools inherently always being deeper than riffles) as discharge increases, the relative difference decreases towards a convergence at bankfull flow levels. Carling (1991) is therefore providing evidence towards a reversal in width, depth and cross-sectional area with increasing discharge. Therefore, even if the convergence in relative depth, as observed by Carling (1991) does occur then there must also be a marked change in relative width for the potential of a velocity reversal to arise.

Analysis of the results returned from the River Swale highlights the occurrence of a convergence in relative effective width between riffle and pool with increased discharge. This highlights that the reach meets the requisite criteria for the potential occurrence of a velocity reversal.

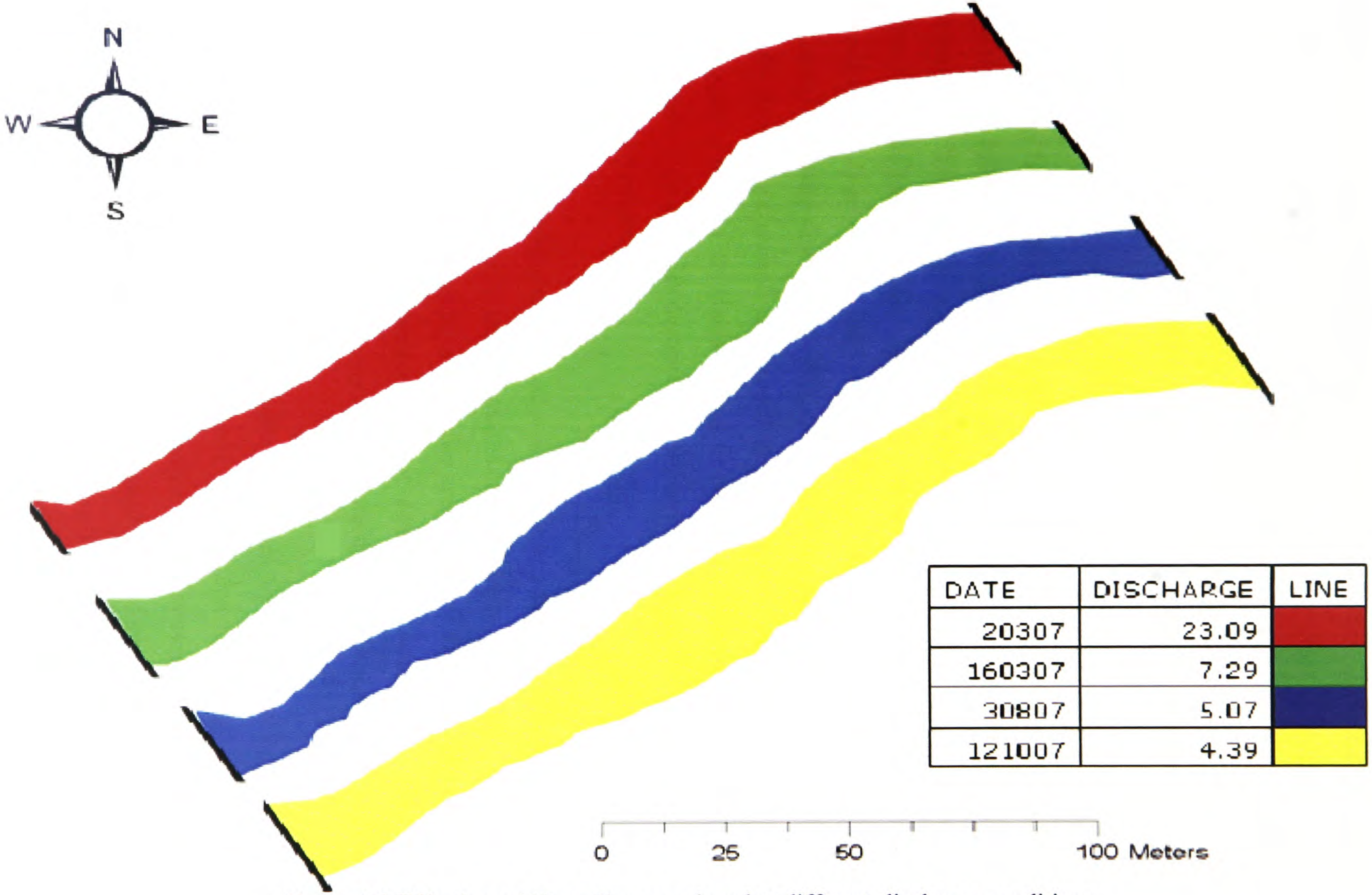

Figure 4.8 Effective width outlines produced at different discharge conditions.

4.3.8 Longitudinal Effective Width Profiles

At all but the highest discharge the longitudinal effective width pattern displays a similar structure (Figure 4.9). Following entry into the reach a common narrowing occurs simultaneously at all discharges as flow narrows into the first riffle located around 20 m - 60 m downstream. The first riffle forms the first of two prominent minimums along the longitudinal effective width profile; the second occurs at the second riffle.

Flow exiting the riffle diverges causing increased effective widths at all discharges reaching an initial peak, marking the pool area of the channel between 98 - 106 m. Downstream from the initial peak, the effective widths of low and higher discharges demonstrate unique behaviour. At lower discharge flow the effective width immediately narrows towards an intermediate trough (130-135 m). The longitudinal effective width pattern of the lower discharge flows then oscillate in a series of steep peaks and shallow troughs providing a overall consistency to the effective width (between 130 - 185 m). The higher discharge flowlines extend through a plateau following the initial peak before again widening with distance downstream to peaks at 160 m (7.29 m^3s^{-1}) and 170 m (23.09 m^3s^{-1}) respectively.

Evidence from the analysis of effective width through the first riffle and pool areas of the test reach (Figure 4.9) is that the magnitude of changes between the effective widths of riffles and pools is of similar magnitudes irrespective of discharge. However, the rate of change is significantly greater at lower discharges. Additionally, the maximum effective width through the pool section occurs further downstream at higher discharges.

This behaviour suggests that at the higher discharges, flow is forced through a narrower core of the overall channel width despite the fact that at the higher discharges the overall width of the channel appears greater. The increased discharge and therefore higher velocities also appear to have deformed the bed structure forcing the relative maximum effective widths further downstream. This would sensibly follow since the bed would be subjected to higher discharges which converge to produce further increased velocities and therefore mobilise bed material.

Following the occurrence of the mid-channel pool, all discharges demonstrate an overall decrease in effective width towards the second minimum and therefore second riffle observed within the reach. The second riffle occurs increasingly further downstream with increasing discharges - a pattern which again follows logically with the effects of converging flow at higher discharges. Following the occurrence of the second riffle, effective widths again increase to the conclusion of the reach.

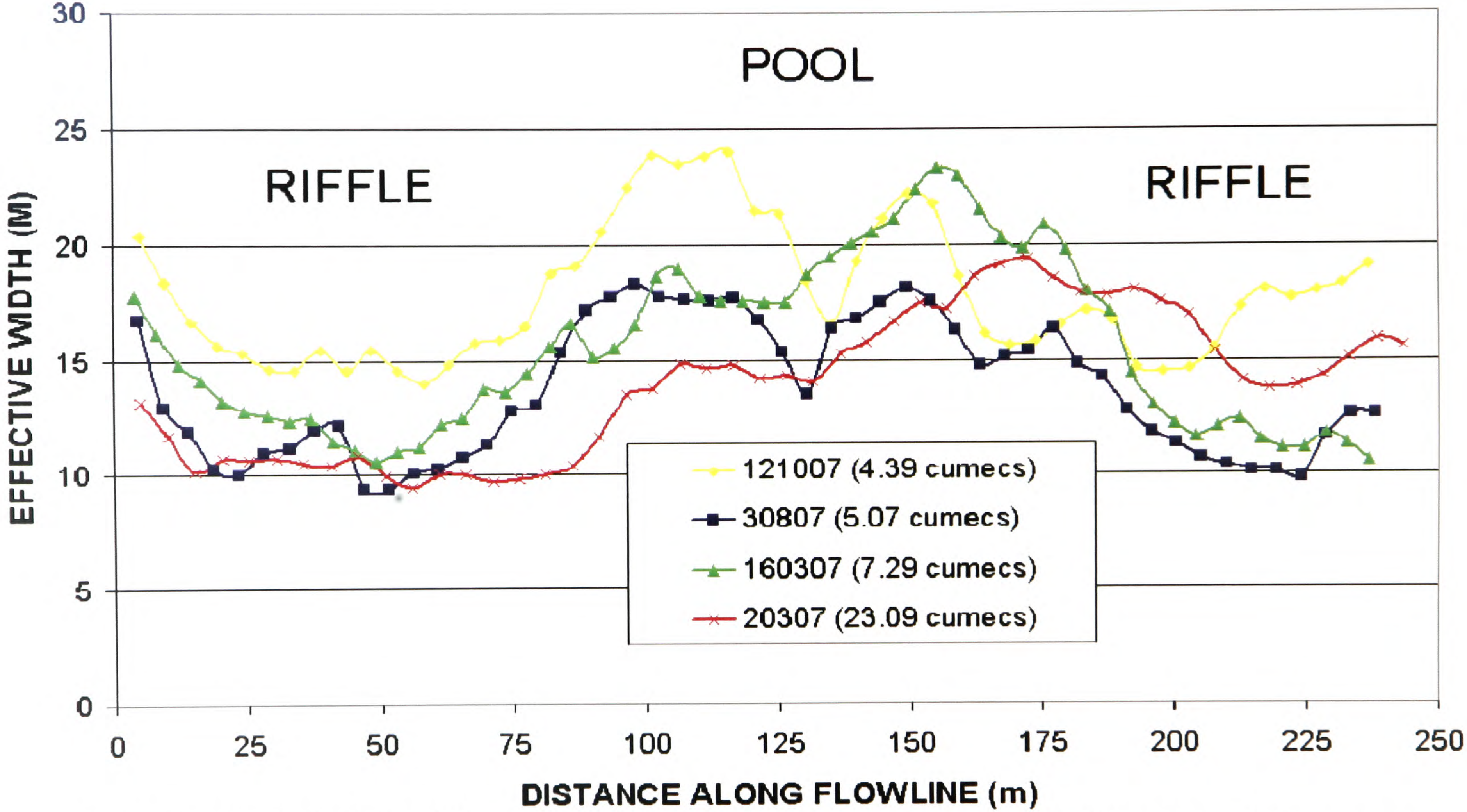

Figure 4.9 Longitudinal effective-width patterns with respect to discharge. The Figure is annotated with broad areas of riffles and pool.

4.3.9 Changes in Cross-Section Effective Width Relative to Base Level Discharge

In addition to accessing the longitudinal effective width patterns that occur relative to specific discharge conditions, it is also possible to determine the change in effective widths which result from changes in discharge. The range of flow conditions investigated therefore allows for discharge increases of +0.68 m^3s^{-1}, +2.9 m^3s^{-1} and +18.7 m^3s^{-1} to be investigated from a base level flow of 4.39 m^3s^{-1} observed on 12/10/07 (Figure 4.10).

Figure 4.10 demonstrates decreases in effective width through the first riffle and pool areas of the channel with any increase in discharge. The magnitude of the decrease is visibly greater throughout the pool region than through the riffle. Additionally, decreases are greatest at the largest discharge increase (+18.7 m^3s^{-1}). A localised point of minimum decrease occurs uniformly around 45m downstream which coincides with the main part of the first riffle. Further downstream the magnitude of decrease increases towards the reach maximum at around $110^{-1}15$ m downstream; at +18.7 m^3s^{-1} the maximum decrease equal -9.78m whilst at +0.69 m^3s^{-1} the maximum decrease measures -6.44 m.

The behaviour of effective width following the mid-channel pool is more varied than that observed previously. A point of equilibrium is reached around 150 m downstream where all changes in discharge exhibit decreases in effective width of between -4.7 and -4.9 m. Following this point the magnitude of decrease in effective width reduces towards 155 m downstream, beyond which all discharge conditions produce an increase in cross-sectional effective width. At 165m increases in discharge of +0.68 m^3s^{-1} and + 18.7 m^3s^{-1} demonstrate an increase in cross-sectional effective width of 0.13m and 3.2m respectively. The result for an increased discharge of +2.9 m^3s^{-1} demonstrates an enlarged cross-section effective width of 3.85m. For the +2.9 m^3s^{-1} data, the relative effective width continues to increase with distance downstream to a peak of +6.78m at 193m downstream. At the 193m cross-section, simultaneous localised peaks occur in both the +0.68 m^3s^{-1} (reduction in magnitude of decrease) and the +18.7 m^3s^{-1} (localised high in increase magnitude) flow. Following these peak increases, the rate of change increase dramatically, decreasing the effective width through to the conclusion of the reach.

An additional point of interest occurs between 115 - 135 m downstream following the mid-channel pool. The magnitude of decrease in cross-section effective width reduces dramatically to an interim minimum / peak where the +2.9 m^3s^{-1} data displays an increase in effective width. Throughout this area there is a switch in the previously observed relationship, as the magnitude of change is no longer ordered relative to increases in discharge. At 135m downstream, with a discharge of +2.9 m^3s^{-1}, the cross-sectional effective width increases for the first time throughout the reach. Concurrently, both the +0.68 m^3s^{-1} and the +18.7 m^3s^{-1} discharges, the rate of decrease reaches a localised minimum.

Within increasing discharge, it appears that flow is forced through the reach at a greater rate intensifying the core flow causing a narrowing of the effective width. It therefore follows that the rate of narrowing is greatest at the highest increases in discharge. The localised magnitudes of narrowing are greatest through the pool where flow inherently converges due to the changes in cross-section structure. Following the pool, flow diverges onto the shallower downstream riffle as the second curve fails to accommodate the higher volume flow causing a widening in effective width.

The point highlighted as diverging from the generally observed pattern to changes in flow structure, observed around 135 m downstream can be explained with reference to the primary flowline data. (Figure 4.7). As the primary flowlines begin to diverge entering the second curve; the 7.29 m^3s^{-1} flowline, which was routed around the left-side of the pool continues to follow a path towards the left channel side, away from the persistent path of lower discharge flows which follow closer to the channel centre and therefore increases relative localised effective widths.

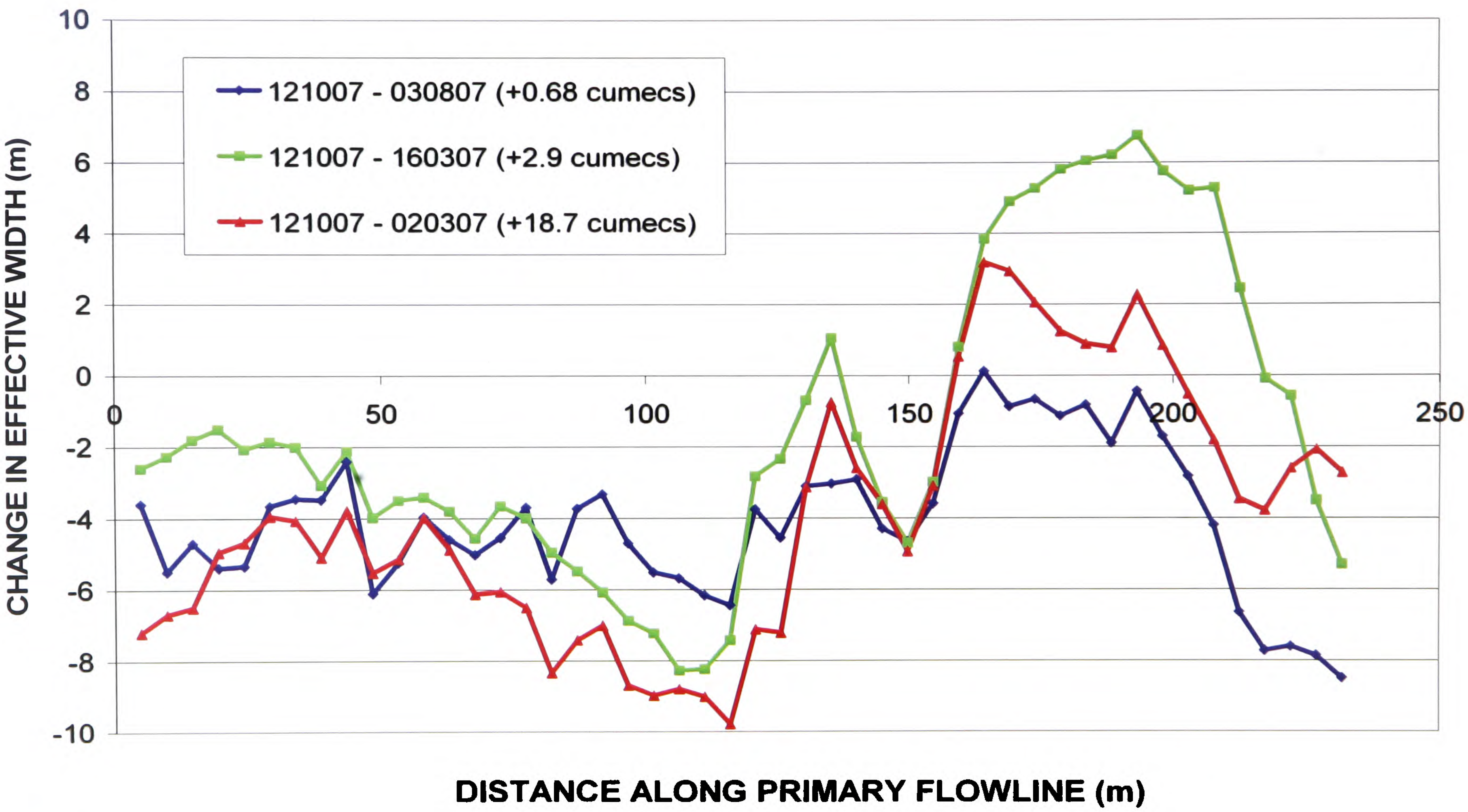

Figure 4.10 Longitudinal changes in effective width from base flow conditions (4.39 m^3s^{-1}).

4.4 Low Velocity Zones and Lateral Flow Patterns

4.4.1 What are Low Velocity Zones (and Flow Separations)

Low velocity zones (LVZ) are specific areas of the channel distinguished from the main body of flow by structural difference in flow speed and direction. These most commonly take the form of regions with a predominately upstream flow direction and / or displaying significantly lower magnitude velocities. In a hydrological context, low velocity zones (and flow separations) most commonly form on the downstream side or parallel to large channel obstacles. As flow passes an obstacle it creates a division in flow, forming a void behind the obstacle which is subsequently filled by secondary flow leaving the main downstream flow.

Lower velocity zones demonstrating rotational or upstream flow directions are regarded in this context as flow separations (where this separation is complete the features can be classified as an eddy). The areas between these LVZs will be classified as the higher velocity core and as such features continuous, relatively higher flow velocities (greater than 0.25 ms^{-1}) predominantly demonstrating a mean downstream flow direction. It is this higher velocity core which is principally responsible for shaping the longitudinal bedform undulation which forms riffle-pool sequences.

4.4.2 The Importance of LVZs (and Flow Separations) to Large-Scale Flow Phenomena

The size, location and type of LVZ are fundamentally important to the development of both longitudinal and lateral flow structures in naturally formed gravel-bed river systems and play a key role in many of the theories that seek to explain the development and maintenance of riffle-pool sequences (MacWilliams et al., 2006). The position and size of LVZ influence the development of constrictions and openings in the downstream flow profile.

These areas have the effect of producing relative convergences and divergences in channel flow which themselves shape and sculpt subsurface channel composition through adjusting relative entrainment and deposition patterns. In addition to creating convergences and divergences, flow separations (specifically separation or eddies featuring partial or full recirculation) can reintroduce flow either upstream or downstream of flow structures and thereby change localised flow patterns and velocities e.g. supplementing converging flow exiting a riffle to form a jet as it enters a subsequent pool (MacWilliams et al., 2006).

4.4.3 How LVZ are Identified / Measured

Utilising the cellular outputs generated from multiple GRiFTers releases it is possible to identify areas of the channel, within the extent of the effective width, with specific flow velocities. In this case, LVZ will be distinguished as continuous areas with average flow velocities less than 0.25 ms^{-1}. Each cell can then featured with an orientated arrow displaying the mean direction of flow within that cell. The direction of flow can then be utilised to make inferences as to the effect that LVZ have on localised and reach scale flow patterns.

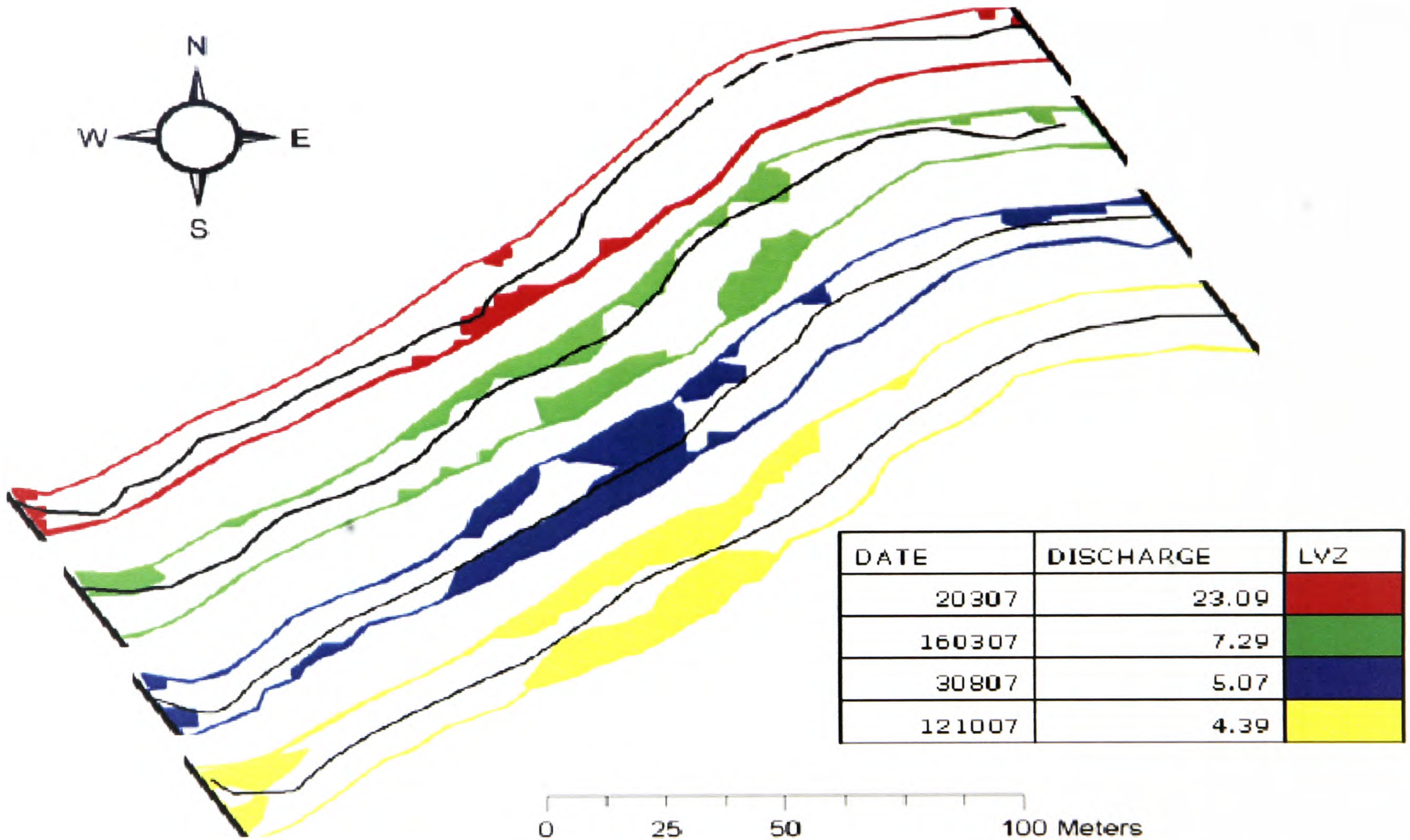

Figure 4.11 Reach scale diagrams highlighting the occurrence of low velocity zones (LVZ).

4.4.4 Location, Type and Role of LVZ

Initially each discharge conditions investigated will be described to highlight the important LVZ, their respective positions, internal flow dynamics and the relationships and role they have in the development of large-scale flow phenomena within the reach (Figure 4.11). Through each subsection the most prominent LVZ referenced will be those at the reach entrance, responsible for determining the passage of flow into the reach and the series of LVZ which develops through the long middle straight determining the behaviour of flow through the pool region of the channel feeding on towards the second riffle.

4.4.4.1 LVZs at a Discharge of 4.39 m^3s^{-1} (12/10/07)

A flow of 4.39 m^3s^{-1} through the test reach has the affect of creating five distinct LVZ. At the entrance to the reach through the initial left-hand curve two LVZ develop. Flow enters the reach through both an unobstructed shoot close to the right channel side and through a constriction created by the two flow separations. At the entrance to the reach the divide between the LVZ is 6.2 m, however 7 m further downstream flow converges to a width of only 1.2 m. Following this constriction, flow rapidly widens and merges with the flow entering through the right shoot and exiting both LVZ. This creates a curvature in flow away from the right channel side up to 20 m downstream where flow runs uniformly downstream across the width of the channel.

The most prominent LVZs at this discharge are present in the long straight region of the channel; two large LVZs occur, one on each side of the channel, creating a series of convergences and divergences in the high velocity core. The left side LVZ is narrow than the right side zone but extends significantly further downstream; the left zone measured 83.7 m whilst the right has a length of 71.8 m. The front face of the left side LVZ is smaller than the corresponding face to the right channel side meaning that less flow is able to enter this separation. Additionally, the width of the left LVZ is also significantly smaller maintaining the predominant downstream flow direction. The left side LVZ does however widen considerably downstream and begins to demonstrate clear rotational and circulating flow. The front face of the right side zone is significantly larger allowing for a great proportion of the higher velocity downstream flow to enter.

Additionally, the average width is significantly greater than that of the left side zone, causing a greater proportion of the area to demonstrate rotational flow. This rotation takes the form of flow from right channel side curving towards the channel centre. These LVZ demonstrate that the wider the LVZ / flow separation the greater the degree of rotation or circulation observed within the area.

The corresponding middle straight separations have significant effects on the flow structures occurring throughout this region of the channel. Flow upstream of the separations has an effective width of 14.9 m however the separations produce a construction (81 m downstream) which causes flow to converge to 3.81 m (12 m along the separations). Following this initial constriction flow diverges to a maximum width of 10.28 m a further 13m downstream (96 m along the reach). An additional 20 m downstream flow progressively converges to a constriction of 2.0 m (120.3 m along the reach). Throughout the next 8 m downstream flow widens again to 9.1 m and continues to widen through and beyond the conclusion of the left side LVZ.

Flow entering the middle straight region divides into three visible strands. The majority of flow passes between the LVZs through the series of constrictions and widenings. The strand of flow towards the left channel side enters the separation and curves away from the higher velocity core at the point of the second constriction. Flow entering the right side LVZ is rotated back towards the central flow intensifying flow through the constriction. The constriction causes the development of a jet which merges with the curved flow exiting the right separation to initiate the development of an elongated "s" like appearance to flow through the reainder of the straight and the initiation of the second curve observed through the reach.

At a discharge of 4.39 m^3s^{-1} it is clear that the presence of LVZ play a fundamental role in influencing both the lateral and longitudinal flow phenomena. The affects upon the lateral flow distribution is highlighted by the path of the primary flowline initially entering the reach through the two LVZ situated at the reach entrance then passing through the centre of the narrowed corridor created through the main channel straight. The longitudinal flow patterns are determined through the creation of a series of narrowing and widenings through the main channel straight. The presence of the LVZ produces a higher velocity corridor forcing flow to converge creating an initial jet which over deepens this part of the channel creating a relative pool. Erosion of the channel due to the higher velocity core being forced through this area creates a relative widening. Flow exiting this widening is supplement by rotational flow form the right side LVZ creating a secondary jet exiting the pool area. Further downstream the absence of LVZ allows the higher velocity core to span the complete effective width throughout the remainder of the reach.

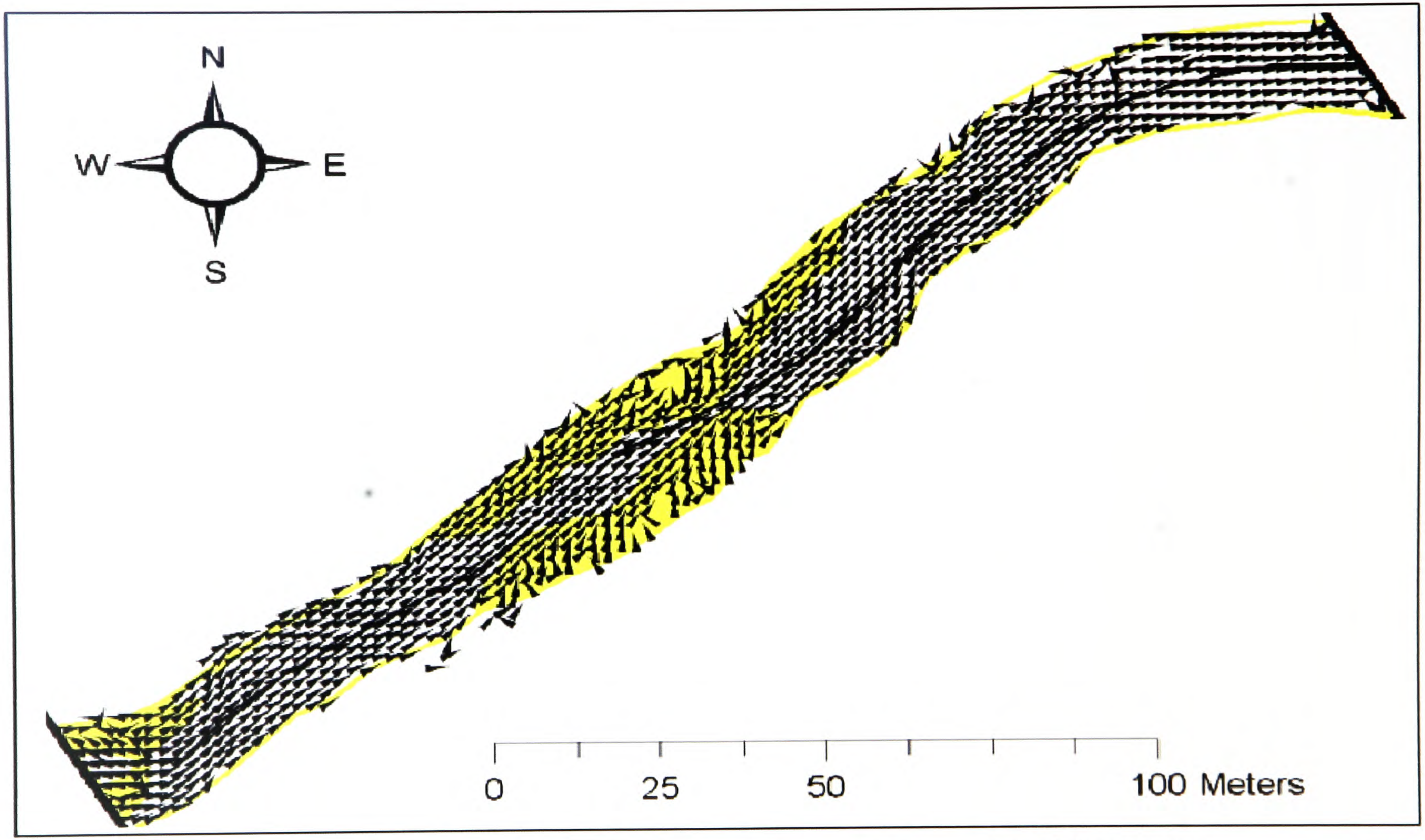

Figure 4.12 Location of LVZ and cellular flow patterns at a discharge of 4.39 $m^3 s^{-1}$ (121007).

4.4.4.2 LVZs at a Discharge of 5.07 m^3s^{-1} (03/08/07)

A flow of 5.07 m^3s^{-1} through the test reach produces ten distinct LVZs. At the entrance of the reach two, approaching rectangular, zones develop producing two clear paths through which flow can enter the reach. Unlike the upstream LVZ observed under the lower discharge flow conditions, although they are sufficient to cause a narrowing they are not sufficient to produce the degree constriction observed previously. Despite the lack of an obvious constriction the primary flow line bisects these LVZ on its entry into the reach.

The two clearly defined flow separations observed under the lower discharge conditions present within the middle straight region of the channel cannot be observed with a discharge of 5.07 m^3s^{-1}. The left side zone has moved further downstream and become fractured creating a divide within the zone measuring 4.55 m. The upstream section of the left side has a relatively short entrance face ensuring that flow within the separation only demonstrates downstream flow and partial curvature (towards the left channel side) as opposed to rotational or circulative flow observed under the lower discharge.

The right side LVZ begins further upstream (64.49 m into the reach) and extends for 42.7 m before merging with the downstream section of the left side zone. The LVZ spans the entire width of the channel at 103.5 m downstream providing a width of around 17 m. Within the LVZ spanning the entire channel width, a prominent line of downstream flow remains following the path of the primary flowline. Flow either side of the primary flowline curves away towards the respective channel sides.

An additional pair of LVZ occurs further downstream on the left channel side, and although they are significantly smaller than those observed previously the effect of both these separations is to compress flow parallel to the LVZs. This creates a curvature of the main body of flow towards the right channel side round the larger, initial LVZ before flow curves back towards the smaller separation, infilling the void between the two LVZs.

The ninth LVZ is situated on the outside of the second curve (left channel side) 171.5 m downstream. This zone is 5.33 m long, has an area of 18.23 m^2 and is approximately triangular extending into the main channel flow. The effect of this zone is to reroute flow curving round the downstream larger left side zone. Flow initial curving from right to left infilling behind the larger zone curves from left to right around this additional triangular LVZ creating another elongated "s" like appearance to the flow entering the main path of the second curve.

Flow through the main straight of the channel possesses many similarities with that observed at the lower discharge. Initially it appears that a narrowing begins to form although the degree of convergence is incomplete as the left side LVZ fail to form completely. This has the affect of allowing the higher velocity core to curve toward the left channel side, dissipating energy and flow momentum which cannot be conveyed downstream in the form of the jet observed previously. This is further supported by the flow paths observed within this area demonstrating similarities in terms of a narrower downstream through flow and either side curved flow towards the extent of the effective width. This would explain the formation of the channel spanning LVZ and the deviation in large-scale flow phenomena from that observed previously.

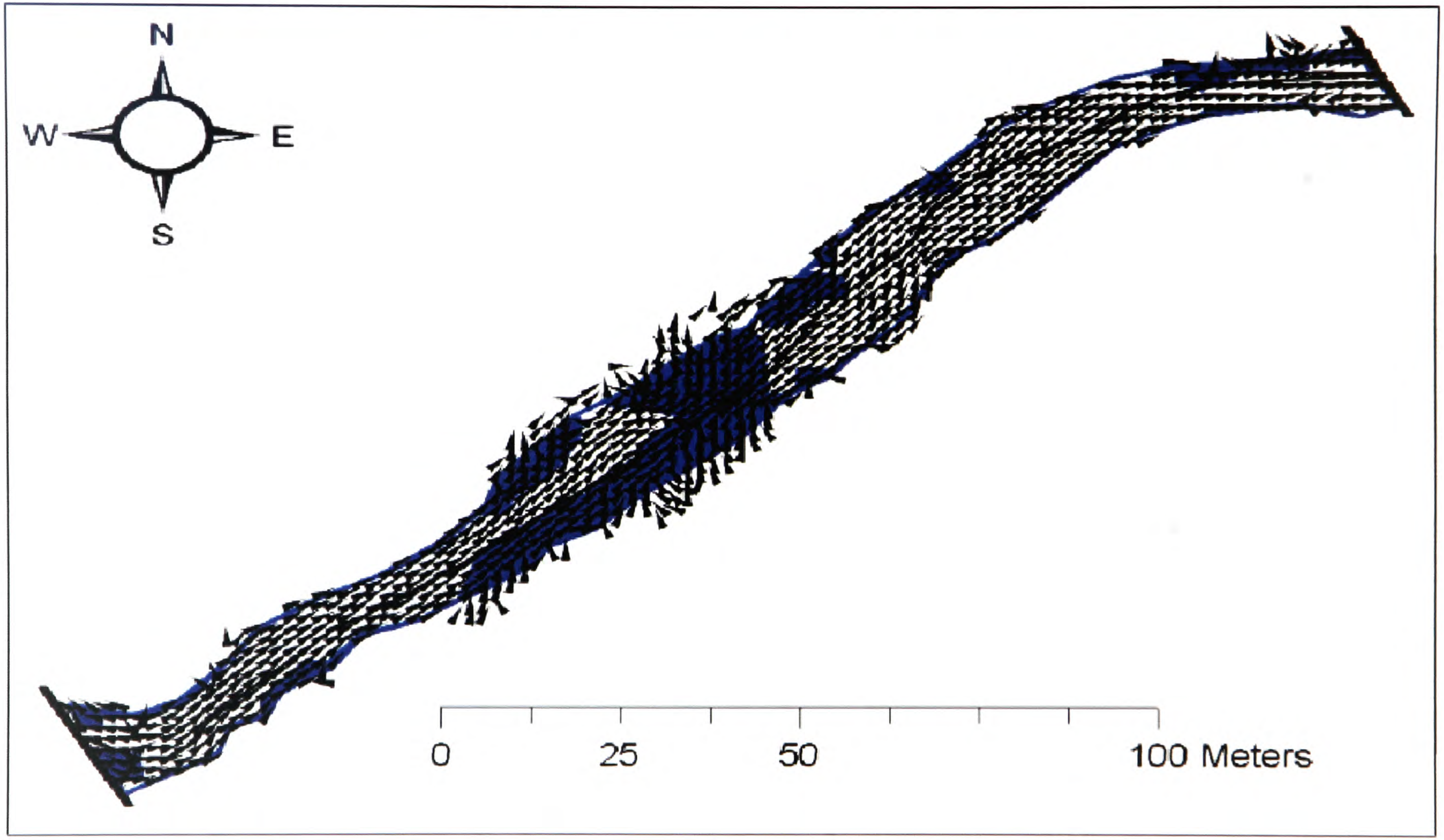

Figure 4.13 Location of LVZ and cellular flow patterns at a discharge of 5.07 m^3s^{-1} (030807).

4.4.4.3 LVZs at a Discharge of 7.29 m^3s^{-1} (16/03/07)

A discharge of 7.29 m^3s^{-1} creates 13 LVZ throughout the test reach. Six larger zones (four of which occur on the left channel side) and seven smaller zones (four of which again occur on the left channel side). The first of the larger LVZ occurs on the left side of the reach entrance and is larger than those observed previously at the reach entrance. Flow enters this zone both from upstream and is also drawn into the zone from the right side channel flow. Within this zone, flow demonstrates rotation and circulation exiting the downstream face of the feature. Flow through the right side of the channel arcs round this zone and merges with flow exiting the area and continues to flow uniformly downstream uniformly towards 35 m.

Around 35 m downstream the first smaller LVZ occurs on the left channel side. This triangular zone is 7.5 m long and has an area of 8.7 m². Flow within this area shows angling away from the channel centre towards the left channel side and again has the effect of compressing flow creating a concave in the general curvature of flow towards the right as it begins to enter the main straight section of the channel. As observed previously the compression of flow occurs upstream and parallel to the LVZ followed by subsequent infilling / realignment of flow.

Throughout the middle and end straight regions of the channel two pairs of larger, almost coincidental LVZ are produced and within the second curve both a larger and two smaller LVZ can be observed on the left channel side. These zones are responsible for dictating the behaviour of flow and the large-scale flow patterns within these regions of the channel.

The higher velocity core which flows between these separations is subjected to a series of constrictions, widenings and lateral flow migrations creating another unique series of flow patterns and structures. Effective width increases prior to the middle of the straight (to a width of 13.7 m) caused by divergent flow exiting the early upstream riffle area (78 m downstream). The two early sections of the initial left side LVZ compress the higher velocity core preserving a width of 12.6 m. The presence of the larger section of the left side zone occurs in parallel to the large right side separation creating a narrowing corridor. The entrance to the corridor occurs at 103 m downstream with a width of 6.2 m and narrows to a maximum constriction of 3.8 m at 121.4 m downstream. Flow on the right side of the channel enters the large separation through the relatively wide entrance face and is curved and spirals downstream being reintroduced to the higher velocity core in the next channel widening (17.9 m) following the constriction at 123 m downstream. The widening of the higher velocity core occurs as flow diverges exiting the constriction.

The next left side zone occurs at 133 m downstream and causes a subsequent compression of flow, with flow entering the LVZ being conveyed further downstream into the next widening. Flow through the right side of the channel enters the LVZ. whilst the main body of channel flow is again compressed creating an additional convergence which arcs around the separation. This convergence is less severe than those previously observed and occurs at 143 m downstream with a width of 10.2 m. Flow through this convergence arcs from right to left until parallel with the smaller triangular LVZ located on the left channel side. Simultaneously, rotational flow exits the right side separation and feed the downstream curving flow. Following this arc in flow the additional left side separation protrudes into the flow altering the flow patterns experienced on the left channel side. Flow within the separation angles away from the right arcing pattern of the higher velocity core (around the second bend), towards the left channel side. This creates a division as flow exiting this separation further downstream orientates directly towards the reach exit straight and merges with the curving flow around 180 m downstream. Following this merger, flow runs almost exclusively downstream throughout the remainders of the reach. This second series of larger LVZs results in the creation of a double "s" like appearance to the compressed flow as it narrows and curves from left to right in the widening, right to left through the second convergence then left to right again at the conclusion of this series of separations.

An elevated discharge and the resultant higher water levels would produce more material and fluid interactions resulting in increased channel roughness and therefore greater turbulence. These factors contribute to the development of more and increasingly large LVZ (relative to coverage of the effective channel width) leading to greater variation and complexity of both lateral and longitudinal flow patterns.

This series of LVZ interacts with the channel bed to adjust but maintain the series of riffles and pool. Flow diverging following the upstream riffle through the early part of the main straight widens the effective width prior to the occurrence of the series of narrowings and widenings. Upon entering the first narrowing flow converges and punches a jet through towards the deepest part of the channel; however as described earlier, at this elevated flow level the primary flow line arcs around to the left of the deepest part of the pool routing sediment away from this area. This results in a widening of the relative higher velocity core through the pool as the narrower corridor observed previous cannot accommodate the increased volume of flow

Again the slowest flows are observed through the pool area itself before secondary flow form the right side separation supplement the downstream flow exiting the pool area. Unlike the pattern produced by the 4.39 m^3s^{-1} data a secondary jet does not leave the pool area due to the curved path of the higher velocity core. Therefore secondary flow form the right side LVZ achieves in forcing the downstream flow from the right channel side and once compressed by the additional right side separation creates the previously identified "s" like pattern through out the remainder of the reach.

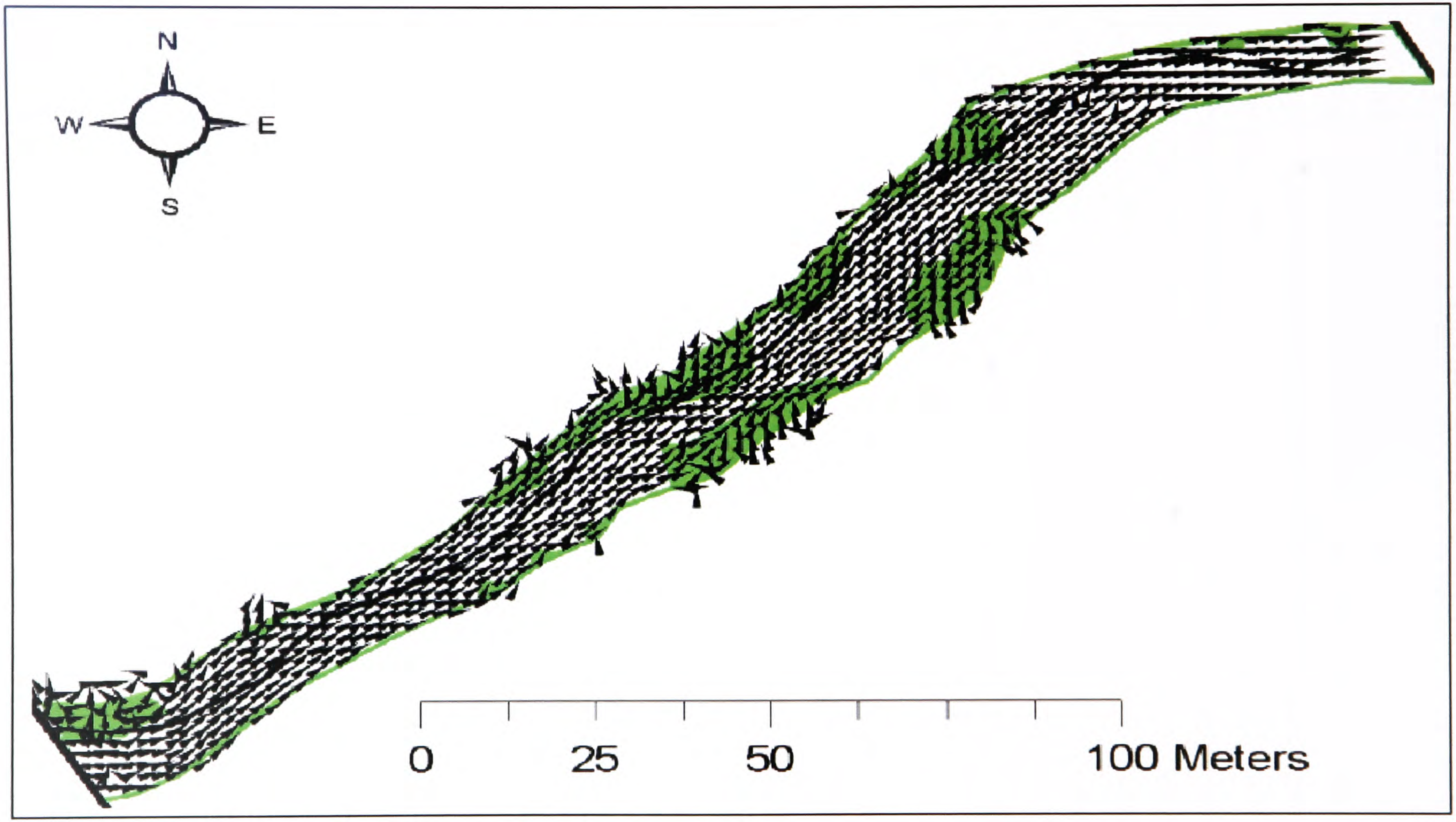

Figure 4.14 Location of LVZ and cellular flow patterns at a discharge of 7.29 m^3s^{-1} (160307).

4.4.4.4 LVZs at a Discharge of 23.09 m^3s^{-1} (02/03/07)

A discharge of 23.09 m^3s^{-1} develops nine (eight smaller and one larger) LVZs through the test reach. A series of three entrance dividing zones develop within the first 5 m of the test reach. These zones create two openings through which flow can enter the reach, the left opening measures 3.14 m and the right 0.9 m wide. These zones create a distinction in the flow observed in the left and central side of the channel as opposed to flow on the right side of the channel. Whilst flow exiting both the left and central separations angles across the channel downstream towards the right channel side; flow between the separations shows average upstream flow directions. Flow on the right side of the channel gently angles towards the right and curves round the outside of the initial left-hand curve. The individual elements of flow merge around 20 m downstream and continue to flow directly downstream.

A pair of small LVZ occurs on the right side of the channel 87.29 m and 98.5 m downstream respectively; the first with an area of 7.8 m^2 and the second with an area of 4.3 m^2. These triangular zones interact with the flow to produce a angling of the higher velocity core away towards the left channel side.

Immediately following these two LVZs, at 101.8 m downstream the single larger separation can be observed. This separation is 19.6 m long with an area of 94.6 m^2 and widths that range from 3.1 m to 5.6 m. A distinction can be observed between flow in the first 7 m of the separation and the remaining 12 m. In the front section, flow entering through the face of the separation continues to flow essentially downstream except for flow closest to the right channel side which curves the widest part of the upper section into the lower section of the separation. Flow entering the lower separation continues to curve towards the right channel side before circling towards the separation exit creating a spiral like pattern to the flow within.

The LVZs highlighted within this 50 m section of the middle straight (between 90 m - 140 m downstream) create a less pronounced and less severe series of narrowings and widenings in the width of the higher velocity core.

Initially, the width of flow entering this series of separations is 13.4 m; a staggered narrowing occurs to 10.2 m, 9.3 m then 6.6 m parallel with the largest right side separation. Following this constriction, flow curves towards the right channel bank diverging to a width of 13.4 m. A secondary compression occurs parallel with the last right LVZ to a width of 15.5 m before the higher velocity core spans the entire effective width through to the conclusion of the reach. This series of LVZ creates an elongated m-like pattern to the higher velocity core as flow through this region of the channel sweeps from right to left around the single large separation before arcing from left to right through the constriction then back from right to left around the final narrowing filling the entire effective width downstream.

With increasing discharge toward bankfull conditions the number, size and complexity of LVZs is reduced. Further the effect of increased discharge appears to punch flow through the reach significantly reducing the degree of lateral flow migration observed at the previous discharge conditions. The only undulation that remain are those produces as flow passes through the LVZs located through the middle channel straight. Despite the decrease in lateral migration the arc in the primary flowline around the deepest part of the pool again appears to occur, however this time it occurs to the right channel side, towards the larger of the two LVZs.

The behaviour of flow through the reach at this discharge appears to demonstrate a smaller convergence occurring as flow arc around the upstream right side separations before entering and curving around the pool and then diverging on the pool exit slope as depth rapidly decreases, thereby filling the entire effective width. This pattern of behaviour would appear sensible as increased discharge would effectively drown out the previously substantial effects of depth changes, increased localised turbulence and small scale flow deviations due to the enormity of the primary flow which fills the entire effective width.

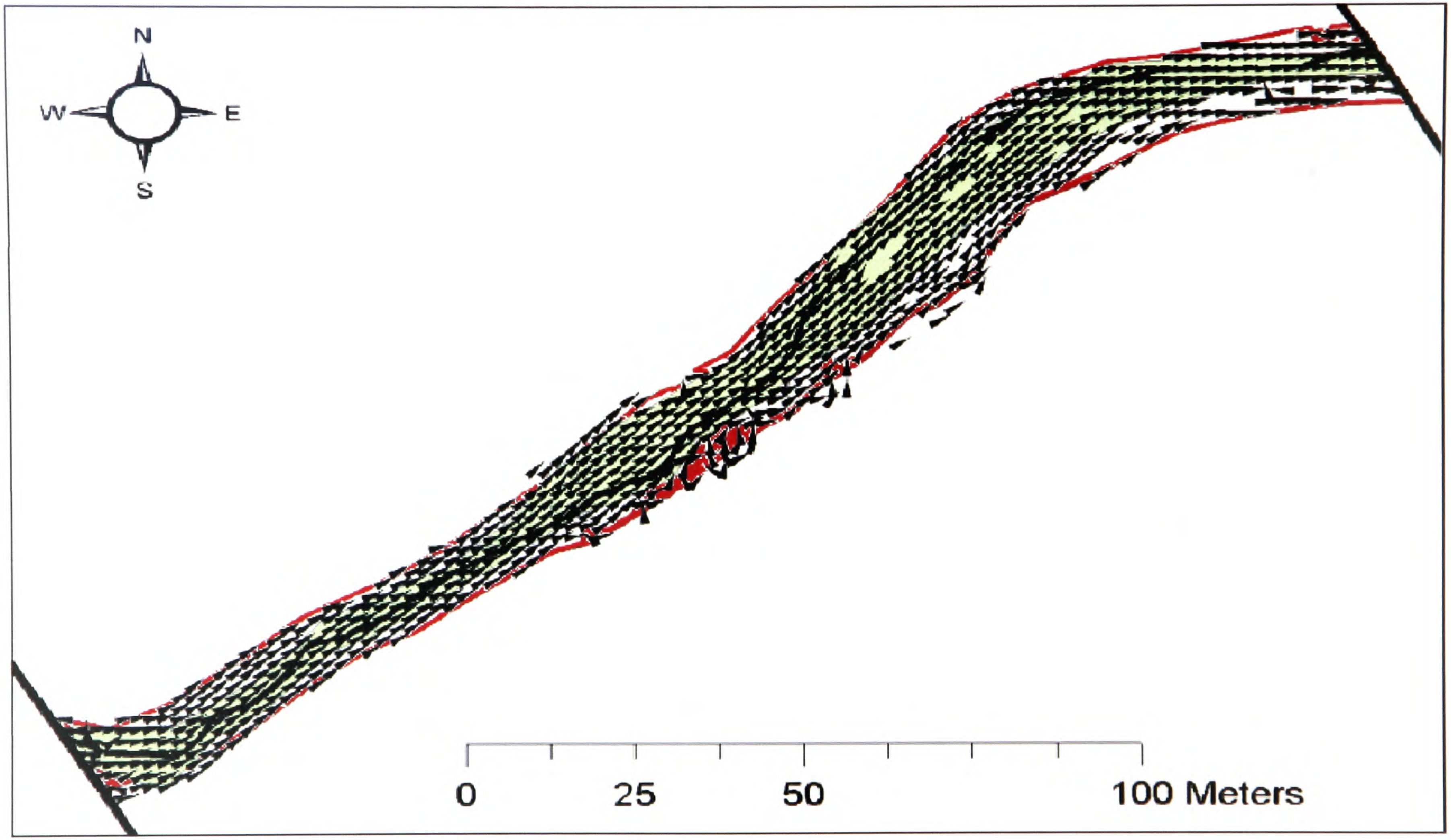

Figure 4.15 Location of LVZ and cellular flow patterns at a discharge of 23.09 m^3s^{-1} (020307).

4.4.5 The Relationship between Low Velocity Zones and Discharge

The effect of increasing discharge from 4.39 m^3s^{-1} though to a bankfull flow of 23.09 m^3s^{-1} produces a unique series of LVZs resulting in different sets of lateral and longitudinal surface flow dynamics. At all discharge conditions the LVZs present within the middle straight section of the channel influence lateral and longitudinal flow patterns through the creation of a series of narrowings and widenings determining the location and size of the pool and the riffle present within the second, longer curve.

At a discharge of 4.39 m^3s^{-1}, the presence of two large coincidental LVZ produces a higher velocity corridor forcing flow to converge creating an initial jet which over deepens the middle straight of the channel creating a pool. Erosion of the channel due to the higher velocity core being forced through this area creates a relative widening. Flow exiting this widening is intensified by rotational flow from the right side LVZ creating a secondary jet exiting the pool area. Further downstream the absence of LVZ allows the higher velocity core to span the complete effective width throughout the remainder of the reach.

Flow through the main straight at 5.07 m^3s^{-1} possesses many similarities with that observed at 4.39 m^3s^{-1}. Although a narrowing begins to form, the degree of convergence is significantly reduced due to the left side LVZ failing to form completely. This has the affect of forcing the higher velocity core to curve toward the left channel side, dissipating energy and flow momentum which cannot be conveyed downstream in the form of the jet observed previously. This would explain the formation of the channel spanning LVZ and the deviation in large-scale flow phenomena from that observed previously.

Increasing the discharge further to 7.29 m^3s^{-1} results in the development of more and increasingly large LVZs (relative to coverage of the effective channel width) leading to greater variation and complexity of both lateral and longitudinal flow patterns. Flow diverging following the upstream riffle through the early part of the main straight widens the effective width prior to the occurrence of the series of narrowings and widenings. Upon entering the first narrowing flow converges and punches a jet through towards the deepest part of the channel. However as described earlier, at this elevated flow level the primary flow line arcs wider around to the left of the deepest part of the pool. This results in a widening of the relative higher velocity core through the pool as the narrower corridor observed previously cannot accommodate the increased volume of flow.

Again the slowest flows are observed through the pool area itself before secondary flow from the right side separation supplement the downstream flow exiting the pool area. Unlike the pattern produced by a discharge of 4.39 m^3s^{-1} a secondary jet does not leave the pool area due to the curved path of the higher velocity core. Therefore secondary flow from the right side LVZ achieves in forcing the downstream flow through the right side of the channel and once compressed by the additional right side separation creates the previously identified meandering pattern throughout the remainder of the reach.

A reversal occurs in the pattern of the increasing prominence of LVZs at a discharge of 23.09 m^3s^{-1}. As discharge approaches bankfull conditions the number, size and complexity of LVZs is reduced. The effect of increased discharge appears to force flow through the reach, significantly reducing the degree of lateral flow migration observed at the previous discharge conditions. Despite the decrease in lateral migration the arc in the primary flowline around the deepest part of the pool again develops, however this time it occurs to the right channel side, towards the larger of the two LVZs. The behaviour of flow through the reach, at this discharge, appears to demonstrate a smaller degree of convergence occurring as flow arcs around the upstream right side separation before entering and curving around the pool and then diverging on the pool exit slope as depth rapidly decreases, thereby filling the entire effective width. This pattern of behaviour would appear sensible as increased discharge would effectively drown out the previously substantial effects of depth changes, increased localised turbulence and small scale flow deviations due to the enormity of the primary flow which fills the entire effective width.

4.5 Velocity Patterns

4.5.1 Alternative Approaches to the Measurement of Surface Flow Velocities

Having utilised the flotilla of GRiFTers to construct a cellular representation of the test reach it is possible to measure surface flow velocities in a variety of ways. The first is through the construction of longitudinal velocity patterns using a series of single cell values taken along the path of the primary flow line. An alternative is to use average cross-sectional flow velocities calculated from every cellular value across 5m spaced cross-sections measured perpendicular to the primary flowline. A third approach uses every cellular velocity value from the entire reach to provide complete flow coverage within the effective channel width. However, measurements of this type cannot be presented as longitudinal patterns.

Each approach uses significantly different numbers of data points and potentially provides different representations of surface flow velocities. Existing literature has highlighted that the variation and disagreement in existing data can be attributed to different measurement methods, statistical techniques and field locations (Milan et al., 2001). Therefore consistency in field site and measurement methods, across four discharge conditions, each exploring a range of statistical techniques will be utilised to access both the relationships between discharge and surface flow velocities and the relative importance of different statistical methods.

4.5.2 Longitudinal Primary Flowline Velocity Patterns

At all discharge conditions three distinct zones can be observed in the longitudinal primary flowline velocity patterns. At the three lower discharges (4.39, 5.07, 7.29 m^3s^{-1}) velocities rise to form an initial peak over the first riffle before falling towards the first transitional point. Following the transition a trough forms through the middle of the reach marking the location of a pool before re-rising to a second peak / riffle and again decreasing towards the conclusion of the test reach. Within the trough an additional smaller peak develops, produced by a localised short rise in velocities.

At a discharge of 23.09 m^3s^{-1} a convergence occurs in magnitude of velocities observed in the pool and through the first riffle; this produces a general pattern featuring three peaks, one at each of the riffle and an additional peak through the mid-channel pool. The magnitudes of velocities at each of the peaks are the maximum observed velocities relative to each peak location. Between each peak, velocities fall to relative troughs; either side of the trough areas observed at each of the other discharge conditions.

In terms of general pattern it is clear that changes in longitudinal primary flowline velocities occur more gradually at lower discharges (4.39 m^3s^{-1} and 5.07 m^3s^{-1}) both in terms of the direction and magnitude of change. This is demonstrated by the absence of velocity spikes, which can clearly be observed at higher discharge; these are particularly prominent at the 7.29 m^3s^{-1} and increase further within the 23.09 m^3s^{-1} data. At all but the highest discharge (23.09) the rate of change in velocities is greatest within the first riffle zone whilst the type of change (increases and decreases) is significantly more varied in the second riffle.

Also apparent is that the range of velocities increases at higher discharges. The magnitude of the minimum observed velocities also decreases as discharge increases, with the exception that the lowest single value (0.09 ms^{-1}) is observed under a discharge of 7.29 m^3s^{-1}. The highest single velocity from all data (2.12 ms^{-1}) is also observed at the highest discharge (23.09 m^3s^{-1}) within the second riffle. This value is distinctive since it is the first second riffle peak that is of a clearly higher magnitude than that observed over the first riffle.

Additionally prominent is the development in an upstream migration in the location of relative transitional points (e.g. peaks or troughs) with increases in discharge. At a discharge of 7.29 m^3s^{-1} the first peak is distinguished from those observed under lower discharges (4.39 and 5.07 m^3s^{-1}) as it occurs further upstream (by 15 m) and spans a shorter distance (only 4 m). A further upstream migration of the first riffle peak can be observed at the highest discharge (23.09 m^3s^{-1}). Further evidence of this migration can be observed at the highest discharge (23.09 m^3s^{-1}) where the second peak, uniquely located within the area of the channel marked as a pool at lower discharges, occurs 90 m downstream with a velocity of 1.83 ms^{-1}. This peak occurs upstream of the relative peaks seen within the troughs of lower discharge flows (4.39, 5.07, 7.29 m^3s^{-1}). This pattern suggests a degree of mobility in the location and structure of the individual elements of riffle-pool sequences which could be utilised to explain the perceived deviation in inter-riffle spacing due to variation in discharge conditions.

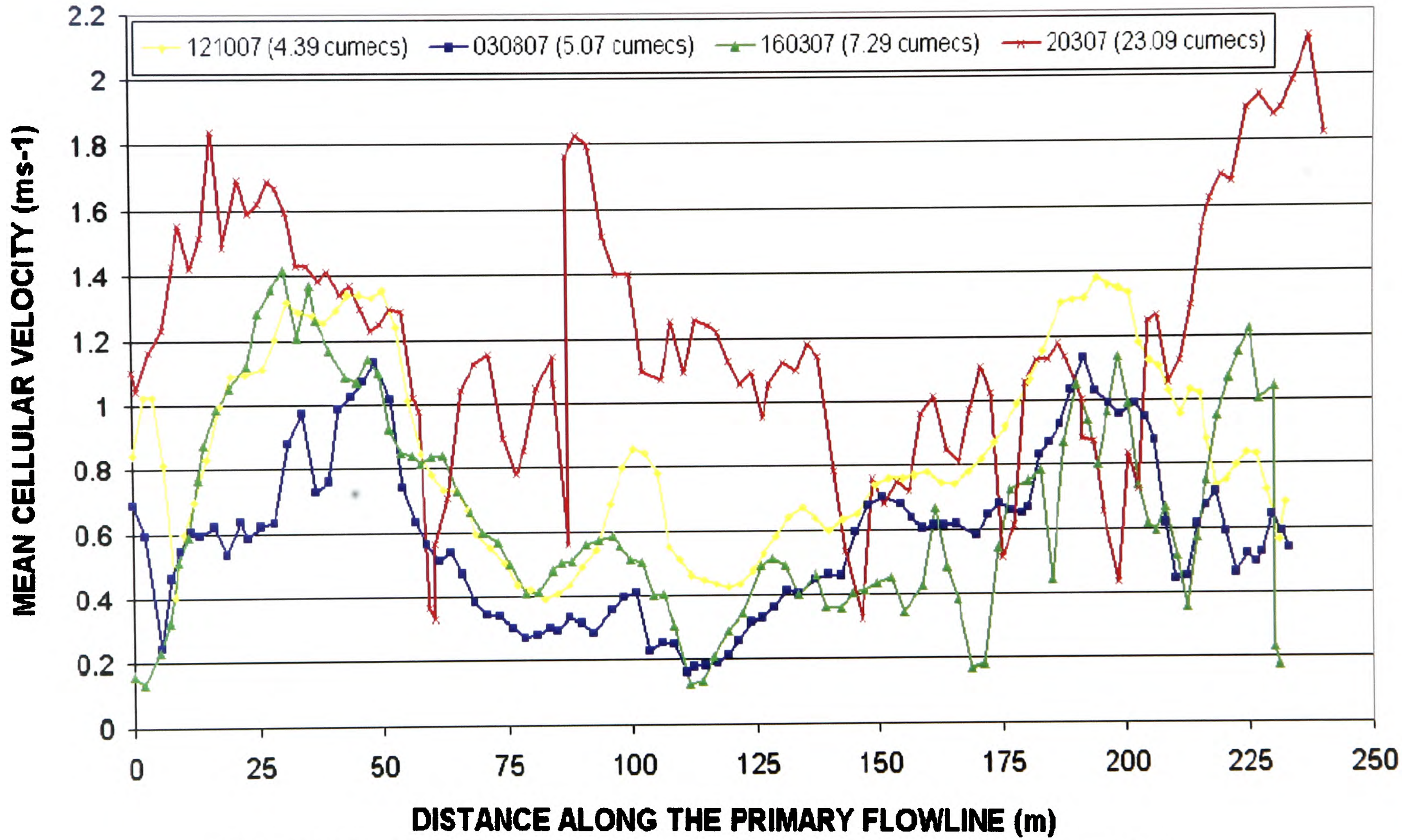

Figure 4.16 Longitudinal primary flowline velocity patterns at different discharge conditions.

4.5.3 Longitudinal "Cross-Sectional" Velocity Patterns

Similarly to the longitudinal primary flowline velocity patterns, the longitudinal cross-section velocity patterns demonstrate three distinct zones (Figure 4.17). From the initiation of the reach velocities increase towards the first large peak, a decrease in velocities then occurs towards a central reach minimum. Following this minimum, velocities increase towards a second peak before again falling towards the conclusion of the reach. All velocity patterns also demonstrate an additional smaller peak on the falling limb towards the mid-reach minimum velocities. An additional feature can be observed between 152 - 172 m downstream where at all discharges, a plateau or decrease in velocities occurs on the upward limb towards the second peak.

The similarity of all longitudinal cross-sectional velocity patterns irrespective of discharge highlights the uniqueness of the primary flowline velocity pattern produced at the highest observed discharge (23.09 m^3s^{-1}). When the primary flowline velocities were analysed it was apparent that a convergence had occurred, where the comparably high velocities now occupied the area of the channel that previously featured the minimum velocities at lower discharges. When cross-section velocity measurements are considered, no such convergence occurs with the same broad structures being produced by the velocity patterns from all discharges.

In terms of general trends, it is clear that the magnitude of velocities increases with increasing discharge; except for the results produced by a discharge of 5.07 m^3s^{-1}. Furthermore, the range of velocities increases with all increasing discharges. Additionally apparent is that flow is more varied at the highest discharge conditions, again excluding the results returned from a discharge of 5.07 m^3s^{-1}. The rate of change in velocity is also again greater during the first riffle area of the velocity profile.

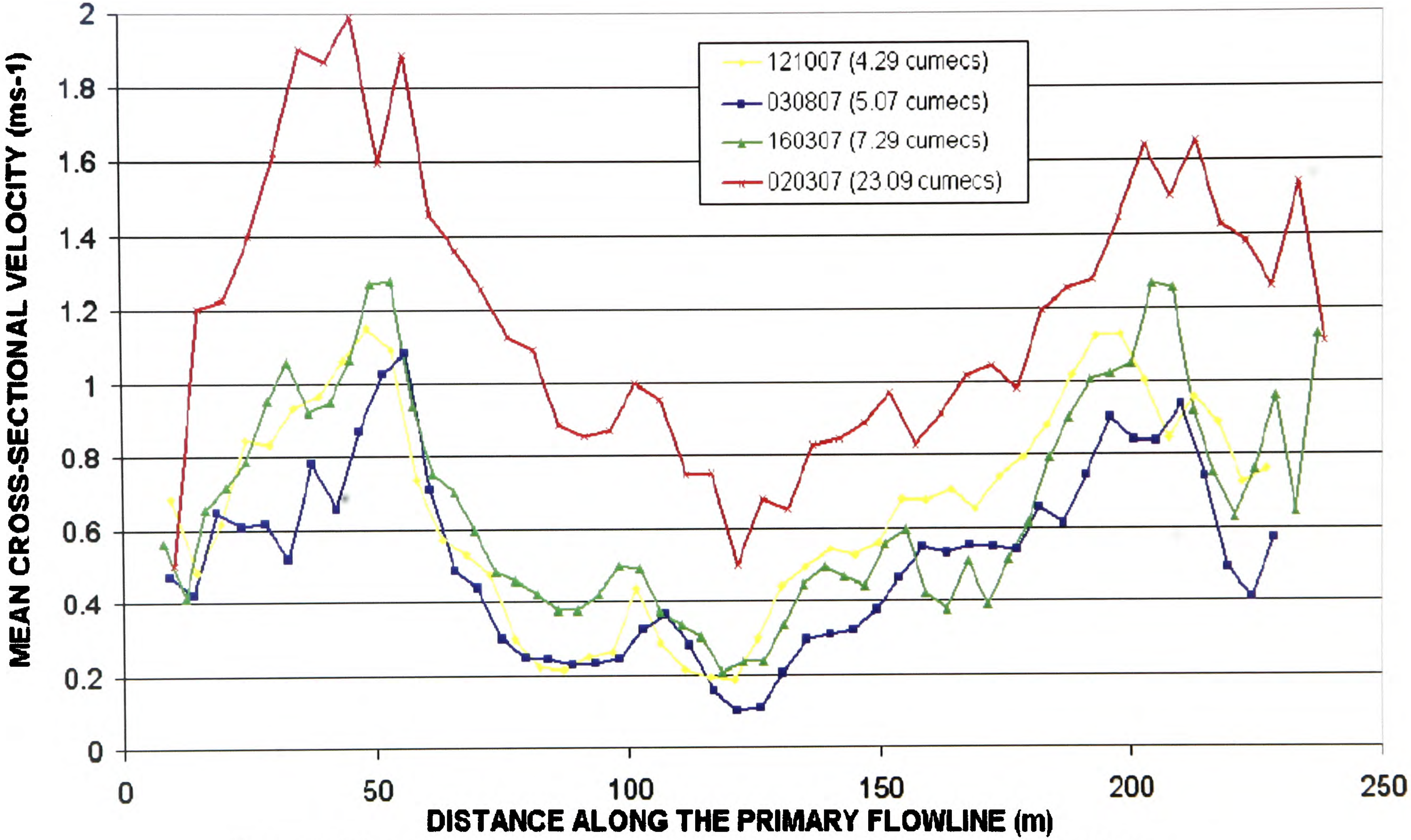

Figure 4.17 Longitudinal cross-section velocity patterns at different discharge conditions.

4.5.4 Deviation between Primary Flowline and "Cross-Sectional" Surface Velocity Patterns

If the structure of surface flow velocities is uniform across the entire width of the channel then the primary flowline velocity patterns should equal those provided by the cross-section averaged velocities. Any deviation between the results provided by the two velocity measurement methods will therefore be informative as to the lateral distributions of velocities within the test reach. The deviation between primary flowline (or any other single point representation of flow velocities) and cross-sectional results could also explain the differences that have occurred in previous investigations of large-scale surface flow dynamics, particular with reference to riffle-pool sequences, where varying measurement strategies have yielded significantly different findings.

At the lower discharges (4.39 and 5.07 m^3s^{-1}) the primary flowline measurements provide higher velocities than the comparative cross-section velocity measurements. At the lowest discharge (4.39 m^3s^{-1}) the structure of velocities from both measurement methods are very similar with all transitional point and the majority of increases and decreases occurring in parallel. It is also apparent that the differences in the magnitude of change are greatest at the transitional points.

At a discharge of 5.07 m^3s^{-1}, the differences in the magnitude of velocities with respect to measurement methods are significantly reduced from those observed previously. Again however, all major transition points and features appear in commonality including a plateau which develops between $158^{-1}78$ m downstream.

An increase in discharge to 7.29 m^3s^{-1} provides that although the velocities from the primary flowline measurements remain higher at the peaks, there is significantly greater cross over and therefore occurrences where the cross-section velocities are higher. With increasing discharge the range of primary flowline velocities increases dramatically and also becomes more varied in terms of the direction of change. This pattern is particularly clear in the third zone of the channel.

At the highest discharge (23.09 m^3s^{-1}) there is an effective reversal in the structure of the primary flowline velocity when compared to cross-sectional velocity pattern.

Differences in the relative velocities are greatest at the peaks and narrowest at the trough. Additionally prominent is that the primary flowline velocities are significantly more varied particularly through the first phase of the channel. This reversal highlights that variation in velocity is greatest at the highest discharges and that the method of velocity measurement has the ability to present significantly different representations of the large-scale surface flow dynamics operating within a particular reach.

The difference between the primary flowline and cross-sectional average velocities are informative as to how location and type of velocity measurement can influence the apparent flow patterns observed throughout specific sections of the reach. This further highlights that in order for the results of different investigations to be compared then reference must be given to differences arising due to variation in measurement method and statistical techniques.

5 Discussion

The development of a GPS River Flow Tracer (GRiFTer) has provided an innovative approach to the acquisition of surface velocity measurements in gravel-bed river systems. Data collected using GRiFTers has been analysed using a suite of tools to investigate and develop current understandings of large-scale surface flow phenomena in gravel-bed river systems and revisit many of the accepted theories relating to riffle-pool sequences.

The suite of GRiFTer based tools developed to date includes; the ability to measure a single primary flowline through a reach, a means of independently measuring the effective width of channel flow, the identification of low velocity zones (and the direction of flow within these areas), three different methods for the measurement of surface flow velocity (primary flowline, cross-sectional averaged and reach scale) and a means of defining riffles and pools from the relationship between depth and surface flow velocities. These tools yield interesting results which that are applicable to many river systems and specifically to flow phenomena in riffle-pool sequences and the development and maintenance of these bedform features.

5.1 GRiFTer Development

The initial concept of a GPS River Flow Tracer (GRiFTer) developed concurrently from the growth in the use of drifter buoys for remotely sensed data acquisition (lakes, estuaries and the surf zone) and a desire to address many of the fundamental questions remaining regarding riffle-pool sequences (largely a result of inadequate or incomplete datasets).

The original conceptual design of the GRiFTer, (GPS, power source and data logger) was subjected to a series of field based development stages in order to reduce the size of the individual units to minimise signal interruption, grounding, submergence and entanglement whilst increasing structural and performance robustness.

The procedural ease of making measurements and the relative quality of GPS performance depends upon the configuration of the environment selected for measurement. GRiFTer performance is optimised where the catchment configuration exhibits a low topographic profile providing a higher number of visible satellites, there are minimal signal impacting obstacles (dense vegetation, buildings, bridges) and the channel has low banks to limit signal shadowing and multipathing.

The effect of many of these fundamental environmental factors can be mitigated by the selection of a wave-based deployment strategy. This strategy benefits from providing full lateral flow coverage concurrent with increased sensitivity to fluctuations in flow velocities by virtue of utilising a time staggered approach. This laterally distributed approach returns the most comprehensive temporal representation of the surface flow dynamics of a particularly reach and therefore maximises GRiFTer performance. Once successful wave deployment is initiated, recovery is most often achieved through the use of a telescopic landing net, or from channel spanning bridges or kayaks when extreme flow conditions limits entry into the channel. This combination of extensive field testing, structural redesign and specific deployment strategy achieves in reducing the number and effect of submergences in highly turbulent areas of channel, groundings in the extreme shallows and entanglements in vegetation or channel banks.

The application of the GRiFTer approach to natural river systems required the creation of a unique data presentation and analysis approach. As a result a cellular based representation was developed. The quality of this cellular representation is determined by two elements, the ability to precisely position individual results within the correct cell and the accuracy of each individual velocity measurement (GPS performance).

The quality of GPS performance (measurement of position and velocity) is directly related to the number of visible satellites, the DOP (dilution of precision and the configuration of each GPS receiver (WAAS). From field based investigation it was determined that unless the presence of WAAS-enabled satellites can be assured throughout the entire duration of data capture then NON-WAAS functionality must be utilised, irrespective of reduce overall performance, in order to avoid the occurrence of widespread drift events. The occurrence of large-scale unpredictable events would have a potentially greater impact on the integrity of GRiFTer performance than overall degraded GPS performance and as such must be avoided.

In addition to determining the appropriate GPS configuration, the use of post capture data filtering (based upon HDOP 1.2) provides the optimal approach to maximising the precision and accuracy of positioning relative to the quantity of data that can be preserved form the original data population. The precise values utilised to facilitate post capture filtration are temporally and spatially specific and as such must be considered prior to any GRiFTer based field investigation. Further development of the GRiFTer approach highlighted that in idealised conditions, GPS performance allowed for velocities within the 0 - 1 ms^{-1} range to be measured within a 3% error. Within environments with poor satellite conditions, specifically intended to degrade GPS performance, the error range increased to 11% however utilising post capture data filtering (as previously outlined) returned errors to within 3% of the alternatively measured velocity.

Having determined confidence intervals for GPS performance in isolation it remained to consider GRiFTer performance against a comparable measurement technique. A direct comparison of 49 propeller meter measurements were made against mean cellular GRiFTer calculated velocities (comprising in excess of 200000 individual data points). Based upon regression analysis it was determined that GRiFTer velocities can be made within 23.5% of propeller meter measured velocities. As before, post capture filtration was then conducted (based on HDOP 1.2) preserving 35 comparable measurements returning a relative error of 4% in the measurement of GRiFTer measured velocities. The combination of representative error ranges for both GPS performance and GRiFTer measurements demonstrates that it is reasonable to utilise the GRiFTer technique for surface flow investigation in natural upland gravel bed river systems.

The development of the GPS River Flow Tracer (GRiFTer) provides the first genuine attempt to return independent lagrangian flow measurements from natural in land waterways. Furthermore, GRiFTers provide surface flow measurements, an element of the velocity profile largely neglected and difficult to measure utilising conventional techniques, particularly in highly turbulent upland flows. Utilising a GPS based approach has the advantage of facilitating detailed flow investigation from an increasing range of environments and conditions. Previously inaccessible channels, either as a result of extreme flow conditions (high or low) or due to access rights prohibiting entry into the channel can be investigated by utilising alternative release and collection points. These investigations can also be facilitated more safely than with any comparable approach (without the need for major engineering operations, such as scaffolding installation) since no direct entry into the channel is required. The use of GRiFTers also allows for rapid field deployment, therefore providing a technique that can be utilised at short notice to capture highly changeable conditions. GRiFTers also offer rapid data collection, allowing for individual velocity measurements to be returned every second, thereby providing an unparalleled ratio of data points to time spent collecting data in the field. Data collected utilising the GRiFTer approach also allows for the identification and measurements of the primarily line of channel flow and determining the effective width channel width through riffle-pool sequences.

5.2 The Flow Convergence Routing Hypothesis

As previously described the most comprehensive explanation of the development and maintenance of riffle-pool sequences is offered by MacWilliams et al's (2006) flow convergence routing hypothesis. The hypothesis of flow convergence routing is based upon an upstream flow constriction producing a convergence and subsequent acceleration of flow at the pool head. This convergence generates a jet of flow into the downstream pool; with the magnitude of the jet increasing at higher discharges, resulting in the development of a defined zone of increased velocity and shear stress (MacWilliams et al., 2006).

At low discharges flow is routed through the centre of the pool increasing shear stress and developing the characteristic longitudinal bedform undulations (MacWilliams et al., 2006). At higher flows, and depending upon the channel geometry, flow and sediment composition, this zone of flow can act to route the coarsest sediment away from the deepest part of the pool maintaining the subsurface bedform composition. Flow exiting the pool diverges leading to deposition on the riffle and the maintenance of a topographic high at the pool tail (MacWilliams et al., 2006).

MacWilliams et al., (2006) quantified the flow convergence routing hypothesis through three-dimensional simulation of the flow processes operating within Dry Creek, California. The use of the suite of GRiFTer based tools and techniques provides the first opportunity to quantify the operation of the flow convergence routing hypothesis from reach scale velocity measurements.

At low flow conditions (4.39 m^3s^{-1}) the presence of concurrent large LVZs in the middle of the channel produces the required constriction and therefore resultant convergence and jetting into the pool. The path of the primary flowline and the presence of elevated surface flow velocities at the pool midpoint provide support for the operation of the flow convergence routing hypothesis. Flow exiting the pool area of the channel diverges providing a transitional zone of lower velocities highlighted within the flow convergence routing hypothesis as necessary for the development of depositional zones required to initiate the building of a riffle. Depositional zones are observed upstream of each riffle suggesting that a riffle forms as a consequence of flow exiting a pool and therefore continues to develop in a series of pool-riffle pairings.

With increasing discharge (7.29 m^3s^{-1}) the flow patterns observed within the River Swale demonstrate a modification to the outlined operation of the flow convergence routing hypothesis. As previously described LVZs occur upstream of each riffle providing the required lower velocity depositional zones and paired LVZs through the mid-channel straight producing the required flow constriction / convergence to develop flow jetting through the pool area of the channel. Additionally clear at this increased discharge is that flow is routed around the deepest part of the pool as demonstrated by the curvature of the primary flowline towards the left side of the channel.

The GRiFTer measured flow patterns differ from those expected in accord with the flow convergence routing hypothesis through the pool area of the channel. At the lower discharge (4.39 m^3s^{-1}) a single convergence caused jet entering the pool area has been replaced by two separate convergences and therefore two jets. The development of a more complex set of lateral and longitudinal flow patterns through the pool element of the channel suggests that the convergence routing hypothesis may not provide a complete explanation for the maintenance of all riffle-pool sequences at all discharge conditions.

One potential explanation of this deviation from the convergence routing framework is that lack of importance placed in the role of recirculating eddies or low velocity zones by MacWilliams et al., (2006). The flow structures produced at a discharge of 7.29 m^3s^{-1} show the impact of recirculating flow causing flow convergence then re-entering the main body of flow further downstream increasing flow velocities beyond the first flow convergence. In this way a single area of flow can act as a catalyst to influence the resultant large-scale surface flow phenomena in two ways. As a result changes in the expected flow patterns may be observed at significantly lower discharges than expected in modelled results.

The pattern of increasingly complex series of convergences and divergences at higher discharges is reversed at bankfull discharge (23.09 m^3s^{-1}) where a simplification of large-scale flow phenomena through the pool area of the channel can be observed. This can be explained by a feedback mechanism which sees the increased discharge providing greater flow momentum forcing flow through the reach decreasing the development of LVZs, the absence of these LVZ therefore fails to produce the pronounced lateral flow changes. As previously described the operation of the flow convergence routing hypothesis requires only a subtle narrowing / convergence of flow to produce the required jet into the pool area (MacWilliams et al., 2006). At bankfull discharge (23.09 m^3s^{-1}) the significantly reduced convergence is still sufficient to produce elevated flow velocities through the pool and divergence of the primary flowline around the deepest part of the pool.

The GRiFTer measured surface flow patterns at the River Swale provide evidence and implied support for the operation of the flow convergence routing hypothesis; with the exception that at high to bankfull flow conditions the hypothesis oversimplifies the development of convergences and subsequent flow jets determining the subsurface bedform composition of the pool area. Therefore, utilising the GRiFTer based findings; a theoretical model of flow behaviour in riffles and pools is presented.

5.3 Large Scale Flow Phenomena in Riffle-Pool Sequences.

The data gathered from the River Swale utilising the GRiFTer technique has enabled the investigation of the large scale surface flow phenomena operating through a riffle-pool sequence. Having determined that the flow convergence routing hypothesis provides the most comprehensive explanation for the development and maintenance of riffle-pool sequences a conceptual model is presented which combines the fundamental principles governing the flow convergence routing hypothesis with the results obtained using the GRiFTers.

5.3.1 Low Flow Conditions - Development

At low flow conditions riffles can be distinguished from pools by narrower effective channel widths, higher surface flow velocities and shallower water depths. Also, the relative differences between riffles and pools are greatest at low discharges(Figure 5.2). Flow entering a riffle increases in surface flow velocity due to the rapid shallowing of flow. The shallower water over the riffle demonstrates close to two dimensional flow processes since the depth is insufficient to allow vertical movement through the flow profile and the development of three-dimensional processes (Figure 5.5).

Flow exiting the riffle diverges as the effective channel width increases and relative flow velocities decrease due to the expanding channel area. This slower, divergent flow develops large LVZs through the pool area of the channel. These LVZs promote flow convergence, rapidly narrowing the HVC which jets flow through the deepest part of the pool. Surface flow convergence in the deeper pool area of the channel causes a downwelling of the highest velocity flows and results in over deepening of the pool (Figure 5.5). Further downstream in the pool, the momentum of the jet is no longer sufficient to scour the bed and the loss of flow momentum results in sediment deposition on the pool tail (preserving this area as a topographic high). Deposition results in reduced flow depth, and a localised divergence in flow which further reduces the propagation of flow momentum downstream from the pool. These processes combine to narrow the effective width downstream towards the second riffle and the building of an additional shallower riffle area of the channel. In this way the development of riffle-pool sequences occurs as a series of mutually-dependent feedback mechanisms performed principally at low flow conditions.

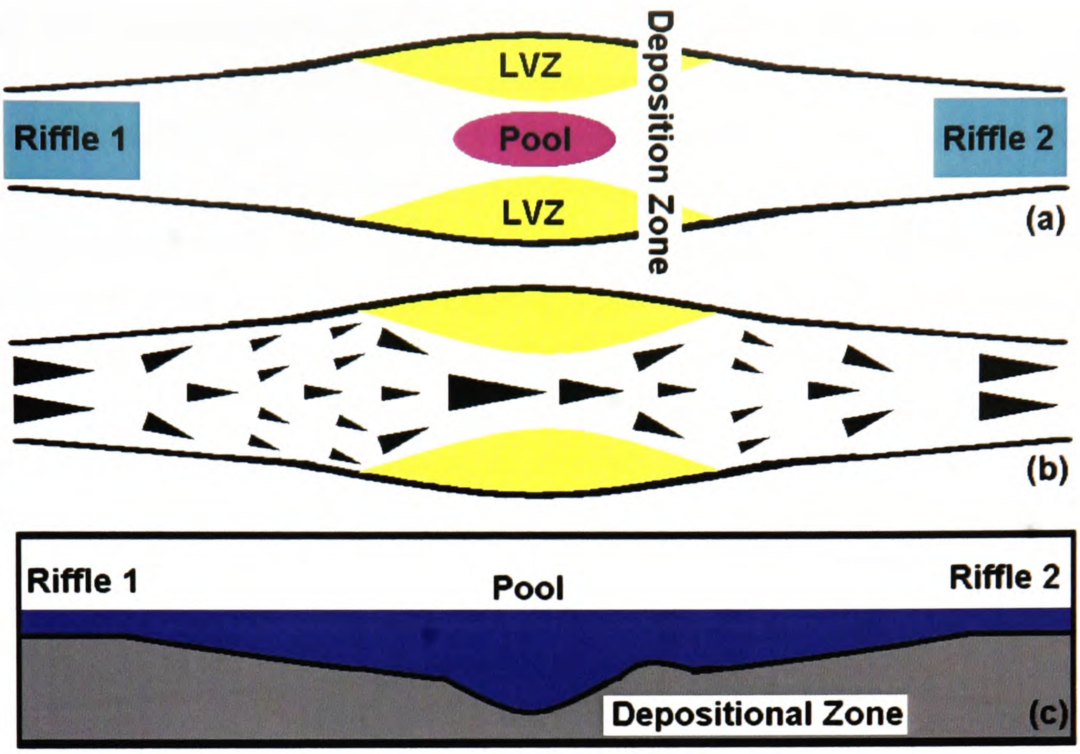

Figure 5.2 Conceptual diagram for the development of riffle-pool sequences at low flow: (a) provides an areal view of the reach highlighting the location of both riffles, the mid-channel pool, convergence producing LVZs and pool exit depositional zone. (b) aerial view to demonstrate main flow patterns through the reach, the size of arrows approximate corresponds to the magnitude of flow velocity (c) cross channel view of the reach highlight the corresponding bedform composition to the surface flow phenomena.

5.3.2 Intermediate Flow Conditions - Modification

At intermediate flow conditions, the dominant flow process act to modify the bedform morphology through the pool area of the channel. Similar to the low flow conditions, flow structure within the riffle is primarily two dimensional and at the exit of the riffle flow diverges towards the channel sides as the effective width increases. Increasing discharge produces greater flow momentum and more complex flow patterns through the pool. Multiple LVZs develop and resultant convergences necessitate a modification of the flow convergence routing hypothesis. These multiple LVZs produce additional convergences and subsequent jetting events with the potential to create numerous bedform undulations through the pool area of the channel (Figure 5.3).

At this increased discharge flow within the LVZs plays a significant role in the modification of large scale flow phenomena through the pool region of the channel. Initially responsible for creating flow convergences, the LVZs begin to demonstrate recirculating flow, reintroducing flow further downstream intensifying the jetting effect, propelling increased flow momentum further downstream and allowing the over deepening of multiple areas of the pool region. This process of converging jets producing additional scour zones continues until the morphological and hydraulic interactions prohibit the development of further convergences. At the conclusion to the final deep area within the pool region the characteristic depositional zone develops causing flow divergence and initiates the building of the second riffle.

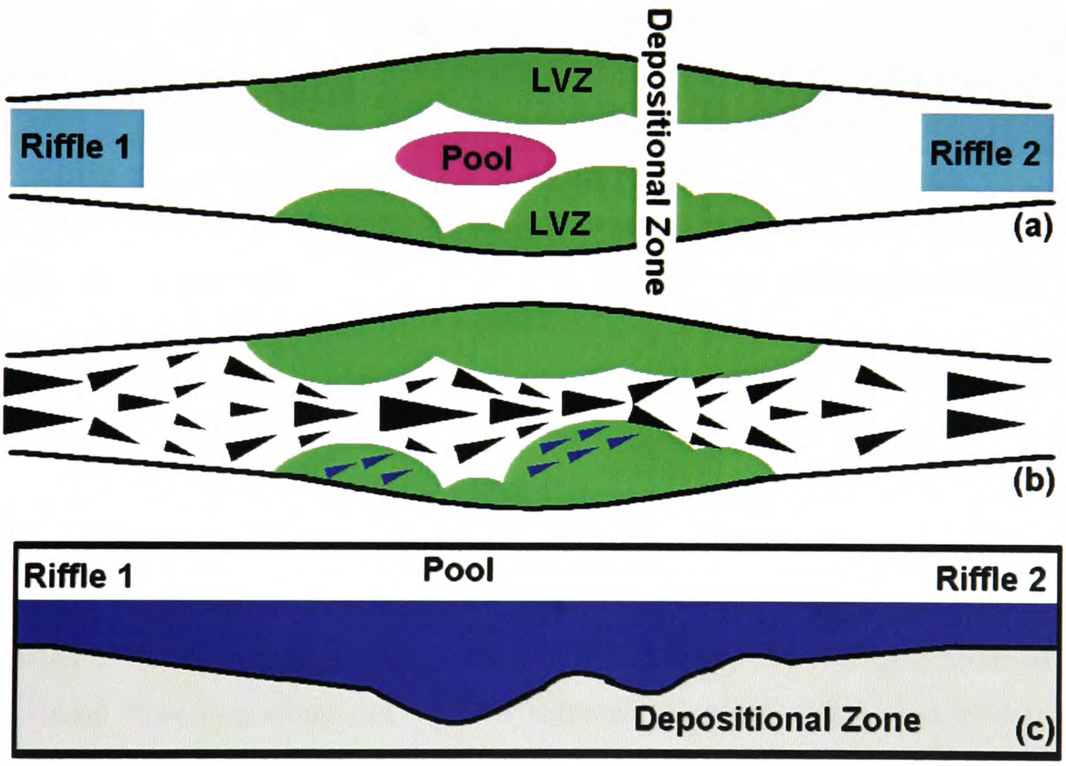

Figure 5.3 Conceptual diagram for the modification of riffle-pool sequences at intermediate flow: (a) provides an areal view of the reach highlighting the location of both riffles, the mid channel pool, convergence producing LVZs and pool exit depositional zone. (b) aerial view to demonstrate broad flow patterns throughout the reach, the size of arrows approximate corresponds to the magnitude of flow velocity (c) cross channel view of the reach highlight the corresponding bedform composition to the surface flow phenomena.

5.3.3 High Flow Conditions - Maintenance

At bankfull discharge the relative difference in morphology and flow velocities between the riffle and pool are at their minimum (Figure 5.5). This results in a simplified series of flow processes acting to maintain the bedform composition of the riffle-pool sequence. At bankfull discharge the significant increase in depth over the riffle allows for the development of three dimensional cellular flow; divergent flow through the riffle causes an upwelling of lower velocity bed flow creating the observed bimodal cross-channel velocity distribution. This type of flow structure is different to that observed at lower discharges where a simpler divergence of flow occurs due to the shallow depth which preserves the two-dimensional flow processes (Figure 5.4).

Figure 5.4 Conceptual diagrams for flow phenomena over individual element of the riffle pool sequences with flow within the riffle distinguished at low and high flows.

Flow divergences through the riffle until after the riffle exit slope when a rapid reduction in the effective width begins the process of flow convergence notably upstream of any flow constricting LVZ. The increased flow momentum at bankfull discharge forces flow through the narrowed effective width creating a much simpler structure to the pool area of the channel. At bankfull discharge significantly fewer and smaller LVZs remain in the pool region of the channel; however as a result of the increased flow momentum the LVZ is sufficient to cause a flow constriction and generate a jet of flow towards the downstream pool. As described by MacWilliams et al., (2006), at the highest discharge this jet can act to route sediment around the deepest part of the pool (Figure 5.5b) preserving the over-deepened pool area of the channel. Flow within the pool area of the channel remains consistent at all discharges demonstrating a rapid convergence producing downwelling of the highest velocity surface flow and therefore deepening of the channel at low to intermediate discharge and flow convergence routing at the highest discharges (Figure 5.5). The relationship between flow in the riffle at high and low flow and in the pool at all discharge conditions provide a potential explanation for the deviation in primary flowline and cross-section average flow velocities observed previously.

Downstream from the deepest part of the pool flow begins to diverge, as the effective width increases. Previously where a loss of momentum has resulted in the development of a depositional zone, at the higher velocity bankfull discharge the dominant factors responsible for the development of the depositional zone is the change to the sediment transport capacity produced by the rapidly widening effective width and the reintroduction of sediment routed around the deepened pool are of the channel. As observed previously this depositional zone initiates the building of the second riffle and the continued propagation of the riffle-pool sequence.

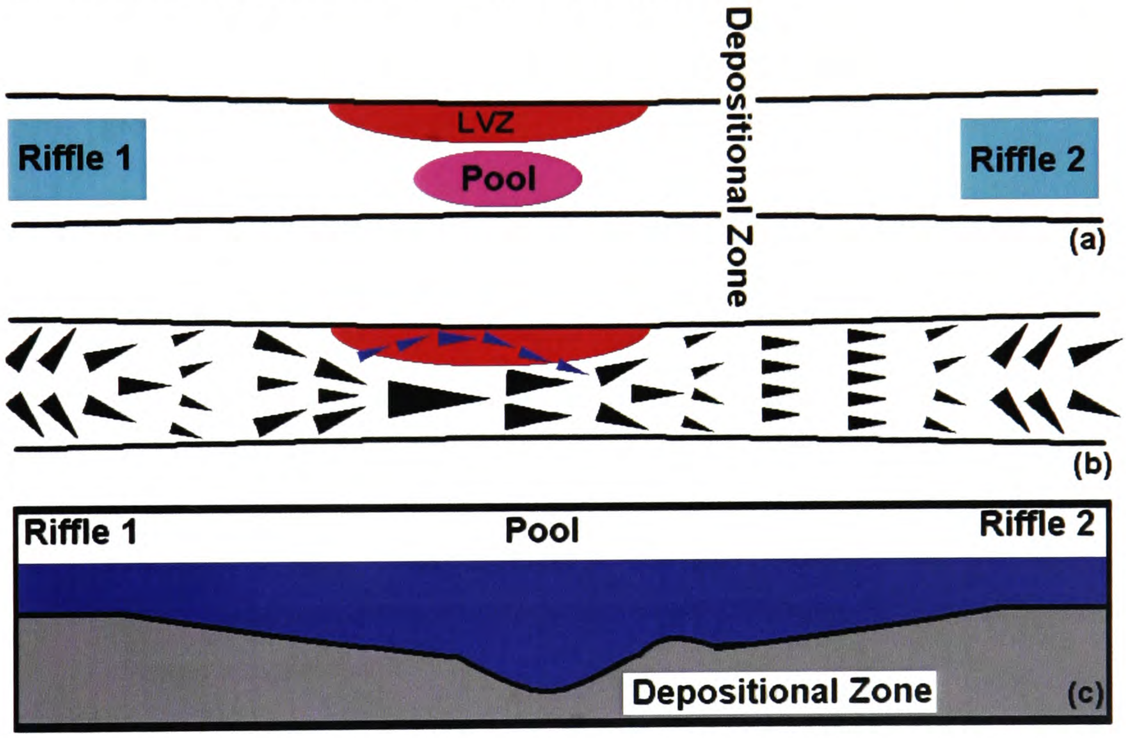

Figure 5.5 Conceptual diagram for the maintenance of riffle-pool sequences at bankfull discharge: (a) provides an areal view of the reach highlighting the location of both riffles, the mid channel pool, convergence producing LVZs and pool exit depositional zone. (b) aerial view demonstrate broad flow patterns throughout the reach, the size of arrows approximate corresponds to the magnitude of flow velocity (c) cross channel view of the reach highlight the corresponding bedform composition to the surface flow phenomena.

5.4 Overall Conclusions

This research has produced many interesting findings, the most important of which are highlighted below.

- It is possible to adapt remote data capture / drifter principles to natural river systems through access to the global positioning system.

- The use of a GRiFTer has allowed for the reinvestigation of many of the traditionally held theories governing the development and maintenance of gravel-bed riffle-pool sequences.

- Measurement of the primary flowline demonstrates convergence through the pool area of the channel at low discharge and flow routing around the deepest part of the pool at higher flow. These findings provide support for the existence and operation of the flow convergence routing hypothesis.

- At low discharges the effective width of the riffle is narrower than that of the pool however with increasing discharge the rate of narrowing is greater through the pool area resulting in a convergence or effective reversal in the structure of effective channel width.

- The primary flowline velocity pattern exhibits three distinct zones through all discharge conditions. At low and intermediate discharges two riffle peaks are separated by a pool trough. However, at the highest discharge an addition peak forms in the pool area of the channel. This highlights an effective reversal or convergence in the magnitude of riffle and pool velocities at the highest discharges and provides implied support for the existence of the velocity reversal hypothesis.

- The cross-section velocity patterns at all discharges demonstrates the formation of two riffle peaks and a single pool trough. This highlights that the observation of a reversal in velocity along the primary flowline is likely a result of measurement location and procedure as opposed to a fundamental change in flow phenomena.

- With increasing discharge there is an increase in the inter-riffle spacing when expressed as a ratio of effective channel width. These values lie within the upper end of the 5 - 7 channel widths frequently cited in the literature.

5.5 Future Work and Technological Advancements

Within additional time and resources there remains immense potential for additional GRiFTer based research. This research can be broadly classified as technological extensions, work extending existing research into riffle-pool sequences and new research projects.

A range of technological advancements are possible for the GRiFTer technique which would extend its potential usage and ability to acquire valuable flow measurements. The incorporation of additional sensors such as a thermometer or chemical sensor would extend potential applications to the measurement of surface pollutants. Additional minor adjustments would include the use of a wider range of NEMA based satellite signals allowing for additional variables to be measured such as water surface slopes (elevation) and further performance indicators to be utilised to provide a more robust data filtering procedure. Additionally increased data storage capacity and power supply would allow for a larger range of environments to be investigated.

As GPS technology develops the accuracy and precision of individual measurements will undoubtedly improve and therefore so will GRiFTer performance. Similarly, the size and cost on individual component and therefore integrated GPS data loggers will also be decreased, resulting in smaller and likely cheaper GRiFTers that can be applied to an even larger range of environments and flow conditions.

Some possible larger scale adaptations would see the incorporation of telemetry functions within individual GRiFTers. A GSM (mobile phone) outstation could be adapted and incorporated into a slightly larger GRiFTer to provide transmission of data direct from the field including a reference point for unit recovery. This would significant raise the cost of a single GRiFTer but would drastically increase unit redundancy, therefore further research would be required to determine a cost-benefit efficiency. A similar scale technological advancement would see the integration of echo-sounder into a larger GRiFTer unit thereby providing longitudinal depth patterns from which vertical velocity profiles can be calculated utilising the relationship between velocity and flow depth.

In terms of extending research conducted into riffle-pool sequences, additional time and resources would see the investigation of a variety of additional field sites and riffle-pool sequences. Primarily, a significantly longer series of riffles and pools (both straight and curved) would further develop the findings detailed within this research particularly if measurement could be performed at the full range of discharge conditions.

One of the greatest advantaged of the GRiFTer approach is the flexibility which it offers for surface flow measurements in terms of environments, flow conditions and therefore research applications. Two of the most exciting potential research projects would be the measurement of over land flow during flood events (with a suitable field site already selected) and for the validation of two and three dimensional flow models (with initial comparisons already conducted based on the flow measurements made during this research)

Appendices

Earth Surface Processes and Landforms
Earth Surf. Process. Landforms (2007)
Published online in Wiley InterScience
(www.interscience.wiley.com) **DOI:** 10.1002/esp.1614

Measuring river velocities using GPS River Flow Tracers (GRiFTers)

R. J. Stockdale,* S. J. McLelland, R. Middleton and T. J. Coulthard
Department of Geography, University of Hull, Hull, UK

Correspondence to: R. J. Stockdale, Department of Geography, University of Hull, Cottingham Road, Hull HU6 7RX, UK. E-mail: r.j.stockdale@geo.hull.ac.uk

Received 17 April 2007; Revised 20 August 2007; Accepted 24 August 2007

Abstract

Existing methods of measuring flow velocities in natural rivers are largely based on series of point measurements. Acquisition of these data can be time consuming and difficult, especially in high flow conditions. This paper introduces the use of GPS drifters (termed GRiFTers) to measure surface flow velocities in a 400 m reach of the River Swale, UK. Over 10 000 measurements were made in a 3 hour period and aggregated over a 2 m grid to generate a genuine distributed representation of flow across the reach. The technique shows great promise to provide new insights into flow patterns over long reaches of rivers, over a range of flow conditions, and may also provide valuable data for numerical model validation. Copyright © 2007 John Wiley & Sons, Ltd.

Keywords: GPS; river velocity; velocity measurement; flow patterns

Introduction and Rationale

Traditional studies of flow dynamics in natural river systems have long been reliant upon point velocity measurements, traditionally obtained using mechanical impellor meters, which produce time-averaged velocities (Carling, 1991; Thompson *et al.*, 1999). More recently, electromagnetic current meters (ECMs) and acoustic Doppler velocimeters (ADVs) have enabled higher resolution measurements of flow velocity and its turbulent fluctuations (see, e.g., Clifford, 1993; Lane *et al.*, 1998; MacVicar *et al.*, 2007).

Despite the relative merits of each approach, all of the above methods are limited as they require the selection of an appropriate point for data acquisition. Furthermore, the use of individual point measurements produces data that are Eulerian by nature and are to some extent detached from the dynamic nature of channel flow (Creutin *et al.*, 2003). Therefore, our understanding of the flow patterns between these point measurements is inferred as opposed to observed or measured (Heritage and Milan, 2004, considering Keller and Florsheim, 1993). All the previously mentioned methods also suffer from being labour intensive, invasive and time consuming, particularly when large spatial coverage is required. For example, significant time is required to position and point measurement devices accurately, and the instruments must remain stationary for a sufficient period to enable representative measurements to be obtained. Some instrumentation is difficult to move, due to power and computer equipment, which can reduce their transportability in less accessible areas, such as upland gravel-bed river systems. All these time factors constrain the number of data points that can be acquired, which can reduce the spatial and temporal resolution of the data as well as the area covered (Creutin *et al.*, 2003).

Additionally, data acquisition using the methods described above is limited both in its ability to return data from the full range of flow conditions (as there are many areas of natural river channels that are inaccessible, particularly at higher discharges) and the time and cost requirements of providing sufficient reach coverage. Many of these issues are solved by the use of particle image/tracking velocimetry (PIV/PTV) techniques, which calculate water surface velocities based on particle movements sensed using cameras (Creutin *et al.*, 2003). However, PIV can also be time consuming to set up and be limited by the field of view of the camera and the need to orthorectify images, and there can be difficulties with sufficient seeding of the flow with tracer particles. These limitations provide a good incentive to revisit the measurement of flow dynamics in natural river systems.

The fields of climatology and oceanography solve many of these difficulties by utilizing remote sensor monitoring techniques, in the form of drifter buoys. Drifter buoys are free-moving floating platforms that are carried by ocean currents charting their position whilst collecting and transmitting data from a variety of inbuilt environmental sensors, and use global position systems (GPS) to determine positions and velocities (Clearwater, 2007). The smallest commercially available GPS equipped drifters measure approximately 40 cm in depth (Metocean – WOCE/OCM and the Clearwater – Argos/GPS marker) making the deployment of these buoys in many inland river systems impracticable. More recently, smaller GPS devices have been deployed in near shore environments to measure velocities of rip currents (Johnson and Pattiaratchi, 2004) and velocity and salinity distributions of plumes at river mouths (Naudin *et al.*, 1997). These devices have demonstrated the potential for using GPS in shallow water environments.

Through the reduced dimensions of GPS devices, the potential now exists for the adaptations of drifter buoy techniques for use in natural river systems. A compact integrated GPS device and data logger, housed within a neutrally buoyant watertight exterior casing, provides a method to deploy GPS devices to study surface flow velocities in natural river systems. This could allow easy deployment from channel banks or bridges facilitating the tracing of flow paths at the full range of flow conditions, thereby solving the problems of restricted access to certain channels, particularly at higher discharge events. The simultaneous deployment of multiple units could also enable a greater spatial distribution of data across and along the channel.

This paper introduces the concept of the GPS River Flow Tracer (GRiFTer) as a new technique to facilitate the investigation of surface flow patterns in natural river systems while outlining its potential use, application and the accuracy with which the collected results can be presented.

Method: Design and Construction of the GRiFTers

The GRiFTer uses a Royaltek™ BlueGPS (RBT3000), which has a built in 12 channel WAAS/EGNOS enabled GPS receiver and (Figure 1(a)) an integral data logger that records up to 30 000 date, time, easting, northing, velocity, course, PDOP (position dilution of precision) and HDOP (horizontal dilution of precision) measurements at up to 1 Hz. It is powered by an internal rechargeable battery, which gives up to 8 hours continuous use. Two designs of GRiFTer have been tested, which are neutrally buoyant with minimal surface area above the water to minimize wind effects. The first design was a hardened plastic, cylindrical exterior casing measuring 0·1 m in depth and 0·3 m in diameter with the device fixed inside the cylinder (Figure 1(b)). The cylinder was weighted using water so that it was neutrally buoyant. The size of the unit was minimized to improve clearance in the shallowest parts of the channel to avoid grounding, whilst the cylindrical shape was intended to reduce the risk of the unit becoming trapped. A second design was tested with the unit placed in a small waterproof bag with sufficient air trapped to maintain neutral buoyancy (Figure 1(c)). Dependent upon the selection of GRiFTer design, complete units can be constructed from commercially available components and range in cost between £100 and 120. Tests conducted with both designs showed that the larger cylindrical unit was more susceptible to grounding and was no less likely to become trapped than the device simply placed in the waterproof bag. In addition, GPS signal reception was better in the waterproof bag, since a signal was received regardless of the device orientation.

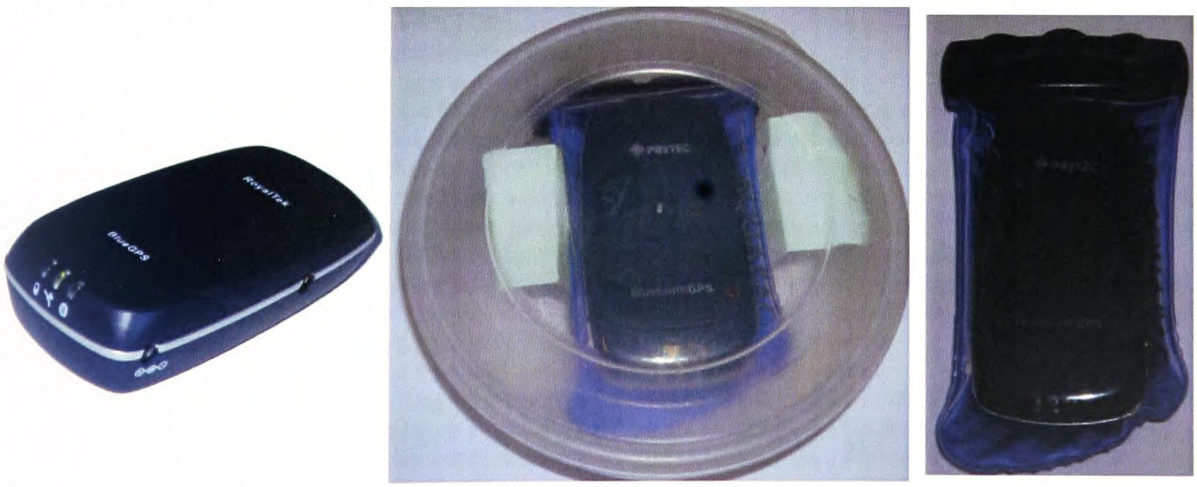

Figure 1. (a) Royaltek™ BlueGPS device; (b) unit design 1; (c) unit design 2. This figure is available in colour online at www.interscience.wiley.com/journal/espl

DOI: 10.1002/esp

Data Processing and error management

Water surface velocity is calculated for two perpendicular horizontal components at time t (u_{Nt} and u_{Et}), which are then used to calculate the resultant velocity (v_t):

$$u_{Nt} = \frac{N_{t+\frac{\Delta t}{2}} - N_{t-\frac{\Delta t}{2}}}{\Delta t} \tag{1}$$

$$u_{Et} = \frac{E_{t+\frac{\Delta t}{2}} \; E_{t-\frac{\Delta t}{2}}}{\Delta t} \tag{2}$$

$$v_t = \sqrt{u_{Et}^2 + u_{Et}^2} \tag{3}$$

where N_t and E_t are the GPS positions in the northerly and easterly directions respectively at a given time t and Δt is the time difference between position measurements.

The GPS signal can be prone to inherent and in some cases uncontrollable errors. The position of the GPS relative to its surrounding environment determines the number of visible satellites from which positions are calculated, whilst the clarity of the path between the receiver and satellites determines the integrity of these calculated positions. Large obstacles, varied terrain and dense vegetation can block and/or deviate satellite signals (multipathing) on their passage to the receiver significantly biasing the calculated positions (Leick, 2004). The magnitudes of these errors are determined by the type of receiver and the specific environment within which the unit is utilized. Signal propagation errors occur when the satellite signals are refracted as they pass through the earth's atmosphere. Although the satellite and receiver units both make modelled adjustments to compensate, inaccuracies often occur, particularly in adverse weather conditions such as heavy rain (GARMIN, 2000). Although the GPS provides an indicator value as to the integrity of the emitted satellite signal in the form of DOP values (dilution of precision), our tests showed there was no direct relationship between increasing DOP values and errors in positioning or timing, therefore an alternative approach was sought to account for the occurrence of error in velocity calculations.

To reduce these errors further, a cellular based approach was developed for calculating the surface velocity field. By dividing the measured section of the river into grid cells, we can total and average velocity measurements from multiple readings for each grid cell. From these averages, we can then determine the quality of the data (standard error and standard deviation) for both velocity and direction. These data may also be used to reveal information about the nature of the flow through identification of convergence in deviation throughout a cell at specific flow conditions (e.g. in turbulent conditions).

Three key factors control the velocity measurement error. The first is the number of GRiFTer measurements within a particular cell. The velocity determines the number of measurements from a single GRiFTer within a given cell and this is multiplied by the number of GRiFTer units that pass through the measurement cell. The latter can be increased by releasing a more GRiFTers and deploying them in successive waves.

Second is the grid cell size, as large cells will capture more data readings, but also reduce the spatial resolution of the data. Hence, the cell size, the local flow velocity, the number of GRiFTers and the number of successive deployments determines the density of data points returned, which can be in turn used to calculate the appropriate dimensions of the grid cells used. For example, in this study a cell size of 2 m was selected, since the channel width was ~20 m and the average velocity was ~0·5 m s^{-1}; therefore, assuming the GRiFTer units were uniformly distributed, three waves of 20 units will yield an average of 24 measurements per cell. This reduces the standard error of the mean velocity measurement in a cell by a factor of approximately five compared to a single measurement.

Third, the time lag used between velocity calculations has an important effect upon the error. To resolve this, static base stations (identical to the units deployed in the river) were deployed adjacent to the river channel to assess the quality of GPS data collected. An appropriate value for Δt was selected by considering the standard deviation of the resultant velocity calculated for the stationary base station (σv_t), which is a measure of the quality of the GPS position information. Figure 2 details how larger values of Δt reduce the relative effect of the GPS error on velocity calculations (and decrease σv_t). However larger values of Δt reduce the ability to resolve small-scale variations in velocity, so the choice of Δt is a compromise between reducing error and retaining detail. For this study (and other deployments), it has been found that $\Delta t = 10$ s is best with a mean velocity error of 0·087 m s^{-1} and an sd of ±0·047 m s^{-1}. Here, σv_t is reduced by at least 50% compared with the raw data output at 1 s intervals. It is important to note that the velocity errors from these base stations change at different times of day according to the position and number of satellites.

DOI: 10.1002/esp

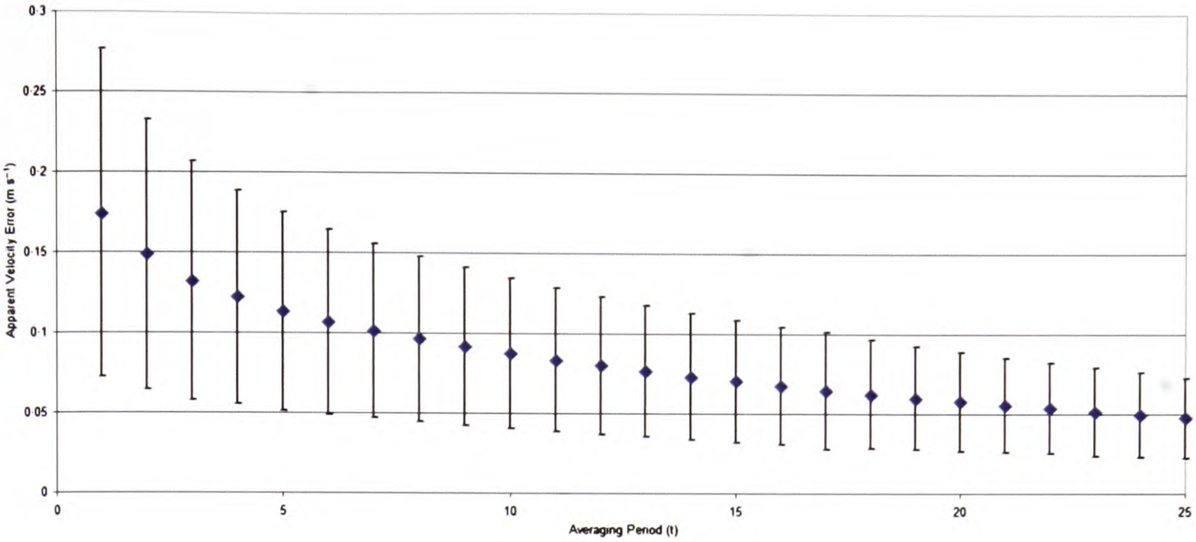

Figure 2. Mean error and standard deviation for stationary base-station velocity calculations using different time steps. This figure is available in colour online at www.interscience.wiley.com/journal/espl

Therefore, these figures are only indicative of the time when the data were acquired, and base-station data should be taken at each GRiFTer application.

Results

An initial surface-flow investigation was conducted of a 400 m section of the River Swale at Low Roe. Twenty units were released in three waves (flowing from left to right in Figure 3), providing in excess of 10 000 paired GPS position measurements from 3 hours of testing (including unit releases and recovery). A time lag of 10 s was used to calculate velocities and data were averaged using a 2 m × 2 m grid. Figure 3 shows the resultant velocity field. The average velocity through the reach was 0·48 m s^{-1} with a minimum measured velocity in pools of 0·1 m s^{-1} and a maximum measured velocity over riffles of 1·72 m s^{-1}. Figure 4(a) shows the number of measurements in each cell. The lowest numbers of measurements are obtained in the fastest moving areas, whilst slower moving regions generally have considerably more measurements. However, the distribution of data points is significantly affected by the paths followed by individual GRiFTer units. Figure 4(b), (c) shows the calculated standard error of the velocity components (U_{nt} and U_{et}) in each cell with an average error of 0·12 (northings) and 0·13 (eastings).

Discussion

Figure 3 illustrates how measured surface velocities and vectors change along the 400 m reach measured. There are clear patterns of low and high velocities that correspond to pools and riffles in the reach. The inset in Figure 3 provides more detail of this reach, showing the high resolution of the data. These results clearly show how this technique can provide a spatially distributed continuous measurement of surface flow velocities that range from close to 0 in pool sections to 1·72 across the riffles. The vectors shown in the inset of Figure 3 clearly show areas of convergent flow at the top of the riffle, and divergent flow at its downstream end. Within this section there are other features of note, with a double downstream peak in velocity, and a definite thalweg with increased velocities in the centre of the channel immediately downstream from the riffle. Furthermore, aside from the main three riffles at the top, middle and lower parts of the reach, in between there are smaller increases in velocity not associated with the main riffle features.

For validation, a direct comparison was made between GRiFTer calculated velocities (across a 2 m × 2 m grid) and velocities measured using a Braystoke impellor meter. Twelve randomly positioned points were selected across through the Swale reach and then plotted against the GRiFTer calculated velocities (Figure 5). Each individual data point

DOI: 10.1002/esp

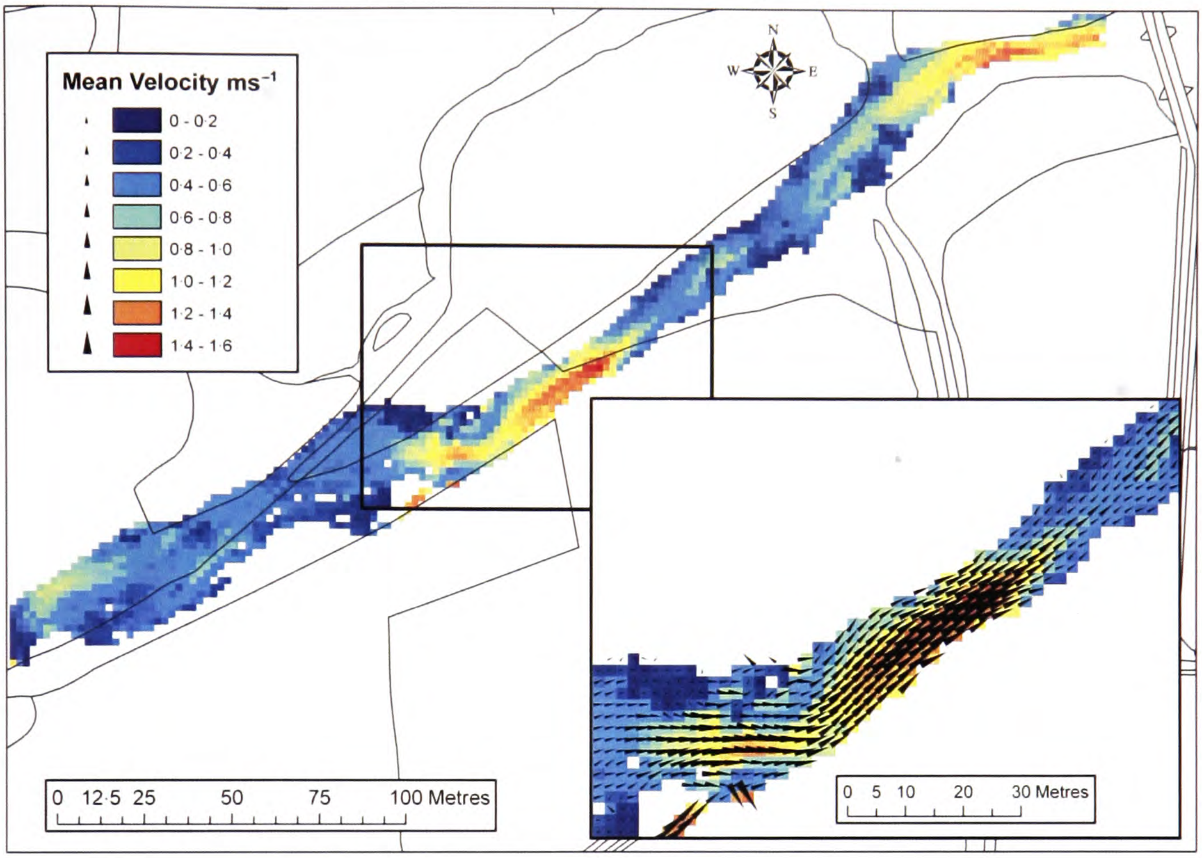

Figure 3. Velocities measured over the study reach of the River Swale, UK. The results are averaged over a 2 m grid; the inset shows detail and vectors from one riffle section. This figure is available in colour online at www.interscience.wiley.com/journal/espl

features error bars representing standard deviation in both the Braystoke measured velocity (y) and the calculated GRiFTer velocity error (x). Apparent from Figure 5 is a strong correlation between the two velocity measurement methods. Interestingly, for the higher velocities the standard deviations for the Braystoke and GRiFTer methods are very similar.

This paper represents the first step in the development of this technique and there are methodological and practical issues that need resolving.

1. They only measure the surface velocity, which is not completely representative of all velocities at all depths. Furthermore, in windy conditions it is possible for GRiFTers to be blown off course, especially in slower moving parts of the channel.
2. The accuracy (velocity and direction) needs to be further assessed in relation to independent measurements. This is difficult since the inherent limitations of point measurement devices described earlier make it problematic to collect comparable datasets, especially for direction. However, one possibility may be comparison with surface-based PIV measurements.
3. There are errors associated with the grounding of GRiFTers on obstructions in the river, though these can be readily filtered in post-processing by removing data points where there has been no movement for a given period (e.g. 300 s).
4. It is important and sometimes difficult to ensure sufficient coverage, as once released there is no control as to where the GRiFTers travel. Subsequently, some areas may receive few or no measurements, though this can be redressed by select releases in these particular areas. Similarly, areas of fast flow also have low coverage and may require repeat releases to ensure enough measurements.

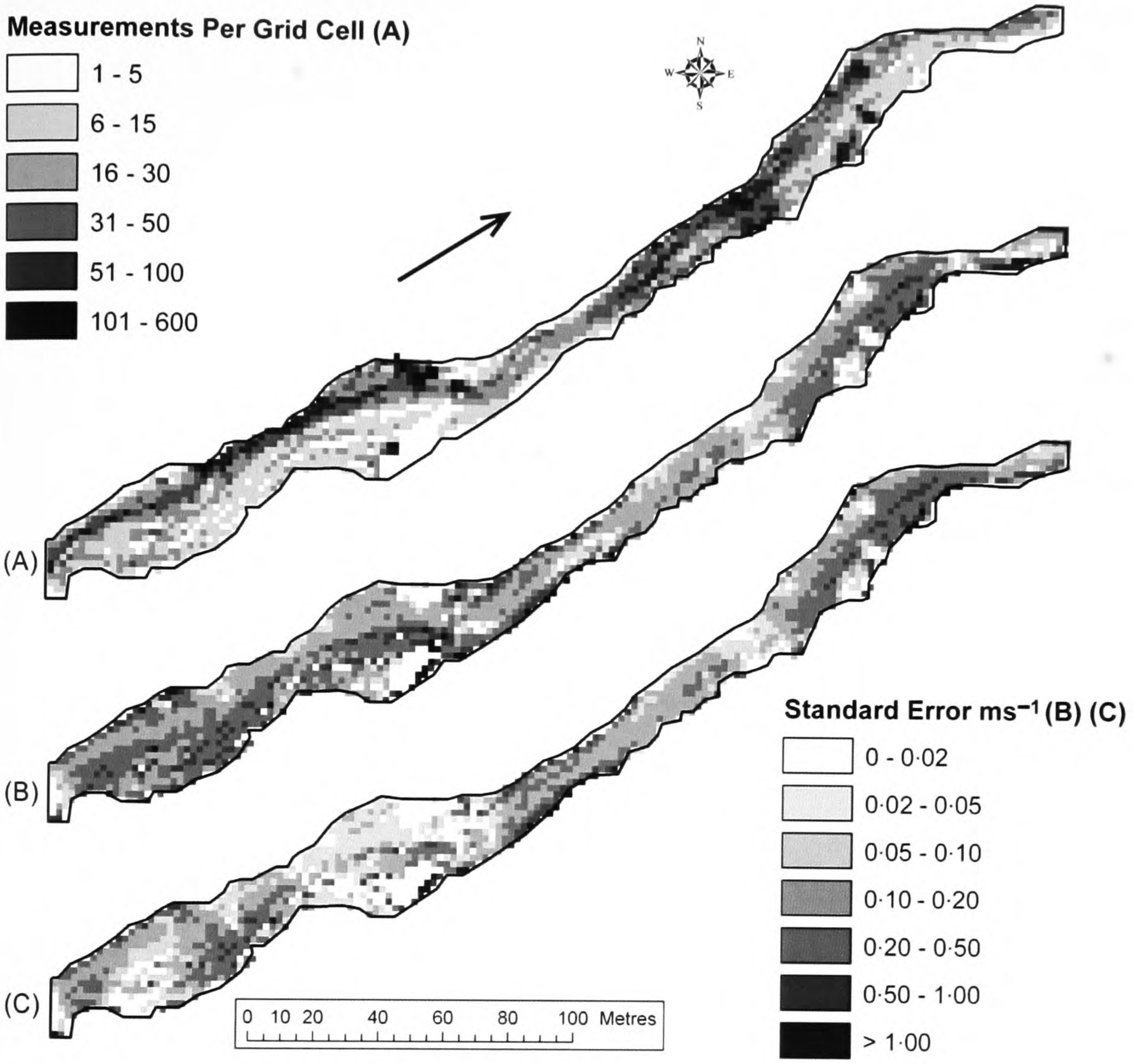

Figure 4. Measurements per grid cell (a) and standard errors in the northing (b) and westing directions (c).

5. There are high standard errors, with the mean error being c. 30% of the mean velocity. Figure 3 show that the areas of high standard error correspond to areas where there are fewer readings; therefore, the error can be significantly reduced by making more measurements. However, it must be remembered that the standard error will also include natural variability in flow patterns within a cell. Within the 2 m cells used here, there will be considerable variation within both mean velocities and in particular directions. These errors are less in faster moving parts of the channel, with more strongly defined flow paths, and these can be seen in Figure 3, where some areas with high velocity have a low standard error despite having relatively few measurements. Due to the nature of turbulence, in particular the capability for flow structures (such as eddies) to migrate short distances, some cells will always return a high error.

However, there are many advantages with this technique. It can be applied easily anywhere in the world where there is sufficient GPS coverage, and can rapidly provide detailed and numerous measurements of flow velocity. Importantly, it provides us with a method for assessing flow patterns and velocities under flood conditions where previous methods have not been suitable. This could allow data to be collected for high velocity, frequently inaccessible areas

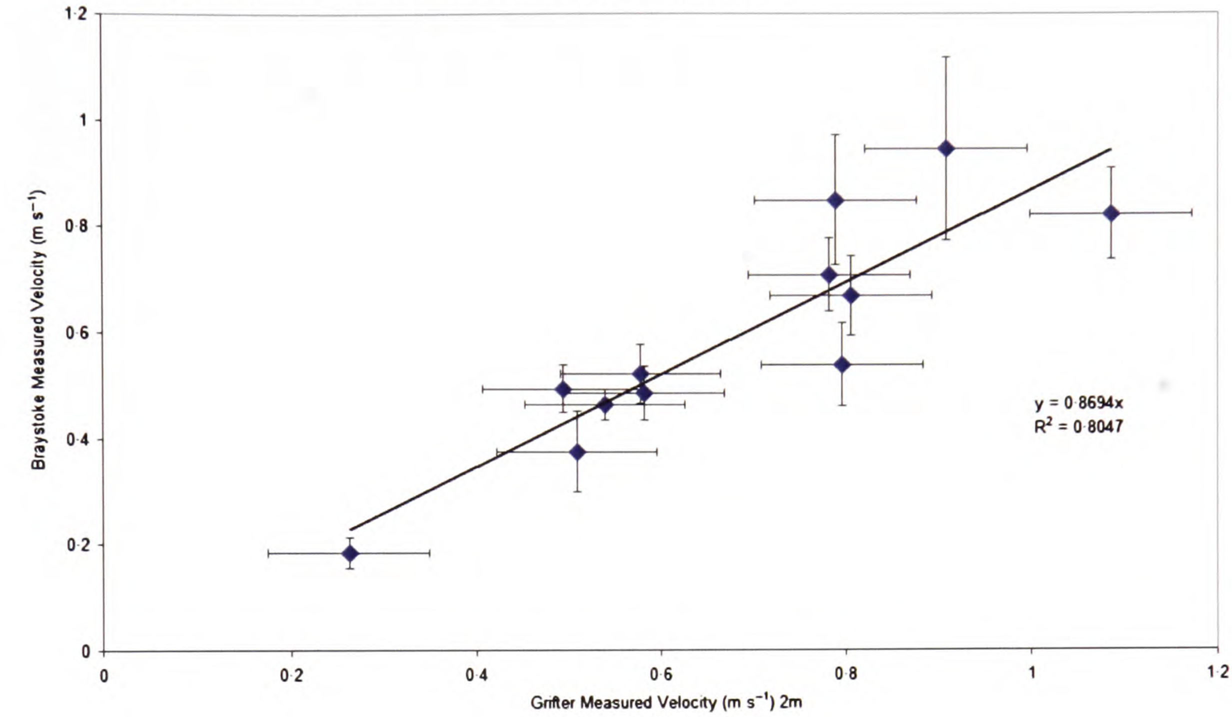

Figure 5. Comparison between GRiFTer and Braystoke measured flow velocities. Error bars indicate the standard deviations for both GRiFTer and Braystoke measurements. This figure is available in colour online at www.interscience.wiley.com/journal/espl

of the channel such as the thalweg, as well as for flow patterns across floodplains, where the flow is distributed across a wide area, disadvantaging point measurements. Furthermore, the Lagrangian nature of the measurements means that, for example, during flood flows the paths of flow through channels and across submerged banks onto floodplains can be tracked and measured. By generating velocity and direction information, the spatially distributed data generated by the GRiFTers would be especially useful for validating 2D numerical flow models. There are many other potential scientific applications and the continuous and spatially distributed nature of the results allows us to observe facets of river flow that are rarely observed. For example, Figure 2 indicates that velocities can change very rapidly over a short distance, and that some parts of rivers move very slowly indeed, with some GRiFTers only moving 10 m in 5 minutes. Furthermore, the method will allow us to measure changes in velocity over long distances of river at a high spatial resolution, providing detailed data on, for example, pool riffle velocity perturbations.

Conclusions

This paper introduces GPS river flow tracers (GRiFTers) that allow the rapid collection of spatially distributed, highly detailed surface velocity data. The technique is easily used with a rapid deployment and can be used in all flow conditions. Initial results provide interesting insights into spatial variations in flow and longitudinal flow structures e.g. riffle–pool sequences. There is excellent scope for using this data to validate numerical flow models (especially under high flow conditions) and combing the GPS recorder with other sensors to simultaneously record (for example) depth, turbidity and acceleration.

Acknowledgements

RJS is funded by an EPSRC studentship. We would like to thank the University of Hull for logistical support and Brendan Murphy for his work in the field. We would also like to thank James Brasington and an anonymous referee for their useful comments.

DOI: 10.1002/esp

References

Carling PA. 1991. An appraisal of the velocity-reversal hypothesis for stable pool–riffle sequences in the River Severn, England. *Earth Surface Processes and Landforms* **16**: 19–31.

Clearwater. 2007. http://www.clearwater-inst.com [1 December 2006].

Clifford NJ. 1993. Differential bed sedimentology and the maintenance of riffle–pool sequences. *Catena* **20**: 456–468.

Creutin JD, Muste M., Bradley AA, Kim SC, Kruger A. 2003. River gauging using PIV techniques: a proof of concept experiment on the Iowa River. *Journal of Hydrology* **277**(13): 182–194.

GARMIN. 2000. www.garmin.com [21 September 2005].

Heritage GL, Milan DJ. 2004. A conceptual model of the role of excess energy in the maintenance of a riffle-pool sequences. *Catena* **58**: 235–257.

Johnson D, Pattiaratchi C. 2004. Application, modelling and validation of surfzone drifters. *Coastal Engineering* **51**: 455–471.

Keller EA, Florsheim JL. 1993. Velocity reversal hypothesis: a model approach. *Earth Surface Processes and Landforms* **18**: 733–740.

Lane SN, Biron PM, Bradbrook KF, Butler JB, Chandler JH, Crowell MD, McLelland SJ, Richards KS, Roy AG. 1998. Three-dimensional measurement of river channel flow processes using acoustic Doppler velocimetry. *Earth Surface Processes and Landforms* **23**(13): 1247–1267.

Leick A. 2004. *GPS Satellite Surveying*. Wiley: New York.

MacVicar BJ, Beaulieu E, Champagne V, Roy AG. 2007. Measuring water velocity in highly turbulent flows: field tests of an electromagnetic current meter (ECM) and an acoustic Doppler velocimeter (ADV). *Earth Surface Processes and Landforms* **32**: 1412–1432.

Naudin JJ, Cauwet G, Chretiennot-Dinet M-J, Deniaux B, Devenon J-L, Pauc H. 1997. River discharge and wind influence upon particulate transfer at the land–ocean interaction: case study of the Rhone River plume. *Estuarine, Coastal and Shelf Science* **45**: 303–316.

Thompson DM, Wohl EE, Jarrett RD. 1999. Velocity reversals and sediment sorting in pools and riffles controlled by channel constrictions. *Geomorphology* **27**: 229–241.

References

- Admiraal, D., Demissie, M., 1996. Velocity and discharge measurements at selected locations on the Mississippi River during the great flood of 1993 using an acoustic Doppler current profiler. Water Int. **21** (3) 1441-51.

- Adrian, R.J., (1991) Particle-imaging techniques for experimental fluid mechanisms. Annu. Rev. Fluid Mech. **23:** 261-304.

- Adrados, C., Girard, I., Gendner, J., and Janeau, G., 2002. Global positioning system (GPS) location accuracy improvement due to selective availability removal. Comptes Rendus Biologies **325**:165–170.

- Andrews, E.D. (1982) Bank stability and channel width adjustment. East Fork River, Wyoming. Water Resource Research **18**(4): 1184-1192.

- Andrews, E.D. (1983) "Entrainment of gravel from naturally sorted riverbed material", Geol. Soc. Am. Bull., **94**, 1225-1231.

- ARGOS Basic Description of the ARGOS System. Available online from http://www.oosa.unvienna.org/unisp-3/docs/backgroundpapers/bp4.pdf accessed 8/11/05 16.06.

- Ashmore, P.E. (1982). Laboratory modelling of gravel, braided stream morphology, Earth Surface Processes and Landforms, 7, 201-225.

- Ashmore, P.E. (1988). Bed load transport in braided gravel-bed stream models, Earth Surf. Proc. Landforms, **13**, 677-695.

- Ashworth, P.J., Ferguson, R.I., and M.D. Powell. (1992) "Bedload transport and sorting in braided channels". Dynamics of Gravel-bed Rivers. Edited by P.Billi, R.D. Hey, C.R. Thorne & P. Tacconi. (1992) John Wiley & Sons Ltd.

- Ashworth, P.J. 1989. Size selective entrainment of bed load in gravel bed streams. Water Resources Research, 25, 627-634.

- Barros, M.S.S., Rosa, L.C.L., Walter, F., Alves, L.H.P.M. (1999). Global positioning system: a methodology for modelling the pseudorange measurements. Adv. Space. Res. **23:** 8 1529^{-1}532.

- Barth, J.A. 2003. Anomalous Southward Advection During 2002 in the Northern California Current: Evidence from Lagrangian Surface Drifters.

- Beardsley, R.C., Limeburner, R., Owens, W.B. (2004) Drifter measurements of surface currents near Marguerite Bay on the western Antarctic Peninsula shelf during austral summer and fall, 2001 and 2002. Deep-Sea Research II **51:** 1947^{-1}964.

- Beechie, T.J., Liermann, M., Pollock, M.M., Baker, S. & Davies, J. (in press). "The dynamics of channel patterns and floodplains in forested mountain river systems".

- Best, J.L. and Kostaschuk, R. 2002. An experimental study of turbulent flow over a low-angle dune. Journal of Geophysical Research Oceans **107**, 3135-54.

- Buffin-Belanger, T., Roy, A.G., (2005). 1 min in the life of a river: selecting the optimal record length for the measurement of turbulence in fluvial boundary layers. Geomorphology **68:** 77-94.

- Bhowmik, N.G. and Demissie, M. (1982). Bed Material Sorting In Pools and Riffles. Journal of Hydraulics Divisions, Proceedings of the American Society of Civil Engineers. **1078**: 1227-1231.

- Bjerklie, D.M., (2005). Estimating discharge in rivers using remotely sensed hydraulic information. Journal of Hydrology **309:** 191-209.

- Bjerklie, D.M., (2007). Estimating the bankfull velocity and discharge for rivers using remotely sensed river morphology information. Journal of Hydrology **341:** 144^{-1}55.

- Bogard, S.J., Tomson, R.E., Rabinovich, A.B., LeBlond, P.H. 1999. Near-Surface Circulation of the Northeast Pacific Ocean derived from WOCE-SVP satellite-tracked drifters.

- Booker, D.J., Sear, D.A., Payne, A.J., 2001. Modelling three-dimensional flow structures and patterns of boundary shear stress in a natural pool-riffle sequence. Earth Surface Processes and Landforms **26:** 553-576.

- Bridge, J.S. (1993). The interaction between channel geometry, water flow, sediment transport and deposition in braided rivers. Best, J.L. & Bristow, C.S. (eds), 1993, Braided rivers, Geological Society Special Publication No. 75, pp. 13-71.

- Brightwaters Products (2000) Available online from www.brightwaters.com/products/GPSDrifters.html. Accessed 31/10/05

- Bristow, C.S. 1987a. Brahmaoutra River: Channel migration and deposition. In: Ethridge, F.G., Flores, R.M., & Harvey, M.D. (eds) Recent Developments in Fluvial Sedimentology. Society of Economic Palaeontologists and Mineralogists Special Publications, **39**, 63-74

- Bristow, C.S. & Best, J.L. (1993). "Braided rivers: perspectives and problems". From Best, J.L. & Bristow, C.S. (eds), Braided Rivers, Geological Society Special Publication No. 75, pp. 1-11.

- Buffington, J.M., Lisle, T.E., Woodsmith, R.D., Hilton, S., 2002. Controls on the size and occurrence of pools in coarse-grained forest rivers. River Research and Applications 18, 507-531.

- Bushnell, M. (1998) NOAA/AOML-Global Drifter Centre. Preliminary results from Global Lagrangian Drifters using GPS receivers. Available online from www.arsc.edu/challenges/oceans3.html accessed 21/10/05. 15:00.

- Cao, Z., Carling, P. and Oakey, R., 2003. Flow reversal over a natural pool-riffle sequence: a computational study. Earth Surf Processes Landform **28**: 689-705.

- Carling, P.A., (1988). The concept of dominant discharge applied to two gravel-bed streams in relation to channel stability thresholds. Earth Surf Processes Landforms **13**: 355-367.

- Carling, P.A., (1991). An appraisal of the velocity-reversal hypothesis for stable pool-riffle sequences in the River Severn, England'. Earth Surf Processes Landforms. **16**: 19-31.

- Carling, P.A., Wood, N. (1994). Simulation of flow over pool-riffle topography: A consideration of the velocity reversal hypothesis. Earth Surface Processes and Landforms **19**: 319-334.

- Carling, P.A, Orr HG, (2000). Morphology of riffle-pool sequences in the River Severn, England. Earth Surface Processes and Landforms **25**: 369-384.

- Carson, M.A. (1984) "The meandering – braiding river threshold: a reappraisal". Journal of Hydrology, **73** (1984) 315-334.

- Cha, J-E., Ahn, Y-C., Kim, M-H., (2002) Flow measurement with an electromagnetic flowmeter in two-phase bubbly and slug flow regimes. Flow Measurement and instrumentation **12:** 329-339.

- Chang, X-W., Paige, C.C., (2002). Numerical linear algebra in the integrity theory of the Global Positioning System. Computational Statistics & Data Analysis **41:** 123-142.

- Chen, Z., Chen, D., Xu, K., Zhao, Y., Wei, T., Chen, J., Li, L., Watanabe, M. (2006). Acoustic Doppler current profiler surveys along the Yangtze River. Geomorphology **85:** 155-165.

- Cherkauer, D.S., (1973). Minimisation of power expenditure in a riffle-pool alluvial channel. Water Resources Research, **9**: 1614-1628.

- Chew, L.C. & Ashmore, P.E. (2001) "Channel adjustment and a test of rational regime theory in a proglacial braided stream". Geomorphology 37 (2001) 43-63.

- Church, M. (1972) Baffin Island sandurs: A study of Arctic fluvial processes: Canada Geol. Survey Bull., v. 216, p. 89-93

- Clague, J.J., Turner, R.J.W., & Reyes, A.V. (2003) "Record of recent river channel instability, Cheakamus Valley, British Columbia". Geomorphology 53 (2003) 317-332.

- Clearwater (2007). Available online from http://www.clearwater-inst.com. Accessed June 2009.

- Clifford, N. J. and Richards, K. S. (1992). The reversal hypothesis and the maintenance of riffle-pool sequences Cited in Carling, P. A. & Petts, G. E. (Eds), Lowland Floodplain Rivers: geomorphological perspectives, Chichester: Wiley & Sons, 43-70.

- Clifford, N.J. (1993a). Differential Bed Sedimentology and the Maintenance of Riffle-pool sequences. CATENA. **20**, 456-468

- Clifford, N.J. (1993b). Formation of riffle-pool sequences: field evidence for an autogenetic process. Sedimentology Geology, 85: 39-51.

- Costa, J.E., Spicer, K.R., Cheng, R.T., Haeni, F.P., Melcher, N.B., Thurman, E.M., Plant, W.J., Keller, W.C. (2000). Measuring stream discharge by non-contact methods: a proof-of-concept experiment. Geophys. Res. Lett. **29:** 553-556.

- Creutin, J.D., Muste, M., Bradley, A.A., Kim, S.C., Kruger, A., (2003) River gauging using PIV technique: proof of concept experiment on the Iowa River. Journal of Hydrology **277:** 182-194.

- Data Buoy Cooperation Panel (2005) available online from www.cls.fr/html.ARGOS/documents/newsletter/nslan53/dbcp_em.html Accessed 31/10/05 11:49

- Data buoy types and background (2005) Available online from www.dbcp.noaa.gov/dbcp/1hb.html#MB Accessed 31/10/05.

- Davoren, A. & Mosley, M.P. (1986) "Observations of bedload movement, bar development and sediment supply in the braided Ohau River". Earth Surf. Proc. Landforms, **11**, 643-652.

- Depriest, D. 2003. A GPS User Manual: Working with Garmin Receivers. Garmin.

- Doeglas, D.J. 1962. The structure of sedimentary deposits of braided rivers. Sedimentology, 1, 167-190.

- Easimap (2010). Environment Agency Internal Map Archive. Accessed April 2010.

- Edina (2006). Digimap - Available online from http://edina.ac.uk/digimap. Accessed June 2006.

- El-Rabbany, A. 2002. Introduction to the Global Positioning System.

- Ergenzinger, P., and de Jong, C., (1996). Linking Hydraulics, Bedload Transport and River Bed Adjustment with the Conceptual FAST Model in Ashworth, P. J., Bennett, S. J., Best, J. L. and McLelland, S. J. (Eds), Coherent Flow Structures in Open Channels,Wiley, Chichester.

- Ettema, R., Fujita, I., Marian, M., Kruger, A., (1997) Particle-image velocimetry for whole-field measurement of ice velocities. Cold Region Science and Technology **26:** 97-112.

- Fan, S., Oey, L.Y., Hamilton, P. (2004) Assimilation of drifter and satellite data in a model of the Northeastern Gulf of Mexico. Continental Shelf Research **24:** 1001-1013.

- Fagan, S.D. & Nanson, G.C. (2004) "The morphology and formation of floodplain-surface channels, Cooper Creek, Australia". Geomorphology 60 (2004) 107-126.

- Ferguson, R.I., Presetegaard, K.L. and Ashworth, P.J. (1989) Influence of sand on the hydraulics and gravel transport in a braided gravel-bed river', Water Resources Research, **25** (4), 635-643.

- Ferguson, R.I. (1993) "Understanding braiding processes in gravel-bed rivers: progress and unsolved problems". From Best, J.L. & Bristow, C.S. (eds), 1983, Braided Rivers, Geological Society Special Publication No. 75, pp. 73-87.

- Fontana, R.D., Wai C, Stansell, T, (2001) The Modernized L2 Civil Signal, GPS World, 10485104, Vol. 12, Issue 9.

- Fox, J.F., Patrick, A., (2008) Large-scale eddies measured with large scale particle-image velocimetry. Flow Measurement and Instrumentation **19:** 283-291.

- Fulford, J.M., (2001) Accuracy and consistency of water-current meters. Journal of the American water resources association. **37: 5** 1215-1224.

- Garmin (2000) – Available online from www.garmin.com Accessed 21/9/05 10:42.

- Garcia, C.M., Cantero, M.I. Nino, Y., Garcia, M.H., 2005. Turbulence measurements with acoustic Doppler velocimeters. Journal of Hydraulic Engineering **131:** 1062-1073.
- Garwood Jr, R.W. Harcourt, R.R. and Stone. R.E. 1998. Simulation of Drifter in a Turbulent Ocean. Naval Research Reviews. Vol. L. 9-13.
- GDP (Global Drifter Programme) (2009). Available online from http://www.aoml.noaa.gov/phod/dac/gdp.html. Accessed August 2009.
- Gilbert, G.K. (1914) The transportation of debris by running water. US Geological Survey Professional Paper 86.
- Gili, J.A., Corominas, J., Rius, J., (2000). Using Global Positioning system techniques in landslide monitoring. Engineering Geology. **55:** 167-192.
- Global drifter buoy centre (2005) Available online from http://noaasis.noaa.gov/ARGOS/ Accessed 1/12/05.
- Goring, D. G.; Nikora, V. I. 2002: Despiking acoustic Doppler velocimeter records. ASCE Journal of Hydraulic Engineering 128: 117-126.
- GPS Explained (2005) www.kowoma.de/en/gps/signals.htm accessed 20/10/05 10.15am.
- GPS (2006). Available online from http://www gpsinformation.org. Now relocated to http://www.gpsinformation.org/ Accessed June 2006.
- Grodsky, S.A. and Carton, J.A. 2002. Surface drifter pathways originating in the equatorial Atlantic cold tongue. Geophysical Research Letters, Vol. 29. No. 23. 2147.
- Grudlingh, M.L. (1998) Surface currents derived form satellite-tracked buoys off Namibia. Deep-Sea Research II **46:** 453-473.

- Hack, J.T., 1957. Studies in longitudinal stream profiles in Virginia and Maryland. USGS Professional paper, 294B.

- Harrison, L.R. & Keller, E.A., (2007) Modeling forced pool-riffle hydraulics in a boulder-bed stream, southern California. Geomorphology **83** 232-248.

- Hauet, A., Creutin, J-D., Belleudy, P., (2008). Sensitivity study of large-scale particle image velocimetry measurement of river discharge using numerical simulation. Journal of Hydrology **349:** 178-190.

- Hay, C., (2000) The GPS Accuracy Improvement Initiative , GPS World, 10485104, Jun2000, Vol. 11, Issue 6.

- Hemp, J., Versteeg, H.K., (1986). Prediction of electromagnetic flow meter characteristics. J. Phys. Appl. Phys. **19:** 1459-1476.

- Hemp, J., (1991). Theory of eddy currents in electromagnetic flow meters. J. Phys. D: Appl. Phys. **24:** 244-251.

- Hemp, J. (2001) A technique for low cost calibration of large electromagnetic flowmeters. Flow measurement and Instrumentation. **12:** 123-134.

- Heritage, G.L. and Milan, D.J, (2004). A conceptual model of the role of excess energy in the maintenance of a riffle-pool sequences. Catena **58**: 235-257.

- Hjellbakk, A. (1997) "Facies and fluvial architecture of a high-energy braided river: the upper proterozoic seglodden member, varanger peninsula, northern Norway" Sedimentary Geology 114 (1997) 131-161.

- Hoey, T.B. & Sutherland, A.J. (1991) "Channel morphology and bedload pulses in braided rivers: a laboratory study". Earth Surface Processes and Landforms, **16**, 447-462.

- Hofmann-Wellenhof, B. Lichtenegger, H. and Collins, J. 2001. GPS: Theory and Practice. SpringerWien NewYork.

- Holland, K.T., Puleo, J.A., Kooney, T.N. (2001). Quantification of swash flows using video-based particle image velocimetry. Coastal Engineering **44:** 65-77.

- Horrevoets, A.C., Savenije, H.H.G., Schuurman, J.N. and Graas, S. 2004. The influence of river discharge on tidal damping in alluvial estuaries. Journal of Hydrology 294 213-228.

- Hosseini, S.A., Shamsai, A., Ataie-Ashtiani, B. (2006). Sychronous measurements of the velocity and concentration in low density turbidity currents using an Acoustic Doppler Velocimeter. Flow Measurement and Instrumentation **17:** 59-68.

- Jaksic, J. (2001) Running Interference, GPS World, 10485104, Feb2001, Vol. 12, Issue 2.

- Jakobson, K.P., Ribergaard, M.H., Quadfasel, D., Schmith, T. and Huges, C.W. (2002). The near surface circulation in the northern North Atlantic as inferred from Lagrangian drifters: variability from the meso-scale to interannual. Journal of Geophysical Research **108** (US) 2002.

- Jiongxin, Xu. (1996) "Channel pattern change downstream from a reservoir: An example of wandering braided rivers". Geomorphology **15** (1996) 147-158.

- Jodeau, M., Hauet, A., Paquier, A., Le Coz, J., Dramais, G., (2008) Application and evaluation of LS-PIV technique for the monitoring of river surface velocities in high flow conditions. Flow Measurement and Instrumentation **19:** 117-127.

- Johnson, D., Stocker, R.,, Head, R., Imberger, J., Pattiaratchi, C. (2003) A compact, low-cost GPS drifter for use in oceanic nearshore zone, lakes and estuaries. Journal of atmospheric and oceanic technology **20:** 1880:1884.

- Johnson, D., Pattiaratchi, C. (2004). Application, modelling and validation of surfzone drifters. Coastal Engineering **51:** 455-471.

- Keller, E.A. (1971). Areal Sorting of Bed-Load Material: The Hypothesis of Velocity Reversal. Geological Society of America Bulletin, **82**: 753-756.

- Keller, E.A. and Melhorn, W.N., (1978). Rhythmic spacing and origin of pools and riffles. Geol. Soc. Am. Bull., 89: 723-730.

- Keller, E.A., and Swanson, F.J., (1979) Effects of large organic material on channel form and fluvial processes. Earth Surface Processes and Landforms, **4:** 361 - 380

- Keller, E.A. and Florsheim, J.L, (1993). Velocity reversal hypothesis: a model approach'. Earth Surf Processes Landforms. **18**: 733-740.

- Kostaschuk, R., Best, J., Villard, P., Peakall, J., Franklin, M. (2004). Measuring flow velocity and sediment transport with an acoustic Doppler current profiler. Geomorphology **68:** 25-37.

- Knighton, D. 1998 Fluvial Forms and Processes: A New Prospective. Arnold, London.

- Lamarre, H., Roy, A.G., (2005). Reach scale variability of turbulent flow characteristics in a gravel-bed river. Geomorphology **68:** 95-113.

- Lamarre, H., Roy, A.G., (2008). A field experiment on the development of sedimentary structures in a gravel-bed river. Earth Surface Processes and Landforms **33**: 1064-1081.

- Lane, E.W. and Borland, W.M. 1954. 'River-bed scour during floods'. Transactions, American society of Civil Engineers, 119, 1069-1079

- Lane, E.W. 1957. A study of the shape of channels formed by natural streams flowing in erodible material. Missouri River Division Sediment Series No.9 U.S. Army Engineer Division, Missouri River Engineers, Omaha, Nebraska.

- Lane, S.N., Richards, K.S., Warburton, J. (1993). Comparison between high frequency velocity records obtained with spherical and discoidal electromagnetic current meters. In Clifford, N.J, French, J.R. and Hardisty, J, ed. Turbulence: Perspectives on Flow and Sediment Transport. 1993 Wiley and Sons Ltd.

- Lane, S.N., Biron, P.M., Bradbrooks, K.F., Butler, J.B., Chandler, J.H., Crowell, M.D., McLelland, S.J., Richards, K.S., Roy, A.G. (1998). Three-dimensional measurement of river channel flow processes using acoustic Doppler velocimetry. Earth Surface Processes and Landforms, **23:** 1247-1267.

- Lane, S.N., Bradbrook, K.F., Richards, K.S., Biron, P.A., Roy, A.G. (1999). The application of computation fluid dynamics to natural river channels: three dimensional versus two-dimensional approaches. Geomorphology **29,** 1-20.

- Langley, Richard B., (2000) Smaller and Smaller: The Evolution of the GPS Receiver , GPS World, 10485104, April 2000, Vol. 11, Issue 4

- Lawless, M. and Robert, A. (2001). Three-dimensional flow structure around small-scale bedform in a simulated gravel-bed environment. Earth Surface Processes and Landforms **26**: 507-522.

- Leick. A. 2004. GPS Satellite Surveying. John Wiley & Sons

- Leigh, D.S. (in press) "Terminal Pleistocene braided to meandering transition in rivers of the south eastern USA". Catena (in press).

- Leonard, L., Croft, A., Childers, D., Mitchell-Bruker, S., Solo-Gabriele, H., Ross, M. (2006) Characteristics of surface-water flows in the ridge and slough landscape of everglades national park: implications for particulate transport. Hydrobiologia **569:** 5-22.

- Leopold, L.B., Wolman M.G., (1957) River channel patterns: meandering, braided and straight. US Geological Survey Professional Paper 282-B.

- Leopold, L.B., Wolman, M.G., and Miller, J.P. (1964). Fluvial processes in geomorphology. San Fransisco: W.H. Freeman

- Lewin, J. & Brewer, P.A. (2001) "Predicting channel patterns". Geomorphology 40 (2001) 329-339.

- Lisle, T.E., 1979. A sorting mechanism for a riffle-pool sequences, Geol. Soc. Am. Bull., 90: 1142-1157.

- Lisle, T.E., 1986. Stabilization of a gravel channel by large streamside obstructions and bedrock bends, Jacoby Creek, northwest California, Geol. Soc. Am. Bull., **97**: 999-1011.

- Lofthouse, C., Robert, A. (2007) Riffle-pool sequences and meander morphology. Geomorphology. doi:10.10.16/j. geomorph.2007.11.002

- Lohrmann, A., R. Cabera, and N.C. Kraus, 1994. Open-channel flow and turbulence measurement by high-resolution Doppler sonar. J. Atmos. Oceanic Technol. **11**, 1295-1308.

- Maa, J.P.-Y., Kwon, J.-J. (2007). Using ADV for cohesive sediment settling velocity measurements. Estuarine, Coastal and Shelf Science **73:** 351-354.

- MacVicar, B.J., Beaulieu, E., Champagne, V., Roy, A.G., (2007). Measuring water velocity in highly turbulent flows: field tests of an electromagnetic current meter (ECM) and an acoustic Doppler velocimeter (ADV). Earth Surface Processes and Landforms **32:** 1412-1432.

o MacWilliams, M.L., (2004). Three-dimensional Hydrodynamic Simulation of River Channels and Floodplains, PhD Dissertation, Stanford University.

o MacWilliams, M.L., Wheaton, J.M., Pasternack, G.B., Street, R.L., Kitanidis, P.K. (2006) Flow convergence routing hypothesis for pool-riffle maintenance in alluvial rivers. Water Resource Research. Vol 42 w10427, doi.1029/2005WR004391, 2006

o Maghrebi, M.F. (2006) Application of the single point measurement in discharge estimation. Advances in Water Resources **29:** 1504-1514.

o Manda, A., Takahashi, T., Komori, S., Kyozuka, Y., Nishimura, S. (2000) Validation of a new type of Lagrangian drifter using a GPS cellular phone. International journal of offshore and polar engineering **12:** 3.

o Manning, J.P., Churchill, J.H. (2006). Estimates of dispersion from clustered-drifter deployments on the southern flank of Georges Bank. Deep-Sea Research II **53:** 2501-2519.

o Manson, J.R., Wallis, S.G. and Wang, D. 2000. A Conservative, Semi-Lagrangian Fate and Transport Model For fluvial Systems – II. Numerical Testing And practical Applications. Wat. Res. Vol. 34. No. 15. pp 3778-3785.

o Markham, A.J. & Thorne, C.R. (1992) "Geomorphology of gravel-bed river bends". Cited in Dynamics of Gravel-bed Rivers. Edited by P.Billi, R.D. Hey, C.R. Thorne & P. Tacconi. (1992) John Wiley & Sons Ltd.

o Marsh McBirney, 2008. Available online from http://www.marsh-mcbirney.com/.Accessed 01/08/2009.

o Martin, N. and Gorelick, S.M. 2005 MOD_FreeSurf2D: A MATLAB surface fluid flow model for rivers and stream. Computers & Geosciences 31. 929-946.

- McLelland, S.J., Nicholas, A.P., (2000). A new method for evaluating errors in high-frequency ADV measurements. Hydrological Processes. **14:** 351-366.
- Melton, M.A. 1962 Methods of measuring the effect of environmental factors on channel properties. Journal of Geophysical Research, **67**, 1485-1490.
- Metivier, F. & Meunier, P. (2003) "Input and output mass flux correlations in an experimental braided stream. Implications on the dynamics of bed load transport". Journal of Hydrology 271 (2003) 22-38.
- Meteo (2009) Available online from http://www.meteo.shom.fr/buoyinfo/svpfig.html. Accessed May 2009.
- Miall, A.D. 1977. A review of the braided stream depositional environment. Earth Science Reviews, 13, 1-62.
- Milan, D.J., Heritage, G.L., Large, A.R.G. and Charlton, M.E. (2001). Stage dependent variability in tractive force distribution through a riffle-pool sequence. CATENA **44:** 85-109.
- Milne, J.A. (1982). Bed-material size and the riffle-pool sequences. Sedimentology. **29**, 267-278.
- Miller, A.J. (1994) Debris fan constrictions and flood hydraulics in river canyons: some implications of two-dimensional flow modelling. Earth Surface Processes and Landforms **19,** 681-697.
- Mosselman, E., Shishikura, T. & Klaassen, G.J. (2000) "Effects of Bank Stabilization on Bend scour in Anabranches of Braided rivers". Phys. Chem. Earth (B) Vol. 25, No. 7-8, pp. 699-704, 2000.
- Montgomery, D.R, Buffington, J.M., Smith, RD., Schmidt, K.M., Pess, G. (1995) Pool spacing in forest channels. Water Resource Research **31**: 1097-1105.

- Montgomery, D.R., Buffington, J.M., 1997. Channel-reach morphology in mountain drainge basins. Geological Society of America Bulletin 109, 596-611.

- Muste, M., Yu, K., Spasojevic, M., (2004). Practical aspects of ADCP data use for quantification of mean river flow characteristics; Part I: moving-vessel measurements. Flow Measurement and Instrumentation **15:** 1-16.

- Muste, M., Yu, K., Pratt, T., Abraham, D. (2004). Practical aspects of ADCP data use for quantification of mean river flow characteristics; Part II: fixed-vessel measurements. Flow Measurement and Instrumentation **15:** 17-28.

- Muste, M., Schone, J., Creutin, J-D., (2005). Measurement of free-surface flow velocity using controlled surface waves. Flow Measurement and Instrumentation **16:** 47-55.

- Naudin, J.J., Cauwet, G., Chretiennot-Dinet, M.-J., Deniaux, B. Devenon, J.-L. and Pauc, H. 1997. River Discharge and Wind Influence Upon Particulate Transfer at the Land-Ocean Interaction: Case Study of the Rhone River Plume. Estuarine, Coastal and Shelf Science 45. 303-316.

- Nicholas, A.P. (2000) "Modelling bedload yield in braided gravel bed rivers". Geomorphology 36 (2000) 89-106.

- NOAA (2005) National Environmental Satellite, Data and Information Service (NESDIS)

- Nystrom, E. A., Oberg, K. A., and Rehmann, C. R. _2002_. "Measurement of turbulence with acoustic Doppler current profilers—Sources of error and laboratory results." Proc., Hydraulic Measurements & Experimental Methods 2002.

- O'Connor, J.E., Webb, R.H., Baker, V.R., 1986. Paleohydrology of pool and riffle pattern development; Boulder Creek, Utah. Geological Scoiety of America Bulletin **97**, 410-420.

- Ohlmann, J.C., White, P.F., Sybrandy, A.L., Niiler, P.P. (2005) GPS-Cellular drifter technology for coastal ocean observing systems. Jounrla of atmospheric and oceanic technology. **22:** 1381:1388.

- Ott (2006). Available online from www.ott-hydrometry.de/web/ott_de.nsf/id/pa_e.html Accessed 17/05/09.

- Pace S. Frost, G. Hackhow, I. Frelinger, D. Fossum, D. Wassem, D.K. and Pinto, M. 1995. The Global Positioning System. Accessing National Policies. Publisher: Rand. Place of Publication: Santa Monica, CA.

- Pacific Gyre (2008). Available online from http://www.pacificgyre.com. Accessed May 2009.

- Pazan, S.E. and Niiler, P. 2004. New Global Drifter Data Set Available. EOS Vol. 85, No. 2. Available online from [www.agu.org/eos_elec/000440e.shtml] Accessed 31/10/05 14:49.

- Rathburn, S. and Wohl E., (2003). Predicting fine sediment dynamics along a pool-riffle mountain channel. Geomorphology **55**: 111-124.

- Richards, K.S. (1976a). The morphology of riffle-pool sequences. Earth Surf Processes Landforms **1**: 71-88.

- Richards, K.S. (1976b). Channel width and the riffle-pool sequences. Geological Society of America Bulletin. **87**: 883-890.

- Richards, K.S, (1978). Simulation of flow geometry in a riffle-pool stream. Earth Surf Processes Landforms **3**: 345-354.

- Richards, K.S. 1982: Rivers. Form and process in alluvial channels. London: Methuen.

- Richardson, W. R. R., Thorne, C. R. and Mahmood, S. 1996. 'Secondary flow and channel changes around a bar in the Brahmaputra River, Bangladesh', in Ashworth, P. J., Bennett, S. J., Best, J. L. and McLelland, S. J. (Eds), Coherent Flow Structures in Open Channels,Wiley, Chichester, 519–544.

- Richardson, R. W. & Thorne, C. R. (2001) "Multiple thread flow and channel bifurcation in a braided river: Brahmaputra-Jamuna river, Bangladesh". Geomorphology 38 (2001) 185-196.

- Robert, A. (1997). Characteristics of velocity profiles along riffle-pool sequences and estimates of bed shear stress. Geomorphology **19**: 89-98.

- Rodriguez, A., Sanchez-Archilla, A., Redondo, J.M., Mosso, C., (1999) Macroturbulence measurements with electromagnetic and ultrasonic sensors: a comparison under high-turbulent flows. Experiments in Fluids **27**: 31-42.

- Roy, A.G., Biron, P., De Serres, B. (1996). On the necessity of applying a rotation to instantaneous velocity measurements in river flows. Earth Surface Processes and Landforms **21:** 817-827.

- Rust, B. R. 1978. A classification of alluvial channel systems. In: Miall, A.D. (ed.) Fluvial Sedimentoogy. Canadian Society of Petroleum Geologists Memoirs, 5, 187-198.

- Sawyer, A.M., Pasternack, G.B., Moir, H.J., Fulton, A.A. In Press. Riffle-pool maintenance and flow convergence routing observed on a large gravel-bed river. Geomorphology (2009), doi: 10.1016/j.geomorph.2009.06.021.

- Schlecht, E., Hulsebusch, F.M., Becker, K., (2004). The use of differential corrected global positioning system to monitor activities of cattle at pasture. Applied Animal Behaviour Science **85:** 185-202.

- Schmidt, JC. 1990. Recirculating flow and sedimentation in the Colorado River in Grand Canyon, Arizona. Journal of Geology. **98:** 709-724.

- Schumm, S.A. & Khan, H.R. 1972. Experimental study of channel patterns. Geological Society of America Bulletin, 83, 1755-1770.

- Schumm, S.A. 1977. The fluvial System, Wiley, New York.

- Schutz, Y., Herren, R,. 2000. Assessment of speed of human locomotion using a differential satellite global positioning systems. Medical Science and Sports Exercise 32, 6420646

- Sear, DA. 1996. Sediment transport processes in pool-riffle sequences. Earth Surface Processes and Landforms **21**: 241-262.

- Shaw, M., (2000) MODERNIZATION OF THE GLOBAL POSITIONING SYSTEM , GPS World, 10485104, Sep2000, Vol. 11, Issue 9

- Shields, F.D., Rigby, J.R., (2005). River Habitat Quality from River Velocities Measured Using Acoustic Doppler Current Profiler. Environmental Management **36:** 565-575.

- Simpson, C.J. & Smith, D.G. (2001) "The braided Milk River, northern Montana, fails the Leopold-Wolman discharge-gradient test". Geomorphology 41 (2001) 337-353.

- SMITHSONIAN NATIONAL AIR AND SPACE MUSEUM, 2005 Available online from http://www.nasm.edu/ Accessed 9/2/06

- Soler, T., Johnson, R.E.,Leland, F.F. Foote, R..H. (2001) Parting the Waters GPS World, 10485104, May2001, Vol. 12, Issue 5.

- SonTek Acoustic Doppler Current Profiler (2006). Avaliable from [www.sontek.com/pics/adpgrp.jpg] Accessed 22/05/06/

- Sphere Diagram (2006) available online from: www.geography.wisc.edu/sco/gps/gps_graphics/inter_spheres.jpg, accessed 09/05/06.

- Stagonas, D., Muller, G. (2007). Wave field mapping with particle image velocimetry. Ocean Engineering **34:** 1781-1785.

- Stockdale, R.J., McLelland, S.J., Middleton, R., Coulthard, T.J., (2007) Measuring river velocities using GPS river flow tracer (GRiFTers). Earth Surface Processes and Landforms **DOI:** 10.1002/esp.1614

- SVP and SVP-B Lagrangian Drifter (WOCE Surface Velocity Programme) Available from www.technocean.com/DOCS/svp_svpb.htm Accessed 31/10/05

- Tait, S.J., Willetts, B.B., Gallagher, M.W., (1996). The application of particle image velocimetry to the study of coherent flow structures over a stabilizing sediment bed in Ashworth, P. J., Bennett, S. J., Best, J. L. and McLelland, S. J. (Eds), Coherent Flow Structures in Open Channels,Wiley, Chichester.

- Taylor, M.A.P., Woolley, J.E., Zito, R., (2000). Integration of the global positioning system and geographical information systems for traffic congestion studies. Transportation Research Part C **8:** 257-285.

- Teisseyre, A.K. (1984): The River Bobr in the Blazkowa study reach (central Sugetes): a case study in fluvial processes and fluvial sedimentology. Geol. Sudetica 19, 7-71.

- Thomas, R. & Nicholas, A.P. (2002) "Simulation of braided river flow using a new cellular routing scheme". Geomorphology 43 (2002) 179-195.

- Thompson, D.M., Wohl, E.E. and Jarrett, R.D, (1996) A revised velocity reversal and sediment sorting model for a high gradient pool-riffle stream. Phys. Geogr. 17(2): 142-156.

- Thompson, D.M., Nelson J.M., Wohl, EE. (1998). Interactions between pool geometry and hydraulics. Water Resource Research **34:** 3673-3681.

- Thompson, D.M., Wohl, E.E. and Jarrett, R.D, (1999). Velocity reversals and sediment sorting in pools and riffles controlled by channel constrictions. Geomorphology **27**: 229-241.

- Thompson, D.M. (2001) Random controls on semi-rhythmic spacing of pools and riffles in constriction-dominated rivers. Earth Surface Processes and Landforms **26**: 1195-1212.

- Thompson, D.M., Hoffman, K.S. (2001) Equilibrium pool dimensions and sediment sorting patterns in coarse-grained, New England channels. Geomorphology **38**: 301-316.

- Thompson, D.M. (2004). The influence of pool length on local turbulence production and energy slope: a flume experiment. Earth Surface Processes and Landforms **29**; 1341-1358.

- Tinkler, K.J. (1970). Pools, Riffles, and Meanders. Geological Society of America Bulletin. **81**, p. 547-552.

- Tracking Drifter Buoys (2005) Available online from http://vathena.arc.nasa.gov/curric/oceans/drifters/ Accessed 22/9/05 9.47am

- Tseng, R.S. and Shen, Y.T. 2002. Lagrangian observations of surface flow patterns in the vicinity of Taiwan. Deep-Sea Research II 50 1107-1115.

- Tsumune, D. Nishioka, J.Shimamoto, A. Takeda, S. and Tsuda, A. Physical behaviour of the SEEDS iron-fertilized patch by sulphur hexafluoride tracer release. Progress in Oceanography 64 (2005) 111-127.

- Van Sickle. J. 1996. GPS for Land Surveying. Ann Arbour Press, Chelsea Michigan.

- Valeport (2009) Available online at [www.valeport.co.uk] Accessed (20/05/09).

- Virant, M., Dracos, T., (1997). 3D PTV and its application on Lagrangian motion. Meas. Sci. Technol. **8:** 1539-1552.

- Voulgaris, G., Trowbridge, J.H. (1997). Evaluation of the acoustic Doppler velocimeter (ADV) for turbulence measurements. Journal of atmospheric and oceanic technology **15:** 272-288.

- Wang, J.Z., Tian, G.Y., Lucas, G.P., (2007) Relationship between velocity profile and distribution of induced potential for an electromagnetic flow meter. Flow Measurement and Instrumentation **18:** 99-105.

- Weitbrecht, V., Kuhn, G., Jirka, G.H., (2002). Large scale PIV-measurements at the surface of shallow water flows. Flow Measurement and Instrumentation **13:** 237-245.

- Wewetzer, S., Duck, R.W., Anderson, J.M., 1999. Acoustic Doppler current profiler measurements in coastal and estuarine environments: examples from the Tay Estuary, Scotland. Geomorphology 29 (1), 21–31.

- Whittaker, J.G. and Jaeggi, M.N.R. 1982. Origin of step-pool systems in mountain streams, J. Hydraul. Div. ASCE. 108, 758-773.

- Wilkinson, S.N., Keller, R.J., Rutherfurd, I.D. (2004) Phase shifts in shear stress as an explanation for the maintenance of pool-riffle sequences. Earth Surface Landforms and Processes **29**: 737-753.

- Williams, P. F. & Rust, B. R. 1969. The sedimentology of a braided river. Journal of Sedimentary Petrology, 39, 649-679.

- Witte, T.H. and Wilson, A.M. 2004. Accuracy of non-differential GPS for the determination of speed over ground. Journal of Biomechanics 37. 1891-1898.

- Witte, T.H. and Wilson, A.M. 2005 Accuracy of WAAS-enabled GPS for the determination of position and speed over ground. Journal of Biomechanics 38. 1717-1722.

- Wohl, E.E., Vincent, K.R., Merrits, D.J. 1993. Pool and riffle characteristics in relation to channel gradients. Geomorphology **6:** 99-110.

- Wolman, M. G., (1958) The natural channel of Brandywine Creek, Pennsylvania. U.S. Geological Survey Professional Paper **271**: 65

- Yalin, M.S., 1971. On the formation of dunes and meanders. International Association of Hydraulic research. 14th Congress, Paris. Proc 3, paper, vol. C13, pp 1-8.

- Yang, C.T. (1971) Formation of riffles and pools. Water Resource Research. 7, 1567-1574.

- Yorke, T.H., Oberg, K.A., (2002). Measuring river velocity and discharge with acoustic Doppler profilers. Flow Measurement and Instrumentation **13:** 191-195.